Characterization of intracranial pressure (ICP) signals

Martinez Tejada, Isabel

Publication date:
2021

Document Version
Publisher's PDF, also known as Version of record

PhD Thesis
Doctor of Philosophy

DTU Health Tech
Department of Health Technology

Characterization of intracranial pressure (ICP) signals

Isabel Martinez Tejada

Kongens Lyngby 2021

DTU Health Technology
Department of Health Technology
Technical University of Denmark

Ørsteds Plads
Building 349
2800 Kongens Lyngby, Denmark
Phone +45 4525 3031
healthtech-info@dtu.dk
www.healthtech.dtu.dk

CSF Study Group
Department of Neurosurgery
Rigshospitalet

Section 6031
Rigshospitalet
Inge Lehmanns Vej 6
2100 Copenhagen Ø, Denmark
Phone +45 3545 6031
neurokir.rigshospitalet@regionh.dk
www.cphcsf.dk

Characterization of intracranial pressure (ICP) signals

Author:
Isabel Martinez Tejada

Supervisors:
Jens E. Wilhjelm, Main Supervisor, Professor, Group Leader, Department of Health Technology, Digital Health Section, Technical University of Denmark, Kongens Lyngby, Denmark
Marianne Juhler, Co-Supervisor, Professor, MD, DMSc, Department of Neurosurgery, Rigshospitalet, Copenhagen Ø, Denmark
Morten Andresen, Co-Supervisor, MD, PostDoc, Department of Neurosurgery, Rigshospitalet, Copenhagen Ø, Denmark

Funded by:
This project has received funding from the Novo Nordisk Foundation Tandem Programme (NNF17OC0024718).

Published by: DTU, Department of Health Technology, Ørsteds Plads, Building 349, 2800 Kgs. Lyngby Denmark
www.healthtech.dtu.dk

Preface

This thesis has been prepared over three years (from August 2018 to July 2021) as a collaboration between the Department of Health Technology, at the Technical University of Denmark, DTU, and the Department of Neurosurgery, at Rigshospitalet, in partial fulfilment for the degree of Doctor of Philosophy in Engineering. The thesis was done under the supervision of Clinical Professor Marianne Juhler, Professor Jens E. Wilhjelm and Clinical PostDoc Morten Andresen, and has resulted in three published scientific articles and three scientific articles in submission. Along with the research work, other activities including teaching assistance in the course *22446 EWH Summer School in biomedical instrumentation*, conference participation and supervision of bachelor and master projects were carried out at the same time.

I hope that the audience enjoys this thesis as much as I have enjoyed the PhD project. From being involved in neurological surgery for data collection, to doing the more technical and mathematical analysis of the data, it has overall been quite a journey for me. This is why I would love any discussion regarding this dissertation with any curious reader.

Isabel Martinez Tejada

Signature

31/July/2021

Date

Abstract

Intracranial pressure (ICP) monitoring is a mainstay of neurosurgical diagnostic and therapeutic procedures. With the development of telemetric monitoring devices in the last decade, ICP monitoring has become feasible in a broader clinical setting, with patients undergoing ICP monitoring with mobile equipment either in-hospital or in the home setting, where a larger variety of ICP waveforms exist. Currently, the identification of these waveforms, the so-called macro-patterns lasting seconds to minutes, is primarily based on visual inspection. This process is not only slow but also subject to investigator bias due to interpretation subjectivity and dependence on experience. The need for objective and more automated identification of these variations emerges as a potential tool for better understanding the physiological underpinnings of the patient's clinical state.

This thesis, divided into three main objectives, presents a new methodology that serves as a foundation for future objective and reproducible macro-pattern identification in the ICP signal with the hope to better understand the morphological characteristics and distribution of these macro-patterns in the ICP signal and their clinical significance.

First, we establish the motivation for the need of algorithm development for the extraction of macro-patterns from the ICP signal as an insight into the brain function. The results show that the current terminology and descriptions of B-waves no longer adequately address the ICP waveforms found in the clinical practice today. Discrepancy also exists regarding their origin. Our results found that ICP B-waves, also observed in healthy subjects during sleep, are associated both with respiratory disturbances and vascular contribution of flow velocity in a limited frequency range.

Second, a new data quality pipeline is designed that integrates all data validation checks to ensure high data quality. This pipeline includes artefact removal based on empirical mode decomposition, which is able to handle the non-linearity and non-stationarity properties of ICP signals. The method is applied to ICP signals before macro-pattern identification, to mitigate the possibility of artefacts masking the true signal.

Finally, a method based on k-Shape clustering is developed to identify the most encountered macro-patterns in ICP signals. We found a total of seven macro-patterns—with varying occurrence and distribution—that describe our ICP signals. These results may be considered benchmarks for the discussed shape clustering method that will be used in our ongoing research. These building blocks together with additional retrospective data could allow the identification of more unencountered macro-patterns besides the seven proposed in this dissertation.

In conclusion, this thesis proposes a new, objective, and more automated method to identify macro-patterns in ICP signals. It walks through all steps from initial ICP recording to the characterization of the ICP signal, including the validation of the data quality. Thanks to this method, disease entities are likely to be identifiable based on the internal distribution and weighting of specific ICP macro-patterns. This information aims at optimizing both disease and treatment identification.

Resumé (Danish)

Intrakranielt tryk (ICP) monitorering er en grundpille i neurokirurgisk diagnostik og terapeutiske procedurer. Med udviklingen af telemetrisk monitoreringsudstyr i det sidste årti er ICP-monitorering blevet mulig i en bredere klinisk sammenhæng, hvor patienter gennemgår ICP-monitorering med mobilt udstyr enten på hospitalet eller derhjemme, hvor en større variation af ICP-bølgeforme eksisterer. Identifikationen af disse bølgeformer, de såkaldte makro-mønstre (der varer sekunder til minutter), er på nuværende tidspunkt baseret på visuel inspektion. Denne proces er ikke kun langsom, men er også genstand for forskerens bias grundet fortolkningssubjektivitet og afhængighed af erfaring. Behovet for objektiv og mere automatiseret identifikation af disse variationer fremstår som et potentielt værktøj til bedre forståelse af den fysiologiske understøttelse af patientens kliniske tilstand.

Denne afhandling, opdelt i tre hovedmål, præsenterer en ny metodologi der tjener som fundament for fremtidigt objektiv og reproducerbar makro-mønsteridentifikation i ICP-signalet, med håbet om bedre at kunne forstå de morfologiske egenskaber og distribuering af disse makro-mønstre i ICP-signalet og deres kliniske betydning.

Først etablerer vi motivationen for behovet af at udvikle algoritmer til ekstraktion af makro-mønstre fra ICP-signalet, som et indblik i hjernens funktion. Resultaterne viste at den nuværende terminologi, og beskrivelser af B-bølger, ikke længere adresserer ICP bølgeformene der findes i den kliniske praksis i dag. Endvidere hersker der også uoverensstemmelser om deres oprindelse. Vores resultater viste at ICP-bølger, også observeret hos raske patienter under søvn, er associeret med både åndedrætsforstyrrelser og vaskulært bidrag af strømhastighed i et begrænset frekvensområde.

Herefter er der designet en ny datakvalitetspipeline, der integrerer alle datavalideringskontroller, for at sikre høj datakvalitet. Denne pipeline inkluderer fjernelse af artefakter baseret på empirical mode decomposition, som er i stand til at håndtere ICP-signalers ikke-lineære og ikke-stationære egenskaber. Metoden bliver anvendt til ICP-signaler før makro-mønsteridentifikation, for at afbøde muligheden for at artefakter maskerer det sande signal.

Endeligt bliver der udviklet en metode, baseret på k-Shape-klyngedannelse, til identifikation af de mest mødte makro-mønstre i ICP-signaler. Vi fandt i alt syv makro-mønstre med varierende forekomst og distribution, der bedre beskriver vores ICP-signaler. Disse resultater kan betragtes som benchmark for den diskuterede formklyngemetode, som vil blive anvendt i vores fortsatte forskning. Disse grundelementer vil, sammen med ekstra retrospektive data, kunne muliggøre identifikation af mindre hyppigt forekommende makro-mønstre udover de syv foreslået i denne afhandling.

Som konklusion foreslår denne afhandling en ny, objektiv og mere automatiseret metode til at identificere makro-mønstre i ICP-signaler. Den gennemgår alle trin fra den indledende ICP-optagelse til karakteriseringen af ICP-signalet, inklusiv validering af datakvaliteten. Takket være denne metode vil sygdomsenheder sandsynligvis være identificerbare baseret på den interne fordeling og vægtning af specifikke ICP-makro-mønstre. Denne information sigter mod at optimere både sygdoms- og behandlingsidentifikation.

Acknowledgements

I would have never reached this point without the help and support of all those that have not only made this project possible but they have also made out of it an unforgettable experience. In fact, I would have never started this project without the opportunity that my three supervisors gave me three years ago. I would like to thank my main supervisor Professor Jens E. Wilhjelm for the many hours of brainstorming, meetings, and the support in writing articles. I also owe huge thanks to my clinical co-supervisor Professor Marianne Juhler, for the enthusiasm, for the incredibly wise advice I always got from her, and for reminding me of the small achievements we were accomplishing along the way. A big thank you also goes to my clinical co-supervisor PostDoc Morten Andresen, for always providing support and guidance, opening my eye for details, and giving me a push when I needed it the most. I need to thank the three of them for their patience, along with their constant support and orientation.

Thanks to my hospital colleague Casper Schwartz for being a big support for me in this project. Thanks for the many hours of coding, coffee, and brainstorming, but also for the fun that came with it. You showed me how to be passionate with the work and to not give up on goals. A big owe also goes to Rikke, for contributing to my project as part as her master thesis, but also for becoming one of my really good friends.

A thanks to Professor Marek Czosnyka, Dr. Zofia Czosnyka, Dr. Peter Smielewski, and the research team from the Brain Physics Lab at University of Cambridge, United Kingdom for hosting me on my research external stay. Although shorter than expected because of COVID, it was truly an inspiration to participate in your research, your clinical work, and dinners at the pubs. I am so grateful for the knowledge I acquired from you.

I would like to thank my colleagues from DTU Health Technology, specially those from the old Biomedical Engineering team. Thanks to PhD students Iman and Jihwan, for making every day at work fun. Rasmus for being my crying partner and Mikkel for teaching me how to be an honest person. To Lasse, because I did not believe on work being done after 17 until I met him. And Sigrid, for always being ready to organize team events.

I am grateful for Novo Nordisk Funding for funding this research, and Otto Mønsteds Fond for supporting my external stay in Cambridge, UK. To everyone part of the same Novo Nordisk Tandem grant, a big thank you for contributing with ideas and research questions in these years. I was able to learn a lot from you and look at my project from different angles.

A big thanks goes to my family, mom, dad, sister and uncle, for always supporting me (from many kilometers away) in every step in my life, understanding that sometimes I could not dedicate as much time to them as I did to my thesis, and loving me undoubtedly. A special mention goes to my sister, because of who she is and what she is becoming, I am truly proud of you, and you are my true inspiration when it comes to hard work.

Approximately halfway through my PhD I met Oscar, who has turned my life in the best way. I am grateful for all the laughs and good energy during the writing of the thesis (and during the thesis also). I could not have been more lucky to meet you and I look forward to what life with you will bring.

And last, but not least, I would not be here today without my friends, who are my family here in Denmark. Maria and Candela for being my older sisters and my go-to persons for anything. Maria de Luna (and Eri) for the fun you brought these last months, the constant chitchats and laughs, undoubting support, inspirational talks, and good runs during this

pandemic. Silje and Ana for being my best friends and my pillars since the first day I arrived to DK. Yvonne for being the other half for my double-trouble, I think that says it all. Toni, Loic, and Rosa for giving me the most fun two years in Copenhagen. Carles, Ayub, and Luis for being them, full of fun no matter what. Marina, Claudia, Andrea, and Iñaki for being my home away from home. And Gordon, for comforting me and bringing a smile when I complain. And although far away, the last thank you goes to my forever friends, Vir, Sara, Pati, Cris, Tito, Criso, and Ele, for understanding me, growing up with me, and always making time when I go visit them.

Contents

Acronyms

AAMI Association for the Advancement of Medical Instrumentation

AASM American Academy of Sleep Medicine

ABP Arterial Blood Pressure

AHI Apnea-Hypopnea Index

AIC Akaike Information Criterion

ANSI American National Standards Institute

BTF Brain Trauma Foundation

CBFV Cerebral Blood Flow Velocity

CBV Cerebral Blood Volume

cGC Conditional Granger Causality

CHI Calinski-Harabasz Index

CNS Central Nervous System

CSF Cerebrospinal Fluid

CVI Cluster Validity Index

DBI Davies-Bouldin Index

ECG Electrocardiogram

EEG Electroencephalogram

EEMD Ensemble Empirical Mode Decomposition

EMD Empirical Mode Decomposition

EMG Electromyogram

EOG Electrooculogram

EVD Extraventricular Drain

FIR Finite-Impulse Response

FV Flow Velocity

GC Granger Causality

ICA Independent Component Analysis

IIH Idiopathic Intracranial Hypertension

ICP Intracranial Pressure

IMF Intrinsic Mode Function

JRD Jensen-Rényi Divergence

KPSS Kwiatkowski–Phillips–Schmidt–Shin

MOCAIP Morphological Clustering and Analysis of Intracranial Pressure

MR Magnetic Resonance

MVAR Multivariate Autoregressive

NE Number of Ensembles

NICU Neurointensive Care Unit

NPH Normal Pressure Hydrocephalus

NREM Non-Rapid Eye Movement

PSD Power Spectral Density

PSG Polysomnography

REM Rapid Eye Movement

RIP Respiratory Inductance Plethysmography

SAH Subarachnoid Haemorrhage

SBD Shape-Based Distance

SDB Sleep-Disordered Breathing

SI Silhouette Index

TBI Traumatic Brain Injury

TCD Transcranial Doppler

VFP Ventricular Fluid Pressure

List of Figures

List of Tables

CHAPTER 1 Introduction

Intracranial pressure (ICP) monitoring was introduced by Guillaume and Janny in 1951 [1]. However, it was not until the 1960s that it grew in popularity thanks to Lundberg, who established a protocol for its routine use in brain-injured patients [2]. Since then, it has unfolded to become a diagnosis modality as integral to neurosurgical practice, as pulse rate is to the larger medical community. Unfortunately, ICP signal analysis in the clinical setting has not evolved to the extent initially hoped for and in the wider clinical community remains largely limited to ICP interpretation as a certain number that must remain within defined boundaries for the brain to function properly. However, the ICP signal represents a tremendously complex interplay of time series with wave patterns that go beyond this previous limited interpretation. This poses a challenge because in our neurosurgical clinic we see patterns in the ICP signal in all sorts of shapes, whose identification is complicated.

1.1 Context and Motivation

Neurosurgical disorders, such as hydrocephalus, traumatic brain injury (TBI), or idiopathic intracranial hypertension (IIH), are conditions characterized by disturbances in the cerebrospinal fluid (CSF) dynamics. The disturbances can involve pathological changes that include abnormal movement of transparenchymal fluids, elevated ICP, and changes in brain morphology, among others [3]. TBI alone is the most common cause of death and disability in children and young adults, according to a recent World Health Organization report on neurological disorders [4]. Lifetime prevalence is 1-2 % of the US population [5] and it is expected to continue rising considering increases in population density, population ageing, and higher number of vehicles in use [6]. Direct annual estimated costs are of approximately $9 billion [7]. IIH draws dangerous parallels to the increasing incidence of TBI. In the UK, the incidence rate increased from 2/100,000 in 2002 to 4.7/100,000 in 2016, induced in part by the current escalating obesity pandemic [8]. The economic burden from frequent hospitalizations and loss of productivity went from 9.2 million pounds in 2002 to 49.9 million [9].

ICP monitoring is explored as a diagnostic and therapeutic modality to better understand these neurosurgical disorders. ICP is monitored invasively with a small pressure transducer inserted in different intracranial anatomical locations (subdural, epidural, intraparenchymal, subarachnoidal, or intraventricular placements) [10]. Although it has been a cornerstone of neurosurgical patient management since the 1960s, there are questions yet to be definitively answered, such as *what is a normal ICP value?*, *can we rely on the numbers we measure at the patient's bedside even though they could be affected by artefacts that might corrupt the ICP signal?*, or *can we characterize the state of the brain pressure-volume relationships based solely on the ICP as a number?* For most intents and purposes the ICP is treated as a value that should remain within certain boundary values. These boundaries are difficult to establish, as there exist ethical concerns in the ICP monitoring of healthy volunteers given the invasive nature of the procedure. Also, they depend on factors like age or body posture, which hinders the definition of universal normal values [11].

This is the simplest way of looking at ICP—as just a number that should remain within certain bounded values. Going beyond that, it is interesting to look at the pressure wave

patterns of the ICP signal as macro-patterns lasting seconds to minutes. Lundberg initially described different macro-patterns in the ICP and categorised them as A-, B-, and C-waves [2]. Telemetric ICP monitoring has allowed us to evaluate the patient's ICP during various activities, either in-hospital or in the home setting, where ICP variations are less accentuated than the classical macro-patterns described by Lundberg. The issue is that these Lundberg's macro-patterns no longer adequately address the waveforms encountered in the clinical practice today. This gives rise to an additional question: *could we identify new macro-patterns in the ICP signal that change in appearance and distribution for the different neurological disorders?*

Automatic algorithms applied to ICP signals can help to answer these questions. Besides being able to provide fast and objective identification of classical macro-patterns in ICP, they also have the potential to reveal signal patterns not easily visible to the human eye, enabling a better characterization of the ICP signal under investigation. This information could later be used to modify and optimize patients' treatment.

The area of research addressed in this thesis focuses on the motivation and algorithm development for the extraction of macro-patterns from the ICP signal for their future use to give insight into the brain function. It has to be acknowledged that many other research groups do work on investigating brain homeostasis with other approaches, including beat-to-beat waveform analysis [12–14], secondary variables [11, 15], and other non-invasive modalities.

1.2 Problem Statement

Macro-patterns lasting seconds to minutes different from the classical ICP waves described by Lundberg in the 60s are encountered in the clinical setting today. Current methods for their identification rely on subjective and time-consuming visual and manual analysis of the ICP signal. Validated automated methods offer the potential advantage of minimal expert intervention and reduction in analysis time. In addition, they permit subsequent access to more advanced analysis techniques in centers without ICP specialists.

As more non-classical ICP patterns have been seen in clinical practice, it might be a promising approach to develop an automated and standard method for the recognition of macro-patterns.

1.3 Thesis Research Questions and Objectives

Based on the motivation and problem and the problem statement aforementioned, together with my consideration of the available literature, we defined the main research question of this dissertation as follows:

> Research Question: ***Is it possible to develop an automated method for the characterization of ICP signals using signal processing and machine learning tools?***

Emerging from this question and to ensure that it is correctly answered, I have formulated the following research sub-questions, with corresponding investigations reported in five papers:

> Research Question 1 (RQ1): ***Can a better understanding of the physiological origin of ICP waves help to define their physical characteristics to ease their identification?*** What initially led us to revisit this question was the lack of agreement with the morphological characteristics, clinical significance, and origin of macro-patterns presented in Paper I [P.I]. The fact that some

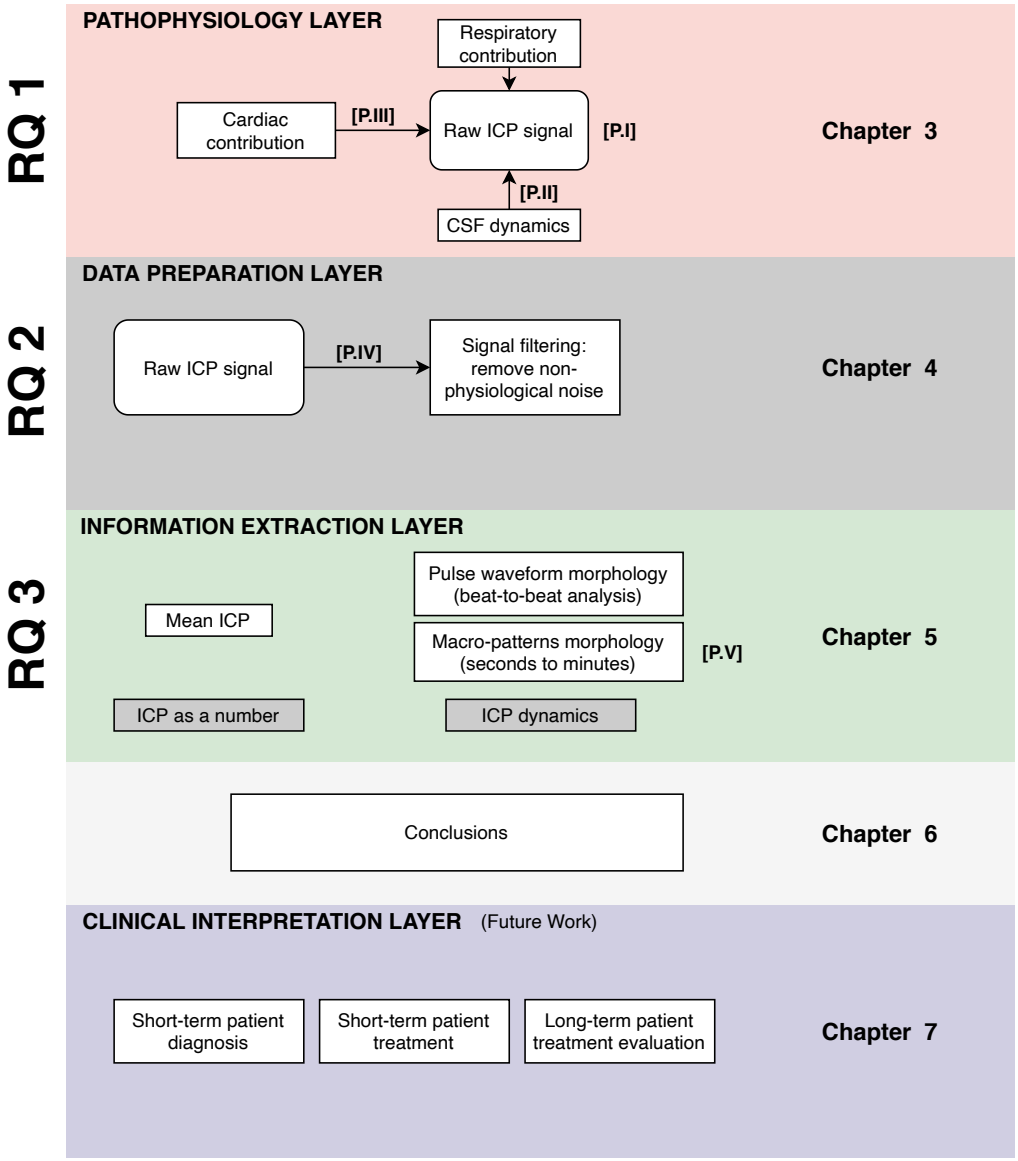

Figure 1.1: An overview of the thesis. The color-coded blocks outline the thesis in its respective chapters with corresponding papers annotated in squared brackets.

of these macro-patterns were present in near-to-normal subjects instead of being a marker of a pathological disorder sparked our curiosity and was the reason for Paper II [P.II]. And finally, we designed Paper III [P.III] with other measured physiological signals besides ICP with the hope of elucidating the source of these macro-patterns.

Research Question 2 (RQ2): ***Is it possible to provide guidelines/workflow for investigating data quality in the ICP data as a pre-processing step before data analysis?*** On the technical side, we saw ICP recordings contaminated by artefacts, so we suspected that some ICP values were flawed and did not represent pathological ICP changes. To better identify these artefacts and mitigate them to reduce their influence on future analysis steps, we wrote Paper IV [P.IV].

Research Question 3 (RQ3): ***Can a new automated method, based on machine learning techniques, be used to identify macro-patterns in ICP signals?*** In Paper V [P.V], we developed the building blocks for an automated method that could identify macro-patterns and characterize ICP signals in neurological patients.

The answers to these questions can serve as the foundation for future research focused on the analysis of ICP dynamics and will potentially shift ICP interpretation from time-consuming manual interpretation to more automated tools. We will thus be leaving the "one size-fits-all" approach behind and start to lean towards a more individualized patient treatment and management.

1.4 Scientific Contributions in Thesis

Figure 1.1 gives an insight of the PhD workflow. Relevant scientific publications which are included as part of this thesis are linked to their corresponding steps in the diagram. These main publications will be summarized in this section. The following chapters will give a short overview of these papers, with additional details added if considered significant for work evaluation.

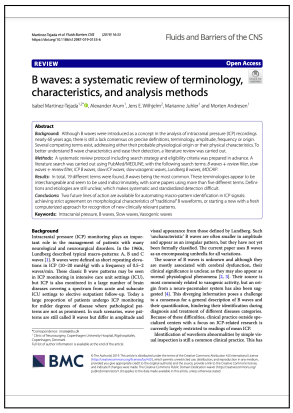
Fluids and Barriers of the CNS

REVIEW Open Access

B waves: a systematic review of terminology, characteristics, and analysis methods

Paper I [P.I]
B-waves: a systematic review of terminology, characteristics, and analysis methods. In: *Fluids and Barriers of the CNS*, 2019

We carried out a literature review on B-waves. The paper contributed to the presentation of the lack of definition and etiologies of these macro-patterns.

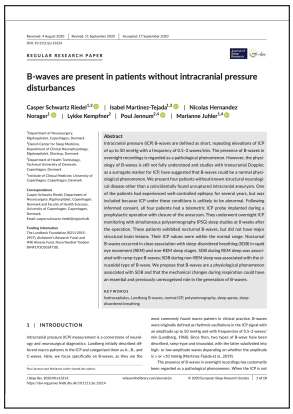
REGULAR RESEARCH PAPER

B-waves are present in patients without intracranial pressure disturbances

Paper II [P.II]
B-waves are present in patients without intracranial pressure disturbances. In: *Journal of Sleep Research*, 2021

We ran ICP B-wave identification and polysomnography analysis in four patients without known structural neurological disease. The main outcome of this study was the identification of mechanical changes during respiration as a potential source of the generation of B-waves, and the presence of these waves as part of a physiological phenomenon in healthy subjects.

Causal relationship between slow waves of arterial, intracranial pressures and blood velocity in brain

Paper III [P.III]
Causal relationship between slow waves of arterial, intracranial pressures and blood velocity in brain. *Submitted*, 2021

We studied the potential role of the arterial blood pressure and flow velocity as a source of ICP. The main outcome was the detection of a causal influence of slow waves of flow velocity on slow waves of ICP.

Empirical Mode Decomposition-Based Method for Artefact Removal in Raw Intracranial Pressure Signals

Paper IV [P.IV]
Empirical Mode Decomposition-Based Method for Artefact Removal in Raw Intracranial Pressure Signals. In: *Intracranial Pressure and Neuromonitoring XVII. Acta Neurochirurgica Supplement, vol 131*, 2021

We developed a method based on modified empirical mode decomposition for automatic spike removal in raw ICP signals. The main contribution of this work came from the application of this method to remove non-physiological artefacts from the ICP signal previous to any further data analysis.

k-Shape clustering for extracting macro-patterns in intracranial pressure signals

Paper V [P.V]
k-Shape clustering for extracting macro-patterns in intracranial pressure signals. *Submitted*, 2021

The paper on k-shape clustering explained the methodology developed for the identification of macro-patterns in the ICP signal. This research sheds the starting point for future automated characterization of ICP signals.

1.5 Thesis Overview

This dissertation carries on with clinical background information on CSF dynamics and ICP monitoring techniques and interpretation in Chapter 2. The latter covers a summary of the state-of-the-art ICP analysis approaches. The next three chapters follow the workflow presented in Figure 1.1. Chapter 3 covers the interplay of ICP with other physiological signals from a technical perspective. Chapter 4 explains the different artifacts encountered in the ICP signal and methods to handle them. Chapter 5 presents the methodology that can be used as a foundation for future ICP characterization. These three chapters all include a research background, a list of objectives and corresponding dissertation papers, and end with a few conclusive remarks. Next, Chapter 6 concludes the thesis by summing up the main work. Finally, Chapter 7 outlines future steps for the automatic identification of macro-patterns in the ICP signal.

CHAPTER 2 Clinical and Technical Background

Physiological phenomena are complex processes that involve the interplay of many inputs and outputs that stimulate, control and lead to actions [16]. These physiological phenomena manifest themselves as signals. Diseases can alter the normal performance of the physiological phenomena and cause pathological processes instead. A good understanding of the system of interest, in our case the intracranial cavity, allows us to observe the signals and assess the performance of the system. The more we understand the system, the better decisions we can take in future technical analysis.

2.1 The ICP signal

2.1.1 CSF dynamics

ICP arises from the partial pressure contributions of the brain, blood, and cerebrospinal fluid inside the skull. The brain accounts for approximately 85% of this volume, the CSF for 10% and the cerebral blood volume for around 5% [17]. The pressure-volume relationship between ICP and the volume of these components is explained by the Monro-Kellie doctrine (see Figure 2.1), which is of paramount importance regarding the understanding of CSF dynamics. Mathematically, the Monro-Kellie doctrine can be described with the expression below:

$$V_{blood} + V_{csf} + V_{brain} = constant \tag{2.1}$$

It states that because the cranial compartment is inelastic and cannot be compressed, the volume inside the cranium must be fixed in order for the pressure inside to be constant [18–20]. Under normal conditions, an increase in volume in any of the cranial constituents must be compensated by a decrease in volume of the other two. A consequence of this is that the introduction of a new intracranial volume due to space-occupying lesions (ie. mass) or a transient increase of arterial cerebral blood volume must be buffered by a decrease of either blood volume or CSF, with the later being the principal buffer.

Although the volume of venous blood is small in the total cerebral blood volume (CBV), it can be promptly changed and thus, ICP changes are rapidly compensated. Compensation from the CSF occurs slowly by extrusion of intracranial CSF into the spinal canal [21]. When the buffer capacity of these two components exhausts, further volume changes can no longer be accommodated, causing the ICP to rapidly rise in a non-linear manner.

2.1.2 ICP waveforms

ICP waveforms have the potential of giving an insight of the intracranial compliance. In the recorded ICP, the dynamic changes consist of three components: (1) pulse waveform, (2) respiratory waveform, and (3) slow waveforms. All three overlap in the time domain but can be separated in the frequency domain via spectral analysis, as observed in Figure 2.2. They each oscillate at different frequencies: pulse waveforms at 40–160 cycles/min, respiratory waveforms at 8–20 cycles/min and slow waves at less than 8 cycles/min [22].

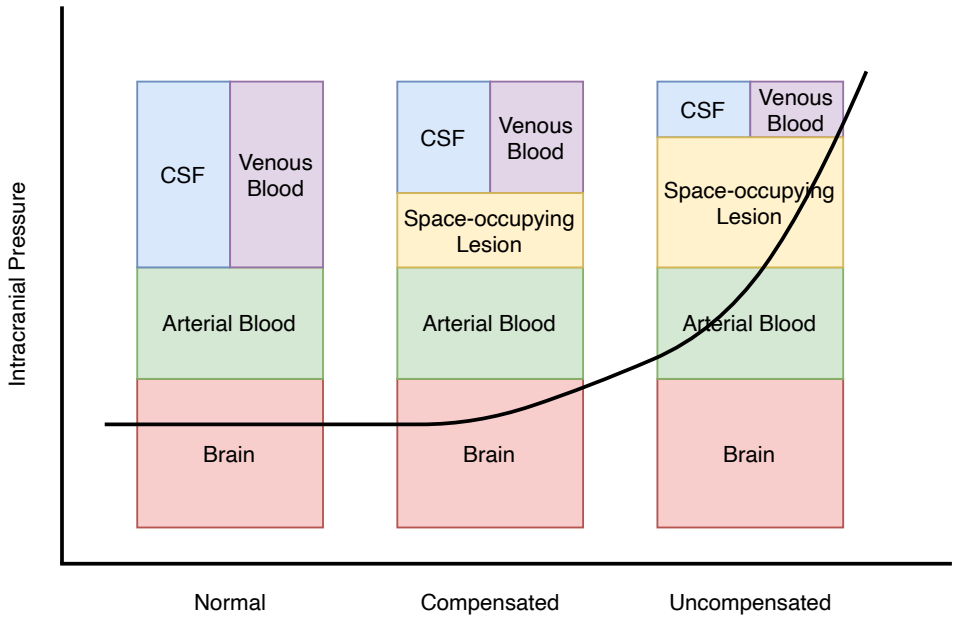

Figure 2.1: The Monro-Kellie doctrine. An increase in volume of cranial constituents must be compensated by a decrease in volume of another. We can see that as the pathology volume becomes larger, the system decompensates and ICP elevates significantly.

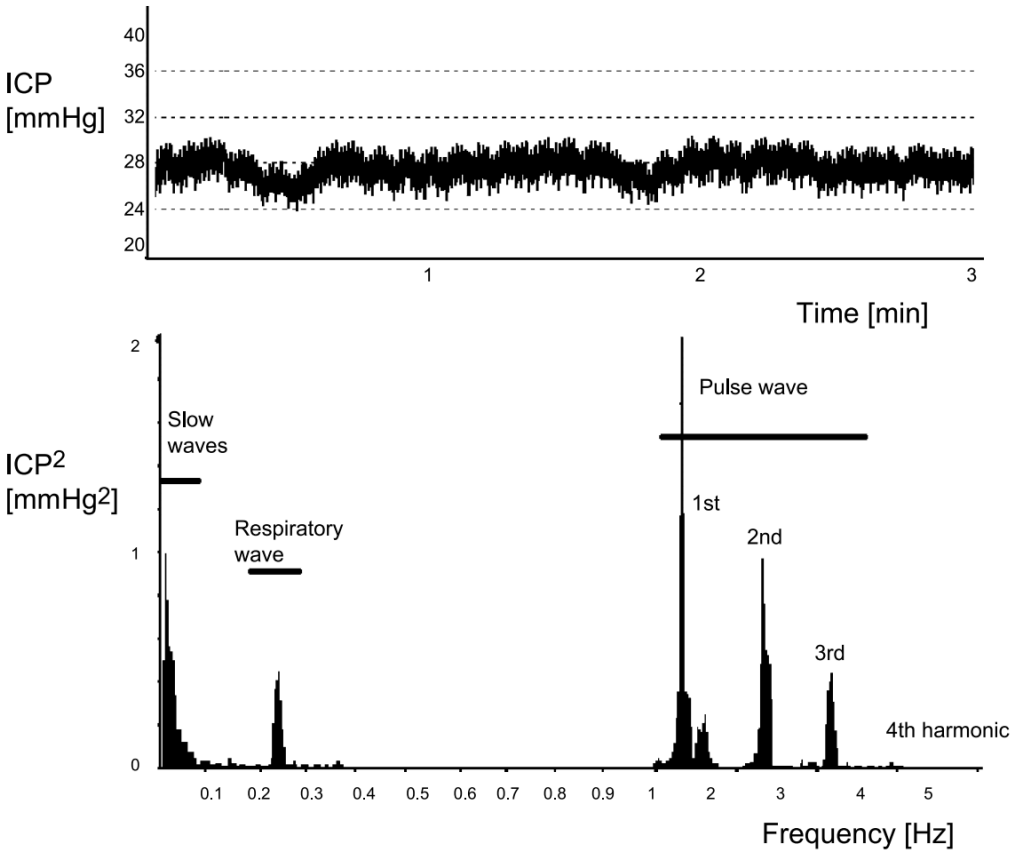

Figure 2.2: Spectrum of ICP signals [23].

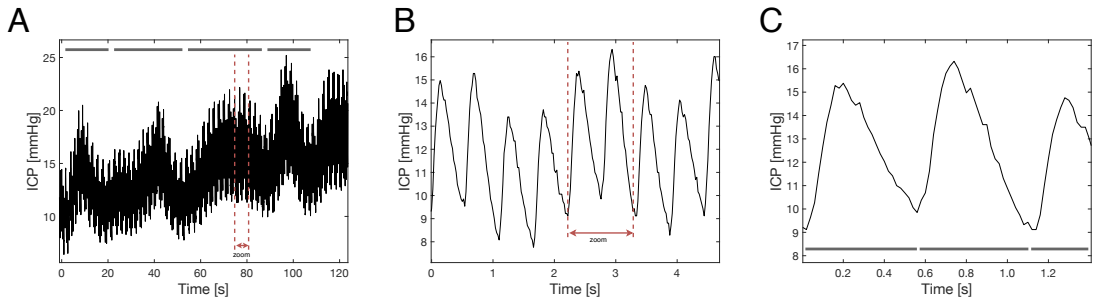

Figure 2.3: ICP waveforms. (A) ICP slow waves, (B) Multiple ICP pulse waveforms, (C) zoomed image of two pulse waveforms to better identify subpeaks P_1, P_2 and P_3.

The latter were classified in the 1960s by Lundberg as A-, B- and C-waves (see Figure 2.4).

Lundberg established that visual interpretation of rhythmic variations, the so-called macropatterns, in the ICP signal combined with related clinical symptoms provided additional value more than just a number [2]. He presented:

- A-waves: ICP increases of 50-100 mmHg for 5 to 20 minutes that appear irregularly. The magnitude of these increases is correlated with the severity of the symptoms. They are believed to reflect reduced cerebral compliance, and thus, dysfunction in the autoregulation of the ICP.
- B-waves: rhythmic oscillations at a frequency of 0.5-2 cycles/minute and a maximum amplitude of 50 mmHg. Their clinical value is still unclear: they have been seen accompanying pathological states, but also as part of a physiological phenomenon present also in healthy subjects [24].
- C-waves: another form of rhythmic oscillations at a frequency of 4-8 cycles/minute and a maximum amplitude of 20 mmHg. They are thought to reflect normal physiological interactions between the cardiac and pulmonary cycles [25].

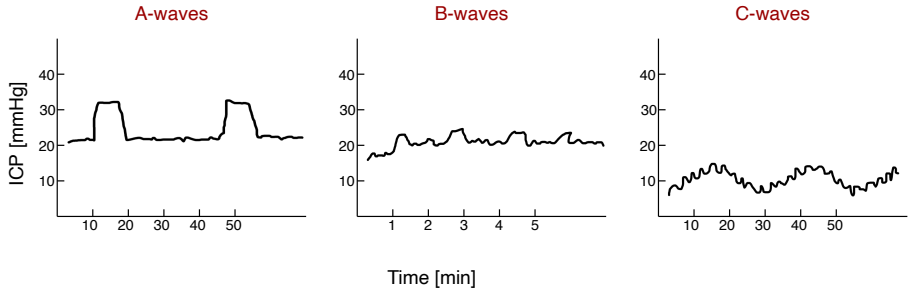

Figure 2.4: Lundberg waves. Lundberg A waves are plateau waves of ICP above 50 mmHg lasting 5-20 minutes. Lundberg B waves are rhythmic oscillations of frequency between 0.5 and 2 per minute, with amplitude lower than 50 mmHg and unclear clinical value. Lundberg C waves are also rhythmic oscillations of an amplitude lower than 20 mmHg and frequency of 4-8 per minute that appear as a normal physiological feature.

Looking now into a smaller time scale, the pulse ICP waveform also contains unique information about the intracranial compliance. It is comprised by three subpeaks (P_1, P_2 and P_3) associated to the arterial blood pressure (ABP). P_1 is the percussion wave simultaneous with the systolic peak in ABP pulse, P_2 is the tidal wave reflecting intracranial

compliance, and P_3 is the dicrotic wave that, when observed, it is synchronous with the venous blood outflow [26, 27]. In general, P_1 is dominant, so P_2 having larger magnitude than P_1 is an indicator for diminishing brain compliance [28].

2.1.3 Changes in ICP

ICP is measured in millimeters of mercury (mmHg) and is normally quoted to be 7-15 mmHg for a supine adult [29], 3-6 mmHg for children, and 1.5-6 mmHg for term infants [30, 31]. Studies reporting normal values are very limited due to ethical concerns given the invasive nature of ICP measurements in healthy subjects. Values are derived from patients with known derangements in ICP [2], or from lumbar CSF pressure [32, 33]. Considering the problems these authors face when defining what is a “normal” subject, Andresen et al. [34] presented a novel model of the normal ICP that excluded patients with any CSF disorders or deviations in ICP. This model showed lower normal ICP values than previously reported for all body postures. It was quoted as 0.5 mmHg (sd, 4.0 mmHg) for the supine position. Changing from supine position to upright led to a decrease of 4.2 mmHg in the normal value. This drop was even higher for those patients with neurosurgical diseases (ie. IIH, NPH), reaching negative values for both supine and vertical positions. From all these different values, we can infer that it is indeed a challenge to establish a “one size fits all” normal value for ICP, since it depends, among others, on several other variables: age, body posture, and clinical state.

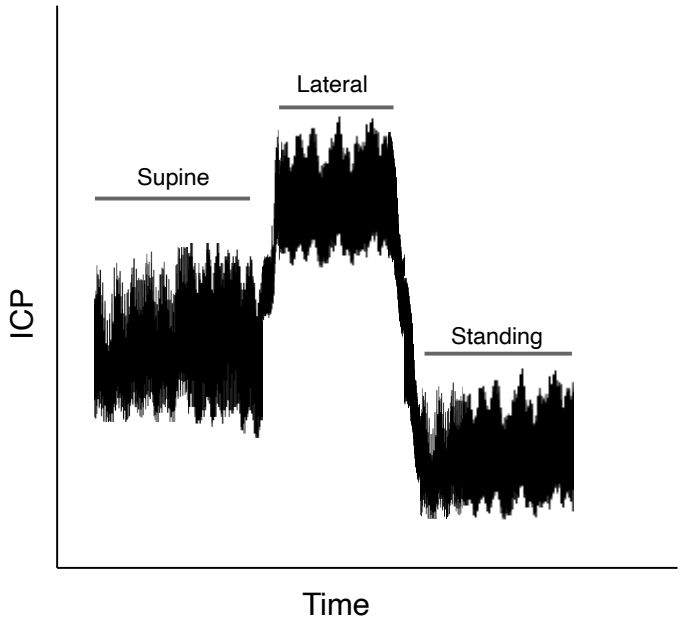

Figure 2.5: Presentation of ICP response to ICP postural changes. It is illustrated by a computer-generated example in which the patients move from supine→lateral→standing position.

Other physiological processes like coughing, sneezing, or talking also influence the ICP values [35]. Coughing is known to momentarily trigger a raise in ICP, as seen in Figure 2.6 [36].

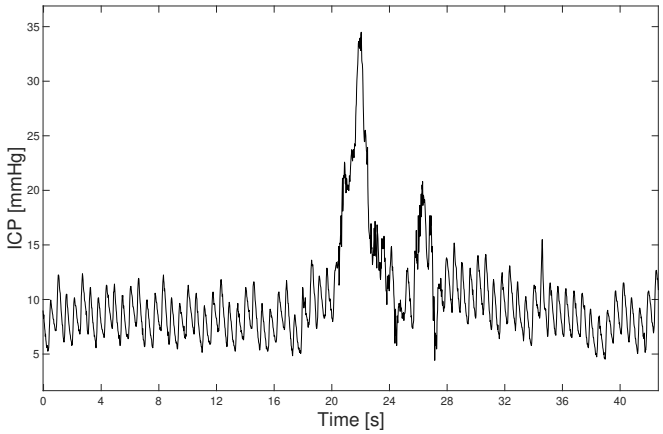

Figure 2.6: Effect of coughing on the ICP signal.

2.2 ICP Monitoring

2.2.1 Indications for ICP monitoring

Today, there are no worldwide guidelines and indications for ICP monitoring, and instead they vary notoriously between centers. However, there are some common monitoring approaches that most of the hospitals follow and that can be branched down into three groups: (1) critically ill patients in the neurointensive care unit suffering from TBI [37]. It is in this unit where ICP monitoring is considered a cornerstone modality [38, 39]. The Brain Trauma Foundation (BTF) has implemented some guidelines for the management and ICP monitoring indications in the case of severe TBI [40]. (2) Non-TBI patients in the intensive care that require ICP monitoring for surveillance, such as patients suffering from subarachnoid haemorrhage (SAH), spontaneous intracerebral haemorrhage, cerebral edema or central nervous system (CNS) infections [41–43]; and (3) patients outside the intensive care with CSF disturbances, including hydrocephalus or idiopathic intracranial hypertension, among others [44–46]. The last group plays an important role in the motivation of this thesis, since how ICP waveforms change in appearance in these categories has not been sufficiently described.

In particular, hydrocephalus occurs when the production and absorption of CSF is unbalanced. Hydrocephalus in both infants and adults causes irreversible damage to the brain, and is a condition without a permanent cure. It requires life-long follow-up and repeated surgeries to fix or replace implanted shunt systems that allow for redirection of cerebrospinal fluid away from the brain [47]. IIH presents elevated pressure inside the skull, due to an increase in volume in one of the three intracerebral components [48]. Monitoring of this disorder is useful both as a diagnostic test and to monitor response to treatment.

2.2.2 Techniques of ICP monitoring

There is a plethora of invasive and non-invasive ICP monitoring devices, which have evolved substantially since first introduced by Lundberg way back in 1960. Lundberg's work on the measurement of ventricular fluid pressure (VFP) for an extended period was the foundation for the use of ICP monitoring as part of the clinical routine [2]. Since then, there has been a multitude of ICP monitoring methods, each with benefits and limitations that have led to the formulation of minimum standards for ICP monitoring by the American National Standards Institute (ANSI)/Association for the Advancement of Medical Instrumentation (AAMI) [49]:

1. Device measured pressure range should lie between 0 and 100 mmHg.
2. Accuracy between 0-20 mmHg should be ±2 mmHg.
3. Between 20-100 mmHg, the error should not exceed 10%.

Many still consider ICP measurements using fluid-filled catheter transducer systems via ventricular catheters as the gold standard. This technique, also referred to as extra-ventricular drain (EVD) technique, consists of an intraventricular drain connected to an external pressure transducer [50]. Such a system offers the advantage of re-calibration to ensure the removal of potential drifts. Besides ICP monitoring, it also has the possibility of facilitating CSF drainage for ICP management [35]. We should stress that there are complications related to ventricular ICP measurement. Among others, mechanical occlusion of the catheter can corrupt the signal, and the risks of infection and haemorrhage only increase with prolonged monitoring duration [51, 52].

The use of this technology is a cornerstone in the neurointensive care unit (NICU) for the management of TBI [53]. In some centers, measurement of ICP is also used for the diagnosis and treatment of patients with CSF disturbances outside the confines of the intensive care. Therefore, ICP monitoring moves beyond being an in-hospital routine that uses cable-based sensors and requires that the patient remains in the bed, to mobile monitoring with the patient being able to move around outside of the confines of the hospital over an extended period of time. Telemetric ICP monitoring can thus be seen as an alternative to traditional cable-fixed ICP sensors. The telemetric probe is implanted below the scalp on the cranial bone and the catheter extends 2 cm into the brain parenchyma, where it records the ICP. To obtain the ICP signal from the sensor, an antenna reader is placed over the probe in the site of implantation [54].

Other ICP monitoring techniques in the present time are based on microtransducer technology. The small pressure transducer can be inserted in CSF filled cavities including subdural, epidural, intraparenchymal, or intraventricular placements, being the parenchyma the most common monitoring location. They are able to shortcut risks of complications and haemorrhage thanks to the absence of fluid-filled coupled systems. But they share a common drawback, re-calibration is not possible after insertion, which can cause imprecise ICP values [41].

2.3 ICP Interpretation

While ICP—in a clinical setting—may often be interpreted purely as a number that needs to stay within a certain range for the brain to function properly, the ICP signal in fact represents a tremendously rich and complex time series with wave patterns that go far beyond this previous limited understanding [55]. ICP as a number is reported as a simple average of the ICP over a short time of time.

Past and present analysis of ICP has also investigated the ICP waveform itself, either in a beat-to-beat basis or over a longer duration lasting from seconds to minutes. Looking at macro-patterns is a markedly different strategy compared to the prevalent ICP morphology analysis approaches that primarily focus on information derived from single beat-to-beat pulse waves lasting less than a second [13, 56, 57], with efforts to see how these subcomponents vary when brain compliance has been compromised [58, 59].

Traditionally, ICP signals are inspected visually for macro-pattern identification [60]. This current gold-standard technique is not only time consuming, but it is also subject to investigator bias do to interpretation subjectivity and clinical experience dependence. With evolving machine learning and mathematical modeling techniques, more emphasis has

been placed on automatizing the study of the presence of repeatable patterns in the ICP signal. Some have attempted to semi-automate the identification of these longer duration waveforms based on temporal and frequency domain analysis [61–63], with most attention placed on the identification of B-waves [64–66]. Others have tried to detect macro-patterns based on morphological changes of ICP pulse waveforms [66], using Morphological Clustering and Analysis of Intracranial Pressure (MOCAIP) for morphological features extraction [13]. However, these techniques have had mainly a research purpose and have not been translated into clinical practice to guide treatment and better predict outcome.

2.4 Thesis Motivation

This chapter has featured the use of ICP monitoring for a variety of neurological and neurosurgical disorders in a broader clinical setting including telemetric monitoring during full mobilization and at home. However, current methods for identification of waveforms in these recordings are based on visual and manual inspection (Section 2.3). As the classical waveforms descriptions no longer resemble what is encountered in the clinical practice, diagnosis and recognition of waveforms is not only time-consuming, but also subject to investigator bias. It is of clear importance to objectively define these new macro-patterns. In this context, the introduction of automatic algorithms to characterize ICP signals has obvious significance, since ICP analysis will become faster and more standardized. This field still remains unexplored and in summary, we can draw the following conclusions on the related gaps:

- There is a poor agreement on the characteristic appearance and origin of macro-patterns to be used for their identification. Of the few that exist, they are all defined on patients with a very severe degree of disease and no longer match the variety seen in clinical practice today.
- ICP signals are likely to be contaminated by artefacts, which may significantly reduce the clinical information that can be obtained from the signals and also hinder the identification of macro-patterns. There is a sparse selection of studies addressing the cleaning of ICP signals. Unfortunately, these methods are tested on specific disease categories. No study has made an automated method and applied it to different disease categories, to understand if there is an optimal method for artefact removal in ICP signals.
- The current method for the identification of macro-patterns is based on visual inspection of the long ICP recordings. Machine learning's underlying mathematical methods are able to extract meaningful information from the data that could otherwise not be visible to the human eye [67]. Published reports on computerized methods to identify macro-patterns have focused only on B-waves [64–66, 68], thus there might be additional patterns with clinical value that are being ignored. There is a current lack of an automatic and standard technique for identification of macro-patterns in ICP signals.

To address these unmet needs, the goal of the thesis was to design and evaluate an automated and standard algorithm that could be used as the foundation for cleaning [P.IV] and analyzing ICP signals, to fill the gaps within data preparation and macro-pattern identification. In this stage, we included clustering to try to identify hidden patterns in the ICP data [P.V]. We also analyzed the interplay of the data with other physiological signals [P.I, P.II and P.III] to better understand the pathophysiology of the patterns, which origin is yet to be elucidated.

CHAPTER 3 Macro-patterns in ICP Signals

In 1849, French physiologist Claude Bernard first postulated the idea of the regulation of the human internal environment [69], but it was not until 1926 that Walter Bradford Cannon named this concept as *homeostasis* [70, 71]. Homeostasis is thus responsible for the stability of natural and artificial systems. Maintaining homeostasis in a complex system requires the interaction of several components with each other.

> *"A complex system is defined as one that is composed of many parts that interact in a non-linear fashion and give rise to emergent behaviour that cannot be understood through the analysis of its constituents." [72]*

In the field of neurosurgery, we can define the intracranial enclosure as a complex system. The intracranial pressure in this system arises from the interaction of three parts: cerebral blood dynamics, cerebrospinal fluid dynamics, and any disease in the central nervous system [11]. If the equilibrium that guarantees homeostasis in these contributions is broken as a result of one of the components failure to harbour an increase in one of the other components, clinical pressure symptoms start to manifest. Clinical pressure symptoms are usually combined with rhythmic variations in ICP, the so-called macro-patterns. B-waves feature the most frequently encountered macro-pattern in the clinical setting.

In the following chapter, we present our research contributions within the origin and characteristics of B-waves to support the difficulties in defining and quantifying macro-patterns. The research work was either drawn from the literature or from studies that we carried out ourselves. This chapter is based upon Papers I, II, and III and addresses our Research Question 1.

3.1 Research Background

Despite the fact that a lot of attention and research has been given to B-waves for diagnosis and treatment of neurosurgical disorders, their automatic detection and quantification is still a challenge because of the difficulties in describing them. The core part of the challenge here may be that the existing terminology used to assess B-waves vary to a tremendous degree, and that it may simply be impossible to expect a computer to identify repeated patterns if humans cannot even agree on how to define these patterns.

Other research groups have previously done comparative analysis of sources of B-waves [60, 73, 74], as well as comparative analysis on their characteristics [60, 75]. However, there are no systematic comparisons of the terminology and descriptions of them. In addition, the clinical implications of the frequency and magnitude values of B-waves remains unclear, with no studies quantifying them in patients without any CSF disturbances and very few looking at their interaction with the vascular system.

3.2 Research Questions and Objectives of this Chapter

Based on the consideration of this background overview, the following sub-questions were formulated:

- Chapter 3 Research Question 1: Regarding classical Lundberg waves, are their terminology and morphological characteristics sufficient to describe the variations seen in daily practice?
- Chapter 3 Research Question 2: To which extent do ICP macro-patterns relate to respiratory disturbances?
- Chapter 3 Research Question 3: To which extent do ICP macro-patterns relate to vascular disturbances?

These research sub-questions led to the formulation of the following objectives:

- Chapter 3 Research Objective 1: To compare systematically the terminology, morphological characteristics, and available automated methods for B-waves identification.
- Chapter 3 Research Objective 2: Multimodal monitoring followed by signal analysis can provide information on the source of the investigated waveforms.
- Chapter 3 Research Objective 3: Causal analysis between the waveforms in the ICP signal and vascular physiological signals can give an insight of the extent of the contribution of the latter to the ICP.

3.3 Paper I: B-waves: a systematic review of terminology, characteristics, and analysis methods

The primary aim of this systematic review was to show the lack of agreement in the terminology and morphological characteristics of the classical B-waves. The different terms, and definitions to describe them, were investigated via a concise literature review. The controversy in the analysis tools applicable to them was also examined as part of the review. The papers included were all specifically mentioning B-waves or related terms as a central or peripheral subject.

By examining these papers, it was possible to certify that there is an unmet need for a clinically acceptable description of B-waves and until this issue is resolved, automated methods for their identification are far from feasible. The simplified overview of the methodology followed in the review is showcased in Figure 3.1.

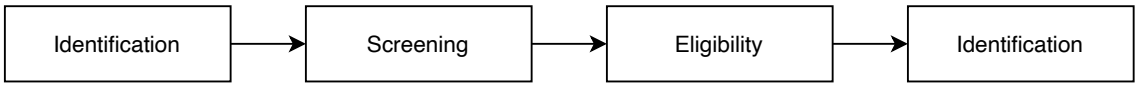

Figure 3.1: PRISMA simplified flow diagram [76] of literature review process for Paper I .

3.3.1 Methods: Systematic review

The PRISMA systematic review provides a reproducible framework to select and evaluate relevant research to help answer a clearly and focused formulated question, while minimizing bias in the results [76]. Our main two questions were:

1. What terminologies are used to describe the concept B-waves, and how are these defined based on frequency, amplitude and possibly other parameters?
2. Which analysis methods have been used in the research to identify B-waves?

Studies were identified in PubMed—by an independent researcher—with the terms “slow vasogenic waves”, “Lundberg B waves”, “slow ICP waves”, “ICP B waves”, “MOCAIP”, “B waves”, and “slow waves”. Articles including the last two terms were also filtered by type to only include reviews to increase the precision of search. Search terms were selected to represent all the variations in B-waves terminology that might be used to describe the concept of B-waves by different research groups. For the sake of dissemination, we will use the term B-waves to designate all variations in terminology. A total of 124 papers from the total of 881 papers searched were considered eligible for review.

3.3.2 Data classification

The extracted terms used to refer to B-waves were categorised based on their terminology, frequency range, and analysis method used for their identification. Table 3.1 shows the different options devised by the researchers for each category.

	Classification
Terminology	(ICP) slow waves ICP waves (ICP) B waves Lundberg B waves B slow waves Vasogenic waves Slow vasogenic (ICP) waves Other
Frequency	Number of waves/min Not applicable
Analysis tool	Visual inspection Spectral analysis Spectral analysis + amplitude Cross-correlation Multiscale entropy Wavelet analysis MOCAIP Not applicable

Table 3.1: Table summarizing the main terms, frequency, and analysis tools used to classify the extracted B-waves information.

3.3.3 Results

The occurrence of terms and frequency range of B-waves was calculated after reviewing all articles and the next subsections will show their distributions.

Terminology

By analyzing the occurrence of the terminology, it was noticed that a total of 19 different terminologies were used in the articles to refer to the concept of B-waves, with the terms “B waves”, “slow waves”, and “ICP slow waves” being the three most used.

It was often that the term “B waves” was used in the introduction, where it is described as a phenomenon originally defined by Lundberg, but a different terminology and frequency range were used in the remaining of the paper. In fact, we found that several papers used more than five different terminologies for this same phenomenon. Part of this terminology divergence arises from the attempt of assigning an etiology to the waves: 22 articles include the word *vasogenic* thereby assuming vasogenic activity of cerebral autoregulation as the origin of the waves. The origin of these waves remains unknown, and authors like Raftopoulos [77], Santamarta [78], Yokota [79], and Kasprowicz [58], have presented further subgroups in an intend to better understand it.

Frequency range
Lundberg described a frequency of 0.5-2 waves/min for B-waves. 27% of the papers defined this frequency range. Recently, some authors have extended this frequency range to encompass a larger variety of B-waves. The frequency range was then redefined to 0.33 to 3 waves/min [11]. Together with this frequency change, the term “slow” was introduced as part of the terminology of the B-waves [73]. We also found that two other papers broadened the frequency upper limit to 4 waves/min [80, 81].

Morphological characteristics
B-waves can also be characterized in terms of their amplitude, with a maximum amplitude of 50 mmHg defined by Lundberg back in the 1960s. This amplification under pathological conditions is no longer seen to such an extent and the upper amplitude limit value is lowered to approximately 35 mmHg [77, 78]. 9% of the articles reviewed specify lower or upper amplitude values, where the lower limit corresponds to the wave trough and the upper limit to the peak.

Besides frequency and amplitude, two additional parameters are also found to be used for describing B-waves: shape and presence or not of plateau. The different combinations of these parameters generate subclasses within B-waves, differing mainly in their morphological characteristics, as seen in Figure 3.2. These sub-classification attempts show that the classical Lundberg waves do not adequately described the waveforms encountered in clinical practice today.

Analysis tools
With the surge of machine learning techniques and their usability for automatically detecting hidden signal patterns, an increasing tendency to apply them to detect B-waves has been observed in more recently published papers [58, 82, 83]. These algorithms use the MOCAIP algorithm to extract morphological information that can then be used to identify B-waves.

These methods have all evolved from the traditional visual inspection of the ICP signal for B wave identification, which was subject to investigator bias due to interpretation subjectivity and clinical experience dependence.

3.3.4 Discussion
This study presents the diversity of terminology and characteristics used to describe B-waves. This diversity highlights the central challenge in studying classical waves in the ICP signal: there is a lack of agreement on their morphological characteristics and the etiology behind their occurrence, and this might serve as supplementary evidence that the classical Lundberg waves no longer fully correspond to the waveforms seen in current clinical practice. In the 1960s, when B-waves where originally identified and defined, patients were admitted with a markedly worse clinical state than what is seen today, mainly due to the lack of therapeutic options. With the introduction of telemetric monitoring devices in the last years, ICP monitoring has become feasible in a broader clinical setting, including monitoring during full mobilization and at home, where a greater diversity of ICP waveforms are present.

The physiological or pathophysiological mechanism underlying the occurrence of B-waves is a research question that remains to be answered, and that will also be addressed in Papers II and III. As B-wave origin remains unknown, sub-classification of B-waves into further subgroups seems to be important for the identification of the mechanisms behind the origin of the waves, which is necessary for the use of B-waves for the diagnosis and treatment of patients. However, attempts in sub-classifying B-waves may also imply that the B-wave category is too broad and thus, not able to address the clinical situations that we see today.

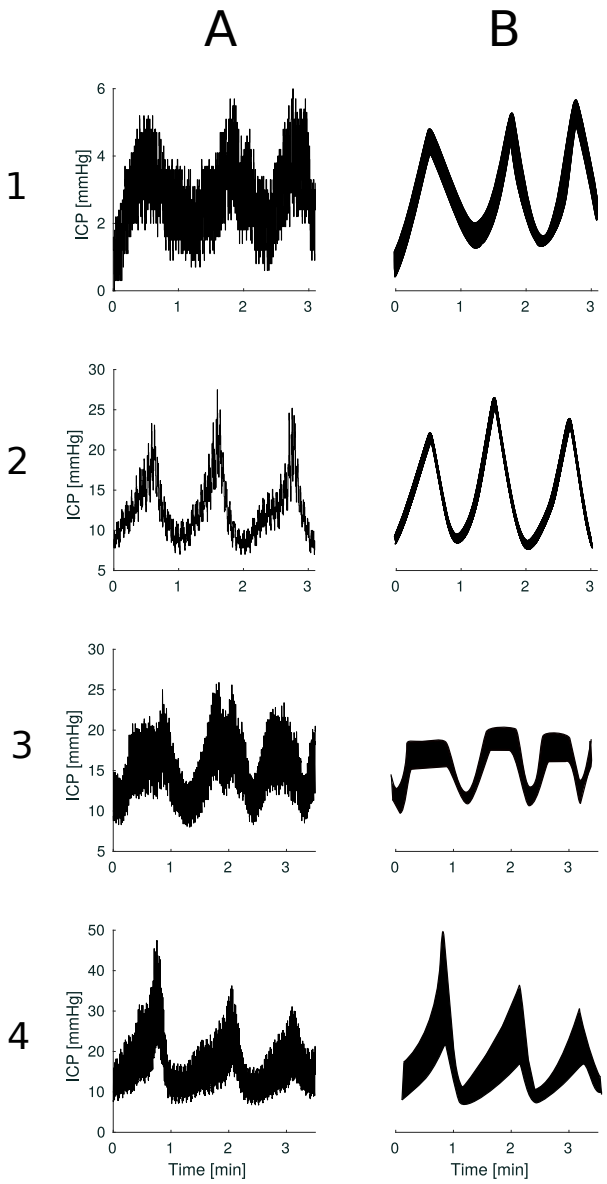

Figure 3.2: B-waves sub-classification patterns illustrated by two computer-generated examples: column A simulating ICP recordings and column B showing an artistic rendering of the ICP. Examples on rows 1 and 2 exhibit B-waves with symmetrical shape and amplitude lower and higher than 10 mmHg, respectively. Examples of row 3 correspond to symmetrical B-waves with plateau. The last row shows examples for asymmetrical B-waves. The time-scale used in all examples is minutes.

Comparison of analysis tools

In terms of appearance, the B-wave is remarkably diverse. Lundberg analyzed and described them visually and this technique has served as the gold standard for B-wave inspection since then. Reliability, however, is very dependent on both subjectivity and clinical experience of the investigator. Many semi-automated analysis techniques have been introduced to identify and quantify B-waves mathematically in a more objective and robust approach, delivering high accuracy at the lowest possible computational cost. Wavelet analysis is another approach to decompose the ICP signal into its spectral components. With the increasing quality of measurements, it has been possible to monitor ICP

at higher sampling frequencies ($\sim$100Hz). Higher sampling frequency means that more time details in the ICP data can be recorded. MOCAIP is a method to extract the features from the pulse waves, which can then be used to recognize B-waves [66]. However, as with spectral and wavelet analysis, this approach works on the assumption that B-waves occupy the classical frequency range introduced by Lundberg.

Automating macro-pattern identification requires either agreement on morphological characteristics of classical waves, or recognition of new clinically relevant patterns. But with current analysis tools limited to identifying classical waves, we are ignoring other patterns that could be related to other potentially relevant waveform deviations. As ICP interpretation is in fundamental transition towards automating ICP analysis to advance diagnostics, management, and treatment, we believe that focus should be placed on the identification of new macro-patterns using automated methods.

3.4 Paper II: B-waves are present in patients without intracranial pressure disturbances

As seen in Paper I, subgroups have been created to clarify the sources underlying the presence of B-waves. Elucidating their source could significantly help in their detection. To better understand whether B-waves occur as a pathological or normal physiological phenomena, if their corresponding ICP values are within the “normal” range and if they have a specific origin, we evaluated the association of B-waves with sleep stages and sleep-disordered breathing (SDB). This evaluation was done in a group of patients with an unruptured intracranial aneurysm. This disorder is not related to any type of CSF disturbances and therefore, these subjects can be classified as near-to-normal subjects.

The mentioned association was computed between B-waves, CO_2 levels, and respiration. In addition, by comparing the occurrence of B-waves in the different sleep stages, it was possible to identify the specific B-wave morphology characteristic of each sleep stage. For this, data processing was required for both sleep and ICP signals. The overview of the methodology is shown in Figure 3.3.

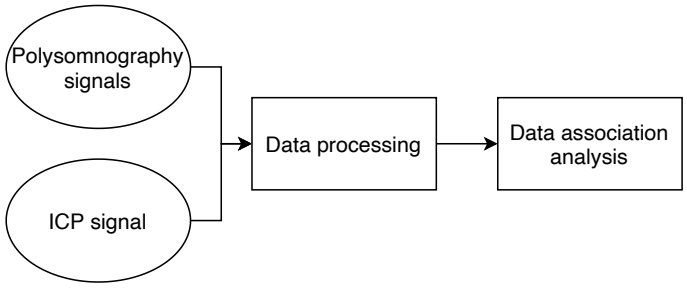

Figure 3.3: Overview of the methodology of Paper II.

3.4.1 Methods: B-wave quantification and association to other physiological signals

Participants and Recordings

A total of 4 participants (3 female, 1 male) were included in the study. Given the invasive nature of the ICP monitoring procedure, healthy subjects cannot be included in the study. Instead, we recruited subjects as near to normal as possible, that fulfilled two conditions: (1) scheduled for surgery for an unruptured aneurysm, and (2) no previous record of any brain disease. This implies that all magnetic resonance (MR) scans were cleaned besides the aneurysm.

Polysomnography (PSG) (SOMNOscreen™ plus, Somnomedics) and ICP (Neurovent-P-tel, recorded using Reader TDT readP, and stored on the Datalogger MPR1, Raumedic Ag), were recorded simultaneously. PSG is a comprehensive multi-parametric test used to study sleep. The PSG monitors many physiological signals, including brain activity (electroencephalogram, EEG), heart rhythm (electrocardiogram, ECG), eye movement (electrooculogram, EOG), oxygen level in the blood (oxyhaemoglobin saturation, SaO_2), airflow, muscle activity (electromyogram, EMG), body position, and breathing effort (respiratory inductance plethysmography, RIP; and end-tidal CO_2). During PSG recording, the ICP signal was transferred from the MPR1 Datalogger to the SOMNOscreener for the synchronous recording of the ICP data and the PSG data. After the test was completed, an experienced neurophysiology assistant analyzed and scored the data according to the American Academy of Sleep Medicine (AASM).

The scoring included the following items:

1. Sleep stage identification: a stage was assigned for each 30-second consecutive epoch, based on the EEG, EOG, and EMG. This assessment was visually represented in a hypnogram. Sleep is made up of cycles of rapid eye movement (REM) and non-rapid eye movement (NREM) stages.

2. Movement patterns: a major body movement was recognized when limb movement or muscle artifact contaminated the EEG for more than half of the 30s-epoch, making it impossible to determine the sleep stage [84].

3. Respiration patterns: annotates any breathing irregularities, focusing on apneas and hypopneas. An apnea is present when the airflow reduces more than 90% for longer than 10 seconds. An hypopnea is present when the reduction of airflow is 30% for at least 10 seconds, and it is accompanied by lowering in blood oxygen levels [85]. Both are utilized to calculate the Apnea-Hypopnea Index (AHI), calculated as $\text{AHI} = (\#\text{ apneas} - \#\text{ hypopneas})/\text{sleep hours}$. AHI was used to detect SDB: AHI <5 indicates no SDB, 5-14 indicates mild SDB, 15-29 is moderate SDB, and more than 30 implies severe SDB.

Data pre-processing
We were in a situation where we were collecting physiological signals from different sensors: the Datalogger MPR1 and the PSG. To further analyze the signals, it was important that they were aligned in time. The PSG ICP signal was used as the reference ICP channel to which the Raumedic ICP signal was aligned to. Our first task was to resample both signals to a common sampling rate. The Raumedic ICP signal, with sampling frequency equal to 100Hz, was upsampled to the sampling frequency of the PSG ICP signal, equal to 256Hz. Besides upsampling the Raumedic ICP signal, also the hypnogram was upsampled to 256Hz, since initially the hypnogram contains just one value per 30 seconds.

Once the ICP signals had common sampling rates, we time-aligned them. Given that both of them were correlated, we could find help in the synchronization by finding a common morphological feature shared by both signals. The problem could then be defined as finding the optimal feature in the signals to calculate the offset which best aligned them. The best time offset was computed as the absolute time difference between the pair of feature points, one from each of the signals. The morphological feature tends to capture a major event that can be seen in both signals, such as a high ICP value. For the remaining of this study, only the aligned Raumedic ICP signal will be used. Before any further ICP analysis, artefacts in the form of very high and rapid spikes were removed using the methodology described in details in the next chapter.

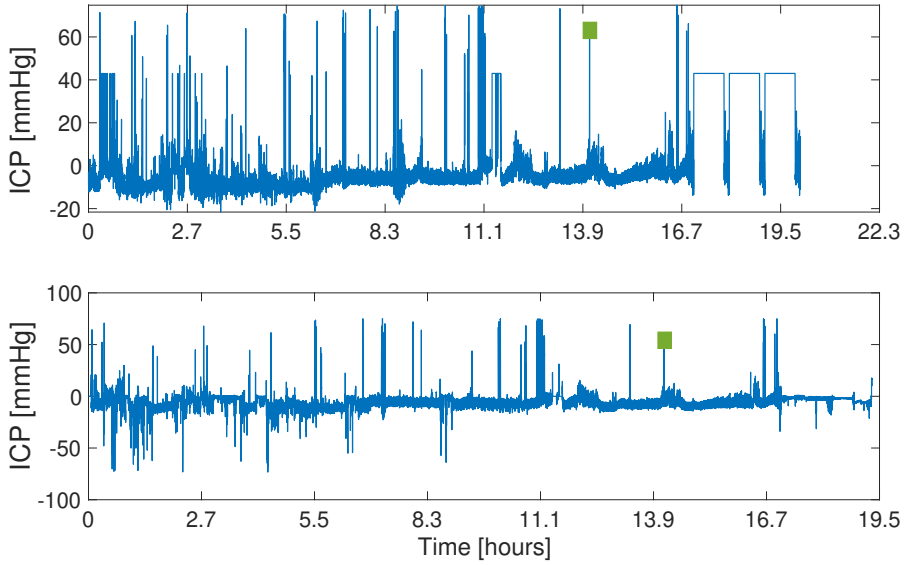

Figure 3.4: ICP signals to be aligned: Raumedic ICP signal (top) and PSG ICP signal (bottom). The time lag to align the two ICP signals was defined by finding the time difference between one correlated morphological feature found in both signals. In this case, we used a spike that was easy to identify in both signals (annotated with a green box). The issue with asynchronous sampling frequencies was handled prior to generating this figure.

Data analysis

The data was inspected visually to detect B-waves, annotate its morphology, and find any correlations between the various physiological signals. B-waves were detected based on Lundberg's criteria: frequency between 0-5-2 waves/min and amplitude of at least 10 mmHg. ICP was considered as elevated when above 10 mmHg.

3.4.2 Results

B-waves analysis

Visual assessment of the ICP signal suggested the presence of B-waves, under Lundberg's descriptive criteria, with varying morphology depending on the sleep stage. Ramp-type B-waves were associated with REM sleep, while sine-type B-waves were associated with NREM sleep (Table 3.2).

	Ramp-type B-waves high amplitude		Sinusoidal B-waves low amplitude		Sinusoidal B-waves high amplitude	
Patient	NREM	REM	NREM	REM	NREM	REM
1	÷	+++	+	÷	÷	÷
2	÷	++	+++	÷	+	÷
3	÷	+	+	÷	÷	÷
4	÷	÷	+++	÷	÷	+

Table 3.2: Morphology of B-waves and sleep stage.

Simultaneous increase in the ICP and SDB was present most of the time that B-waves occurred. Table 3.3 shows that SDB were present in at least 50% of B-wave events in all patients. All four patients had an average AHI above 5, indicating mild to severe SDB.

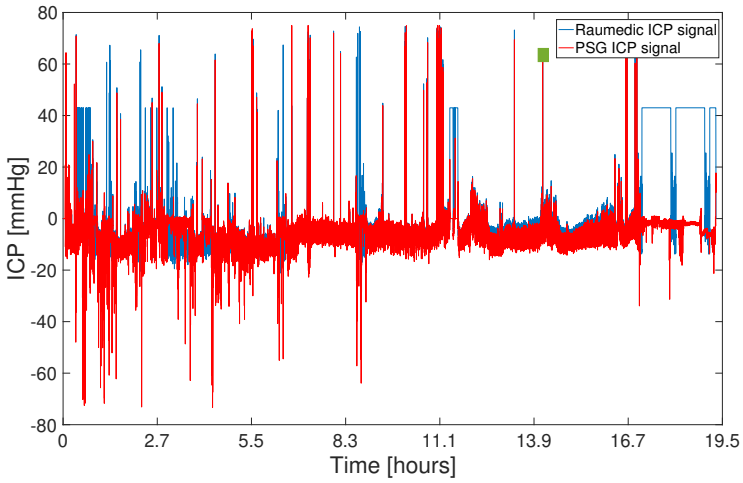

(a) The same ICP signals displayed in Figure 3.4, but now synchronized after temporal alignment.

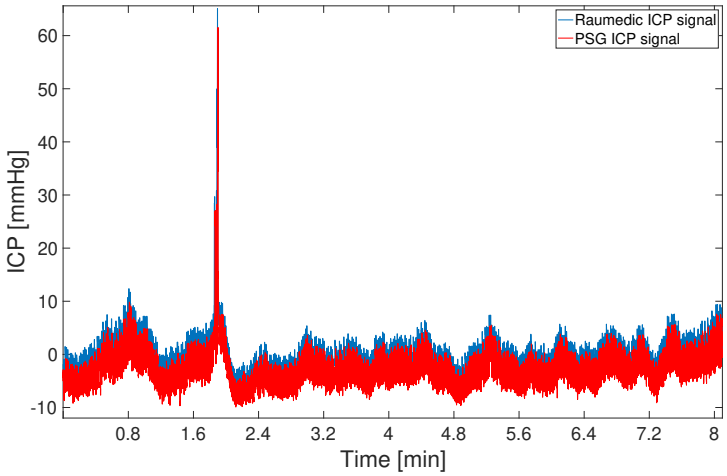

(b) Zoomed in display of the alignment at the location of the spike used as morphological feature.

Figure 3.5: Example of temporal alignment for ICP and PSG recordings of one patient.

Patient	Total	SDB	%	Excluded
1	114	101	88.6	3
2	183	166	91.0	20
3	172	86	50.0	11
4	139	139	100	0

Table 3.3: B-waves during sleep and association with sleep-disordered breathing (SDB).

3.4.3 Discussion

The presented study has four main outcomes: i) B-waves occur during sleep in near-to-normal patients, with normal ICP values defined by Andresen et al. [34]; ii) morphology of B-waves depends on the sleeping cycle: ramp-type B-waves are present during REM sleep, while sine-type B-waves occur during NREM sleep; iii) B-waves occur simultaneously to episodes of apneas and hypopneas; and iv) B-waves are associated with SDB.

B-waves and sleep
B-waves presence is increased during sleep and varies according to sleep cycles [75, 86, 87]. This presence is long known and accentuated during REM sleep, as previously described by [75, 79, 88]. Most of these studies reported conclusions using ICP signals from patients with CSF disturbances. Few studies reported the presence of B-waves [75, 89, 90] in healthy subjects. Six other studies reported B-wave surrogates [86, 90–94] in healthy subjects. Any signal occurring in the same frequency range as ICP and correlated to it, is considered a B-wave surrogate. Näsi [95], Weerakkody [96] found prevalence of a B-wave surrogate in REM sleep of healthy subjects, as we reported in outcome ii).

As a technical consideration, when analyzing B-waves in sleep, it is important to take into account the sleep stages. Otherwise, for instance, patients that do not enter REM phase could potentially show less B-wave activity than expected during sleep.

B-waves origin
It is a common belief that B-waves are largely governed by cardiovascular and respiratory contributions. The attribution of B-waves to SDB has been previously reported [79, 97, 98]. The latter study found a relationship between increasing ICP and apneas during sleep in patients with severe SDB. These apneas were accentuated during REM sleep. During these episodes of apneas, B-waves had a ramp-type morphology that resembled ICP A-waves, given their high ICP values [90, 98]. Our results support these findings, as we see ramp-type waves during REM sleep.

Limitations
This study presents a few limitations. First, it might be that the aneurysm operation or the implementation of the telemetric ICP probe may have disturbed the CSF dynamics and accentuated the presence of B-waves. Second, the resolution of the telemetric ICP probe is low (5Hz), which gives a lower resolution that might hinder the identification of B-waves.

In summary, we report that B-waves occur as a normal physiological phenomena related to SDB and mechanical respiratory changes, which differs from previously suggested cardiovascular origin. It also shows evidence on the existence of low amplitude B-waves not described by Lundberg.

3.5 Paper III: Causal relationship between slow waves of arterial, intracranial pressure and blood velocity in brain

As mentioned in Paper I, there exists a discrepancy in the frequency range used to describe B-waves. This discrepancy is also present when trying to define their origin. In Paper II, we reported the contribution of respiratory changes to their generation. In this paper (Paper III) we aim to elucidate the influence of the cardiovascular system as a source of B-waves and how its contribution may vary over time. The schematic overview of the methodology implemented in this paper is shown in Figure 3.6. The proposed method is not aiming just at identifying the causality between the cerebral and systemic signals, but also at exploring if the non-linearity and non-stationarity of these signals can be tackled using empirical nonlinear analysis tools.

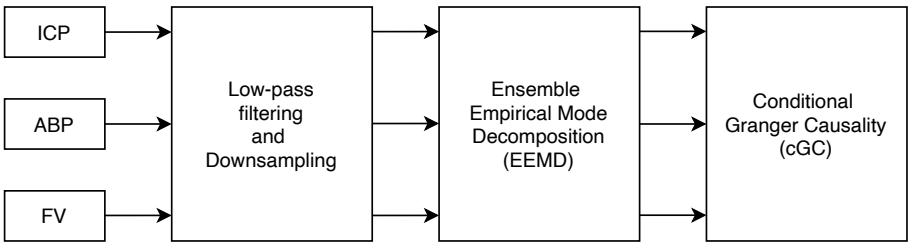

Figure 3.6: Overview of the methodology of Paper III. ICP, ABP, and FV signals are first lowpass filtered and downsampled. Then, each of them are decomposed using Ensemble empirical mode decomposition. The association between the extracted components is then analyzed using conditional Granger causality.

3.5.1 Methods:

Participants and Recordings

The cohort included for the analysis of the causality of ICP with cardiovascular signals consisted in randomly selected data from 45 CSF infusion studies (28 male, 17 female) with a mean age of 54 years old(range 25-78 years old). The studies included simultaneous recordings of ICP, arterial blood pressure (ABP), and transcranial doppler (TCD) cerebral blood flow velocity (CBFV) carried out between 1994 and 2006 in subjects with hydrocephalus.

Data pre-processing

We first applied a lowpass filter to remove high frequency signal components from the three input signals (ICP, ABP, and FV). The filter design is a finite-impulse response (FIR) lowpass filter with a cutoff frequency of 0.12Hz (Figure 3.7), as we want to focus on slow waves. Other filter specifications include passband ripple of 0.001 dB and stopband attenuation of 60 dB.

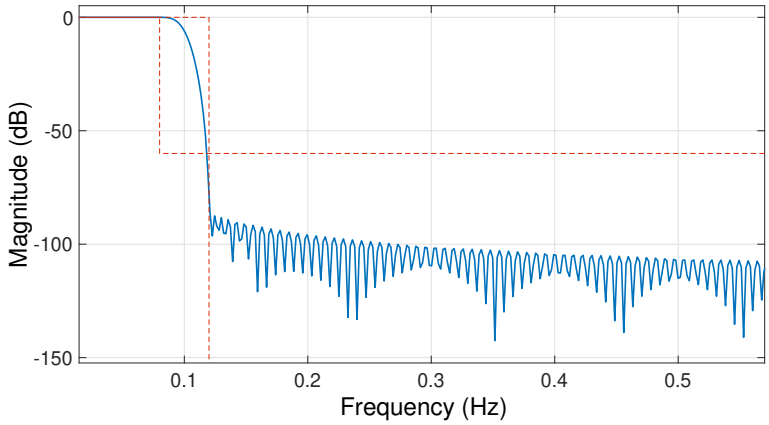

Figure 3.7: Visualization of the magnitude response (in dB) of the lowpass FIR-filter.

After applying lowpass filtering to the signals, we downsampled them to 1Hz. The main motivation for downsampling was to reduce the future cost of processing. Downsampling was done after filtering to mitigate the distortion due to aliasing. When downsampling is done before filtering, aliasing from undesired noise in the frequency bands that are not of interest could be present, raising the noise level of the resulting signals.

Ensemble Empirical Mode Decomposition
We used Ensemble Empirical Mode Decomposition (EEMD) to decompose each of the signals with different white noise series added into intrinsic mode functions (IMF) using empirical mode decomposition (EMD). Further mathematical details of this method can be found in Appendix B.2. In our work, the amplitude of the added noise was 0.1 of the standard deviation of the signal, the total number of IMFs, K, that were extracted in each trial was set to 10, and the ensemble number was set to 100, as recommended in [99]. The noise amplitude was chosen upon suggestion by Wu and Huang [99] but considering that when the signal contains high-frequency components a smaller amplitude than 0.2 is recommended.

The statistical significance of the extracted IMFs was checked to ensure that they did not contain any of the noise added.

IMF selection
The decomposed IMFs were divided in two groups: slow wave representative IMFs and non-slow wave dominant IMFs. Thus, the first set contained the relevant information we were interested in. The slow wave dominant IMFs were selected using the Jensen-Rényi divergence (JRD) and the Minkowski distance (d_{mink}) [100]. If the original signal and the ith IMF were somewhat identical, then d_{mink} and JRD would be low and therefore selected as slow wave dominant IMF.

Granger Causality
We tested the causal relation between IMFs of ICP, ABP, and FV using conditional Granger Causality (cGC). Further details of this methodology can be found in Appendix B.3. Significance of the existence and strength of connection was tested both for a single subject and at group level. For a single subject, the existence of a significant connection between two of the time series was analyzed using the cGC values under a Bonferroni-corrected significance threshold of p=0.01. The strength of significant connections was calculated as the mean Granger Causality (GC) values between the two signals. At group level, if the connection between two signals was significant in at least 75% of the subjects, the existence of a connection between these two signals was considered.

3.5.2 Results

Data pre-processing
The effect of applying lowpass filtering on the three signals can be seen in Figure 3.8. The high frequencies corresponding to the cardiovascular and respiratory components can no longer be seen.

Ensemble Empirical Mode Decomposition
Data from the three signals after pre-processingwas decomposed by the EEMD, as illustrated in Figure 3.9. Ten IMFs were extracted for each of the signals in each of the 45 patients. Initial visual inspection suggests that the last IMF (IMF_{10}) contains the trend of the signal and the first IMFs (IMF_1 and IMF_2) contain high frequencies that seem to be higher than those present in the slow waves.

Statistical significance of IMFs
In Figure 3.10 we show an example of the statistical significance of the extracted IMFs for the three signals of one subject. The majority of the IMFs were all above the 99% confidence level, meaning that the IMFs were significant components for the selected number of ensembles (NE) and amplitude of added noise. IMFs significance notably decreased when NE was lowered down to five or when the amplitude of the added white noise was increased to 0.9 times the standard deviation of the original signal, suggesting that our parameters choice was correct.

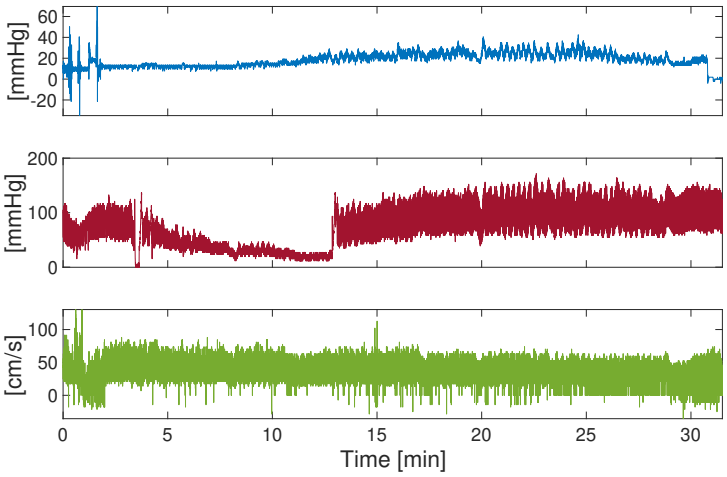

(a) Before pre-processing.

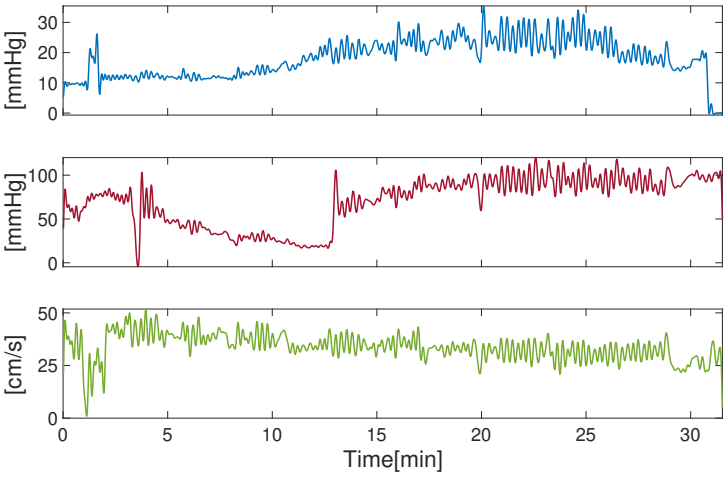

(b) After pre-processing.

Figure 3.8: ICP in blue (top), ABP in red (middle) and FV in green (bottom) signals of one subject before (left) and after (right) pre-processing. The X-axis shows the time in minutes whereas the Y-axis represents the magnitude of the signals.

IMF selection

The values of d_{mink} and JDR decreased rapidly from the sixth IMF and forward, leading to our selection of IMFs from 6 to 9 as the most slow wave dominant IMFs. In accordance with this selection of IMFs, Table 3.4 shows that the average power spectral density (PSD) is larger with increasing IMF order. The power of slow waves was higher in the infusion stage than in the baseline, suggesting that slow waves are predominant in the infusion phase. Slow waves reconstructed with the selected IMFs occupy a frequency range from 0.013 to 0.155Hz.

Directional causality

The only significant connection observed was from FV to ICP in IMF_6 during infusion and not at baseline, probably because slow waves are of less power in the baseline stage. This difference in power between baseline and infusion can also be seen in the other IMFs, as we observed in Table 3.4.

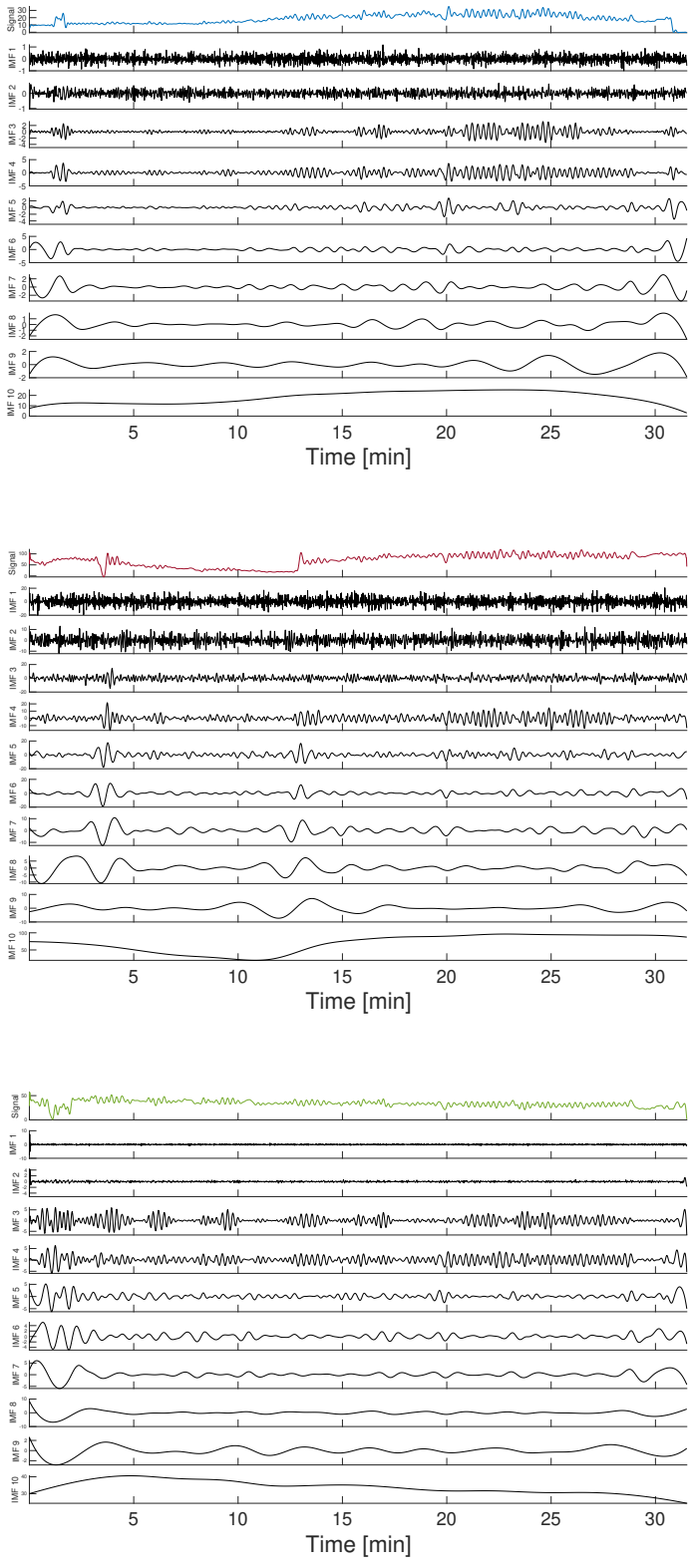

Figure 3.9: An example of EEMD in one subject for each of the three signals: ICP (top), ABP (middle), and FV (bottom). Each of the plots represents the filtered signal (first row), and its corresponding EEMD including the trend (last row).

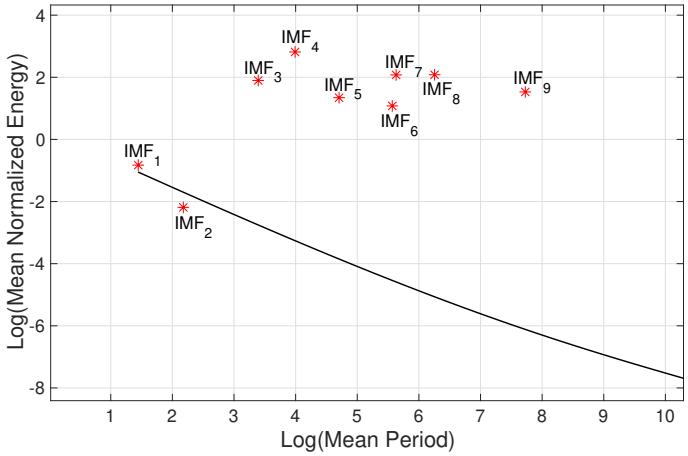

(a) ICP signal

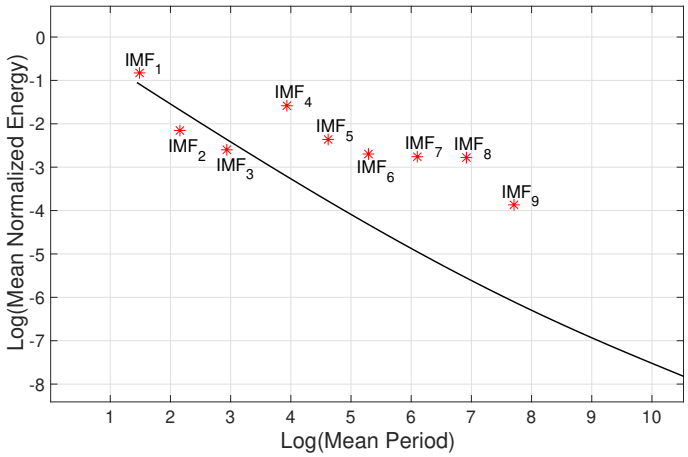

(b) ABP signal

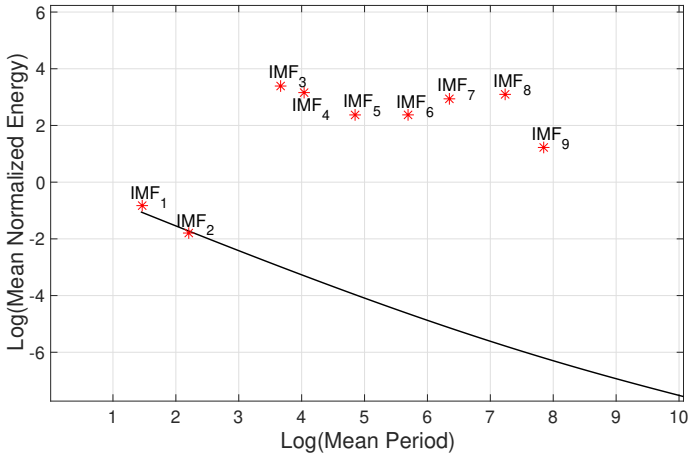

(c) FV signal

Figure 3.10: Statistical significance test of IMF components for IMFs extracted using number of ensembles equal to 100, from the ICP, ABP, and FV signals of one subject.

Power / IMF	Baseline	Infusion
IMF_1	0.022	0.124
IMF_2	0.025	0.165
IMF_3	0.047	0.050
IMF_4	0.068	0.218
IMF_5	0.090	0.471
IMF_6	0.098	0.700
IMF_7	0.098	0.561
IMF_8	0.082	1.735
IMF_9	0.052	1.871
IMF_{10}	82.765	373.442

Table 3.4: Mean power of different IMFs during baseline and infusion stages.

3.5.3 Discussion

The suggested EEMD method can successfully handle the problem of non-linearity and non-stationarity of the cerebral and systemic signals. There are two main outcomes of this study: i) slow waves in ICP, ABP, and FV can be described by oscillatory modes of frequencies between 0.013 and 0.155Hz, and ii) within the 0.095 and 0.155Hz frequency band, there is an influence of slow waves of FV on slow waves of ICP.

As reported in Paper I, there is controversy in the definition of a frequency band of ICP slow waves. In fact, the term “slow waves” was introduced to extend the frequency range of Lundberg’s B-waves and cover a greater variety of variations of slow waves. We reported a frequency range between 0.013-0.155Hz in our data. We found a higher frequency range than those previously suggested by other authors [2, 77, 78, 101] (see Figure 3.11).

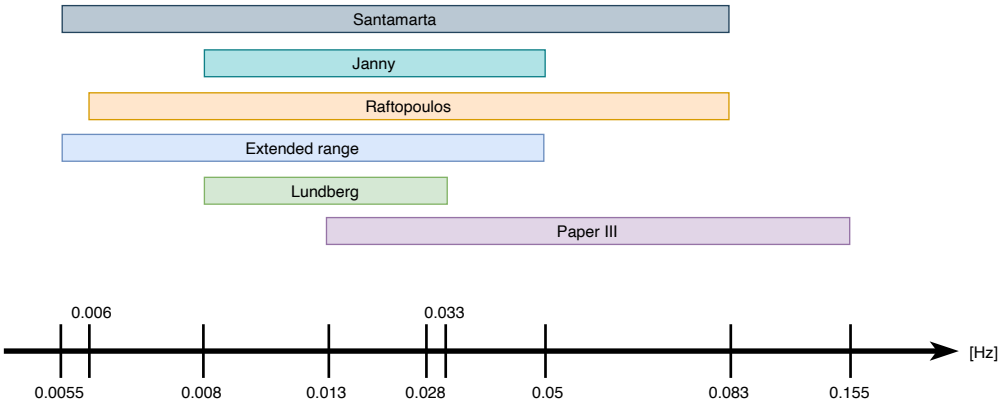

Figure 3.11: Visual comparison of the frequency ranges of ICP slow waves defined by different authors [2, 77, 78, 101] with the frequency range we found in Paper III.

In this study, EEMD was applied for the calculation of the frequency range encompassing slow waves. While EMD has previously been implemented in the field of ICP analysis for removal of artifacts [102, 103], only one study has been found on the use of EEMD in ICP analysis [104]. We selected EEMD over more traditional spectral decomposition (i.e. Fourier analysis) to tackle the non-linearity and non-stationarity of our signals. Using EEMD, the slow waves in all three signals were better described by $IMF_{6\text{-}9}$.

Conditional GC analysis applied to these selected IMFs showed that FV has an influence in ICP in the frequency band between 0.095 and 0.155Hz. However, the physiological

reason behind this association is not clear, with hypotheses suggesting intrinsic brainstem sympathetic nerve discharges [105], and regulatory mechanisms systemic to arterial smooth-muscle cells [106] as potential reasons.

Limitations
This study has some limitations. First, the connectivity between signals may not be constant throughout time and GC might not capture it. Second, other physiological variables (heart rate, oxygen levels...) were ignored. Third, GC results depend on the extracted IMFs, which depend on the choice of both the added noise amplitude and the value of the number of ensembles. Finally, the study was limited to a cohort of patients with NPH condition. Results could be different if other disorders were also included.

3.6 Summary and Final Remarks

In this chapter, we present the lack of clarity for naming, describing morphological characteristics, and analyzing solely B-waves since they are the classic macro-pattern most likely to be encountered in the clinical practice. The results shown in Papers I, II, and III address the research questions of this chapter. We will now again present these research questions, but now together with their corresponding replies based on our research output.

- Chapter 3 Research Question 1: Regarding classical Lundberg waves, are their terminology and morphological characteristics sufficient to describe the variations seen in daily practice?
  Answer to Chapter 3 Research Question 1: Paper I shows that the terminology and description of B-waves varies across research groups and has stopped addressing the ICP waveforms found in the clinical practice today, where patients are now also being monitored in non-acute scenarios. The results presented in Paper III further confirm those presented in Paper I. Specifically, that the frequency range of slow B waves needs to be expanded as an umbrella to cover more pattern variations.
- Chapter 3 Research Question 2: To which extent do ICP macro-patterns relate to respiratory disturbances?
  Answer to Chapter 3 Research Question 2: In Paper II we show that ICP B-waves are found to be associated with respiratory disturbances. They are also observed in healthy subjects during sleep, as part of a physiological phenomenon.
- Chapter 3 Research Question 3: To which extent do ICP macro-patterns relate to vascular disturbances?
  Answer to Chapter 3 Research Question 3: In Paper III, we observed the vascular contribution of flow velocity to ICP in a limited frequency range within slow waves.

These research outcomes highlight the need for moving beyond the definition of classical waves and focusing instead in the recognition of new clinically relevant patterns. The remainder of this thesis will focus on developing a more robust and generalized automated method to identify macro-patterns in the ICP signal.

CHAPTER 4 Investigating Data Quality of ICP Signals

Known data quality issues are costing companies tremendous amounts of money. Only in the United States, the total yearly cost of data quality issues summed up to $3.1 trillion in 2016, as estimated by data quality consultant Thomas Redman in an article in Harvard Business Review [107]. He later on wrote for the MIT Sloan Management Review that the cost of bad data to be 15% to 25% of annual revenue for most companies.

Understanding the importance of data quality as a guarantee of robust results is one of the most relevant processes of data analysis and interpretation. Yet, we are often prone to accept the values presented by a monitor or computer without any thought given to uncertainty, missing values, reliability of the equipment employed, among many other flaws. These problems are rarely taken into consideration in the context of neurosurgery. However, it is of key importance to ensure good ICP quality that researchers check that it is not altered or inaccurate, either by human error or sensor defects.

This chapter addresses our Research Question 2 and describes the design of a data quality pipeline [P.IV] to integrate all required data validation checks to make sure high data quality is ensured before any further data analysis is performed.

4.1 Research Background

Before applying any ICP analytical tools it is important to consider that the signal may be contaminated by noise. Some computer monitors might present deviated measured numbers that represent neither normal physiological nor pathological values. Some actions, like patient movement, provide changes in the ICP signal that are physiological responses to the change, but what is certain is that noise does not come from a physiological cause [108]. Table 4.1 shows a summary of certain problems that are associated ICP time series, with Table 4.2 showing further division of low frequency noise.

Data loss and wrong timestamps are likely to be caused by sensor detachment the first, and network transmission interruptions both of them. High and low frequency noise, and spikes can lead to difficulties in identifying the underlying true signal. Signals with different sampling frequencies can introduce misleading results, specially when combined for comparison. Accuracy in sensor calibration is also important given the context where clinical decisions are made based on threshold values.

One would think that fixing all these artefacts would improve the signal quality, but this is not always the case, and decisions on handling them or not should depend on future signal analysis technique and application. As an example, imputing values in a missing signal segment could be useful for the correct performance of certain algorithms, but it may be harmful for algorithms searching for patterns in the signal. Two questions arise from this discussion: (1) *which type of artefacts should we focus our efforts on removing for latter macro-pattern identification in the signal?*, and (2) *which kind of tools could we offer to the clinicians or researchers for quality check of ICP signals?*

Artefact Name	Artefact Description
Data Loss*	There are gaps in the ICP signal.
Wrong Timestamps*	Timestamps are repeated.
Spikes*	Sudden changes of high magnitude in a short duration, which are physiologically implausible.
Data Formats	Different data formats depending on the reading monitor.
Diverging sampling frequency*	Different sampling frequencies depending on ICP sensor used.
High frequency noise*	Small changes due to inaccurate measurement amplifier devices, electrical interference, quantization noise...
Low frequency noise	Slow changes that can be both physiological or due to environmental effects.

Table 4.1: Summary of challenges that can be encountered in the ICP signal. Marked with an asterisk "*" are those artefacts that will be further discussed in this chapter.

Physiological origin	Device-related origin
Patient movement	Connection errors
Coughing	Sensor calibration
	Sensor shift

Table 4.2: Examples of origin of certain low frequency noises.

In the literature, lowpass filtering is the most common method for artefact removal. However, lowpass filtering is limited to stationary signals, whose time period and spectral content value are constant. The concept of stationarity does not apply to ICP signals. Adaptive filtering is a more advanced technique, but requires a reference signal to estimate the noise in the ICP signal. This reference signal is lacking in ICP monitoring. Independent Component Analysis (ICA) is a widely used algorithm for removing different artefacts. It separates the signal into additive subcomponents under the assumption that they are statistically independent, assumption that does not hold for ICP signals [102]. To tackle these shortcomings, non-linear methods based on wavelets have emerged. Wavelet techniques rely on the idea that the signal is concentrated in certain wavelet coefficients [109]. The drawback of wavelet transformation is that the basis functions are fixed, so they do not adapt to the nature of the ICP signal. In this chapter, we propose the use of EMD to effectively detect artefacts, in particular high and rapid spikes, given its basis functions are derived from the ICP signal itself.

4.2 Research Questions and Objectives of this Chapter

Based on the consideration of this background overview, the following concrete sub-questions that guided the research for investigating the data quality of ICP signals were defined:

- Chapter 4 Research Question 1: Which artefacts are present in ICP signals? Is the removal of such artefacts always necessary?
- Chapter 4 Research Question 2: Can we identify the noise components in ICP signals based on non-linear and non-stationary techniques?

These research sub-questions led to the formulation of the following objectives:

- Chapter 4 Research Objective 1: Two types of noise can be identified in the ICP signal: high-frequency noise from measurement devices and electrical interference, and low-frequency noise due to environmental factors. The goal is the removal these artefacts but limited to those with non-physiological origin.
- Chapter 4 Research Objective 2: To recover the underlying structure of the signal of interest using signal decomposition techniques such as EMD.

4.3 Paper IV: Empirical Mode Decomposition-Based Method for Artefact Removal in Raw Intracranial Pressure Signals

As mentioned before, ICP signals are contaminated by artefacts that mask the true signal. Creating a roadmap to handle these artefacts could significantly help in the accuracy of posterior ICP analysis. To facilitate this process, and with focus on the removal of non-physiological artefacts, we built a series of data quality checks. The overview of this pipeline is presented in Figure 4.1.

Figure 4.1: Overview of the methodology of Paper IV. The ICP signal is first anonymized, and then check, successively for missing data fragments, artefacts, and differences in sampling frequency.

Imagine we are in a car starting our trip in Copenhagen and finishing in Madrid, but the car we are taking is old and needs to be checked at a few pit stops before making it to our final destination. The same goes with the ICP signal, we will do three validity checks before it can be used for macro-pattern identification analysis. In the first stop we will check for missing data. Then, we remove artefacts contaminating the signal. And as the last pit stop, we correct the sampling frequency of the signal. As an end result, the system will return as output a more cleaned ICP signal. The mentioned workflow was tested on ICP signals from a retrospective database.

4.3.1 Methods

Recordings

This study was carried out on ICP records retrieved from the database at Rigshospitalet, Denmark. Five patients with various neurosurgical disorders were included. We made a conscious decision to focus on the basic methodology and leave disease entity stratification for a subsequent investigation.

ICP was continuously monitored using the ICP probe (Neurovent-P; Raumedic AG). The ICP readings were sampled at 100Hz. For all ICP sessions of patients included in this study, the ICP records had a mean of 29.2 hours and a standard deviation of 5.5.

Data anonymization

The protocol for data anonymization shown in Figure 4.2 encompassed data handling from the measured raw files to the final anonymized files, as well as the inclusion of the corresponding demographic patient information. A new encrypted database in a secure web application known as REDCap was built [110]. REDCap was set up to store patient data (including measurement techniques, age, diagnosis...) and to assign serial IDs to each of them. This was specifically done to aid in the process of data anonymization for its use in our research studies.

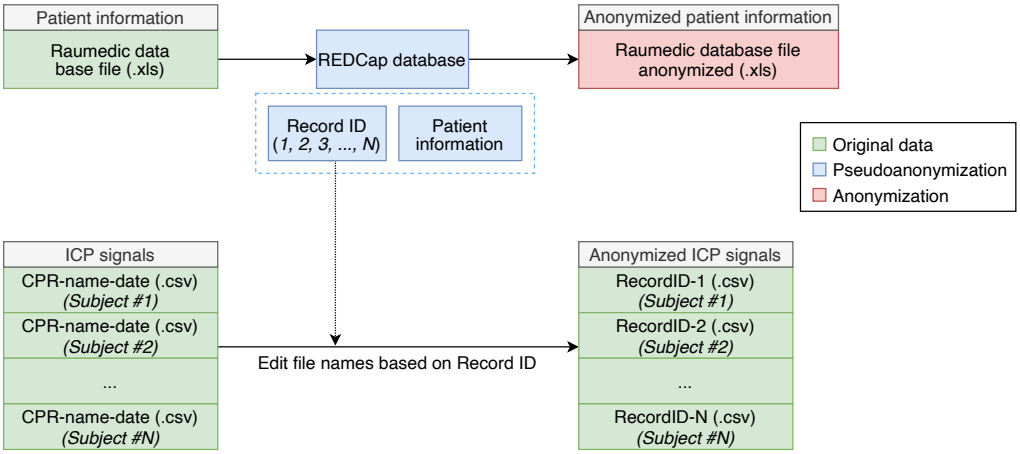

Figure 4.2: Overview of the data anonymization protocol.

Quality check 1: Data loss

The first stop in the quality check pipeline ensured that only complete ICP signals were moved forward in the process. If more than 30% of the data was missing, the ICP recording was discarded and did not continue in the validation pipeline. Otherwise, the gaps with missing data were removed. The idea of removing gaps by joining the fragments together was discarded because it could cause discontinuities in the data. Instead, the signal was split at the location of the missing data.

Quality check 2: Spike removal

The second stop in the quality check searched for spikes in the ICP signal, and the overview of this check is show in Figure 4.3. Spikes are defined as high and rapid changes in the ICP magnitude that are physiologically impossible. To detect and filter them out, we relied on the fact that sharp changes in time domain result in spikes also in the frequency domain. Thus, we proposed the following method based on EMD:

1. Break down ICP signal into a maximum of sixteen IMFs via EMD, as described in Appendix B.1.
2. Detection of spikes: location and duration estimation of spikes based on extracted IMFs.
3. Imputation of spikes in the original signal.

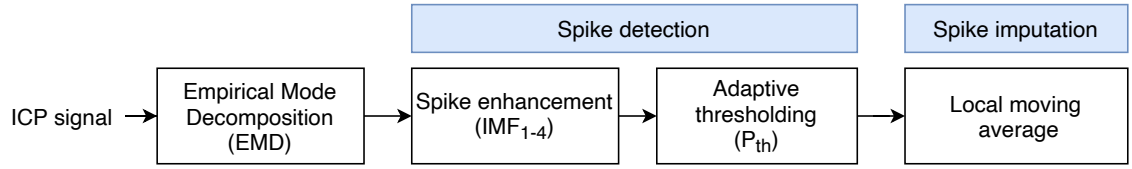

Figure 4.3: Overview of the methodology for spike removal. The ICP signal is first decomposed into intrinsic mode functions, which are then used to detect the location and estimate the duration of the spikes. The spike is then imputed in the original signal using a moving mean average of 10 seconds.

Spike detection involved two additional steps: first, spike enhancing; and second, thresholding for locating the spike. After decomposition, we observed that the original spikes were also present in the first consecutive IMFs, and this is due to the band-limited characteristic of spikes. Based on the first IMF (IMF_1) the location of the spike event could be identified. The next consecutive IMFs were used to estimate the duration of the events. In our case, summing the first four intrinsic modes as in Equation 4.1 enhanced the spike event.

$$IMF_{1\text{-}4} = \sum_{i=1}^{4} IMF_i(t) \tag{4.1}$$

The spikes were identified within this sum using adaptive thresholding. The threshold was calculated from the noise level in $IMF_{1\text{-}4}$

$$P_{th} = \hat{\sigma}\sqrt{2 \cdot \log(L)} \tag{4.2}$$

where L is the length and σ the standard deviation of $IMF_{1\text{-}4}$. As artefacts are present in the summation, the standard deviation is unknown and it must be estimated as [111]

$$\hat{\sigma} = \frac{MAD}{0.6745} \tag{4.3}$$

MAD is the median absolute deviation as is calculated using the median value

$$MAD = Me[IMF_{1\text{-}4}] - Me(IMF_{1\text{-}4})] \tag{4.4}$$

Those samples in the summed IMFs beyond the threshold values [-P_{th},P_{th}] were marked as spike events.

After spike detection, the spike in the original ICP signal was suppressed by replacing the value of the spike samples with the local average calculated for each sample using a sliding window of 10s. If another spike was present during those 10s, the window size was reduced to 5s. But, if the other spike lied within a window of 0.4s, the ICP samples between them were considered one spike event.

Quality check 3: Diverging sampling frequency
The last stop was to resample the ICP signal to the base frequency of 30Hz. A small sampling frequency was selected to reduce the computational cost of future applications.

Performance evaluation
To investigate the performance of the proposed algorithm, a segment from one of the ICP recordings containing a typical spike was selected as a spike template (Figure 4.4). A typical spike fulfills two characteristics: a duration shorter than 0.5s and an abrupt ICP value increase. The real data was then inspected visually by an expert to identify ICP segments with spikes, using the spike template. These annotated spikes were used as the ground truth to examine the performance of our algorithm. The performance of the proposed method was quantified based on how well it estimated the location of the spikes using precision and recall metrics [112]:

$$\text{precision } = \frac{TP}{TP + FP} \quad \text{recall } = \frac{TP}{TP + FN} \tag{4.5}$$

where TP is the number of correctly identified spikes, FP is the number of spikes identified that were not spikes, and FN is the number of not detected spikes. A total of 26 hours from the ICP recordings described before were used for this evaluation. The closer both values are close to 100%, the better the performance.

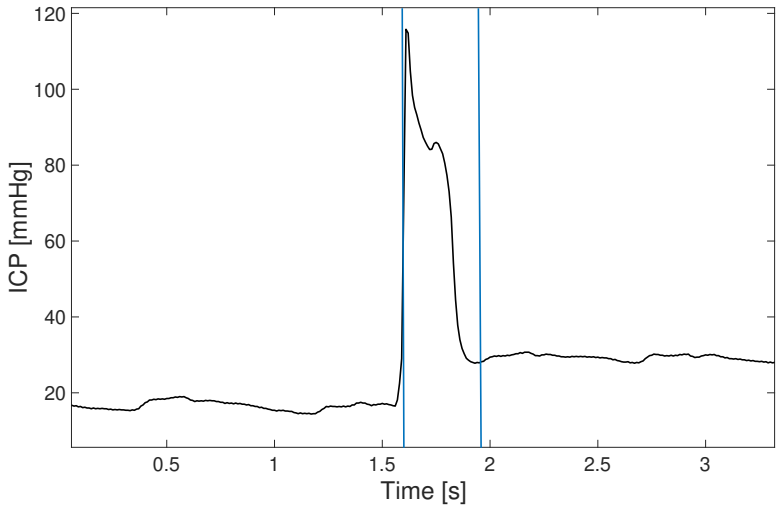

Figure 4.4: Spike template used for visual identification of spike-dominant fragments in the ICP recordings. Other magnitude values (above 50 mmHg), durations below 0.5s, and other morphologies similar to the spike template are also considered as spike-dominant fragments.

4.3.2 Results

A typical result is presented in Figure 4.5, where an ICP signal contaminated by high spikes was run through the data validation pipeline.

Data Loss

It is important to address missing values because they can jeopardize the accuracy and credibility of later analysis and if not handled, they can lead to false interpretation of results and false discovery of macro-patterns. Our ICP recordings had a maximum 1.3% of missing data (see Table 4.3). This is lower than previously reported values by [102], whose data loss accounted for 5-20% of the recordings. This percentage can vary considerably given the complicated environment of ICP monitoring, where missing values can be caused by many reasons: patient movement, sensor detachment, connection problems, among others [113].

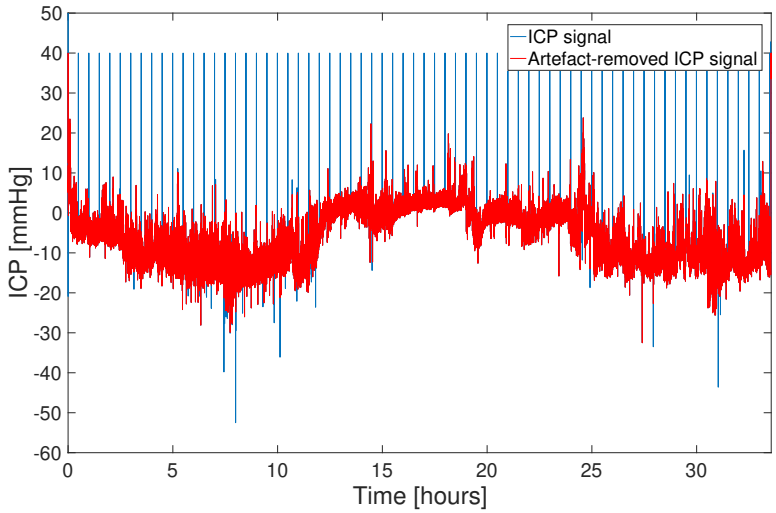

Figure 4.5: Example of ICP signal before (blue) and after artefact removal (red) for one subject from the selected patient's data.

	Total duration of missing data [min]	Total duration of monitoring~[min]	Percentage duration of missing data [%]
Subject #1	19.36	1487	1.3
Subject #2	1.33	2189	0.1120
Subject #3	2.10	1438	0.15
Subject #4	0	2013	0
Subject #5	1.83	1640	0.11

Table 4.3: Summary of missing data in each of the ICP recordings.

Signal stationarity

The Kwiatkowski–Phillips–Schmidt–Shin (KPSS) test for stationarity was applied to selected artefact-free segments of increasing size [114]. ICP signals of window size equal to 1s were non-stationary. Their p-values were around 0.03 for a significance level for the hypothesis test of 0.05.

EMD

Given that a previous study [102] for artefact removal in ICP signals used a maximum of sixteen IMFs, we chose to develop our algorithm using this number. As seen in Figure 4.6, the first four IMFs ($IMF_{1\text{-}4}$) were sufficient for estimating the location and duration of the spike episodes.

The extracted IMFs were all significant except for IMF_2, as seen in Figure 4.7. We are aware that IMF_2 was not significant, so using EEMD might have solved this problem. However, EEMD is more computationally expensive. For our artefact removal algorithm using EMD is sufficient to obtain good results, since we only want to estimate a location that spreads over certain IMFs, and not take any statistical analysis on the extracted IMFs. It must be noted also that spikes can have a big effect on the presence of artefacts on the decomposition [115], which might also be the reason of the lack of significance of our second IMF. Table 4.4 shows increasing occupied bandwidth of the power spectrum for decreasing intrinsic function index. This is expected, as the frequency content is the highest in the first IMF (IMF_1) and lowest in the last extracted IMF.

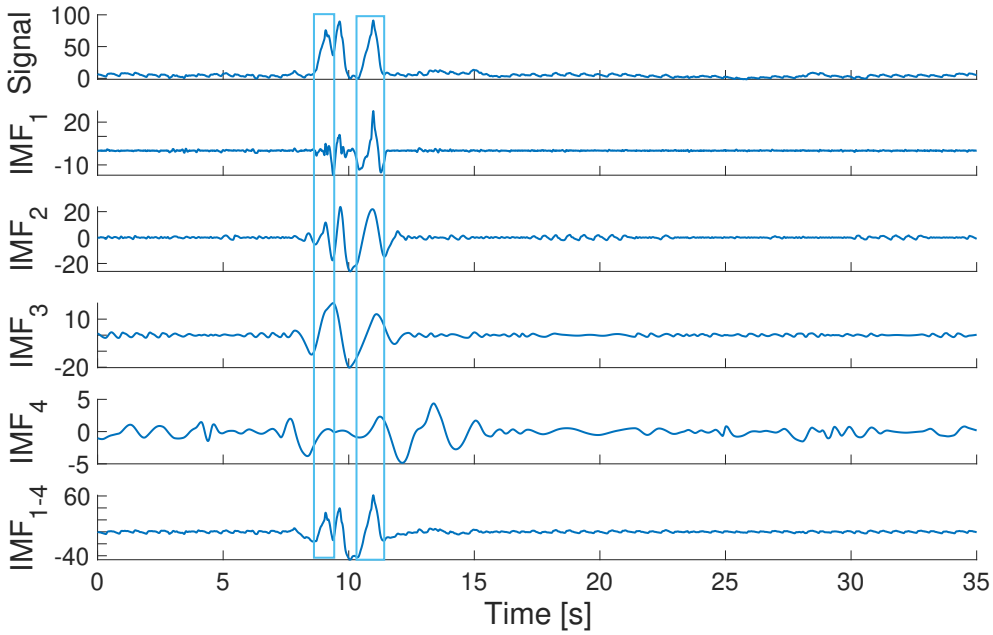

Figure 4.6: Example of IMFs extracted after Empirical Mode Decomposition zoomed at the location of a spike. The duration of the spike is annotated with a blue rectangle in both cases.

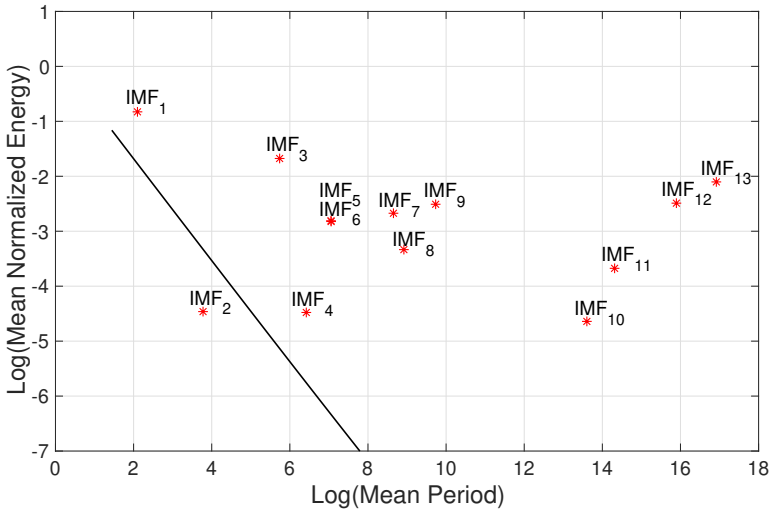

Figure 4.7: Statistical significance test of IMF components for IMFs extracted using a maximum of sixteen IMFs.

IMF	Frequency Band [Hz]
1	0.020-25.041
2	0.013-15.056
3	0.011-4.426
4	0.008-2.870

Table 4.4: Frequency band of selected IMFs.

Spike detection

An overview of the statistics of the spikes detected in our ICP monitoring signals is displayed in Tables 4.5 and 4.6. This latter table shows that the number of artefacts varies depending on the recording, and this is most likely due to environmental factors. Initial screening of the ICP signals of Subject #2 with 156 detected spikes, and Subject #5 with 1018 detected spikes (see Figure 4.8), also suggests than this last one is contaminated by significantly more spikes than the first.

Statistics	Values
Median monitoring length [min]	1640
Median number of artefact events	166
Total number of artefact events	1741

Table 4.5: Statistics of the detected spikes.

Subject	Number of spikes
Subject #1	101
Subject #2	156
Subject #3	166
Subject #4	300
Subject #5	1018

Table 4.6: Number of spikes in the selected ICP recordings.

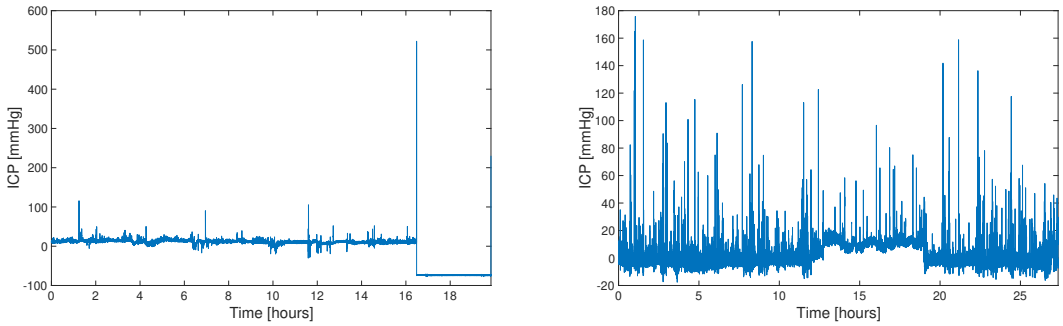

(a) Subject #2. (b) Subject #5.

Figure 4.8: Example of ICP recordings from two different patients.

Spike imputation

Figure 4.9 illustrates how ICP samples in the original signal are imputed with the moving average values. This is done to maintain the underlying structure of the original signal. We can observe that our artefact removal method tends to estimate a wider width of artefact events than the actual spike duration. Part of our future work will focus on modifying the algorithm to achieve a better width estimation of artefacts.

Performance results

When evaluating the performance of the proposed algorithm in a total of 26 hours of spike-dominant fragments, spikes are detected with 84% precision and a 77% recall, given that TP = 114, FP = 21, and FN = 34.

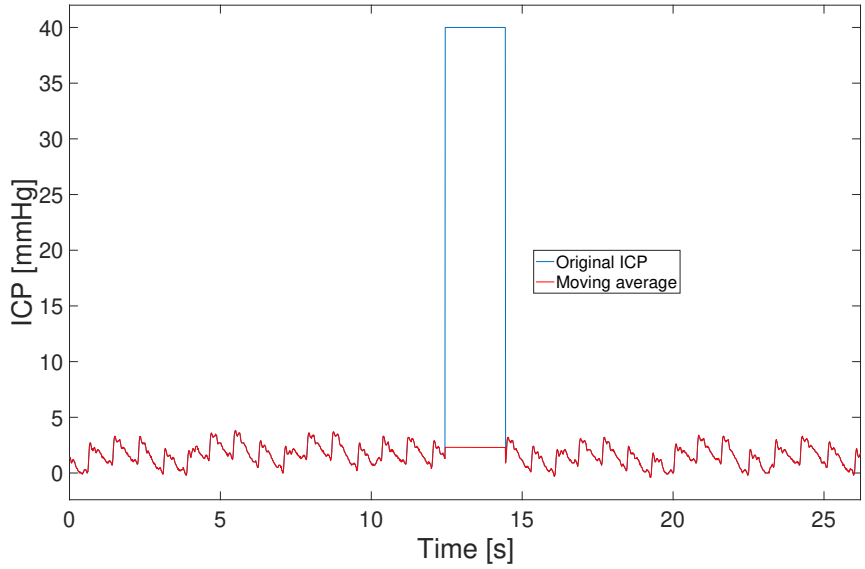

Figure 4.9: Example of ICP imputation using moving average to replace sample values corresponding to spikes.

4.3.3 Discussion

The method proposed for artefact removal effectively removes spikes using EMD, which is appropriate given its ability to handle non-stationary and non-linear signals. The method relies on two main ideas: (1) spikes are band-limited so their frequency content is limited to some successive IMFs; and (2) adaptive thresholding ensures that the width estimation adapts for each individual case.

Although our method is demonstrated to be efficient on 26 hours of ICP signals, we observed some limitations. First of all, we are aware that the proposed methodology is computationally expensive, as it requires repetitive sifting. More advanced signal processing techniques come at a cost, that of computation complexity. For our specific future application of identification of macro-patterns, we chose artefact removal performance over computational cost.

Another limitation is the overestimation of the artefact width. Tuning of the algorithm needs to be done to address this problem. A possible solution could be to use EEMD instead of EMD, although more computationally expensive, or to tune the parameters from the EMD (i.e. spline interpolation type, convergence method...). Future work will further investigate on this topic, and in addition, work will also be placed on increasing the recall. As suggested in [102], the recall can be improved by iterating the algorithm a few times, to prevent tall artifacts from masking smaller artifacts and thus hindering their detection.

4.4 Summary and Final Remarks

The investigation carried in Paper IV addresses the research questions introduced in this chapter. The answer to each of the questions is reported below:

- Chapter 4 Research Question 1: Which artefacts are present in ICP signals? Is the removal of such artefacts always necessary?
  Answer to Chapter 4 Research Question 1: Among the noise sources explored, it is clear that those with a non-physiological origin that affect the appearance of the signal should be tackled before any shape-based analysis.
- Chapter 4 Research Question 2: Can we identify the noise components in ICP signals based on non-linear and non-stationary techniques?
  Answer to Chapter 4 Research Question 2: EMD can be elected as method to decompose the signal into intrinsic mode functions that allow the reconstruction of artefacts. The EMD-based method developed permits a more generalized approach for handling artefacts in the ICP signal.

Given the capability of the presented method for artefact removal in ICP signals as part of the data cleaning pre-processing step, we can proceed to further analyze the data. The goal is to develop an automated method to identify macro-patterns in the ICP signals. This topic will be investigated in the next chapter.

CHAPTER 5 Development of a Method for Automatic Identification of Macro-patterns in ICP Signals

We are on a constant journey of unraveling patterns. Even as babies barely able to speak one word, we are already looking for patterns. Babies gradually understand the pattern of sounds and start to mimic it until they are able to speak. We grow up and we go to school, where we learn new behavioral patterns. For instance, when the teacher enters the class every morning, we all need to stand up and say good morning. As we continue with having a job, we also acquire new patterns needed to adapt to the new workplace. Life is based on patterns, and living beings use pattern recognition in everyday life because they embody structure and order.

"To understand is to perceive patterns."
Isaiah Berlin

How can we cure cancer if not knowing the mechanism of how it originates and spreads? How can we defeat COVID without understanding the process of how it attacks the body, how it mutates, and how it proliferates? Are not all of these also different types of pattern recognition? The answer is yes, and if we bring these questions to the field of neurosurgery we can ask ourselves many questions: can we identify neurosurgical disease entities based on the internal distribution of macro-patterns in the ICP signal? can specific shift configurations in macro-patterns allow us to identify "at risk" patients before critical changes in ICP?

5.1 Research Background

The combined efforts of understanding the source of macro-patterns and cleaning data from spurious artefacts allowed us to move forward on to looking how macro-patterns beyond classical A- and B-waves, unfolding over seconds to minutes, can be described and identified. So, as we explained in Chapter 2, while ICP in a clinical setting may often be interpreted purely as a number that needs to stay within a certain range for the brain to function properly, the ICP signal represents a tremendously complex time series with macro-patterns that go far beyond this previous limited understanding.

Looking at macro patterns is a markedly different approach compared to the prevalent ICP morphology-analysis approaches that primarily focus on information derived from single beat-to-beat pulse waves. Some have attempted to identify longer duration waveforms based on these pulse wave metrics [66], but they have not seen widespread clinical use. Part of the challenge here may, as explained in Chapter 2, that the existing terminology used to assess B-waves vary to a tremendous degree, and that it may simply be impossible to expect a computer to identify these type of classical patterns if humans cannot

even agree on how to define these patterns. In addition, an extra challenge is that in the last decade, new telemetric ICP monitoring has become available, allowing recordings to be more representative of daily life conditions with a higher signal diversity. The need for identification of these macro-pattern variations emerges as a potential tool for better understanding the physiological underpinnings of patient symptoms. In this chapter, we address our Research Question 3 as we introduce the first steps in the development of a methodology for future automatic macro-pattern identification in ICP signals whose quality has previously been validated. The technical path introduced in Chapter 4 is responsible for this part.

5.2 Research Questions and Objectives of this Chapter

From this research background, we defined the following questions:

- Chapter 5 Research Question 1: Is it possible to develop an automated algorithm to find more general macro-patterns that could help to better describe the ICP signal?
- Chapter 5 Research Question 2: Is the developed method generalized? And does it perform equally in data from different disease categories?
- Chapter 5 Research Question 3: Can the macro-pattern information be presented to a clinical end user in a fashion that is operationally useful?

These research sub-questions led to the formulation of the following objectives:

- Chapter 5 Research Objective 1: To develop a fully automated system that, based on ICP signals, performs i) identification and ii) labeling of macro-patterns.
- Chapter 5 Research Objective 2: To test the method introduced in a dataset different from the one used to create the template library. This additional dataset should include subjects with different disease entities.
- Chapter 5 Research Objective 3: To create a strategy, among all the many alternatives, to look at the raw ICP signal with specific features accentuated, which might not be easily spotted during the visual interpretation of the ICP monitoring.

5.3 Paper V: k-Shape clustering for extracting macro-patterns in intracranial pressure signals

This leads us to propose a new methodology based on shape clustering to extract macro patterns from the ICP signal that permits a more appropriate description of the larger timescale ICP variations seen in the clinical setting. Our approach produces a universal scalable library of seven that we intend to use to automatically segment each individual ICP signal into shorter sequences and in the future, link with additional clinical data. The overview of the methodology is presented in Figure 5.1.

5.3.1 Methods

We have devised an adaptable pipeline that steps through segmentation into variable duration subsequences, z-normalization to deal with scale and translation invariance by prioritizing shape over amplitude features, and finally, shape-based clustering to divide the extracted ICP subsequences into a number of characteristic-preserving groups.

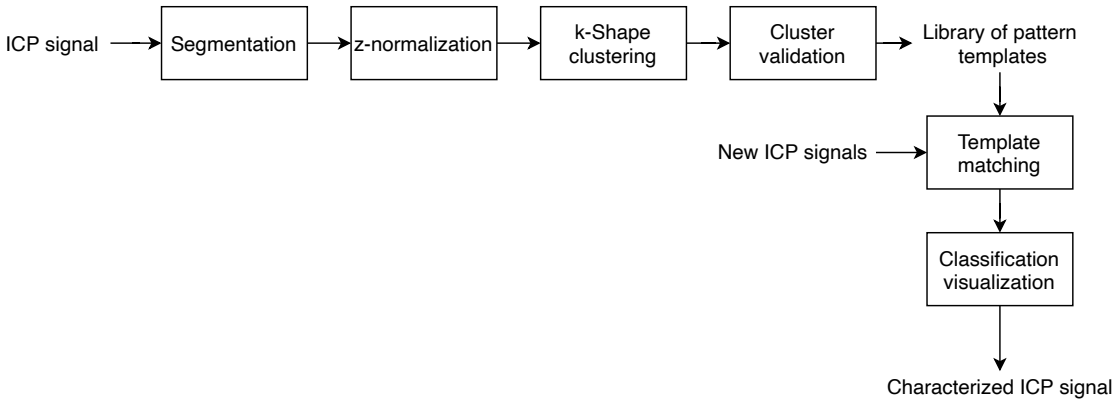

Figure 5.1: Overview of the methodology of Paper V. After being checked for data quality, the ICP signals are segmented into ICP subsequences, z-normalized, and clustered. Clustering results are used for template matching to label ICP subsequences in new incoming data.

Creation of the library of templates
As in any clustering technique, in this subsection we will step through six steps:

1. Choosing the data for the clustering
2. Normalizing the selected data
3. Deciding on the similarity measure for data comparison
4. Choosing the shape-based clustering method
5. Setting the number of clusters to group the data
6. Validating the clustering results

Segmentation and z-normalization. The starting step is choosing the data for clustering, for which we decomposed the signal into a discrete number of ICP subsequences lasting from seconds to minutes. To decide where to locate the start and end points of the subsequences, we first smoothed the signal using a FIR lowpass filter with a cut-off frequency between 0.05 and 0.1Hz. From this lowpass filtered signal, we then calculated the local extrema, from which the minima were used for the segmentation. These minima fulfilled two requirements:

1. The time difference between a minima, g_i, and its neighboring maxima, g_j, was above a threshold η_{dur}, between 0.5 and 2 minutes, and
2. The amplitude difference between a minima, g_i, and its neighboring maxima, g_j, was above a threshold η_{mag}, that takes values between 0.5 and 1.5.

The segmented ICP window (i.e. ICP subsequence) was defined as $g[i,j]$ with i and j corresponding to the discrete indices of the selected minima.

Once the ICP subsequences were generated, the second step was to normalize the data. Normalization is importance to deal with scale and translation invariance to focus on shape features instead of amplitude features [116, 117]. We applied z-normalization to each subsequence to ensure zero mean and standard deviation close to one:

$$z(g[i,j]) = \frac{g[i,j] - \mu_{g[i,j]}}{\sigma_{g[i,j]}} \tag{5.1}$$

where $\mu_{g[i,j]}$ and $\sigma_{g[i,j]}$ were the mean and standard deviation of the ICP subsequence $g[i,j]$, respectively. To simplify the notation, we will refer to each z-normalized ICP subsequence $z(g[i,j])$ as z_{icp}. An example of segmentation and z-normalization is illustrated in Figure 5.2.

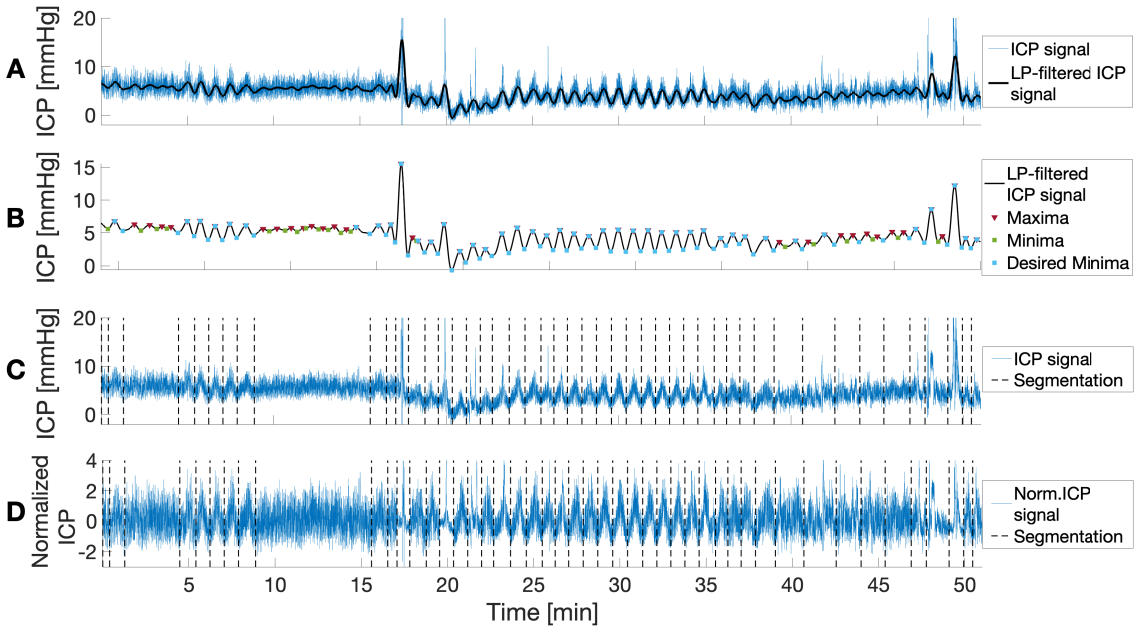

Figure 5.2: Example of the ICP signal segmentation of one subject: (A) after lowpass filtering the ICP signal, with respiratory and pulse contributions to the signal removed to generate the filtered ICP signal; (B) after extracted extrema from filtered ICP signal; (C) after segmentation using desired minima; and (D) after z-normalization of the segmented ICP signal.

Clustering. Deciding on the similarity measure for data comparison goes together with choosing the shape-based clustering method. We implemented k-Shape clustering to group our ICP subsequences into a predefined number of groups, the so-called clusters. ICP subsequences in the same cluster share similar shape characteristics. Each cluster is represented by a centroid determined as the sequence that minimizes the sum of squared distances to the remaining z_{icp}. K-Shape iterates continuously between (i) an assignment step, where each z-normalized ICP subsequences is assigned to the centroid with maximum shape similarity given by the so-called Shape-Based Distance (SBD) from Equation 5.2, and (ii) a refinement step where centroids from each cluster are updated based on new members of each group.

$$SBD(\overrightarrow{x}, \overrightarrow{c_k}) = 1 - max_w \left(\frac{CC_w(\overrightarrow{x}, \overrightarrow{c_k})}{\sqrt{R_0(\overrightarrow{x}, \overrightarrow{x}) \cdot R_0(\overrightarrow{c_k}, \overrightarrow{c_k})}} \right) \tag{5.2}$$

where w is the position at which the cross-correlation $CC_w(\overrightarrow{x}, \overrightarrow{c_k})$ between the z-normalized ICP subsequence ($\overrightarrow{x} = z_{icp}$) and the centroid vector of each cluster ($\overrightarrow{c_k}$) is maximized; and R_0 the autocorrelation of either $\overrightarrow{x}$ or $\overrightarrow{c_k}$. The generated clusters conform the library of scalable templates.

K-shape also required that we predefined the number of clusters to group the data. Medical input suggested a maximum of 20 clusters for clinical relevance. To obtain a more objective measure for optimal selection of number of clusters [118], the so-called silhouette index (SI) was calculated for a range of number of clusters between five and 20. As this metric measures the clustering quality based on the similarity between members from the same cluster and across different clusters, the optimal value of K corresponds to that which maximizes the silhouette metric. The silhouette metric is calculated as follows:

$$S(i) = \frac{b(l) - a(i)}{max\{b(l), a(l)\}} \tag{5.3}$$

where $a(l)$ is the average distance between subsequence l and every subsequence within the same cluster and $b(l)$ is the minimum average distance between subsequence l and every subsequence in different clusters [119].

After walking through the steps presented above, we reached the last step, which involves cluster validation. For this, and given the lack of annotated ground truth data, we selected three internal cluster validation indices (CVI): Silhouette index, Davies-Bouldin index (DBI), and Calinski-Harabasz index (CHI). More thorough mathematic description of these indices can be found in Paper V. For all three—SI, 1-DBI, CHI—higher values are an indication of better clustering solutions.

Characterization of ICP signals
The overall workflow for classifying new ICP subsequences is presented in Figure 5.3. The generated library of templates was used for labeling ICP subsequences (z-normalized) from new data. These query subsequences were compared to each template to find the closest match in shape. SBD was used for this comparison. It might be the case that the closest template match is not meaningful. So, in addition to computing SBD, we added a rule to ensure that the correlation to the closest match ($CC(z_{icp}, \overrightarrow{c_k})$) was meaningful: $CC(z_{icp}, \overrightarrow{c_k}) > 0.50$. The correlation threshold can be specified by the user. This also implies that with our current template library, we will be able to classify only a subset of the ICP signal.

Labeling visualization
Among all the possible ICP subsequence labeling visualization approaches, we introduced a colored box-based representation (Figure 5.4), where each ICP subsequence is displayed as a colored box. The dimensions of the box were given by the duration and difference between the absolute maximum and minimum values of the non-normalized subsequence for the width and height, respectively. Box coloring was done according to the template to which the corresponding ICP subsequence had been matched to, with black color if the correlation requirement was not fulfilled.

5.3.2 Results

The algorithm was developed using data from five patients: two male and three female. This data was randomly selected from overnight monitoring sessions from our continuously updated database at the Department of Neurosurgery, Rigshospitalet, Denmark. A cable ICP probe (Neurovent-P; Raumedic AG, Germany), with sampling frequency equal to 100Hz was used for all these measurements. The length of the measurements summed up to a total of 88 hours. The disease entities of these subjects included hydrocephalus, aneurysm, and craniotomy. Note that further signal analysis was performed on the anonymized recordings without reference to any clinical information.

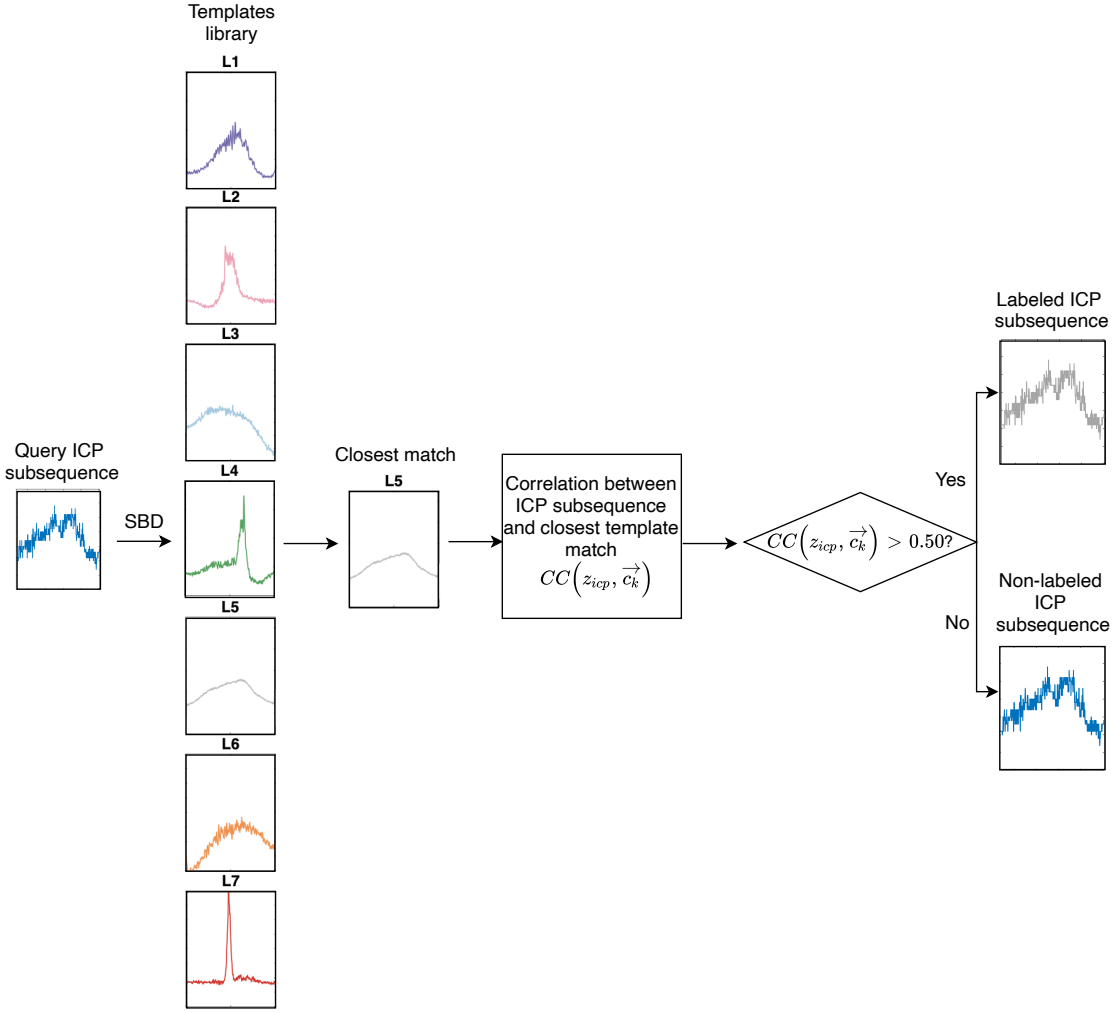

Figure 5.3: Template matching workflow. The SBD between the query ICP subsequence and each of the templates is first calculated. The one with the smallest distance is selected as the closest match. To ensure that the closest match is meaningful, the correlation rule is calculated. If above 0.5, then the ICP subsequence is annotated with the label of the closest match.

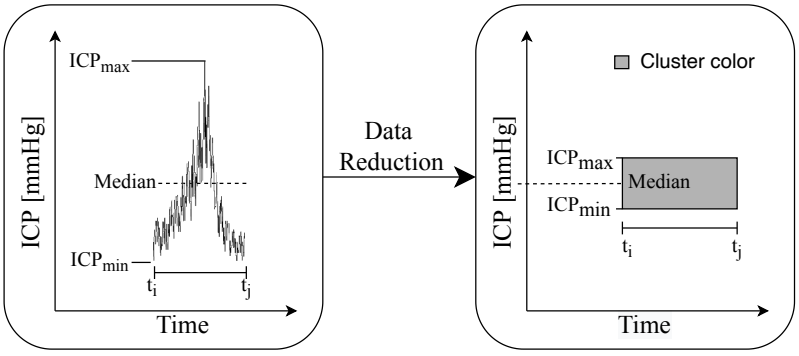

Figure 5.4: Detailed description of data reduction for each labeled ICP subsequence.

As part of the quality validation of the data that was done before the creation of the template library, 18 spikes of less than one second duration were identified as an average, in each of the monitoring sessions, accounting for less than 0.000087% of the total monitoring time. For the last step of the validation, we downsampled all signals to a base frequency of 30Hz.

From the main dataset of 88 hours, after quality validation, we were able to generate 5579 ICP subsequences. After z-normalization, the 5579 ICP subsequences were clustered using the k-Shape algorithm into seven groups. We set K=7 because it gave us the maximum silhouette value for the search range of K=5–20, as seen in Figure 5.5.

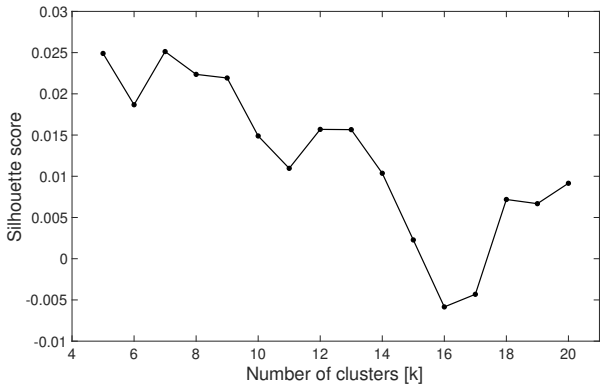

Figure 5.5: Number of optimal K using Silhouette score on the main ICP subsequences.

The clustering results are shown in Figure 5.6. A subset of the ICP recordings can be represented by a combination of these seven generated templates, which can vary in duration and amplitude.

Clustering results were validated using CVIs. Table 5.1 shows how introducing the correlation rule increases the value of the three CVIs. For additional validation of the results, we used an additional dataset of three different subjects, for a total of 55 monitoring hours, to visually confirm that the pattern templates can also be observed in this new data.

CVI	k-Shape	k-Shape with correlation rule
Sil	0.02	0.06
1-DBI	-9.96	-8.19
CHI	115.91	123.15

Table 5.1: Three CVIs for k-Shape clustering without and with correlation rule for the main dataset.

To display the clustering results we must take into consideration that the ICP template matching output should be clinically and visually intelligible for clinicians to find it relevant to use. Figure 5.7 shows an example of our visualization approach for displaying the ICP characterization results.

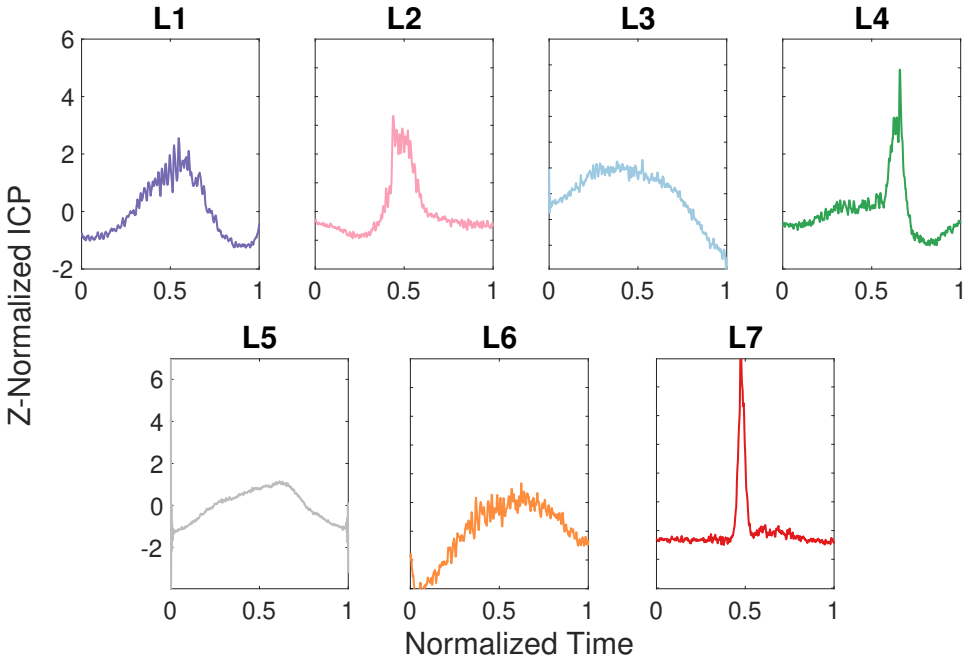

Figure 5.6: Main extracted reproducible ICP subsequences from the 88 hours of ICP recordings. These patterns are the foundation for identifying clinically relevant macro-patterns across a wide cohort of patients, moving away from Lundberg's A and B waves. In contrast to the classical approach, our subsequences could be chained to generate a new macro-pattern.

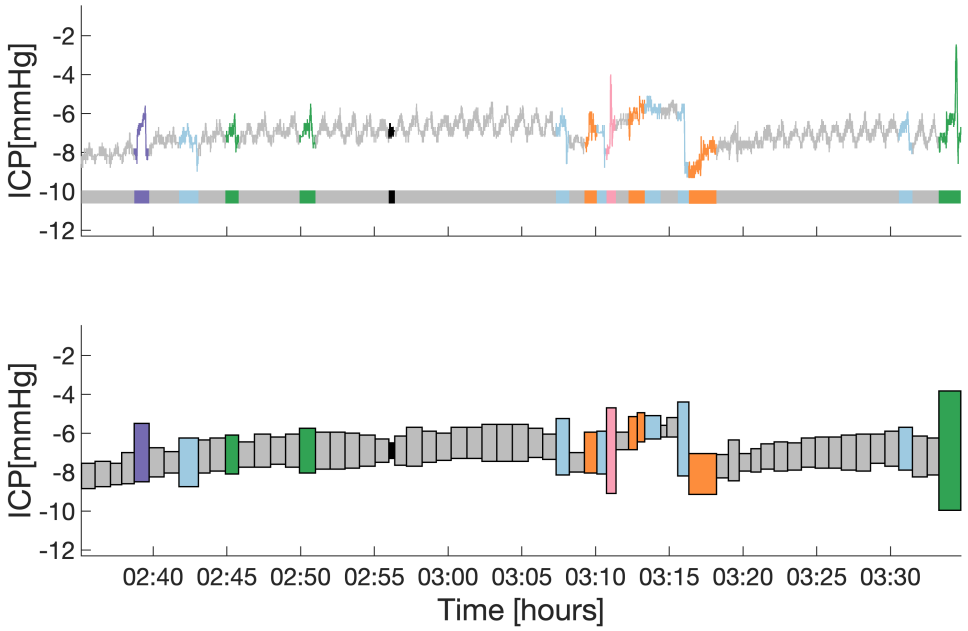

Figure 5.7: Example of the ICP signal segmentation and classification into labels for one subject visualized in the raw signal (top) and in the data reduced signal representation (bottom).

5.3.3 Discussion

Our approach has produced a universal scalable library of seven representative macro-patterns that we intend to use to automatically segment each individual ICP signal into subsequences and link them to additional clinical data. Visual assessment of the templates leads to some preliminary conclusions. Clusters *L1*, *L2*, and *L5* could belong to the same category of clinically well-known waveforms since they show similarity to A- and B-waves.

B-waves have previously been classified, as mentioned in Paper I, according to their shape into symmetrical (sinousoidal), with ascending and descending phases of similar duration; and asymmetrical (ramp-like) waveforms, with duration of the ascending phase longer than that of the descending [73, 77, 78]. Cluster *L1* in our template library resembles these asymmetrical waves, while clusters *L2* and *L5* present more similarity with symmetrical waves. They mainly differ in the presence (*L2*) or absence (*L5*) of a plateau. Pressure values of *L2*-like waveforms would dictate its degree of relation to either A- or B-waves. Clusters *L6* and *L3* are simple ascending and descending segments and could appear before or after a plateau segment, respectively. This plateau can differ in duration and even contain other clinically relevant macro-patterns. Both clusters could also be chained to generate a new macro-pattern described as *L6* followed by *L3*. Cluster *L7* is likely to represent an artefact, given the morphology of the peak. Finally, cluster *L4* is believed to be a non-classified macro-pattern, with clinical relevance yet to be determined. Knowledge of some of these macro-patterns possibly being more indicative of particular disease entities, opens doors to a more personalized management and treatment of each patient as well as better predicting and understanding the possible outcome.

With this library of seven templates, approximately half of the ICP session is labeled. This fact leads to two reasonings: (1) ICP signals are likely to be made up of the same repeated patterns, but distributed differently; and (2) it might be that the current macro-pattern library needs to be expanded to be able to label a larger percentage of the ICP signal. Building on the building blocks set by our methodology and with additional retrospective data, the template library could be extended to include previously unencountered macro-patterns.

To visualize the labeled ICP signal, we introduced a visualization strategy, among many other possibilities, to highlight the encountered seven macro-patterns. The internal distribution and clinical significance of the boxes could be used as an indicator of a certain clinical state.

Limitations

K-Shape clustering presents the limitation that the number of clusters needs to be prespecied by the user and different values of K generates different results if our algorithm is to be used by different research groups. We tried to mitigate this limitation by combining visual inspection of the signals with the Silhouette index, for a more objective choice. Another limitation is that the selection of ICP monitorings for the generation of the template library will likely affect the resulting templates, given that some patterns have more distinguishable macro-patterns than others, which often depends on the pathological state. However, applying the developed algorithm to a wider cohort of patients could minimize this problem.

5.4 Summary and Final Remarks

The investigation carried in Paper V addresses the research questions introduced in this chapter. The answer to each of the questions is reported below:

- Chapter 5 Research Question 1: Is it possible to develop an automated algorithm to find macro-patterns that could help to better describe the ICP signal?
  Answer to Chapter 5 Research Question 1: For our feasibility study presented in Paper V, we used a dataset of a total of 88 hours and extracted seven representative macro pattern subsequences. We expect the addition of additional retrospective data to give rise to new previously unencountered macro patterns. Yet, our developed algorithm can be seen as the benchmark for the shape clustering method that will be used in our ongoing research. Our approach is flexible and allows for custom additional workflows based on the division into subsequences.
- Chapter 5 Research Question 2: Is the developed method generalized? And does it perform equally in data from different disease categories?
  Answer to Chapter 5 Research Question 2: When the proposed method was applied to ICP signals from patients with different diagnoses, it was able to identify the macro-patterns from our template library. However, the method needs to be applied to a bigger cohort of patients to ensure its generalization.
- Chapter 5 Research Question 3: Can the macro-pattern information be presented to a clinical end user in a fashion that is operationally useful?
  Answer to Chapter 5 Research Question 3: We developed a box-based visualization approach that can be seen as a prototype, among all possibilities of graphical representations. The box approach is based on the presence in the ICP signal of the seven identified labels, with many other visualization alternatives yet to be considered.

CHAPTER 6 Conclusions

This dissertation is built upon the research question of whether it is possible to characterize ICP signals using both signal processing and machine learning tools. The scope of this thesis focuses on developing the foundations for a new automatic algorithm for the identification of macro-patterns in ICP signals that could help to characterize the clinical state of the patient. The application of this algorithm has the potential to enable individualized patient treatment and management. This research question is further subdivided into three subquestions with the aim of ensuring a correct workflow that helps to answer the main question. These subquestions are answered below based on the results presented throughout the previous chapters.

Research Question 1 (RQ1): ***Can a better understanding of the physiological origin of ICP waves help to define their physical characteristics to ease their identification?***
Answer to Research Question 1 (RQ1): The sources underlying the presence of ICP waves are helpful in the definition of their characteristic morphology. In Chapter 3 we show that a particular type of ICP waves, the so-called B-waves, are found to be associated with respiratory disturbances. We also observe the vascular contribution of flow velocity to ICP in a limited frequency range within ICP slow waves. This further supports the results presented in this chapter addressing the need for a more adequate description of variations seen in daily clinical practice to better associate the probable physiological origin of the macro-patterns to specific physical characteristics. However, this can only be achieved without solely relying on classical macro-patterns. Therefore, this suggests that there is a need to exploit the potential role of macro-patterns in ICP dynamics beyond Lundberg classical waves and to automate their identification for diagnostic or therapeutic purposes.

Research Question 2 (RQ2): ***Is it possible to provide guidelines/workflow for investigating data quality in the ICP data as a pre-processing step before data analysis?***
Answer to Research Question 2 (RQ2): Chapter 4 shows that before the development and application of an algorithm for the identification of macro-patterns in ICP signals, the quality of the signals needs to be guaranteed through a consistent data quality. This pipeline addresses missing data, non-physiological artefacts in the form of high and rapid spikes, and diverging sampling frequencies in ICP signals. This data quality check workflow prepares the ICP signal before the identification of macro-patterns to avoid that data patterns corresponding to artefacts or missing data mask the underlying structure. The method proposed for spike removal is based on empirical mode decomposition, which is able to handle the non-stationarity and non-linearity of ICP signals.

Research Question 3 (RQ3): ***Can a new automated method, based on machine learning techniques, be used to identify macro-patterns in ICP signals?***
Answer to Research Question 3 (RQ3): Chapter 5 presents the foundations for building an automated method to identify macro-patterns in ICP signals. Our results produced seven distinct and scalable macro-patterns. These findings suggest that ICP signals can be classified into a number of reproducible subsequences, identifiable across a wide cohort of patients. So far, the proposed method seems to be generalized, as it was able to identify the macro-patterns from our template library when applied to ICP signals from patients with different disease entities. We also developed a box-based visualization approach as one among many strategies to ensure that macro-pattern information is presented

in an operationally useful fashion. The entire pipeline can be seen as a flexible starting point that allows for custom additional workflows based on the division into subsequences with the prospect of being able to quantitatively describe how pattern occurrence and distribution varies across diseases.

Based on our contributions, we can conclude that there is a strong potential for automated algorithms to provide good and objective identification of macro-patterns in ICP signals. They permit a more adequate description of the longer timescale ICP variations seen in the broader clinical setting today, with patients undergoing ICP monitoring with mobile equipment. The main advantage is that the clinical use of this technique will reveal a better understanding of the patients underlying physiological status, contributing to a more personalized treatment and disease management. We hope that in the future, with the validation of the algorithm on a larger cohort, it will be used in the clinic as a diagnostic tool, therefore minimizing the time-consuming visual inspection of the long ICP recordings.

CHAPTER 7 Future Work

Establishing reproducible ICP signal macro-patterns without error-prone visual inspection by clinicians will alone be a huge boon in introducing a much needed common nomenclature and it has great potential for personalized management and treatment of neurological disorders. Being able to quantitatively describe how waveform occurrences shift between normal individuals and patients with disturbances of intracranial pressure will have a direct impact on patient care. This thesis has proposed new methods for data quality validation and characerization of ICP signals which have the potential to help other research groups and clinicians with this purpose. In direct continuation of this proposal, this research field needs further investigations which include the following aims:

- To investigate whether it is possible to fully automate our method, not requiring user specific input for η_{dur} and η_{mag} during ICP signal segmentation.
- To ensure that the developed algorithm can be applied to ICP signals with a large percentage of missing data.
- To repeat the template generation algorithm in a larger cohort of patients, to evaluate whether it is possible to identify previously unencountered macro-patterns that could be added to our template library. We will retrospectively ingest and review data from our existing database of over 200 patients, which to the best of our knowledge, is unique in its composition and detail in the world.
- To relate the generated macro-pattern templates to clinical data to ensure that macro-patterns are reproducible and identifiable across a wide cohort of patients with different disease entities. The same database suggested before could be used for this purpose.
- To investigate whether the extracted macro-pattern can be identified in a cohort representing a general (near-to-normal) population, and if there exist identifiable shifts in ICP subsequence pattern distribution between the normal and the pathological population.
- To investigate if disease entities are identifiable based on their internal distribution and weighting of specific ICP signal subsequences. With this in mind, we expect ICP subsequences from the same disease category to contain distinctive reproducible patterns, which will allow us to generate reusable anonymized datasets for each disease category (hydrocephalus, traumatic brain injury etc.).
- To analyze the existence of specific shift configurations that could identify “at risk” patients before critical changes in ICP, mainly in long-term ICP monitoring in the neurointensive care unit.
- To integrate the developed method for ICP signals with multimodal monitoring analysis to clarify sources contributing to distinctive macro-patterns in the ICP signal.
- To implement the proposed methodologies in clinical software and clinical patient bedside management.

Bibliography

[1] J Guillaume and P Janny. “Continuous intracranial manometry; importance of the method and first results”. In: *Revue Neurologique* 84.2 (1951), pp. 131–42.

[2] Nils Lundberg. “Continuous recording and control of ventricular fluid pressure in neurosurgical practice”. In: *Acta Psychiatrica Scandinavica. Supplementum* 36.149 (1960), pp. 1–193.

[3] I. Johnston and Charles Teo. “Disorders of CSF hydrodynamics”. In: *Child’s Nervous System* 16.10-11 (Nov. 2000), pp. 776–799. ISSN: 0256-7040. DOI: 10.1007/s003810000383.

[4] World Health Organization. “Neurological disorders: a public health approach (Neurological disorders associated with malnutrition, Pain associated with neurological disorders, Parkinson’s disease, Stroke, Traumatic brain injuries)”. In: *Neurological Disorders: Public Health Challenges*. 2006. Chap. 3, pp. 41–110. ISBN: 92 4 156336 2.

[5] Daniel F. Kelly, M.D. and Donald P. Becker, M.D. “Advances in Management of Neurosurgical Trauma: USA and Canada”. In: *World Journal of Surgery* 25.9 (Sept. 2001), pp. 1179–1185. ISSN: 0364-2313. DOI: 10.1007/s00268-001-0080-x.

[6] Spencer L James et al. “Global, regional, and national burden of traumatic brain injury and spinal cord injury, 1990–2016: a systematic analysis for the Global Burden of Disease Study 2016”. In: *The Lancet Neurology* 18.1 (Jan. 2019), pp. 56–87. ISSN: 14744422. DOI: 10.1016/S1474-4422(18)30415-0.

[7] K. T. Ragnarsson et al. “Rehabilitation of persons with traumatic brain injury”. In: *Journal of the American Medical Association* 282.10 (Sept. 1999), pp. 974–983. ISSN: 00987484. DOI: 10.1001/jama.282.10.974.

[8] John Chen and Michael Wall. “Epidemiology and Risk Factors for Idiopathic Intracranial Hypertension”. In: *International Ophthalmology Clinics* 54.1 (2014), pp. 1–11. ISSN: 0020-8167. DOI: 10.1097/IIO.0b013e3182aabf11.

[9] Susan P. Mollan et al. “The expanding burden of idiopathic intracranial hypertension”. In: *Eye* 33.3 (Mar. 2019), pp. 478–485. ISSN: 0950-222X. DOI: 10.1038/s41433-018-0238-5.

[10] Maya Harary, Rianne G. Dolmans, and William Gormley. “Intracranial Pressure Monitoring—Review and Avenues for Development”. In: *Sensors* 18.2 (Feb. 2018), p. 465. ISSN: 1424-8220. DOI: 10.3390/s18020465.

[11] M Czosnyka. “Monitoring and interpretation of intracranial pressure”. In: *Journal of Neurology, Neurosurgery and Psychiatry* 75.6 (June 2004), pp. 813–821. ISSN: 0022-3050. DOI: 10.1136/jnnp.2003.033126.

[12] Antonio Di Ieva, Erika M. Schmitz, and Michael D. Cusimano. “Analysis of Intracranial Pressure”. In: *The Neuroscientist* 19.6 (Dec. 2013), pp. 592–603. ISSN: 1073-8584. DOI: 10.1177/1073858412474845.

[13] Xiao Hu et al. “Morphological Clustering and Analysis of Continuous Intracranial Pressure”. In: *IEEE Transactions on Biomedical Engineering* 56.3 (Mar. 2009), pp. 696–705. ISSN: 0018-9294. DOI: 10.1109/TBME.2008.2008636.

[14] Seung-Bo Lee et al. “Artifact removal from neurophysiological signals: impact on intracranial and arterial pressure monitoring in traumatic brain injury”. In: *Journal of Neurosurgery* 132.6 (June 2020), pp. 1952–1960. ISSN: 0022-3085. DOI: 10.3171/2019.2.JNS182260.

[15] Christian Zweifel et al. “Continuous monitoring of cerebrovascular pressure reactivity in patients with head injury”. In: *Neurosurgical Focus* 25.4 (Oct. 2008), E2. ISSN: 1092-0684. DOI: 10.3171/FOC.2008.25.10.E2.

[16] Alexandros Karagiannis, Philip Constantinou, and Demosthenes Vouyioukas. “Biomedical Time Series Processing and Analysis Methods: The Case of Empirical Mode Decomposition”. In: *Advanced Biomedical Engineering*. InTech, Aug. 2011. DOI: 10.5772/20906.

[17] Peter Reinstrup et al. “Cerebral Blood Volume (CBV) in Humans during Normo- and Hypocapnia”. In: *Anesthesiology* 95.5 (Nov. 2001), pp. 1079–1082. ISSN: 0003-3022. DOI: 10.1097/00000542-200111000-00009.

[18] B. Mokri. “The Monro-Kellie hypothesis: Applications in CSF volume depletion”. In: *Neurology* 56.12 (June 2001), pp. 1746–1748. ISSN: 0028-3878. DOI: 10.1212/WNL.56.12.1746.

[19] Alexander Monro. “Observations on the Structure and Functions of the Nervous System, Illustrated with Tables”. In: *London Medical Journal* 4.2 (1783), pp. 113–135. DOI: 10.11588/diglit.4812.

[20] George Kellie. “An account of the appearances observed in the dissection of two of three individuals presumed to have perished in the storm of the 3d, and whose bodies were discovered in the vicinity of Leith on the morning of the 4th, November 1821: with some reflections on the pathology of the brain”. In: *Transactions of the Medico-Chirurgical Society of Edinburgh* (1824), pp. 84–122.

[21] Alifia Tameem and Hari Krovvidi. “Cerebral physiology”. In: *Continuing Education in Anaesthesia Critical Care and Pain* 13.4 (Aug. 2013), pp. 113–118. ISSN: 17431816. DOI: 10.1093/bjaceaccp/mkt001.

[22] M. Kasprowicz et al. “Intracranial pressure, its components and cerebrospinal fluid pressure-volume compensation”. In: *Acta Neurologica Scandinavica* 134.3 (Sept. 2016), pp. 168–180. ISSN: 00016314. DOI: 10.1111/ane.12541.

[23] M. Balestreri et al. “Intracranial hypertension: what additional information can be derived from ICP waveform after head injury?” In: *Acta Neurochirurgica* 146.2 (Feb. 2004), pp. 131–141. ISSN: 0001-6268. DOI: 10.1007/s00701-003-0187-y.

[24] Mohammad I Hirzallah and H Alex Choi. “The Monitoring of Brain Edema and Intracranial Hypertension”. In: *Journal of Neurocritical Care* 9.2 (Dec. 2016), pp. 92–104. ISSN: 2508-1349. DOI: 10.18700/jnc.160093.

[25] C. Strik et al. “Slow Rhythmic Oscillations in Intracranial CSF and Blood Flow: Registered by MRI”. In: *Intracranial Pressure and Brain Biochemical Monitoring*. Vienna: Springer Vienna, 2002, pp. 139–142. DOI: 10.1007/978-3-7091-6738-0_36.

[26] Marek Czosnyka and Zofia Czosnyka. “Origin of intracranial pressure pulse waveform”. In: *Acta Neurochirurgica* 162.8 (Aug. 2020), pp. 1815–1817. ISSN: 0001-6268. DOI: 10.1007/s00701-020-04424-4.

[27] Gustavo Frigieri et al. “Intracranial Pressure Waveform: History, Fundamentals and Applications in Brain Injuries”. In: *Advancement and New Understanding in Brain Injury [Working Title]*. IntechOpen, Oct. 2020. DOI: 10.5772/intechopen.94077.

[28] Usmah Kawoos et al. “Advances in Intracranial Pressure Monitoring and Its Significance in Managing Traumatic Brain Injury”. In: *International Journal of Molecular Sciences* 16.12 (Dec. 2015), pp. 28979–28997. ISSN: 1422-0067. DOI: 10.3390/ijms161226146.

[29] Michael J. Albeck et al. “Intracranial pressure and cerebrospinal fluid outflow conductance in healthy subjects”. In: *Journal of Neurosurgery* 74.4 (Apr. 1991), pp. 597–600. ISSN: 0022-3085. DOI: 10.3171/jns.1991.74.4.0597.
[30] Nicolas Canac et al. “Review: pathophysiology of intracranial hypertension and noninvasive intracranial pressure monitoring”. In: *Fluids and Barriers of the CNS* 17.1 (Dec. 2020), p. 40. ISSN: 2045-8118. DOI: 10.1186/s12987-020-00201-8.
[31] Martin Smith. “Monitoring Intracranial Pressure in Traumatic Brain Injury”. In: *Anesthesia and Analgesia* 106.1 (Jan. 2008), pp. 240–248. ISSN: 0003-2999. DOI: 10.1213/01.ane.0000297296.52006.8e.
[32] Olof Gilland et al. “Normal cerebrospinal fluid pressure”. In: *Journal of Neurosurgery* 40.5 (May 1974), pp. 587–593. ISSN: 0022-3085. DOI: 10.3171/jns.1974.40.5.0587.
[33] J. J. Corbett and M. P. Mehta. “Cerebrospinal fluid pressure in normal obese subjects and patients with pseudotumor cerebri”. In: *Neurology* 33.10 (Oct. 1983), pp. 1386–1386. ISSN: 0028-3878. DOI: 10.1212/WNL.33.10.1386.
[34] Morten Andresen et al. “Effect of postural changes on ICP in healthy and ill subjects”. In: *Acta Neurochirurgica* 157.1 (Jan. 2015), pp. 109–113. ISSN: 0001-6268. DOI: 10.1007/s00701-014-2250-2.
[35] Laurence T Dunn. “Raised Intracranial Pressure”. In: *Journal of Neurology, Neurosurgery and Psychiatry* 73.suppl 1 (Sept. 2002), pp. i23–i27. ISSN: 0022-3050. DOI: 10.1136/jnnp.73.suppl_1.i23.
[36] Charles W Mcmonnies. “The interaction between intracranial pressure, intraocular pressure and lamina cribrosal compression in glaucoma”. In: *Clinical and Experimental Optometry* 99.3 (May 2016), pp. 219–226. ISSN: 0816-4622. DOI: 10.1111/cxo.12333.
[37] P. J. Hutchinson et al. “Intracranial pressure monitoring in severe traumatic brain injury”. In: *BMJ* 346.feb15 1 (Feb. 2013), f1000–f1000. ISSN: 1756-1833. DOI: 10.1136/bmj.f1000.
[38] Karen Brastad Evensen and Per Kristian Eide. “Measuring intracranial pressure by invasive, less invasive or non-invasive means: limitations and avenues for improvement”. In: *Fluids and Barriers of the CNS* 17.1 (Dec. 2020), p. 34. ISSN: 2045-8118. DOI: 10.1186/s12987-020-00195-3.
[39] Sunil Munakomi and Joe M Das. *Intracranial Pressure Monitoring*. 2021.
[40] Susan L. Bratton et al. “VI. Indications for Intracranial Pressure Monitoring”. In: *Journal of Neurotrauma* 24.supplement 1 (May 2007), S–37–S–44. ISSN: 0897-7151. DOI: 10.1089/neu.2007.9990.
[41] P. H. Raboel et al. “Intracranial Pressure Monitoring: Invasive versus Non-Invasive Methods—A Review”. In: *Critical Care Research and Practice* 2012 (2012), pp. 1–14. ISSN: 2090-1305. DOI: 10.1155/2012/950393.
[42] Raimund Helbok et al. “Intracranial Pressure and Cerebral Perfusion Pressure Monitoring in Non-TBI Patients: Special Considerations”. In: *Neurocritical Care* 21.S2 (Dec. 2014), pp. 85–94. ISSN: 1541-6933. DOI: 10.1007/s12028-014-0040-6.
[43] Lykke Larsen et al. “Use of intracranial pressure monitoring in bacterial meningitis: a 10-year follow up on outcome and intracranial pressure versus head CT scans”. In: *Infectious Diseases* 49.5 (May 2017), pp. 356–364. ISSN: 2374-4235. DOI: 10.1080/23744235.2016.1269265.
[44] Aswin Chari et al. “Intraparenchymal intracranial pressure monitoring for hydrocephalus and cerebrospinal fluid disorders”. In: *Acta Neurochirurgica*

159.10 (Oct. 2017), pp. 1967–1978. ISSN: 0001-6268. DOI: 10.1007/s00701-017-3281-2.
[45] Kelly J. Bridges and Ahmed M. Raslan. “Utility of Intracranial Pressure Monitoring for Diagnosis of Idiopathic Intracranial Hypertension in the Absence of Papilledema”. In: *World Neurosurgery* 111 (Mar. 2018), e221–e227. ISSN: 18788750. DOI: 10.1016/j.wneu.2017.12.036.
[46] Susan P Mollan et al. “Idiopathic intracranial hypertension: consensus guidelines on management”. In: *Journal of Neurology, Neurosurgery and Psychiatry* 89.10 (Oct. 2018), 1088 LP –1100. DOI: 10.1136/jnnp-2017-317440.
[47] G. Kesava Reddy, Papireddy Bollam, and Gloria Caldito. “Long-Term Outcomes of Ventriculoperitoneal Shunt Surgery in Patients with Hydrocephalus”. In: *World Neurosurgery* 81.2 (Feb. 2014), pp. 404–410. ISSN: 18788750. DOI: 10.1016/j.wneu.2013.01.096.
[48] Venessa L. Pinto, Prasanna Tadi, and Adebayo Adeyinka. *Increased Intracranial Pressure*. 2021.
[49] Institute AftAoMIICPDSANS. *Intracranial Pressure Monitoring Devices*. 1993.
[50] Deb Sanjay Nag et al. “Intracranial pressure monitoring: Gold standard and recent innovations”. In: *World Journal of Clinical Cases* 7.13 (July 2019), pp. 1535–1553. ISSN: 2307-8960. DOI: 10.12998/wjcc.v7.i13.1535.
[51] Samon Tavakoli et al. “Complications of invasive intracranial pressure monitoring devices in neurocritical care”. In: *Neurosurgical Focus* 43.5 (Nov. 2017), E6. ISSN: 1092-0684. DOI: 10.3171/2017.8.FOCUS17450.
[52] Herbert I. Fried et al. “The Insertion and Management of External Ventricular Drains: An Evidence-Based Consensus Statement”. In: *Neurocritical Care* 24.1 (Feb. 2016), pp. 61–81. ISSN: 1541-6933. DOI: 10.1007/s12028-015-0224-8.
[53] S. Rot et al. “Comparative investigation of different telemetric methods for measuring intracranial pressure: a prospective pilot study”. In: *Fluids and Barriers of the CNS* 17.1 (Dec. 2020), p. 63. ISSN: 2045-8118. DOI: 10.1186/s12987-020-00225-0.
[54] Mahmoud Omidbeigi et al. “Telemetric Intracranial Pressure Monitoring: A Systematic Review”. In: *Neurocritical Care* 34.1 (Feb. 2021), pp. 291–300. ISSN: 1541-6933. DOI: 10.1007/s12028-020-00992-6.
[55] Marek Czosnyka et al. “Intracranial Pressure: More Than a Number”. In: *Neurosurgical Focus* 22.5 (May 2007), pp. 1–7. ISSN: 1092-0684. DOI: 10.3171/foc.2007.22.5.11.
[56] Xiao Hu, Nestor Gonzalez, and Marvin Bergsneider. “Steady-state indicators of the intracranial pressure dynamic system using geodesic distance of the ICP pulse waveform”. In: *Physiological Measurement* 33.12 (Dec. 2012), pp. 2017–2031. ISSN: 0967-3334. DOI: 10.1088/0967-3334/33/12/2017.
[57] F. Scalzo et al. “Intracranial Pressure Signal Morphology: Real-Time Tracking”. In: *IEEE Pulse* 3.2 (Mar. 2012), pp. 49–52. ISSN: 2154-2287. DOI: 10.1109/MPUL.2011.2181024.
[58] Magdalena Kasprowicz et al. “Association Between ICP Pulse Waveform Morphology and ICP B Waves”. In: 2012, pp. 29–34. DOI: 10.1007/978-3-7091-0956-4_6.
[59] Fabien Scalzo et al. “Robust Peak Recognition in Intracranial Pressure Signals”. In: *BioMedical Engineering OnLine* 9.1 (2010), p. 61. ISSN: 1475-925X. DOI: 10.1186/1475-925X-9-61.

[60] J J Lemaire et al. “Slow pressure waves in the cranial enclosure”. eng. In: *Acta Neurochirurgica* 144.3 (2002), pp. 243–254. ISSN: 0001-6268. DOI: 10.1007/s007010200032. URL: http://www.ncbi.nlm.nih.gov/pubmed/11956937.

[61] J.-J. Lemaire et al. “A computer software for frequential analysis of slow intracranial pressure waves”. In: *Computer Methods and Programs in Biomedicine* 42.1 (Feb. 1994), pp. 1–14. ISSN: 01692607. DOI: 10.1016/0169-2607(94)90133-3.

[62] K. Hara et al. “A Minicomputer System for Analysis and Display of ICP Related Data”. In: *Intracranial Pressure VII*. Berlin, Heidelberg: Springer Berlin Heidelberg, 1989, pp. 132–134. DOI: 10.1007/978-3-642-73987-3_35.

[63] Sverre Holm and Per Kristian Eide. “The frequency domain versus time domain methods for processing of intracranial pressure (ICP) signals”. In: *Medical Engineering and Physics* 30.2 (Mar. 2008), pp. 164–170. ISSN: 13504533. DOI: 10.1016/j.medengphy.2007.03.003.

[64] Anders Eklund et al. “Two computerized methods used to analyze intracranial pressure B waves: comparison with traditional visual interpretation”. In: *Journal of Neurosurgery* 94.3 (Mar. 2001), pp. 392–396. ISSN: 0022-3085. DOI: 10.3171/jns.2001.94.3.0392.

[65] Eduard Ramon Maldonado. “Algorithms for B waves detection”. PhD thesis. 2013.

[66] Magdalena Kasprowicz et al. “Pattern recognition of overnight intracranial pressure slow waves using morphological features of intracranial pressure pulse”. In: *Journal of Neuroscience Methods* 190.2 (July 2010), pp. 310–318. ISSN: 01650270. DOI: 10.1016/j.jneumeth.2010.05.015.

[67] Steven L. Brunton and J. Nathan Kutz. *Data-Driven Science and Engineering*. Cambridge University Press, Jan. 2019. ISBN: 9781108380690. DOI: 10.1017/9781108380690.

[68] Rolf R. Diehl et al. “Spontaneous blood pressure oscillations and cerebral autoregulation”. In: *Clinical Autonomic Research* 8.1 (Feb. 1998), pp. 7–12. ISSN: 0959-9851. DOI: 10.1007/BF02267598.

[69] D Bernard. “Du suc pancreatique et de son role dans les phenomenes de la digestion”. In: *Mémoires du Société de Biologie* 1 (1849), pp. 99–115.

[70] W B Cannon and A Pettit. “A Charles Richet: ses amis, ses collègues, ses élèves”. In: *Paris: Les Éditions Médicales* (1926).

[71] Steven J. Cooper. “From Claude Bernard to Walter Cannon. Emergence of the concept of homeostasis”. In: *Appetite* 51.3 (Nov. 2008), pp. 419–427. ISSN: 01956663. DOI: 10.1016/j.appet.2008.06.005.

[72] Cheng-Wei Lu et al. “Complexity of intracranial pressure correlates with outcome after traumatic brain injury.” In: *Brain : a journal of neurology* 135.Pt 8 (Aug. 2012), pp. 2399–408. ISSN: 1460-2156. DOI: 10.1093/brain/aws155.

[73] Andreas Spiegelberg, Matthias Preuß, and Vartan Kurtcuoglu. “B-waves revisited”. In: *Interdisciplinary Neurosurgery* 6 (Dec. 2016), pp. 13–17. ISSN: 22147519. DOI: 10.1016/j.inat.2016.03.004.

[74] Erta Beqiri et al. “Influence of mild-moderate hypocapnia on intracranial pressure slow waves activity in TBI”. In: *Acta Neurochirurgica* 162.2 (Feb. 2020), pp. 345–356. ISSN: 0001-6268. DOI: 10.1007/s00701-019-04118-6.

[75] J. K. Krauss et al. “The relation of intracranial pressure B-waves to different sleep stages in patients with suspected normal pressure hydrocephalus”. In: *Acta Neurochirurgica* 136.3-4 (Sept. 1995), pp. 195–203. ISSN: 0001-6268. DOI: 10.1007/BF01410626.

[76] Alessandro Liberati et al. “The PRISMA statement for reporting systematic reviews and meta-analyses of studies that evaluate healthcare interventions: explanation and elaboration.” In: *BMJ (Clinical research ed.)* 339 (2009). ISSN: 14685833. DOI: 10.1136/bmj.b2700.

[77] Christian Raftopoulos et al. “Morphological quantitative analysis of intracranial pressure waves in normal pressure hydrocephalus”. In: *Neurological Research* 14.5 (Jan. 1992), pp. 389–396. ISSN: 0161-6412. DOI: 10.1080/01616412.1992.11740091.

[78] David Santamarta et al. “The Prediction of Shunt Response in Idiopathic Normal-Pressure Hydrocephalus Based on Intracranial Pressure Monitoring and Lumbar Infusion”. In: 2016, pp. 267–274. DOI: 10.1007/978-3-319-22533-3_53.

[79] Akira Yokota et al. “Overnight Recordings of Intracranial Pressure and Electroencephalography in Neurosurgical Patients”. In: *Journal of UOEH* 11.4 (1989), pp. 371–381. ISSN: 0387-821X. DOI: 10.7888/juoeh.11.371.

[80] P. W. Hanlo et al. “Relationship between anterior fontanelle pressure measurements and clinical signs in infantile hydrocephalus”. In: *Child’s Nervous System* 12.4 (Apr. 1996), pp. 200–209. ISSN: 0256-7040. DOI: 10.1007/BF00301251.

[81] Despina Afroditi Lalou et al. “Are Slow Waves of Intracranial Pressure Suppressed by General Anaesthesia?” In: 2018, pp. 129–132. DOI: 10.1007/978-3-319-65798-1_27.

[82] Robert Hamilton et al. “Intracranial pressure pulse waveform correlates with aqueductal cerebrospinal fluid stroke volume”. In: *Journal of Applied Physiology* 113.10 (Nov. 2012), pp. 1560–1566. ISSN: 8750-7587. DOI: 10.1152/japplphysiol.00357.2012.

[83] Xiao Hu et al. “Automated Extraction of Decision Rules for Predicting Lumbar Drain Outcome by Analyzing Overnight Intracranial Pressure”. In: 2012, pp. 207–212. DOI: 10.1007/978-3-7091-0956-4_40.

[84] Manjari Tripathi. “Technical notes for digital polysomnography recording in sleep medicine practice”. In: *Annals of Indian Academy of Neurology* 11.2 (2008), p. 129. ISSN: 0972-2327. DOI: 10.4103/0972-2327.41887.

[85] Vina Meliana et al. “Interpretation of sleep studies for patients with sleep-disordered breathing: What the anesthesiologist needs to know”. In: *Canadian Journal of Anesthesia/Journal canadien d’anesthésie* 65.1 (Jan. 2018), pp. 60–75. ISSN: 0832-610X. DOI: 10.1007/s12630-017-0988-8.

[86] D W Droste et al. “Middle Cerebral Artery Blood Flow Velocity in Healthy Persons During Wakefulness and Sleep: A Transcranial Doppler Study”. In: *Sleep* 16.7 (Oct. 1993), pp. 603–609. ISSN: 0161-8105. DOI: 10.1093/sleep/16.7.603.

[87] Marek Czosnyka et al. “Cerebrospinal fluid dynamics”. In: *Physiological Measurement* 25.5 (Oct. 2004), R51–R76. ISSN: 0967-3334. DOI: 10.1088/0967-3334/25/5/R01.

[88] J.C. Hirsch, P. Pierre-Kahn, and J.F. Hirsch. “Experimental study of intracranial pressure during rapid eye movement sleep in the chronic cat”. In: *Neuroscience Letters* 7.2-3 (Feb. 1978), pp. 245–249. ISSN: 03043940. DOI: 10.1016/0304-3940(78)90176-3.

[89] G Martin. “Lundberg’s B waves as a feature of normal intracranial pressure”. In: *Surgical Neurology* 9.6 (1978), pp. 347–8.

[90] Dirk Droste and Joachim Krauss. “Oscillations of cerebrospinal fluid pressure in nonhydrocephalic persons”. In: *Neurological Research* 19.2 (Apr. 1997), pp. 135–138. ISSN: 0161-6412. DOI: 10.1080/01616412.1997.11740786.

[91] Doreen Mautner-Huppert et al. “B-waves in healthy persons”. In: *Neurological Research* 11.4 (Dec. 1989), pp. 194–196. ISSN: 0161-6412. DOI: 10.1080/01616412.1989.11739891.

[92] David W. Newell et al. “The relationship of blood flow velocity fluctuations to intracranial pressure B waves”. In: *Journal of Neurosurgery* 76.3 (Mar. 1992), pp. 415–421. ISSN: 0022-3085. DOI: 10.3171/jns.1992.76.3.0415.

[93] Ralf Steinmeier et al. “Slow Rhythmic Oscillations of Blood Pressure, Intracranial Pressure, Microcirculation, and Cerebral Oxygenation”. In: *Stroke* 27.12 (Dec. 1996), pp. 2236–2243. ISSN: 0039-2499. DOI: 10.1161/01.STR.27.12.2236.

[94] D W Droste and J K Krauss. “Simultaneous recording of cerebrospinal fluid pressure and middle cerebral artery blood flow velocity in patients with suspected symptomatic normal pressure hydrocephalus.” In: *Journal of Neurology, Neurosurgery and Psychiatry* 56.1 (Jan. 1993), pp. 75–79. ISSN: 0022-3050. DOI: 10.1136/jnnp.56.1.75.

[95] Tiina Näsi et al. “Spontaneous Hemodynamic Oscillations during Human Sleep and Sleep Stage Transitions Characterized with Near-Infrared Spectroscopy”. In: *PLoS ONE* 6.10 (Oct. 2011). Ed. by Pedro Antonio Valdes-Sosa, e25415. ISSN: 1932-6203. DOI: 10.1371/journal.pone.0025415.

[96] Ruwan Alwis Weerakkody et al. “Near Infrared Spectroscopy as Possible Non-invasive Monitor of Slow Vasogenic ICP Waves”. In: 2012, pp. 181–185. DOI: 10.1007/978-3-7091-0956-4_35.

[97] R. Cooper and A. Hulme. “Intracranial pressure and related phenomena during sleep”. In: *Journal of Neurology, Neurosurgery and Psychiatry* 29.6 (Dec. 1966), pp. 564–570. ISSN: 0022-3050. DOI: 10.1136/jnnp.29.6.564.

[98] Poul Jennum and Svend Erik Børgesen. “Intracranial Pressure and Obstructive Sleep Apnea”. In: *Chest* 95.2 (Feb. 1989), pp. 279–283. ISSN: 00123692. DOI: 10.1378/chest.95.2.279.

[99] Zhaohua Wu and Norden E. Huang. “ENSEMBLE EMPIRICAL MODE DECOMPOSITION: A NOISE-ASSISTED DATA ANALYSIS METHOD”. In: *Advances in Adaptive Data Analysis* 01.01 (Jan. 2009), pp. 1–41. ISSN: 1793-5369. DOI: 10.1142/S1793536909000047.

[100] Daoud Boutana, Messaoud Benidir, and Braham Barkat. “On the selection of Intrinsic Mode Function in EMD method: Application on heart sound signal”. In: *2010 3rd International Symposium on Applied Sciences in Biomedical and Communication Technologies (ISABEL 2010)*. IEEE, Nov. 2010, pp. 1–5. ISBN: 978-1-4244-8131-6. DOI: 10.1109/ISABEL.2010.5702895.

[101] P. Janny. “La pression intracrânienne chez l’homme. Méthode d’enregistrement. Etude de ses variations et de ses rapports avec les signes cliniques et ophtalmologiques.” PhD thesis. 1950.

[102] Mengling Feng et al. “Artifact removal for intracranial pressure monitoring signals: A robust solution with signal decomposition”. In: *2011 Annual International Conference of the IEEE Engineering in Medicine and Biology Society*. IEEE, Aug. 2011, pp. 797–801. ISBN: 978-1-4577-1589-1. DOI: 10.1109/IEMBS.2011.6090182.

[103] Mengling Feng et al. *Artifact correction with robust statistics for non-stationary intracranial pressure signal monitoring*. eng. 2012.

[104] A. Zeiler et al. “Sliding Empirical Mode Decomposition-Brain Status Data Analysis and Modeling”. In: 2013, pp. 311–349. DOI: 10.1007/978-3-642-28696-4_12.

[105] S. Higashi et al. “The Role of Vasomotor Center and Adrenergic Pathway in B-Waves”. In: *Intracranial Pressure VII*. Berlin, Heidelberg: Springer Berlin Heidelberg, 1989, pp. 220–224. DOI: 10.1007/978-3-642-73987-3_60.

[106] L. M. Auer and I. Sayama. “Intracranial pressure oscillations (B-waves) caused by oscillations in cerebrovascular volume”. In: *Acta Neurochirurgica* 68.1-2 (Mar. 1983), pp. 93–100. ISSN: 0001-6268. DOI: 10.1007/BF01406205.

[107] Thomas C. Redman. “Bad Data Costs the U.S. $3 Trillion Per Year”. In: *Hardvard Business Review* (2016).

[108] Ralf Gitzel. “Data Quality in Time Series Data An Experience Report”. In: *Ceur Workshop Proceedings*. 2016, pp. 41–49.

[109] Cigdem Polat Dautov and Mehmet Sirac Ozerdem. “Wavelet transform and signal denoising using Wavelet method”. In: *2018 26th Signal Processing and Communications Applications Conference (SIU)*. IEEE, May 2018, pp. 1–4. ISBN: 978-1-5386-1501-0. DOI: 10.1109/SIU.2018.8404418.

[110] Paul A. Harris et al. “Research electronic data capture (REDCap)—A metadata-driven methodology and workflow process for providing translational research informatics support”. In: *Journal of Biomedical Informatics* 42.2 (Apr. 2009), pp. 377–381. ISSN: 15320464. DOI: 10.1016/j.jbi.2008.08.010.

[111] A. O.; Boudraa, J. C.; Cexus, and Z. Saidi. “EMD-Based Signal Noise Reduction”. In: *Proceedings of World Academy of Science, Engineering and TechnologyEngineering and Technology* 2 (2005), pp. 93–96.

[112] David L. Olson and Dursun Delen. *Advanced Data Mining Techniques*. Berlin, Heidelberg: Springer Berlin Heidelberg, 2008, p. 138. ISBN: 978-3-540-76916-3. DOI: 10.1007/978-3-540-76917-0.

[113] Donald B. Rubin. “Inference and missing data”. In: *Biometrika* 63.3 (1976), pp. 581–592. ISSN: 0006-3444. DOI: 10.1093/biomet/63.3.581.

[114] Denis Kwiatkowski et al. “Testing the null hypothesis of stationarity against the alternative of a unit root”. In: *Journal of Econometrics* 54.1-3 (Oct. 1992), pp. 159–178. ISSN: 03044076. DOI: 10.1016/0304-4076(92)90104-Y.

[115] Angela Stallone, Antonio Cicone, and Massimo Materassi. “New insights and best practices for the successful use of Empirical Mode Decomposition, Iterative Filtering and derived algorithms”. In: *Scientific Reports* 10.1 (Dec. 2020), p. 15161. ISSN: 2045-2322. DOI: 10.1038/s41598-020-72193-2.

[116] Saeed Aghabozorgi et al. “A hybrid algorithm for clustering of time series data based on affinity search technique”. In: *The Scientific World Journal* 2014 (2014). ISSN: 1537744X. DOI: 10.1155/2014/562194.

[117] Ali Javed, Byung Suk Lee, and Donna M. Rizzo. “A benchmark study on time series clustering”. In: *arXiv* 1.July (2020), p. 100001. ISSN: 23318422. DOI: 10.1016/j.mlwa.2020.100001. arXiv: 2004.09546.

[118] Alexis Sardá-Espinosa. “Comparing time-series clustering algorithms in R using the dtwclust package”. In: *R Journal* 11.1 (2019), pp. 1–45. ISSN: 20734859.

[119] Artur Starczewski and Adam Krzyżak. “Performance Evaluation of the Silhouette Index”. In: 2015, pp. 49–58. DOI: 10.1007/978-3-319-19369-4_5.

[120] Qin Wei et al. “Analysis of EEG via Multivariate Empirical Mode Decomposition for Depth of Anesthesia Based on Sample Entropy”. In: *Entropy* 15.12 (Aug. 2013), pp. 3458–3470. ISSN: 1099-4300. DOI: 10.3390/e15093458.

[121] Ke Fang et al. “Comparison of EMD and EEMD in rolling bearing fault signal analysis”. In: *2018 IEEE International Instrumentation and Measurement Technology Conference (I2MTC)*. IEEE, May 2018, pp. 1–5. ISBN: 978-1-5386-2222-3. DOI: 10.1109/I2MTC.2018.8409666.

[122] N E Huang et al. “The empirical mode decomposition and the Hilbert spectrum for nonlinear and non-stationary time series analysis”. eng. In: *Proceedings of the Royal Society A-mathematical Physical and Engineering Sciences* 454.1971 (1998), pp. 903–995. ISSN: 14712946, 13645021.

[123] Shiqiang Qin, Qiuping Wang, and Juntao Kang. “Output-Only Modal Analysis Based on Improved Empirical Mode Decomposition Method”. In: *Advances in Materials Science and Engineering* 2015 (2015), pp. 1–12. ISSN: 1687-8434. DOI: 10.1155/2015/945862.

[124] R. K. ; Niazy et al. “Performance evaluation of ensemble empirical mode decomposition”. In: *Advances in Adaptive Data Analysis* 01.02 (Apr. 2009), pp. 231–242. ISSN: 1793-5369. DOI: 10.1142/S1793536909000102.

[125] C. W. J. Granger. “Investigating Causal Relations by Econometric Models and Cross-spectral Methods”. In: *Econometrica* 37.3 (Aug. 1969), p. 424. ISSN: 00129682. DOI: 10.2307/1912791.

[126] Lionel Barnett and Anil K. Seth. “The MVGC multivariate Granger causality toolbox: A new approach to Granger-causal inference”. In: *Journal of Neuroscience Methods* 223 (Feb. 2014), pp. 50–68. ISSN: 01650270. DOI: 10.1016/j.jneumeth.2013.10.018.

[127] H. Akaike. “A new look at the statistical model identification”. In: *IEEE Transactions on Automatic Control* 19.6 (Dec. 1974), pp. 716–723. ISSN: 0018-9286. DOI: 10.1109/TAC.1974.1100705.

[128] J Durbin and G S Watson. “Testing for serial correlation in least squares regression”. eng. In: *Biometrika* 38.1-2 (1951), pp. 159–178. ISSN: 00063444.

[129] Anil Seth. “Granger causality”. In: *Scholarpedia* 2.7 (2007), p. 1667. ISSN: 1941-6016. DOI: 10.4249/scholarpedia.1667.

[130] John Geweke. “Measurement of Linear Dependence and Feedback between Multiple Time Series”. In: *Journal of the American Statistical Association* 77.378 (June 1982), pp. 304–313. ISSN: 0162-1459. DOI: 10.1080/01621459.1982.10477803.

CHAPTER A Scientific Papers

A.1 Paper I

Title: B-waves: a systematic review of terminology, characteristics, and analysis methods

Authors: Isabel Martinez-Tejada, Alexander Arum, Jens E. Wilhjelm, Marianne Juhler, and Morten Andresen

Journal: Fluids and Barriers of the CNS

Status: Published

DOI: 10.1186/s12987-019-0153-6

Martinez-Tejada *et al. Fluids Barriers CNS* (2019) 16:33
https://doi.org/10.1186/s12987-019-0153-6

Fluids and Barriers of the CNS

REVIEW Open Access

B waves: a systematic review of terminology, characteristics, and analysis methods

Isabel Martinez-Tejada[1,2*], Alexander Arum[1], Jens E. Wilhjelm[2], Marianne Juhler[1] and Morten Andresen[1]

Abstract

***Background*:** Although B waves were introduced as a concept in the analysis of intracranial pressure (ICP) recordings nearly 60 years ago, there is still a lack consensus on precise definitions, terminology, amplitude, frequency or origin. Several competing terms exist, addressing either their probable physiological origin or their physical characteristics. To better understand B wave characteristics and ease their detection, a literature review was carried out.

***Methods*:** A systematic review protocol including search strategy and eligibility criteria was prepared in advance. A literature search was carried out using PubMed/MEDLINE, with the following search terms: *B waves* + *review filter*, *slow waves* + *review filter*, *ICP B waves*, *slow ICP waves*, *slow vasogenic waves*, *Lundberg B waves*, *MOCAIP*.

***Results*:** In total, 19 different terms were found, *B waves* being the most common. These terminologies appear to be interchangeable and seem to be used indiscriminately, with some papers using more than five different terms. Definitions and etiologies are still unclear, which makes systematic and standardized detection difficult.

***Conclusions*:** Two future lines of action are available for automating macro-pattern identification in ICP signals: achieving strict agreement on morphological characteristics of "traditional" B waveforms, or starting a new with a fresh computerized approach for recognition of new clinically relevant patterns.

Keywords: Intracranial pressure, B waves, Slow waves, Vasogenic waves

Background

Intracranial pressure (ICP) monitoring plays an important role in the management of patients with many neurological and neurosurgical disorders. In the 1960s, Lundberg described typical macro-patterns: A, B and C waves [1]. B waves were defined as short repeating elevations in ICP (10–20 mmHg) with a frequency of 0.5–2 waves/min. These classic B wave patterns may be seen in ICP monitoring in intensive care unit settings (ICU), but ICP is also monitored in a large number of brain diseases covering a spectrum from acute and subacute ICU settings to elective outpatient follow-up. Today a large proportion of patients undergo ICP monitoring for milder degrees of disease where pathological patterns are not as prominent. In such scenarios, wave patterns are still called B waves but differ in amplitude and visual appearance from those defined by Lundberg. Such 'uncharacteristic' B waves are often smaller in amplitude and appear as an irregular pattern, but they have not yet been formally classified. The current paper uses B waves as an encompassing umbrella for all variations.

The source of B waves is unknown and although they are mostly associated with cerebral dysfunction, their clinical significance is unclear, as they may also appear as normal physiological phenomena [2, 3]. Their source is most commonly related to vasogenic activity, but an origin from a neuro-pacemaker system has also been suggested [4]. This diverging information poses a challenge to a consensus for a general description of B waves and their quantification, hindering their identification during diagnosis and treatment of different diseases categories. Because of these difficulties, clinical practice outside specialized centers with a focus on ICP-related research is currently largely restricted to readings of mean ICP.

Identification of waveform abnormalities by simple visual inspection is still a common clinical practice. This has

*Correspondence: imate@dtu.dk
[1] Clinic of Neurosurgery, Copenhagen University Hospital, Rigshospitalet, Copenhagen, Denmark
Full list of author information is available at the end of the article

an obvious bias from reliance on personal empiric experience and raises questions of interobserver reproducibility. Automated and standardized detection of B wave patterns would increase the usefulness in both clinical and research settings. This automated detection is only possible if the waveform morphological characteristics are clearly defined; preferably by consensus in the scientific community. A systematic quantitative detection system could allow for identification of B wave variations and other 'non-Lundberg' patterns, replacing traditional visual inspection.

The aim of this study was to assess the various terms and definitions used to describe classical B waves in order to highlight the lack of consensus in terms of terminology and morphological characteristics, frequency and amplitude. Therefore, a systematic review was carried out to summarize the different terminologies and definitions regarding B waves and the methods used for B wave identification.

Methods

Relevant studies were identified by a single reviewer using the online database PubMed/Medline. The diagram in Fig. 1 gives an overview of the literature search based on the PRISMA systematic review methodology [5]. Studies were selected if they included the key terms *slow vasogenic waves*, *Lundberg B waves*, *slow ICP waves*, *ICP B waves*, *MOCAIP*, *B waves + review filter*, and *slow waves + review filter*. A total sum of 816 paper abstracts were screened initially for content relevance and 124 papers were included in the search review.

Results

Terminologies

A total of 19 terminologies were found to describe B waves in the reviewed papers (Table 1). The most common terms being *B waves* and *(ICP) slow waves* (Fig. 2). Nine articles used four or more terms to refer to B waves. The choice of terminology is often related to the ongoing etiology discussion: 22 articles include the word *vasogenic* thereby implying cerebrovascular changes as the origin of the waves. Raftopoulos [6], Santamarta [7], Yokota [8], and Kasprowicz [9], defined further subgroups in order to clarify the sources underlying the presence of B waves (Table 2).

Characteristics

B waves were identified based on two major wave parameters: frequency and amplitude. Frequency is the number of waves that fit into a certain time period, usually measured as waves per minute and 27% of the papers defined a frequency of 0.5–2 waves/min, as originally defined by Lundberg [1]. To accommodate B waves of a lower frequency, the term *slow* was introduced [10]. The term *slow waves* was then used to define waves with a frequency window of 0.33 to 3 waves/min [11]. Two other papers extended the frequency upper limit to 4 waves/min [12, 13].

As mentioned, B waves can also be characterized by their amplitude. Lundberg defined a maximum amplitude of 50 mmHg back in the 1960s. Under pathological conditions, this level of elevation is less often seen to such an extent today, and B waves with lower amplitudes are more likely to be present. As an example, lower amplitude B waves are present in cases of normal pressure hydrocephalus, where the occurrence of B waves is not related to high ICP [14].

Sub-classification

In addition to frequency and amplitude, two other parameters are generally defined for the analysis of B waves. B waves can also be characterized by their shape and whether a plateau phase is present or not. The shape is considered symmetrical if the duration of ascending and descending phases is the same. If the ascending phase is longer, then the shape is asymmetrical. The use of these parameters gives rise to different subclasses within B waves (Table 2). All subclasses fit into the traditional definition of B waves with an extended frequency spectrum, but mainly differ in their morphological characteristics (Fig. 3).

Besides these four parameters, Raftopolous et al. and Santamarta et al. also use the duration of the ICP wave to characterize B waves. They distinguish between three morphological subclasses: (1) small symmetrical waves with an amplitude below 10 mmHg, (2) great symmetrical waves with an amplitude above 10 mmHg, and (3) intermediate waves, with the same frequency as symmetrical waves but an amplitude similar to plateau waves [6, 7].

Kasprowicz et al. describe three subcategories of B waves based on the investigation of their unique shape: (1) symmetrical ICP B waves, (2) asymmetrical ICP B waves, and (3) slow ICP B waves with plateau phase. They show how the different subtypes of B waves are related to changes in the ICP pulse shape, which indicate that each has a unique origin [9]. Similarly, Yokota et al. also suggest the existence of three subgroups but from the analysis of ICP amplitude and occurrence: (1) episodic B-waves, (2) persistent, high pressure B-waves, and (3) continuous, regular B-waves, and that these patterns may better distinguish between different origins of ICP waves [8].

The intermediate waves described by Raftopolous et al. [6] and Santamarta et al. [7] contain amplitudes similar to plateau waves, Kasprowicz et al. [9] describe B waves

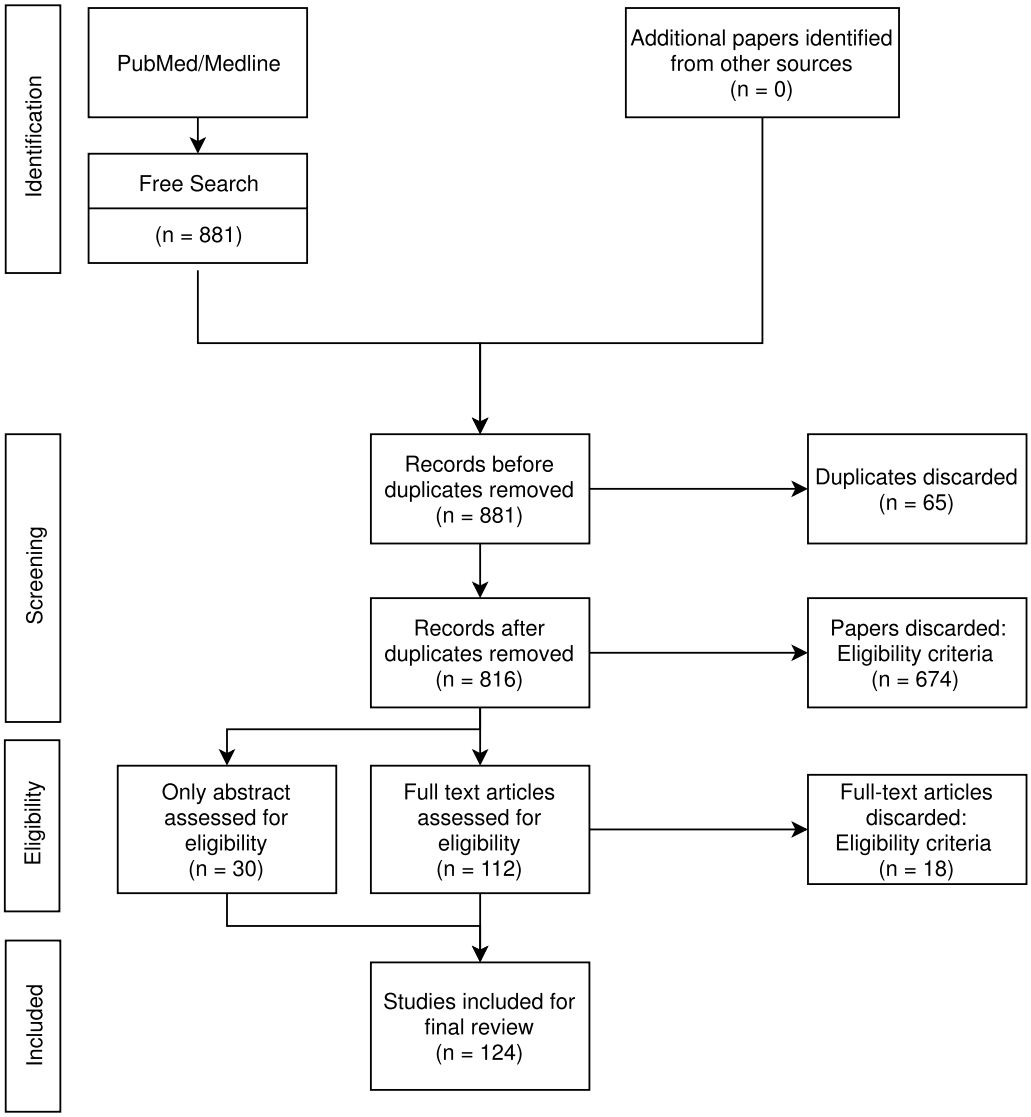

Fig. 1 Modified PRISMA 2009 flow diagram. Systematic literature search and selection process overview. Given that the goal of this literature review was to give an insight into the different terminologies and definitions of B waves, only articles specifically mentioning B waves or related terms were included in the study selection. As an example: *slow waves of ABP* was not included. Papers simultaneously published by different journals were considered as duplicates and also excluded. The remaining articles (n = 124) were thoroughly examined and included in this study following the PRISMA flow-diagram. Terminologies, definitions, and methods were identified individually by two independent reviewers and categorized according to a predefined protocol. Disagreements were resolved by consensus. No importance was given to the order of words, *ICP B waves* was treated equally to *B ICP waves*. Hyphens were removed, *B-waves* were grouped together with *B waves*. *Of* and *in* were disregarded, *slow waves of ICP* were registered as *slow waves ICP*. Only terminologies associated with ICP B waves were included (i.e. *slow waves of ABP* was not included). Terminologies in singular form were registered as plural, *B wave* was registered as *B waves*. Terms used less than three times were categorized as *other*

with a plateau phase, and Yokota et al. [8] describe persistent high pressure B waves. It is noteworthy that all sub-classification attempts contain a B wave subtype with plateau-like features. This raises the question whether there is a continuous transition from B waves to plateau waves or whether they have different etiology.

To summarize, B waves are categorized into different subclasses if they have distinct shapes *and/or* if their amplitude is different. These sub-classification attempts may be used as supplementary evidence that the classical waveform categories do not adequately address waveforms identified in clinical practice today.

Table 1 Summary of reviewed B waves terminology and characteristics

Article	Terminology								Frequency (waves/min)	Analysis tool	Additional comments
	(ICP) slow waves	ICP waves	(ICP) B waves	Lundberg B waves	B slow waves	Vasogenic waves	Slow vasogenic (ICP) waves	Other			
Spiegelberg et al. [26]			X				X		0.5–2 0.33–3	Cross-correlation	
Lalou et al. [12]	X		X			X			0.3–4	Spectral analysis	
Czosnyka et al. [27]	X						X				
Cabella et al. [28]	X										
Kojoukhova et al. [29]			X							Visual inspection	
Lalou et al. [30]	X		X			X	X	X	0.3–4	Spectral analysis	Slow wave
Czosnyka et al. [31]	X						X		0.33–3		
Santamarta et al. [7]	X		X						0.5–2		4 types, N:5
Hamilton et al. [32]	X		X	X							
Moyse et al. [33]	X										
Lu et al. [34]	X								0.5–3	Multiscale entropy	
Antes et al. [35]	X		X	X				X	0.5–3		Lundberg wave
Horcajadas Almansa et al. [36]			X								
Horcajadas Almansa et al. [37]			X						0.5–2	Visual inspection	
Varsos et al. [38]	X								0.33–3		
Cordero Tous et al. [39]			X								
Weerakkody et al. [40]	X						X	X	0.3–2	Visual inspection	Vasogenic ICP wave
Lewis et al. [41]	X		X								
Budohoski et al. [42]	X			X			X		0.3–3		
Elixmann et al. [43]			X						0.5–3		N:3
Smielewski et al. [44]	X		X				X				
Jetzki et al. [45]			X						0.5–2		
Kasprowicz et al. [9]	X		X						0.5–2	MOCAIP	3 types
Hamilton et al. [15]	X									MOCAIP	
Hu et al. [16]			X							MOCAIP	
Kim et al. [46]							X				
Shahsavari et al. [47]	X										
Horcajadas Almansa et al. [48]			X						0.5–2	Visual inspection	
Asgari et al. [49]			X								
Weerakkody et al. [50]	X		X	X		X	X		0.5–3	Spectral analysis	

Table 1 (continued)

Article	Terminology								Frequency (waves/min)	Analysis tool	Additional comments
	(ICP) slow waves	ICP waves	(ICP) B waves	Lundberg B waves	B slow waves	Vasogenic waves	Slow vasogenic (ICP) waves	Other			
Weerakkody et al. [51]	X	X	X						0.5–2 0.5–3		
Eide et al. [52]		X	X	X							
Hu et al. [17]	X										
Kasprowicz et al. [53]	X		X						0.5–2	MOCAIP	
Ursino et al. [54]			X								
Hamilton et al. [55]	X		X							Visual inspection	N:20, O:30
Lee et al. [56]			X						0.2–3		
Damasceno et al. [57]			X								
Czosnyka et al. [58]	X								0.3–3	Wavelet analysis	
Brady et al. [59]	X		X								
Stevens et al. [60]			X					X			Hypertensive ICP spikes
Petrella et al. [61]	X		X					X	0.33–3	Spectral analysis	Lundberg ICP B wave
Schuhmann et al. [62]	X		X			X		X		Spectral analysis	Vasogenic intracranial wave
Minns et al. [63]	X		X					X		Visual inspection	Slow ICP pressure wave
Jantzen et al. [64]			X	X							
Geocadin et al. [65]			X						0.5–2		N:3
Czosnyka et al. [66]	X						X		0.33–3	Spectral analysis	
Wang et al. [67]	X										
Delavallee et al. [68]			X								
Czosnyka et al. [69]	X								0.33–3		
Guendling et al. [70]	X								0.33–3		
Czosnyka et al. [71]	X		X								
Schmidt et al. [72]			X							Visual inspection	
Agren-Wilsson et al. [73]			X								
Lescot et al. [4]			X	X				X	0.5–2		Lundberg ICP B wave
Balestreri et al. [74]	X		X				X	X	0.33–3		Vasogenic ICP wave
Stephensen et al. [75]			X						0.5–2	Spectral analysis and amplitude	
Czosnyka et al. [76]	X								0.2–3		
Fountas et al. [77]	X				X			X	0.5–2		ICP slow B wave

Table 1 (continued)

Article	Terminology								Frequency (waves/min)	Analysis tool	Additional comments
	(ICP) slow waves	ICP waves	(ICP) B waves	Lundberg B waves	B slow waves	Vasogenic waves	Slow vasogenic (ICP) waves	Other			
Czosnyka et al. [78]	X		X			X	X		0.33–2	Spectral analysis and amplitude	
Momjian et al. [14]	X		X	X			X	X	0.33–3	Spectral analysis	Lundberg ICP B wave
Lenfeldt et al. [79]			X						0.5–2		N:1
Edsbagge et al. [80]			X							Spectral analysis	
Balestreri et al. [81]	X		X						0.33–3	Spectral analysis	
Ragauskas et al. [82]	X				X			X	0.3–2		
Strik et al. [83]	X		X						0.5–3	Spectral analysis	
Daley et al. [84]		X	X						0.5–2	Spectral analysis	
Stephensen et al. [85]		X	X								
Poca et al. [86]			X								
Lemaire et al. [87]	X	X	X	X					0.5–2		
Czosnyka et al. [88]	X	X	X			X			0.5–3		
Walter et al. [89]			X						0.5–2	Spectral analysis	
Schmidt et al. [90]	X								0.5–2		
Eklund et al. [23]			X						0.5–2	Spectral analysis and amplitude	
Vanneste et al. [91]			X						0.5–2		
Schoeman et al. [92]			X						0.5–2	Visual inspection	
Schuhmann et al. [93]			X								
Czosnyka et al. [94]			X							Spectral analysis	
Droste et al. [95]			X						0.5–2	Visual inspection	
Qureshi et al. [96]			X						1–2		N:3
Czosnyka et al. [97]	X							X			Slow spontaneous waves in ICP
Czosnyka et al. [98]	X	X									
Newell et al. [99]			X						0.5–2		
Lemaire et al. [100]	X		X						0.5–2		
Steinmeier et al. [101]		X	X						0.5–2		
Hanlo et al. [13]			X						3–4		O:15
Krauss et al. [102]			X						0.5–2	Visual inspection	
Wayenberg et al. [103]			X						0.5–3		

Table 1 (continued)

Article	Terminology								Frequency (waves/min)	Analysis tool	Additional comments
	(ICP) slow waves	ICP waves	(ICP) B waves	Lundberg B waves	B slow waves	Vasogenic waves	Slow vasogenic (ICP) waves	Other			
Lemaire et al. [104]	X		X						0.5–3	Spectral analysis	
Krauss et al. [105]			X						0.5–2		
Droste et al. [106]			X							Visual inspection	
Takeda et al. [107]			X								
Newell et al. [108]		X	X						0.5–2	Spectral analysis	
Raftopoulos et al. [6]			X						0.5–3		
Sahuqillo et al. [109]			X								N:10
Hara et al. [110]			X						0.5–2	Spectral analysis	
Handa et al. [111]]			X						0.5–2		
Yokota et al. [8]			X						0.5–2	Visual inspection	
Takeuchi et al. [112]			X								
Yokota et al. [113]			X							Visual inspection	
Sato et al. [114]								X			Lundberg's B
Maeda et al. [115]			X								
Gjerris et al. [116]			X								
Hayashi et al. [117]			X						0.5–2		
Schoeman et al. [118]			X							Visual inspection	
Kosteljanetz et al. [119]			X								
Hayashi et al. [120]			X						0.5–2		
Brock et al. [121]			X								
Kuchiwaki et al. [122]								X			B type pressure wave
Tamaki et al. [123]			X								
Auer et al. [124]			X						0.5–2		
Terzano et al. [125]				X				X			Lundberg B-type CSF pressure waves
Gjerris et al. [126]			X						1–2		N:5
Tomei et al. [127]			X								
Kaye et al. [128]			X								N:10
Bilz et al. [129]			X								
Munari et al. [130]	X							X			Pressure waves of the Lundberg type b
Guieu et al. [131]			X	X				X	0.5–2		type B pressure waves

Table 1 (continued)

Article	Terminology								Frequency (waves/min)	Analysis tool	Additional comments
	(ICP) slow waves	ICP waves	(ICP) B waves	Lundberg B waves	B slow waves	Vasogenic waves	Slow vasogenic (ICP) waves	Other			
Wilkinson et al. [132]			X								
Liguoi et al. [133]			X								
Fuentes et al. [134]			X								
Munari et al. [135]			X	X				X			Lundberg's B waves
Hayashi et al. [136]			X								N:15, O:45
Martin et al. [2]				X							
Total sum	49	9	96	13	2	6	13	19			

Table summarizing the main terms and characteristics used to describe B waves with articles sorted based on year of publication. Under *terminology*, terms that appeared more than five times are given their own column. Less frequent terms are included under *other* and the term is listed under *additional comments*. The column *frequency* describes the occurrence in waves/min of the B waves as described in the corresponding article, while the column *analysis tool* lists the methodology used to detect B waves. Under *additional comments*, besides including other terms used to refer to the B waves, extra notes are added: N with an associated number value: Lower amplitude value of X mmHg. O with an associated number value: Upper amplitude value of X mmHg. N types: B waves subclassification into N subgroups

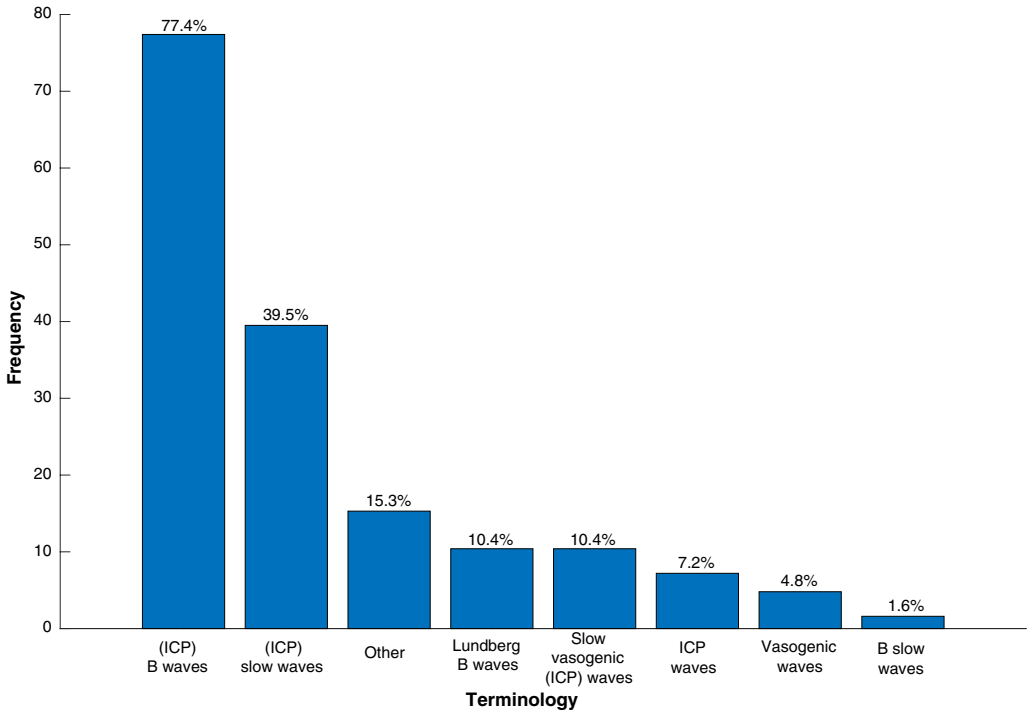

Fig. 2 Frequency of terminology usage in the reviewed papers. The term *B waves* was used in most articles, followed by *slow waves* and *ICP slow waves*

Table 2 Major morphological B wave subclasses

	Term	Shape	Plateau	Frequency (waves/min)	Amplitude (mmHg)
Raftopolous et al. [6] Santamarta et al. [7]	Small symmetrical wave (SSW)	Symmetrical	No	0.36–5	< 10
	Great symmetrical wave (GSW)	Symmetrical	No	0.36–5	> 10
	Intermediate wave (IW)	Asymmetrical	No	0.33–1.67	6–34
Kasprowicz et al. [9]	Slow symmetrical ICP wave	Symmetrical	No	–	–
	Slow asymmetrical ICP wave	Asymmetrical	No	–	–
	Slow ICP B with plateau phase	Symmetrical	Yes	–	–
Yokota et al. [8]	Type II episodic B-wave	–	–	–	25–75
	Type III persistent, high pressure B-wave	–	–	0.5–2	40–100
	Type IV continuous, regular B-wave	–	–	0.5–2	10–30

Analysis tools

32% of the papers had an explicitly stated analysis method. While traditionally the most common analytical method used was either spectral analysis (40%) or spectral analysis with an amplitude threshold (7%), there is now an increasing tendency (10%) to detect B waves using trained machine learning algorithms, as observed in more recently published papers [9, 15, 16]. These algorithms use as input morphological features extracted from the ICP pulse wave via the Morphological clustering and analysis of ICP pulse (MOCAIP) algorithm. Thus, instead of defining B waves in terms of amplitude and frequency, they define them according to different morphological parameters of the pulse wave. These parameters are based on the three subpeaks (P_1, P_2, and P_3) of the pulse wave: systolic peak, tidal peak, and dicrotic peak, respectively [9]. Examples of these ICP pulse metrics include the amplitude of the subpeaks, the latency between subpeaks, and the start of the ICP pulse wave and the pulse wave period, among others [17].

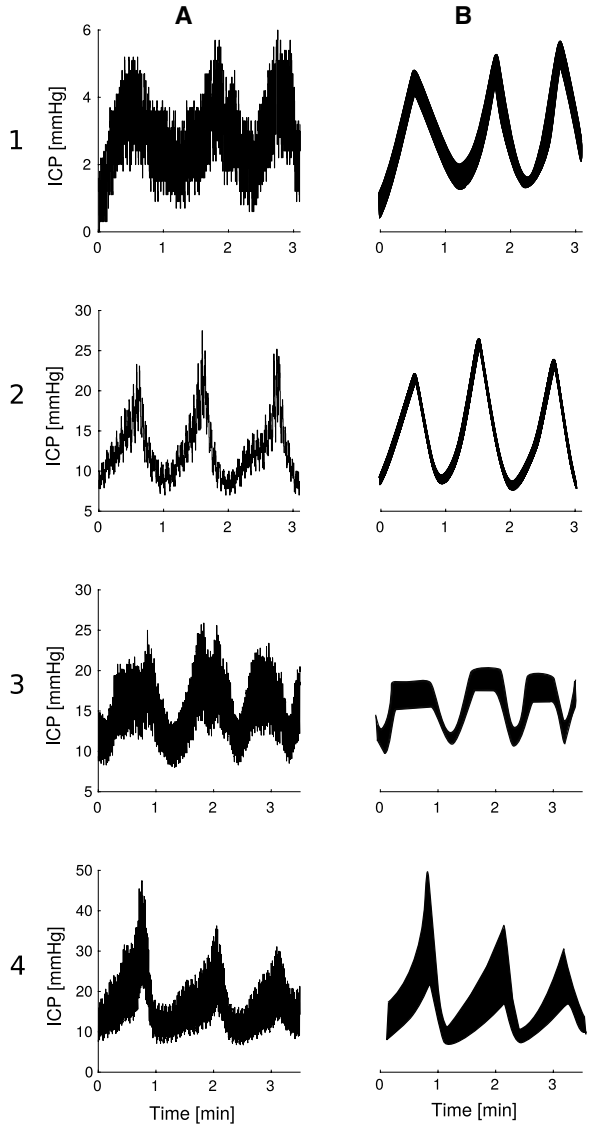

Fig. 3 Presentation of different B waves sub-classification patterns. Each is illustrated by two computer-generated examples: column A simulating ICP recordings and column B showing an artistic rendering. Examples on rows 1 and 2 exhibit B waves with symmetrical shape and amplitude lower and higher than 10 mmHg, respectively. Examples of row 3 correspond to symmetrical B waves with plateau. The last row shows examples for asymmetrical B waves. The time-scale used in all examples is minutes

Discussion

ICP arises from pressure contributions from the brain, the heart, and the cerebrospinal fluid (CSF) inside the skull [18]. ICP is monitored invasively with a pressure transducer inserted either intracranially (subdural, epidural, intraparenchymal or intraventricular placements) or in the spinal compartment (lumbar puncture). As the brain is enclosed within the skull and its expandability is restricted, the ability to compensate for pressure-volume changes (auto-regulation) is also limited (i.e. compliance is low). Under normal conditions, auto-regulatory processes are responsible for keeping the intracranial volume constant. As brain compliance starts to decrease, the compensatory capacity is exhausted so that further volume changes are no longer accommodated; this causes ICP to increase. Space-occupying lesions are the main causes for the changes in intracranial volume. Hydrocephalus, intracranial haemorrhage, haematoma, and brain edema are examples of such lesions [19].

Under normal compensatory adaptations, the ICP stays within a narrow pressure range for each assumed body posture [20, 21]. This is the simplest way of looking at ICP, as just a number that should remain within certain boundary values. Going beyond that, the ICP signal can be analyzed from a different perspective by studying the presence of macro-patterns. The diversity of B waves is the most commonly encountered macro-wave in clinical practice.

This study demonstrates the lack of agreement with regard to the terminology and characteristics used to define B waves. Different names are used to refer to the same phenomena, in order to either describe characteristics and morphological variations of the wave or the etiology behind their occurrence. This makes mathematical modeling of B waves more difficult, which consequently complicates the selection or development of an analysis tool that could be used to automatically interpret them. Automating B wave identification may be a way to detect and better understand ICP deviations from a normal physiological state at an earlier stage. But with the focus of current analysis tools on identifying previously defined B waves, they share a limitation of throwing away data related to other potentially relevant waveform deviations. Thus, underlying patterns of ICP that may contain important information on the interplay of physiological systems affecting the brain are potentially neglected. Opening up the analysis of ICP signals without being limited to previously defined patterns and conventions could enable fruitful new investigative and diagnostic techniques.

Sub-classification

B waves were first defined from ICP monitoring sessions recorded in severely ill patients. Sub-classifications, which have mainly been qualitative, are the only attempts at modernizing the description of B waves to fit the clinical situations we see today [6–9].

The existence of multiple attempts at B wave subgrouping suggests that the overarching B wave

category is not satisfactory for classification purposes today. A future avenue of research may instead be to direct attention away from classical B wave detection and instead focus on the identification of new parameters to automate the analysis of repeatable patterns in the ICP signal. Pattern recognition algorithms will be the fundamental approach used for this purpose.

Analysis tools

ICP signals arise from the interaction of multiple physiological factors (e.g. heart pump, respiration, ...) that vary over time. Thus, it may be seen as a time series signal [22]. Traditionally, ICP signals have been inspected visually for B wave identification. In addition to being a time consuming technique, it is also subject to investigator bias due to interpretation subjectivity and dependence on clinical experience. Since the introduction of computerized algorithms, spectral analysis has led the way in B wave detection. A general agreement on a certain frequency range that this wave occupies may explain why spectral analysis is the most reported methodology. However, there is low frequency activity within the B-wave range that is unrelated to vasomotor activity (i.e. respiratory changes associated with sleep), thereby introducing a severe limitation in the use of spectral analysis. We might get unwanted contributions from these signals in the B-wave frequency range when breaking down the signal into frequency components. Eklund et al. developed an algorithm that strives to overcome this problem by also taking into account the wave amplitude [23].

Defining B waves in terms of amplitude is, however, very ambiguous. In particular, the term amplitude can be approached as the trough to peak pressure difference in the signal. If the wave has a sinusoidal appearance there is no problem in the identification of both its maximum and minimum values, but their identification becomes a challenge when the waveform is irregular. At the same time, the term amplitude can also refer to the distance from the peak of the wave to the baseline.

MOCAIP extracts morphological parameters from the pulse wave that are then used to characterize B waves instead of defining them based on their amplitude and frequency [24]. With the advantage of no longer depending on the classical B wave definition, this algorithm presents other drawbacks that prevents it from proper implementation in clinical practice. It rejects ICP pulses if a corresponding matching template is not included within the reference library proposed. This library is limited to intraparenchymal ICP signals from patients with hydrocephalus and does not comprise any ICP pulses from other pathologies, so that ICP pulses could be falsely rejected. Another limitation is the requirement of a simultaneous acquisition of ECG signal to help in the identification of the ICP pulse wave. Also, identifying B waves using MOCAIP assumes that the pulse waves are affected during the B waves, which is not definitively settled. Another approach proposed by Elixmann also isolates the pulse waves and classifies them based on predefined templates [25].

Conclusion

To exploit the potential role of macro-patterns in ICP dynamics and to automate their identification for diagnostic or therapeutic purposes, two approaches for future work may be considered.

There could be efforts to arrive at strict agreement on morphological characteristics of classical macro-patterns, which requires consensus-based definitions to enable the derivation of relevant metrics to characterize them.

Alternatively, a new approach could be attempted without relying on classical macro-patterns. Instead it could be based on recognition of new patterns that more adequately describe variations seen in daily clinical practice today. This de novo pattern recognition approach requires relating macro-patterns to clinical information to ensure that they are biologically relevant.

Abbreviations

ICP: intracranial pressure; CSF: cerebrospinal fluid; ICU: intensive care unit; MOCAIP: morphological clustering and analysis of ICP pulse.

Acknowledgements

The authors are thankful for contributions from the Novo Nordisk Fonden Tandem Programme.

Authors' contributions

Study conception and design: AA, MA, MJ. Analysis and interpretation of the papers for the work: AA and IMT. Drafting of manuscript: IMT with input from the other authors. Critical revision: MJ, MA, JW. All authors read and approved the final manuscript.

Funding

Funding was provided by Novo Nordisk Fonden (Grant Number: NNF17OC0024718).

Availability of data and materials

Data sharing is not applicable to this article as no datasets were generated or analysed during the current study.

Ethics approval and consent to participate

Not applicable.

Consent for publication

Not applicable.

Competing interests

The authors declare that they have no competing interests.

Author details
[1] Clinic of Neurosurgery, Copenhagen University Hospital, Rigshospitalet, Copenhagen, Denmark. [2] Department of Health Technology, Technical University of Denmark, Kongens Lyngby, Denmark.

Received: 12 June 2019 Accepted: 15 September 2019
Published online: 15 October 2019

References

1. Lundberg N. Continuous recording and control of ventricular fluid pressure in neurosurgical practice. Acta Psychiatrica Scandinavica Supplementum. 1960;36:1–193.
2. Martin G. Lundberg's B waves as a feature of normal intracranial pressure. Surg Neurol. 1978;9(6):347–8.
3. Droste DW, Krauss JK, Berger W, Schuler E, Brown MM. Rhythmic oscillations with a wavelength of 0.5–2 min in transcranial Doppler recordings. Acta Neurologica Scandinavica. 2009;90(2):99–104.
4. Lescot T, Naccache L, Bonnet MP, Abdennour L, Coriat P, Puybasset L. The relationship of intracranial pressure Lundberg waves to electroencephalograph fluctuations in patients with severe head trauma. Acta Neurochir. 2005;147(2):125–9 **(discussion 129)**.
5. Liberati A, Altman DG, Tetzlaff J, Mulrow C, Gotzsche PC, Ioannidis JPA, et al. The PRISMA statement for reporting systematic reviews and meta-analyses of studies that evaluate healthcare interventions: explanation and elaboration. Br Med J. 2009;339(b2700):b2700.
6. Raftopoulos C, Chaskis C, Delecluse F, Cantrainet F, Bidauti L, Brotchi J. Morphological quantitative analysis of intracranial pressure waves in normal pressure hydrocephalus. Neurol Res. 1992;14:389–96.
7. Santamarta D, González-Martínez E, Fernández J, Mostaza A. The prediction of shunt response in idiopathic normal-pressure hydrocephalus based on intracranial pressure monitoring and lumbar infusion. Acta Neurochir Suppl. 2016;122:267–74.
8. Yokota A, Matsuoka S, Ishikawa T, Kohshi K, Kajiwara H. Overnight recordings of intracranial pressure and electroencephalography in neurosurgical patients. Part I: intracranial pressure waves and their clinical correlations. J UOEH. 1989;11(4):371–81.
9. Kasprowicz M, Bergsneider M, Czosnyka M, Hu X. Association between ICP pulse waveform morphology and ICP B waves. Acta Neurochir Suppl. 2012;114:29–34.
10. Spiegelberg A, Preuß M, Kurtcuoglu V. B-waves revisited. Interdisciplin Neurosurgery: Adv Tech Case Manage. 2016;6:13—7.
11. Czosnyka M, Pickard JD. Monitoring and interpretation of intracranial pressure. J Neurol Neurosurg Psychiatry. 2004;75(6):813–21.
12. Lalou DA, Czosnyka M, Donnelly J, Lavinio A, Pickard JD, Garnett M, et al. Are slow waves of intracranial pressure suppressed by general anaesthesia? Acta Neurochir Suppl. 2018;126:129–32.
13. Hanlo PW, Gooskens RH, Faber JA, Peters RJ, Hermsen AA, Nijhuis IJ, et al. Relationship between anterior fontanelle pressure measurements and clinical signs in infantile hydrocephalus. Childs Nerv Syst. 1996;12(4):200–9.
14. Momjian S, Czosnyka Z, Czosnyka M, Pickard JD. Link between vasogenic waves of intracranial pressure and cerebrospinal fluid outflow resistance in normal pressure hydrocephalus. Br J Neurosurg. 2004;18(1):56–61.
15. Hamilton R, Baldwin K, Fuller J, Vespa P, Hu X, Bergsneider M. Intracranial pressure pulse waveform correlates with aqueductal cerebrospinal fluid stroke volume. J Appl Physiol. 2012;113(10):1560–6.
16. Hu X, Hamilton R, Baldwin K, Vespa PM, Bergsneider M. Automated extraction of decision rules for predicting lumbar drain outcome by analyzing overnight intracranial pressure. Acta Neurochir Suppl. 2012;114:207–12.
17. Hu X, Xu P, Asgari S, Vespa P, Bergsneider M. Forecasting ICP elevation based on prescient changes of intracranial pressure waveform morphology. IEEE Trans Biomed Eng. 2010;57(5):1070–8.
18. Raboel PH, Bartek J, Andresen M, Bellander BM, Romner B. Intracranial pressure monitoring: Invasive versus non-invasive methods—a review. Crit Care Res Pract. 2012;2012:950393.
19. Lavinio A, Menon DK. Intracranial pressure: why we monitor it, how to monitor it, what to do with the number and what's the future? Curr Opin Anesthesiol. 2011;24:117–23.
20. Andresen M, Hadi A, Petersen LG, Juhler M. Effect of postural changes on ICP in healthy and ill subjects. Acta Neurochir. 2014;157(1):109–13.
21. Petersen LG, Lawley JS, Lilja-Cyron A, Petersen JCG, Howden EJ, Sarma S, et al. Lower body negative pressure to safely reduce intracranial pressure. J Physiol. 2019;597(1):237–48.
22. Pham H. Springer handbook of engineering statistics. London: Springer; 2006.
23. Eklund A, Agren-Wilsson A, Andersson N, Bergenheim AT, Koskinen LO, Malm J. Two computerized methods used to analyze intracranial pressure B waves: comparison with traditional visual interpretation. J Neurosurg. 2001;94(3):392–6.
24. Hu X, Xu P, Scalzo F, Vespa P, Bergsneider M. Morphological clustering and analysis of continuous intracranial pressure. IEEE Trans Biomed Eng. 2009;56(4667641):696–705.
25. Elixmann IM, Hansinger J, Goffin C, Antes S, Radermacher K, Leonhardt S. Single pulse analysis of intracranial pressure for a hydrocephalus implant. In: Proceedings of the annual international conference of the IEEE engineering in medicine and biology Society, Embs, vol. 2012, no. 6346828. 2012. p. 3939–42.
26. Spiegelberg A, Krause M, Meixensberger J, Seifert B, Kurtcuoglu V. Significant association of slow vasogenic ICP waves with normal pressure hydrocephalus diagnosis. Acta Neurochir Suppl. 2018;126:243–6.
27. Czosnyka M, Donnelly J, Calviello L, Smielewski P, Menon DK, Pickard JD. Do ICP-derived parameters differ in vegetative state from other outcome groups after traumatic brain injury? Acta Neurochir Suppl. 2018;126:17–20.
28. Cabella B, Donnelly J, Cardim D, Liu X, Cabeleira M, Smielewski P, et al. An association between ICP-derived data and outcome in TBI patients: the role of sample size. Neurocrit Care. 2017;27(1):103–7.
29. Kojoukhova M, Vanha KI, Timonen M, Koivisto AM, Nerg O, Rummukainen J, et al. Associations of intracranial pressure with brain biopsy, radiological findings, and shunt surgery outcome in patients with suspected idiopathic normal pressure hydrocephalus. Acta Neurochir. 2017;159(1):51–61.
30. Lalou DA, Czosnyka M, Donnelly J, Lavinio A, Pickard JD, Garnett M, et al. Influence of general anaesthesia on slow waves of intracranial pressure. Neurol Res. 2016;38(7):587–92.
31. Czosnyka M, Varsos GV, Czosnyka ZH, Smielewski P, Saadoun S, Jamous A, et al. Waveform analysis of intraspinal pressure after traumatic spinal cord injury: an observational study (O-64). Acta Neurochir Suppl. 2016;122:335–8.
32. Hamilton R, Fuller J, Baldwin K, Vespa P, Hu X, Bergsneider M. Relative position of the third characteristic peak of the intracranial pressure pulse waveform morphology differentiates normal-pressure hydrocephalus shunt responders and nonresponders. Acta Neurochir Suppl. 2016;122:339–45.
33. Moyse E, Ros M, Marhar F, Swider P, Schmidt EA. Characterisation of supra- and infratentorial ICP profiles. Acta Neurochir Suppl. 2016;122:37–40.
34. Lu CW, Czosnyka M, Shieh JS, Pickard JD, Smielewski P. Continuous monitoring of the complexity of intracranial pressure after head injury. Acta Neurochir Suppl. 2016;122:33–5.
35. Antes S, Tschan CA, Heckelmann M, Breuskin D, Oertel J. Telemetric intracranial pressure monitoring with the Raumedic Neurovent P-tel. World Neurosurg. 2016;91:133–48.
36. Horcajadas Almansa A, Cordero Tous N, Roman Cutillas A, Jorques Infante A, Saura Rojas E, Ibanez Velasco B, et al. Usefulness of continuous intracranial pressure monitoring in long-standing overt ventriculomegaly in adults. Neurocirugia. 2015;26(2):64–72.
37. Horcajadas Almansa A, Cordero Tous N, Roman Cutillas A, Jorques Infante A, Saura Rojas E, Ibanez Velasco B, et al. Usefulness of intracranial pressure continuous monitoring in pseudotumor cerebri. Neurocirugia. 2015;26(4):157–66.
38. Varsos GV, Werndle MC, Czosnyka ZH, Smielewski P, Kolias AG, Phang I, et al. Intraspinal pressure and spinal cord perfusion pressure after spinal cord injury: an observational study. J Neurosurg Spine. 2015;23(6):763–71.

39. Cordero Tous N, Roman Cutillas AM, Jorques Infante AM, Olivares Granados G, Saura Rojas JE, Ibanez Velasco B, et al. Adult chronic idiopathic hydrocephalus-diagnosis, treatment and evolution. Prospective study. Neurocirugia. 2013;24(3):93–101.
40. Weerakkody RA, Czosnyka M, Zweifel C, Castellani G, Smielewski P, Brady K, et al. Near infrared spectroscopy as possible non-invasive monitor of slow vasogenic ICP waves. Acta Neurochir Suppl. 2012;114:181–5.
41. Lewis PM, Smielewski P, Rosenfeld JV, Pickard JD, Czosnyka M. Monitoring of the association between cerebral blood flow velocity and intracranial pressure. Acta Neurochir Suppl. 2012;114:147–51.
42. Budohoski KP, Schmidt B, Smielewski P, Kasprowicz M, Plontke R, Pickard JD, et al. Non-invasively estimated ICP pulse amplitude strongly correlates with outcome after TBI. Acta Neurochir Suppl. 2012;114:121–5.
43. Elixmann IM, Walter M, Kiefer M, Leonhardt S. Simulation of existing and future electromechanical shunt valves in combination with a model for brain fluid dynamics. Acta Neurochir Suppl. 2012;113:77–81.
44. Smielewski P, Czosnyka Z, Kasprowicz M, Pickard JD, Czosnyka M. ICM+: a versatile software for assessment of CSF dynamics. Acta Neurochir Suppl. 2012;114:75–9.
45. Jetzki S, Weinzierl M, Krause I, Hahne S, Rehbaum H, Kiausch M, et al. A multisensor implant for continuous monitoring of intracranial pressure dynamics. IEEE Trans Biomed Circuits Syst. 2012;6(4):356–65.
46. Kim DJ, Czosnyka Z, Kasprowicz M, Smieleweski P, Baledent O, Guerguerian AM, et al. Continuous monitoring of the Monro-Kellie doctrine: is it possible? J Neurotrauma. 2012;29(7):1354–63.
47. Shahsavari S, McKelvey T, Ritzén CE, Rydenhag B. Cerebrovascular mechanical properties and slow waves of intracranial pressure in TBI patients. IEEE Trans Biomed Eng. 2011;58(7):2072–82.
48. Horcajadas Almansa A, Roman A, Olivares G, Saura E, Jorques A, Cordero N, et al. Usefulness of IPC continuous monitoring in shunt dysfunction. Neurocirugia. 2011;22(4):310–23.
49. Asgari S, Vespa P, Bergsneider M, Hu X. Lack of consistent intracranial pressure pulse morphological changes during episodes of microdialysis lactate/pyruvate ratio increase. Physiol Meas. 2011;32(10):1639–51.
50. Weerakkody RA, Czosnyka M, Schuhmann MU, Schmidt E, Keong N, Santarius T, et al. Clinical assessment of cerebrospinal fluid dynamics in hydrocephalus. Guide to interpretation based on observational study. Acta Neurol Scand. 2011;124(2):85–98.
51. Weerakkody RA, Czosnyka M, Zweifel C, Castellani G, Smielewski P, Keong N, et al. Slow vasogenic fluctuations of intracranial pressure and cerebral near infrared spectroscopy—an observational study. Acta Neurochir. 2010;152(10):1763–9.
52. Eide PK, Sorteberg W. Simultaneous measurements of intracranial pressure parameters in the epidural space and in brain parenchyma in patients with hydrocephalus. J Neurosurg. 2010;113(6):1317–25.
53. Kasprowicz M, Asgari S, Bergsneider M, Czosnyka M, Hamilton R, Hu X. Pattern recognition of overnight intracranial pressure slow waves using morphological features of intracranial pressure pulse. J Neurosci Methods. 2010;190(2):310–8.
54. Ursino M, Giannessi M, Frapparelli M, Magosso E. Effect of cushing response on systemic arterial pressure. IEEE Eng Med Biol Mag. 2009;28(6):63–71.
55. Hamilton R, Xu P, Asgari S, Kasprowicz M, Vespa P, Bergsneider M, et al. Forecasting intracranial pressure elevation using pulse waveform morphology. Conf Proc IEEE Eng Med Biol Soc. 2009;2009:4331–4.
56. Lee JK, Kibler KK, Benni PB, Easley RB, Czosnyka M, Smielewski P, et al. Cerebrovascular reactivity measured by near-infrared spectroscopy. Stroke. 2009;40(5):1820–6.
57. Damasceno BP. Normal pressure hydrocephalus: diagnostic and predictive evaluation. Dement Neuropsychol. 2009;3(1):8–15.
58. Czosnyka M, Brady K, Reinhard M, Smielewski P, Steiner LA. Monitoring of cerebrovascular autoregulation: facts, myths, and missing links. Neurocrit Care. 2009;10(3):373–86.
59. Brady KM, Lee JK, Kibler KK, Easley RB, Koehler RC, Shaffner DH. Continuous measurement of autoregulation by spontaneous fluctuations in cerebral perfusion pressure: comparison of 3 methods. Stroke. 2008;39(9):2531–7.
60. Stevens SA, Stimpson J, Lakin WD, Thakore NJ, Penar PL. A model for idiopathic intracranial hypertension and associated pathological ICP wave-forms. IEEE Trans Biomed Eng. 2008;55(2 Pt 1):388–98.
61. Petrella G, Czosnyka M, Keong N, Pickard JD, Czosnyka Z. How does CSF dynamics change after shunting? Acta Neurol Scand. 2008;118(3):182–8.
62. Schuhmann MU, Sood S, McAllister JP, Jaeger M, Ham SD, Czosnyka Z, et al. Value of overnight monitoring of intracranial pressure in hydrocephalic children. Pediatr Neurosurg. 2008;44(4):269–79.
63. Minns RA, Jones PA, Chambers IR. Low frequency pressure waves of possible autonomic origin in severely head-injured children. Acta Neurochir Suppl. 2008;102:85–8.
64. Jantzen JPAH. Prevention and treatment of intracranial hypertension. Best Pract Res Clin Anaesthesiol. 2007;21(4):517–38.
65. Geocadin RG, Varelas PN, Rigamonti D, Williams MA. Continuous intracranial pressure monitoring via the shunt reservoir to assess suspected shunt malfunction in adults with hydrocephalus. Neurosurg Focus. 2007;22(4):E10.
66. Czosnyka M, Smielewski P, Timofeev I, Lavinio A, Guazzo E, Hutchinson P, et al. Intracranial pressure: more than a number. Neurosurg Focus. 2007;22(5):E10.
67. Wang EC, Ang BT, Wong J, Lim J, Ng I. Characterization of cerebrovascular reactivity after craniectomy for acute brain injury. Br J Neurosurg. 2006;20(1):24–30.
68. Delavallée M, Raftopoulos C. Normal pressure hydrocephalus in a patient with myotonic dystrophy: case report with a 10-year follow-up. Neurosurgery. 2006;58(4):E796 **(discussion E796)**.
69. Czosnyka M, Hutchinson PJ, Balestreri M, Hiler M, Smielewski P, Pickard JD. Monitoring and interpretation of intracranial pressure after head injury. Acta Neurochir Suppl. 2006;96:114–8.
70. Guendling K, Smielewski P, Czosnyka M, Lewis P, Nortje J, Timofeev I, et al. Use of ICM+ software for on-line analysis of intracranial and arterial pressures in head-injured patients. Acta Neurochir Suppl. 2006;96:108–13.
71. Czosnyka Z, van den Boogaard F, Czosnyka M, Momjian S, Gelling L, Pickard JD. The relationship between CSF circulation and cerebrovascular pressure-reactivity in normal pressure hydrocephalus. Acta Neurochir Suppl. 2005;95:207–11.
72. Schmidt B, Bocklisch SF, Pässler M, Czosnyka M, Schwarze JJ, Klingelhöfer J. Fuzzy pattern classification of hemodynamic data can be used to determine noninvasive intracranial pressure. Acta Neurochir Suppl. 2005;95:345–9.
73. Agren-Wilsson A, Eklund A, Koskinen LOD, Bergenheim AT, Malm J. Brain energy metabolism and intracranial pressure in idiopathic adult hydrocephalus syndrome. J Neurol Neurosurg Psychiatry. 2005;76(8):1088–93.
74. Balestreri M, Czosnyka M, Steiner LA, Hiler M, Schmidt EA, Matta B, et al. Association between outcome, cerebral pressure reactivity and slow ICP waves following head injury. Acta Neurochir Suppl. 2005;95:25–8.
75. Stephensen H, Andersson N, Eklund A, Malm J, Tisell M, Wikkelsö C. Objective B wave analysis in 55 patients with non-communicating and communicating hydrocephalus. J Neurol Neurosurg Psychiatry. 2005;76(7):965–70.
76. Czosnyka M, Balestreri M, Steiner L, Smielewski P, Hutchinson PJ, Matta B, et al. Age, intracranial pressure, autoregulation, and outcome after brain trauma. J Neurosurg. 2005;102(3):450–4.
77. Fountas KN, Sitkauskas A, Feltes CH, Kapsalaki EZ, Dimopoulos VG, Kassam M, et al. Is non-invasive monitoring of intracranial pressure waveform analysis possible? Preliminary results of a comparative study of non-invasive vs. invasive intracranial slow-wave waveform analysis monitoring in patients with traumatic brain injury. Med Sci Monit. 2005;11(2):CR58–63.
78. Czosnyka M, Czosnyka Z, Momjian S, Pickard JD. Cerebrospinal fluid dynamics. Physiol Meas. 2004;25(5):R51–76.
79. Lenfeldt N, Andersson N, Agren-Wilsson A, Bergenheim AT, Koskinen LOD, Eklund A, et al. Cerebrospinal fluid pulse pressure method: a possible substitute for the examination of B waves. J Neurosurg. 2004;101(6):944–50.
80. Edsbagge M, Tisell M, Jacobsson L, Wikkelso C. Spinal CSF absorption in healthy individuals. Am J Physiol Regul Integr Comp Physiol. 2004;287(6):R1450–5.

81. Balestreri M, Czosnyka M, Steiner LA, Schmidt E, Smielewski P, Matta B, et al. Intracranial hypertension: what additional information can be derived from ICP waveform after head injury? Acta Neurochir. 2004;146(2):131–41.
82. Ragauskas A, Daubaris G, Ragaisis V, Petkus V. Implementation of non-invasive brain physiological monitoring concepts. Med Eng Phys. 2003;25(8):667–78.
83. Strik C, Klose U, Kiefer C, Grodd W. Slow rhythmic oscillations in intracranial CSF and blood flow: registered by MRI. Acta Neurochir Suppl. 2002;81:139–42.
84. Daley ML, Pasley RL, Connolly M, Timmons SD, Angel J, Stidham G, et al. Spectral characteristics of B-waves and other low-frequency activity. Acta Neurochir Suppl. 2002;81:147–50.
85. Stephensen H, Tisell M, Wikkelsö C. There is no transmantle pressure gradient in communicating or noncommunicating hydrocephalus. Neurosurgery. 2002;50(4):763–71 **(discussion 771–773)**.
86. Poca MA, Sahuquillo J, Ibañez J, Amorós S, Arikan F, Rubio E. Intracranial hypertension after surgery in patients with Chiari I malformation and normal or moderate increase in ventricular size. Acta Neurochir Suppl. 2002;81:35–8.
87. Lemaire JJ, Khalil T, Cervenansky F, Gindre G, Boire JY, Bazin JE, et al. Slow pressure waves in the cranial enclosure. Acta Neurochir. 2002;144(3):243–54.
88. Czosnyka ZH, Czosnyka M, Whitfield PC, Donovan T, Pickard JD. Cerebral autoregulation among patients with symptoms of hydrocephalus. Neurosurgery. 2002;50(3):526–32 **(discussion 532–533)**.
89. Walter M, Kiefer M, Leonhardt S, Steudel WI, Isermann R. Online analysis of intracranial pressure waves. Acta Neurochir Suppl. 2002;81:161–2.
90. Schmidt EA, Czosnyka M, Smielewski P, Piechnik SK, Pickard JD. Asymmetry of cerebral autoregulation following head injury. Acta Neurochir Suppl. 2002;81:133–4.
91. Vanneste JA. Diagnosis and management of normal-pressure hydrocephalus. J Neurol. 2000;247(1):5–14.
92. Schoeman JF, Laubscher JA, Donald PR. Serial lumbar CSF pressure measurements and cranial computed tomographic findings in childhood tuberculous meningitits. Childs Nerv Syst. 2000;16(4):203–8 **(discussion 209)**.
93. Schuhmann MU, Engel M, Runge L, Samii M, Brinker T. Application of clinically recorded ICP patterns-an extension of conventional shunt testing. Childs Nerv Syst. 2000;16(12):856–61.
94. Czosnyka M, Smielewski P, Piechnik S, Al-Rawi PG, Kirkpatrick PJ, Matta BF, et al. Critical closing pressure in cerebrovascular circulation. J Neurol Neurosurg Psychiatry. 1999;66(5):606–11.
95. Droste DW, Krauss JK. Intracranial pressure B-waves precede corresponding arterial blood pressure oscillations in patients with suspected normal pressure hydrocephalus. Neurol Res. 1999;21(7):627–30.
96. Qureshi AI, Williams MA, Razumovsky AY, Hanley DF. Magnetic resonance imaging, unstable intracranial pressure and clinical outcome in patients with normal pressure hydrocephalus. Acta Neurochir Suppl. 1998;71:354–6.
97. Czosnyka M, Smielewski P, Kirkpatrick P, Piechnik S, Laing R, Pickard JD. Continuous monitoring of cerebrovascular pressure-reactivity in head injury. Acta Neurochir Suppl. 1998;71:74–7.
98. Czosnyka M, Smielewski P, Kirkpatrick P, Laing RJ, Menon D, Pickard JD. Continuous assessment of the cerebral vasomotor reactivity in head injury. Neurosurgery. 1997;41(1):11–7 **(discussion 17–19)**.
99. Newell DW, Aaslid R, Stooss R, Seiler RW, Reulen HJ. Evaluation of hemodynamic responses in head injury patients with transcranial Doppler monitoring. Acta Neurochir. 1997;139(9):804–17.
100. Lemaire JJ. Slow pressure waves during intracranial hypertension. Ann Fr Anesth Reanim. 1997;16(4):394–8.
101. Steinmeier R, Bauhuf C, Hübner U, Bauer RD, Fahlbusch R, Laumer R, et al. Slow rhythmic oscillations of blood pressure, intracranial pressure, microcirculation, and cerebral oxygenation. Dynamic interrelation and time course in humans. Stroke. 1996;27(12):2236–43.
102. Krauss JK, Droste DW, Bohus M, Regel JP, Scheremet R, Riemann D, et al. The relation of intracranial pressure B-waves to different sleep stages in patients with suspected normal pressure hydrocephalus. Acta Neurochir. 1995;136(3–4):195–203.
103. Wayenberg JL, Hasaerts D, Franco P, Valente F, Massager N. Anterior fontanelle pressure variations during sleep in healthy infants. Sleep. 1995;18(4):223–8.
104. Lemaire JJ, Boire JY, Chazal J, Irthum B. A computer software for frequential analysis of slow intracranial pressure waves. Comput Methods Programs Biomed. 1994;42(1):1–14.
105. Krauss JK, Droste DW. Predictability of intracranial pressure oscillations in patients with suspected normal pressure hydrocephalus by transcranial Doppler ultrasound. Neurol Res. 1994;16(5):398–402.
106. Droste DW, Krauss JK, Berger W, Schuler E, Brown MM. Rhythmic oscillations with a wavelength of 0.5–2 min in transcranial Doppler recordings. Acta Neurol Scand. 1994;90(2):99–104.
107. Takeda Y, Onitsuka T, Haraoka J, Koba T, Ito H, Miwa T. Clinical assessment of meningeal carcinomatosis; from the viewpoint of the analysis of intracranial pressure. No Shinkei Geka. 1993;21(3):213–20.
108. Newell DW, Aaslid R, Stooss R, Reulen HJ. The relationship of blood flow velocity fluctuations to intracranial pressure B waves. J Neurosurg. 1992;76(3):415–21.
109. Sahuquillo J, Rubio E, Codina A, Molins A, Guitart JM, Poca MA, et al. Reappraisal of the intracranial pressure and cerebrospinal fluid dynamics in patients with the so-called "normal pressure hydrocephalus" syndrome. Acta Neurochir. 1991;112(1–2):50–61.
110. Hara K, Nakatani S, Ozaki K, Ikeda T, Mogami H. Detection of the B waves in the oscillation of intracranial pressure by fast Fourier transform. Med Inform. 1990;15(2):125–31.
111. Handa Y, Hayashi M, Hirose S, Noguchi Y, Kobayashi H. The effect of increased intracranial pressure during the appearance of pressure waves on the brainstem. Neurol Med Chir. 1990;30(5):301–8.
112. Takeuchi S, Koike T, Sasaki O, Kamada K, Tanaka R, Arai H. Intracranial extradural pressure monitoring after direct operation on ruptured cerebral aneurysms. Neurosurgery. 1989;24(6):878–83.
113. Yokota A, Matsuoka S, Ishikawa T, Kohshi K, Kajiwara H. Overnight recordings of intracranial pressure and electroencephalography in neurosurgical patients. Part II: changes in intracranial pressure during sleep. J UOEH. 1989;11(4):383–91.
114. Sato H, Sato N, Tamaki N, Matsumoto S. The critical threshold of cerebral perfusion pressure in intracranial pressure circumstance of hydrocephalus during infancy. No Shinkei Geka. 1988;16(4):385–92.
115. Maeda M, Matsuura S, Tanaka K, Katsuyama J, Nakamura T, Sakamoto H, et al. Effects of electrical stimulation on intracranial pressure and systemic arterial blood pressure in cats. Part I: stimulation of brain stem. Neurol Res. 1988;10(2):87–92.
116. Gjerris F, Børgesen SE, Sørensen PS, Boesen F, Schmidt K, Harmsen A, et al. Resistance to cerebrospinal fluid outflow and intracranial pressure in patients with hydrocephalus after subarachnoid haemorrhage. Acta Neurochir. 1987;88(3–4):79–86.
117. Hayashi M, Kobayashi H, Kawano H, Handa Y, Yamamoto S, Kitano T. ICP patterns and isotope cisternography in patients with communicating hydrocephalus following rupture of intracranial aneurysm. J Neurosurg. 1985;62(2):220–6.
118. Schoeman JF, le Roux D, Bezuidenhout PB, Donald PR. Intracranial pressure monitoring in tuberculous meningitis: clinical and computerized tomographic correlation. Dev Med Child Neurol. 1985;27(5):644–54.
119. Kosteljanetz M. CSF dynamics in patients with subarachnoid and/or intraventricular hemorrhage. J Neurosurg. 1984;60(5):940–6.
120. Hayashi M, Kobayashi H, Kawano H, Yamamoto S, Maeda T. Cerebral blood flow and ICP patterns in patients with communicating hydrocephalus after aneurysm rupture. J Neurosurg. 1984;61(1):30–6.
121. Brock M, Cervos-Navarro J, Holdorff B. Changes in intracranial pressure associated with delayed cerebral radionecrosis. Surg Neurol. 1984;22(1):8–16.
122. Kuchiwaki H, Kageyama N, Hirai N, Takada S, Inao S, Terashima M, et al. A biological rhythm in a patient with normal pressure hydrocephalus-comparative studies in pre- and postoperative patients by a polygraphy. No To Shinkei. 1984;36(9):911–6.
123. Tamaki N, Kusunoki T, Kose S, Matsumoto S. Continuous intracranial pressure monitoring in normal pressure hydrocephalus-with special reference to clinical significance of B wave and prognostic criteria for CSF shunting. No To Shinkei. 1983;35(2):131–7.

124. Auer LM, Sayama I. Intracranial pressure oscillations (B-waves) caused by oscillations in cerebrovascular volume. Acta Neurochir. 1983;68(1–2):93–100.
125. Terzano MG, Gatti PL, Manzoni GC, Formentini E, Mancia D. Is the EEG cyclic alternating pattern a true autonomous entity? Analytic study in a case of post-traumatic coma with good prognosis. Eur Neurol. 1982;21(5):324–34.
126. Gjerris F, Børgesen SE, Hoppe E, Boesen F, Nordenbo AM. The conductance to outflow of CSF in adults with high-pressure hydrocephalus. Acta Neurochir. 1982;64(1–2):59–67.
127. Tomei G, Gaini SM, Giovanelli M, Rampini P, Granata G, Villani R. Intracranial pressure in subarachnoid hemorrhage. Preliminary report in 36 cases. J Neurosurg Sci. 1981;25(2):57–66.
128. Kaye AH, Brownbill D. Postoperative intracranial pressure in patients operated on for cerebral aneurysms following subarachnoid hemorrhage. J Neurosurg. 1981;54(6):726–32.
129. Bilz D, Pásztor A, Paraicz E. Rhythmic correlations between regional intracranial blood volume and intracranial pressure within minutes during continuous simultaneous recording in infants. Psychiatr Neurol Med Psychol. 1981;33(8):483–90.
130. Munari C, Calbucci F, Casaroli D, Bonora M. Correlations between E.E.G. findings and intracranial pressure (ICP) during treatment of acute post-traumatic intracranial hypertension (preliminary report) (author's transl). Rev Electroencephalogr Neurophysiol Clin. 1980;10(4):319–30.
131. Guieu JD, Lapierre M, Blond S, Hurtevent JF, Jomin M, Pruvot P. Correlations between intracranial pressure variations and EEG changes in patients with cranial trauma (author's transl). Rev Electroencephalogr Neurophysiol Clin. 1979;9(2):194–201.
132. Wilkinson HA, Schuman N, Ruggiero J. Nonvolumetric methods of detecting impaired intracranial compliance or reactivity: pulse width and wave form analysis. J Neurosurg. 1979;50(6):758–67.
133. Liguori G, Fiordirosa M, Cicchiello LR, Ambrosio A. Long-term monitoring of intracranial pressure in hydrocephalic children not affected by cerebral tumor. J Neurosurg Sci. 1979;23(4):295–302.
134. Fuentes JM, Bouscarel C, Choucair Y, Roquefeuil B, Vlahovitch B, Blanchet P. Monitoring of intracranial pression in acute neurotrauma by extra-dural screw (author's transl). Anesth Analg. 1979;36(9–10):429–33.
135. Munari C, Calbucci F. Correlations between intracranial pressure (I.C.P.) and EEG changes during traumatic coma (author's transl). Rev Electroencephalogr Neurophysiol Clin. 1979;9(2):185–93.
136. Hayashi M, Marukawa S, Fujii H, Kitano T, Kobayashi H, Yamamoto S. Intracranial hypertension in patients with ruptured intracranial aneurysm. J Neurosurg. 1977;46(5):584–90.

Publisher's Note

A.2 Paper II

Title: B-waves are present in patients without intracranial pressure disturbances

Authors: Casper Schwartz Riedel, Isabel Martinez Tejada, Nicolas Hernandez Norager, Lykke Kempfner, Poul Jennum, and Marianne Juhler

Journal: Journal of Sleep Research

Status: Published

DOI: 10.1111/jsr.13214

Received: 4 August 2020 | Revised: 11 September 2020 | Accepted: 17 September 2020

DOI: 10.1111/jsr.13214

REGULAR RESEARCH PAPER

Journal of Sleep Research

B-waves are present in patients without intracranial pressure disturbances

Casper Schwartz Riedel[1,2] | Isabel Martinez-Tejada[1,3] | Nicolas Hernandez Norager[1] | Lykke Kempfner[2] | Poul Jennum[2,4] | Marianne Juhler[1,4]

[1]Department of Neurosurgery, Rigshospitalet, Copenhagen, Denmark

[2]Danish Center for Sleep Medicine, Department of Clinical Neurophysiology, Rigshospitalet, Glostrup, Denmark

[3]Department of Health Technology, Technical University of Denmark, Copenhagen, Denmark

[4]Institute of Clinical Medicine, University of Copenhagen, Copenhagen, Denmark

Correspondence
Casper Schwartz Riedel, Department of Neurosurgery, Rigshospitalet, Copenhagen, Denmark and Faculty of Health Sciences, University of Copenhagen, Copenhagen, Denmark.
Email: casper.schwartz.riedel@regionh.dk

Funding information
The Lundbeck Foundation (R211-2015-2937), Alzheimer's Research Fund, and IMK Almene Fund, Novo Nordisk Tandem (NNF17OC0024718).

Abstract

Intracranial pressure (ICP) B-waves are defined as short, repeating elevations of ICP of up to 50 mmHg with a frequency of 0.5–2 waves/min. The presence of B-waves in overnight recordings is regarded as a pathological phenomenon. However, the physiology of B-waves is still not fully understood and studies with transcranial Doppler, as a surrogate marker for ICP, have suggested that B-waves could be a normal physiological phenomenon. We present four patients without known structural neurological disease other than a coincidentally found unruptured intracranial aneurysm. One of the patients had experienced well-controlled epilepsy for several years, but was included because ICP under these conditions is unlikely to be abnormal. Following informed consent, all four patients had a telemetric ICP probe implanted during a prophylactic operation with closure of the aneurysm. They underwent overnight ICP monitoring with simultaneous polysomnography (PSG) sleep studies at 8 weeks after the operation. These patients exhibited nocturnal B-waves, but did not have major structural brain lesions. Their ICP values were within the normal range. Nocturnal B-waves occurred in close association with sleep-disordered breathing (SDB) in rapid eye movement (REM) and non-REM sleep stages. SDB during REM sleep was associated with ramp-type B-waves; SDB during non-REM sleep was associated with the sinusoidal type of B-wave. We propose that B-waves are a physiological phenomenon associated with SDB and that the mechanical changes during respiration could have an essential and previously unrecognised role in the generation of B-waves.

KEYWORDS

hydrocephalus, Lundberg B-waves, normal ICP, polysomnography, sleep apnea, sleep-disordered breathing

1 | INTRODUCTION

Intracranial pressure (ICP) measurement is a cornerstone of neurology and neurosurgical diagnostics. Lundberg initially described different macro patterns in the ICP and categorised them as A-, B-, and C-waves. Here, we focus specifically on B-waves, as they are the most commonly found macro pattern in clinical practice. B-waves were originally defined as rhythmic oscillations in the ICP signal with an amplitude up to 50 mmHg and with frequencies of 0.5–2 waves/min (Lundberg, 1960). Since then, two types of B-wave have been described, ramp-type and sinusoidal, with the latter subdivided into high- or low-amplitude waves depending on whether the amplitude is > or <10 mmHg (Martinez-Tejada et al., 2019).

The presence of B-waves in overnight recordings has customarily been regarded as a pathological phenomenon. When the ICP is not

Poul Jennum and Marianne Juhler shared last author.

raised, B-waves alone are often used to support decisions for invasive ICP management. However, the physiology of B-waves is still not understood, and it has been proposed, based on studies with non-invasive ICP methods, e.g. transcranial Doppler, that B-waves may be a normal physiological phenomenon that is also seen in healthy subjects (Droste et al., 1993; Droste & Krauss, 1997; Mautner-Huppert et al., 1989; Newell et al., 1992). Previous studies have suggested a correlation of B-waves with sleep, and particularly rapid eye movement (REM) sleep, in patients with known or suspected abnormal ICP (Hirsch et al., 1978; Krauss et al., 1995; Pierre Kahn et al., 1976; Yokota et al., 1989). B-waves are also associated with sleep-disordered breathing (SDB) (Cooper & Hulme, 1966; Jennum & Børgesen, 1989; Lundberg, 1960; Yokota et al., 1989), and a highly significant correlation between the duration of apneas and B-waves was found in six patients with severe SDB (Jennum & Børgesen, 1989).

Only a few cases of invasive ICP have been published to date, suggesting that B-waves may be present in healthy subjects (Droste & Krauss, 1997; Lundberg, 1960; Martin, 1978). However, these reports were of single cases and in direct relation to surgical intervention, which could have influenced the findings. Current telemetric ICP equipment allows for long-term ICP monitoring, thus reducing short-term confounding effects after surgery. The technological advantages of current telemetric ICP equipment make long-term ICP monitoring possible (Norager et al., 2018), and any short-term confounding effects of the surgery on the ICP measurements less likely.

The present study aimed to investigate whether B-waves occur in subjects without major structural brain lesions and with ICP values within the normal range and, if possible, to determine their origin. To this end, telemetric ICP signals were recorded 8 weeks after surgery and combined with simultaneous polysomnography (PSG) sleep studies, to enable us to search for possible associations between B-waves, sleep stages, and SDB.

2 | METHODS

This study focusses mainly on the nocturnal occurrence of B-waves. It is part of a more extensive research programme investigating sleep and the glymphatic system in humans.

The study was approved by the Committee on Health Research Ethics for the Capital Region of Denmark (H-1-2014-123 and H-17011472), and was performed according to the standards set by the Helsinki declaration. All patients gave their written informed consent.

2.1 | Study population

Due to the invasive nature of ICP measurement, completely healthy persons could not be recruited. The option was thus to select pseudo-normal individuals, in whom it was both ethically acceptable to measure, and feasible to obtain measurements that had a high probability of being normal.

We recruited patients who were scheduled for surgery for an unruptured aneurysm and who had no previously diagnosed brain disease. Four patients consented to participate in the study. None of the patients had previous symptoms of elevated ICP, and all magnetic resonance (MR) scans were normal except for the aneurism. Three had no history of other neurological diseases, and the fourth patient had experienced well-controlled epilepsy for several years, but was included because ICP under these conditions is unlikely to be abnormal. Details of these four patients are shown in Table 1.

2.2 | Surgery and the telemetric device

All four patients were operated for an unruptured aneurysm of the right middle cerebral artery. A standard right-sided approach was made in which the aneurysm was accessed through the Sylvian fissure. After placing one or more clips, the aneurysm sack was punctured, and blood flow in the arteries was ensured by endo-Doppler. At the end of the surgery, a commercially available telemetric ICP probe (Neurovent-P-tel; Raumedic AG) was inserted 2 cm into the brain parenchyma through the top of the craniotomy. Calibration was not necessary before insertion. Fixation of the bone flap and soft-tissue closure were done according to the usual surgical standards. All operations were completed without complications, and all patients were discharged the next day. Follow-up in the outpatient clinic showed that their neurological function continued to be normal.

TABLE 1 Patient demographics

Variable	Patient 1	Patient 2	Patient 3	Patient 4
Age, years	54	55	56	74
Gender	Female	Female	Female	Male
Disease	No known diseases	Type 1 diabetes mellitus	Hypertension, epilepsy, hyperthyroidism	Hypertension, ischaemic heart disease, follicular lymphoma
Medication	No	Insulin	Enalapril, levetiracetam, thiamazol, centyl	Amlodipine, statins, aspirin, omeprazole
Smoking	Yes	Yes	Yes	No
Height, cm	162	158	176	176
Weight, kg	60.0	53.0	72.0	79.6
BMI, kg/m^2	22.9	21.2	23.2	26.5

2.3 | Polysomnography and ICP recording

The study was performed 8 weeks after surgery, as this period is sufficient to allow postoperative recovery and to minimise the influence of the surgical procedure on the results, while at the same time providing telemetric ICP data before the 3-month implantation period established by the manufacturer. The PSG (SOMNOscreen™ plus, Somnomedics) and telemetric ICP recordings (NEUROVENT-P-tel, recorded using Reader TDT readP, and stored on the Datalogger MPR1, RAUMEDIC AG), were recorded simultaneously. During PSG recording, the ICP signal was transferred from the Datalogger to the SOMNOscreener by an analogue cable to ensure the correct and fully synchronised time incorporation of the ICP signal into the PSG data.

Polysomnography is a criterion standard method of sleep monitoring and the only method that allows assessment of sleep architecture. PSG was based on the recording of an electroencephalogram (EEG) together with several other physiological signals (electro-oculography, submental- and anterior tibialis electromyography, electrocardiography (ECG), airflow, respiratory inductance plethysmography (RIP), snoring, oxyhaemoglobin saturation (SaO_2), end-tidal CO_2 (LoFlo, Respironics, Inc.)). Recordings were scored manually by an experienced neurophysiology assistant according to the guidelines of the American Academy of Sleep Medicine (AASM). SDB was detected by the Apnea–Hypopnea Index (AHI), wherein a value of <5 indicates no SDB, 5–14 indicates mild SDB, 15–29 indicates moderate SDB, and ≥30 indicates severe SDB.

2.4 | Respiratory disturbances

We defined respiratory disturbances (RDs) as events lasting for ≥5 s, with flattening of the RIP and a reduction in flow from baseline, which did not meet the flow criteria for apnea or hypopnea and was not associated with oxygen desaturation. It is important to note that these RDs are not respiratory effort-related arousals (RERAs) as defined by the AASM. We found it was more important to score RD events than RERAs, because our primary interest was in the disturbances in the respiratory movements, regardless of arousal.

2.5 | Data processing after PSG recording

After manually scoring the PSG, all data were transferred to Matlab 2019b (MathWorks®). The signals were recorded by two sensors: the Datalogger MPR1 and the PSG. The data were collected asynchronously by these two sensors, so time alignment was necessary to remove the delay between them. As a result, the signal recorded by the Datalogger MPR1 was integrated into the PSG signal. Only the synchronised Datalogger MPR1 ICP signal was analysed further. Before carrying out the ICP analysis, artefacts were identified and removed from the Datalogger MPR1 ICP signal.

3 | RESULTS

3.1 | Measurement quality

The process of overnight measurement with PSG and ICP was well tolerated by all patients. The unusual sleep environment created by the equipment caused overall sleep quality to be poorer than was habitual for all patients, but it was sufficient to provide a sleep hypnogram of acceptable quality, with all sleep stages present in all patients. A telemetric ICP signal of technically good quality was obtained from the four patients throughout the night. Due to the temporary displacement of the reader on the scalp, there were minor periods of signal loss in patient 1 (2 min) and patient 3 (15 min). The median ICP values ranged between −6.00 and 6.20 mmHg for the whole recording (including upright and supine awake positions and sleep). In parts of the PSG recording, patient 1 dislodged the saturation monitor from the finger, and the oxygen saturation data was lost. However, it was still possible to score SDB with the RIP signal during most of these periods.

3.2 | The occurrence of B-waves

While asleep, all patients had periodic elevations of ICP, with amplitudes and frequencies fulfilling the Lundberg criteria for B-waves (Lundberg, 1960). These were seen to have different morphologies during various sleep stages. B-wave morphology during REM sleep was of the ramp type. Sinusoidal B-waves of smaller amplitudes were present during non-REM sleep stages.

3.3 | Relationship between B-waves and respiration

Mild to severe SDB (Table 2) was observed in all four subjects. The duration of respiratory changes and of B-waves was closely correlated. The ICP pattern followed all respiratory events, forming a continuum of SDB from complete (apnea) to partial (hypopnea) obstruction of the airways to only RDs, with a decrease in respiratory movements, which did not meet the criteria for apnea or hypopnea. ICP elevations synchronous with SDB accounted for the majority of B-wave episodes (50%–100%) (Table 3). All four patients had SDB with ICP elevations that were too small to be classified as B-waves. The relationship between the ICP and SDB is shown in Figures 1–3 and Figure S1. The ICP of all four patients was higher during the night than during the day, and highest during episodes with B-waves (Figure 4). The most pronounced B-waves were present when respiration resumed with a ventilatory overshoot, marked by increased flow and respiratory movements in the thorax and abdominal RIP. All four patients also had ICP elevations due to movement during short periods of wakefulness. These ICP elevations were not included in the calculation of the total B-wave frequency. Details of the B-waves and their association with SDB for each patient are summarised in Tables 2–5.

TABLE 2 Apnea–hypopnea and respiratory disturbances

	Apnea–Hypopnea (index)			Respiratory disturbances (index)		
	Sleep stage			Sleep stage		
Patient	Non-REM	REM	Total	Non-REM	REM	Total
1	53 (7.8)	59 (46.0)	112 (13.9)	59 (8.7)	12 (9.4)	71 (8.8)
2	62 (17.1)	35 (48.3)	97 (22.3)	191 (52.8)	49 (67.6)	240 (55.3)
3	63 (10.7)	9 (9.7)	70 (10.9)	5 (5.4)	8 (1.4)	13 (2.0)
4	278 (55.4)	13 (18.8)	291 (53.4)	66 (13.9)	12 (17.3)	78 (14.3)

Apnea with complete obstruction and hypopnea with partial obstruction of the airways. Respiratory disturbances: events lasting ≥5 s with flattening of the respiratory inductance plethysmography and a reduction in flow from baseline, which did not meet the flow criteria for apnea or hypopnea and was not associated with oxygen desaturation. Index in parenthesis indicates the total number divided by the hours of sleep (or sleep stage).

TABLE 3 B-waves during sleep and association with sleep-disordered breathing (SDB)

Patient	Total	SDB	%	Excluded
1	114	101	88.6	3
2	183	166	91.0	20
3	172	86	50.0	11
4	139	139	100	0

3.4 | B-waves and CO_2

Patient 4 was also monitored with LoFlo CO_2, but during parts of the night (2 hr and 30 min in total), the CO_2 signal was lost due to water condensation. Most of the B-waves coincided with a small increase in CO_2 tension (1–3 mmHg), but CO_2 tension remained within the normal range of 32–42 mmHg (4.2–5.6 kPa; Figure 3). Very few B-waves were associated with slightly higher CO_2 tension (total increases of up to 8 mmHg/49 mmHg), and their morphologies and amplitudes did not differ from those of the vast majority of other B-waves. Therefore, no overall correlation between B-waves and CO_2 levels was concluded for this patient.

4 | DISCUSSION

Our main finding is that B-waves seem to occur during sleep in patients who have no major structural brain lesions, and whose ICP values fall within traditional and recently accepted normal ranges (Andresen & Juhler, 2014). Our observations suggest that high-amplitude ramp-like B-waves are associated with REM sleep, while smaller, sinusoidal waves, which are also generally classified as B-waves, are associated with non-REM sleep stages. Both types of B-wave occur in conjunction with apneas and hypopneas. We also observed a close association between RDs and the onset and duration of B-waves in all four patients. None of the included patients had a history consistent with pre-existing sleep apnea or other respiratory disorders.

4.1 | B-waves during sleep

B-waves have long been known to occur during sleep, and particularly during REM sleep (Hirsch et al., 1978; Krauss et al., 1995; Pierre Kahn et al., 1976; Yokota et al., 1989), but this information comes from studies that were performed on patients with known or suspected abnormal ICP. Four cases (Droste & Krauss, 1997; Lundberg, 1960; Martin, 1978) and a few studies with ICP surrogate markers have suggested that B-waves may be present in healthy people (Droste et al., 1993; Droste & Krauss, 1997; Mautner-Huppert et al., 1989; Newell et al., 1992). Lundberg, reporting on one healthy patient undergoing invasive ICP measurement, found many sinusoidal B-waves during sleep, similar to what we observed in patient 4. Lundberg also stated that the ICP pattern resembled that of patients with intracranial lesions, but no signs of intracranial hypertension (Lundberg, 1960). Droste and Krauss reported B-waves with a relative frequency of 50%–60% in two non-hydrocephalic men with normal ICP (Droste & Krauss, 1997). Furthermore, they found ramp-type B-waves to be more frequent in the early morning hours where REM sleep is more prevalent, suggesting ramp-type B-waves to be associated with REM sleep, in agreement with our present findings.

4.2 | B-wave equivalents

Droste et al. (Droste & Krauss, 1997) studied 10 healthy young adults with transcranial Doppler and found rhythmic changes in blood flow velocity (ICP B-wave equivalents) with a varying frequency (from 35% to 75%) between sleep stages, and most frequently during REM sleep. These observations support the findings of our present study, but unfortunately, respiratory and other clinical data were not reported, making it impossible to assess whether the reported B-wave equivalents were related to SDB.

Changes in blood flow have been reported in 70%–80% of healthy people (Droste & Krauss, 1997; Mautner-Huppert et al., 1989; Newell et al., 1992), indicating that this ICP B-wave equivalent is a common finding. Interestingly, Newell et al. observed small changes

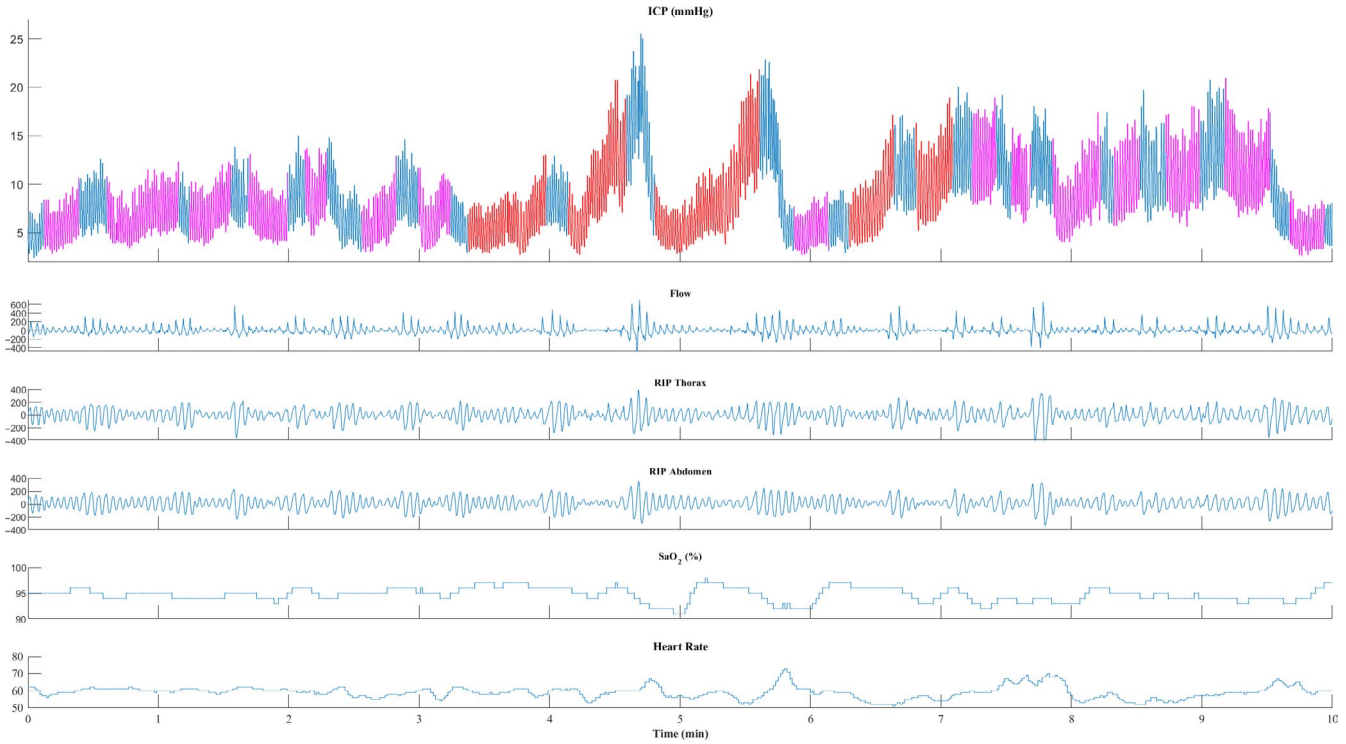

FIGURE 1 Example of intracranial pressure (ICP) B-waves during sleep-disordered breathing in patient 2. This figure illustrates the underlying respiratory changes summarised in the ICP signal as apneas (red) or respiratory disturbances (purple). The peak of the B-waves is seen when respiration resumes with a ventilatory overshoot, marked by increased flow and respiratory movements in the thorax and abdominal RIP. ICP is shown in blue, with red and purple indicating duration of apneas and respiratory disturbances, respectively. Flow: nasal cannula registering flow changes (arbitrary units). RIP, respiratory inductance plethysmography; thorax and abdomen movements (arbitrary units). SaO_2 (%), oxyhaemoglobin saturation measured on the finger. Heart rate, beats/min

in the respiratory rate in some of their subjects at a frequency similar to that of the changes in blood flow (Newell et al., 1992).

4.3 | B-waves and sleep-disordered breathing (SDB)

The relationship between B-waves and SDB is not a new finding, Lundberg having reported it in 1960. Since then, other studies have confirmed an association between B-waves, sleep stages, and SDB (Cooper & Hulme, 1966; Jennum & Børgesen, 1989; Yokota et al., 1989). Jennum and Børgesen found significant increases in ICP, coinciding with apneas during sleep, in six patients with severe SDB (Jennum & Børgesen, 1989). They found that the apneas in REM sleep were longer and featured greater pressure variations than in non-REM sleep. ICP and ICP equivalents are highest during REM sleep, when apneas are typically prolonged, giving rise to high-amplitude ramp-type waves with an almost ICP A-wave (plateau) morphology (Droste & Krauss, 1997; Jennum & Børgesen, 1989). Some authors have suggested that the amplitude, rather than the occurrence of B-waves, is more critical for evaluating the patients. In the results presented here, the amplitudes of the B-waves varied markedly within each patient, and the greatest amplitudes were seen during REM sleep. Furthermore, the distribution of SDB between REM sleep and non-REM sleep varied considerably between the four patients. Thus, the amplitude of the B-waves could be more a matter of the sleep stages in which SDB-associated B-waves occur than one of reduced compliance of the brain. This calls into question the importance of B-wave amplitude in clinical settings.

4.4 | Possible physiological contexts

Several mechanisms have been suggested as causes of nocturnal ICP abnormalities in patients with SDB: transient hypoxia and hypercapnia causing cerebral vasodilatation during hypoventilation during the night; severe arterial pressure variations during apnea combined with intracerebral vasodilation (due to hypoxia, hypercapnia); intrathoracic pressure variation with initial negative pressure during apnea, with terminal pressure increase. All of these contribute to the severe pressure variations that occur during apnea.

CO_2 is an essential and primary factor in altering the overall level of ICP through vasodilation or constriction of the cerebral blood vessels, altering the cerebral blood flow and volume. With CO_2 values ranging from 20 to 80 mmHg, cerebral blood flow changes 1–2 ml 100 g^{-1} min^{-1} for each 1 mmHg change in CO_2, and cerebral blood volume changes 0.05 ml/100 g for each 1 mmHg change in CO_2 (Brian, 1998). CO_2 and change in arterial blood pressure are usually hypothesised as being involved in the

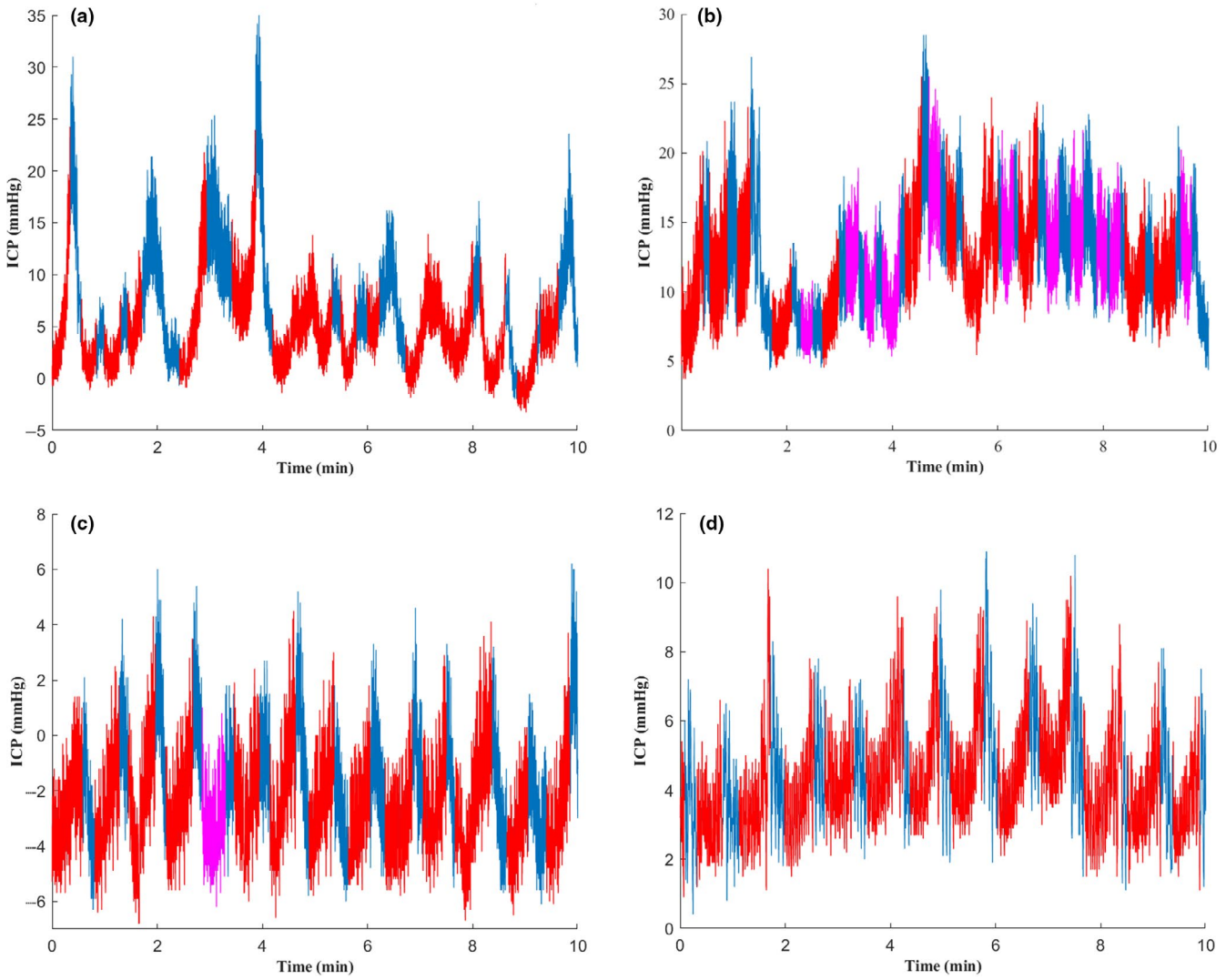

FIGURE 2 Example of an intracranial pressure (ICP) B-wave segment during sleep-disordered breathing in each patient. ICP is shown in blue, with red and purple indicating duration of apneas and respiratory disturbances, respectively. (a) patient 1, (b) patient 2, (c), patient 3, (d) patient 4. ICP (mmHg) and time (min)

generation of B-waves and the rise in ICP. However, we suggest that the mechanical effect of respiratory movements may be more important than CO_2 to the occurrence of B-waves during sleep. Thus, we observed B-waves in association with RDs in all four patients, where only the respiratory movements are affected and not the oxygen saturation of the blood. Moreover, there was no association between the changes in CO_2 and the occurrence of B-waves in patient 4. When most of the B-waves arose, the CO_2 tension changed by only 1–3 mmHg, which is equivalent to the regular change in CO_2 when going from awake to asleep (Madsen et al., 1991). Although early studies of ICP dynamics suggested that CO_2 was instrumental for the formation of B-waves, later reports have indicated that this may not be the case. Thus in 1960, Lundberg originally suggested a role for CO_2 in B-waves, inspired by his observation that they disappeared once respirations were controlled (Lundberg, 1960). He speculated that variations in arterial CO_2 would provide the best explanation for the presence of B-waves. Yet, many later attempts have failed to verify this causal relationship. Interestingly, as early as 1972, Tindall et al. investigated 27 patients with head injuries and found CO_2 changes in association with B-waves (Tindall et al., 1972), concluding that CO_2 generated the B-waves; however, their data show only small changes in CO_2 compared with the significant changes in respiratory impedance signals. Also, subsequent studies found B-waves to be present at constant CO_2 levels in artificially ventilated and spontaneously respiring patients (Børgesen & Espersen, 1986; Venes, 1979). Furthermore, Jennum and Børgesen also suggested that cerebral hypoxia or hypercapnia during SDB alone could not account for the significant increases in ICP and that other factors, like systemic blood pressure or central venous pressure, most likely contributed to these changes (Jennum & Børgesen, 1989). Experimental data also suggest that CO_2 is unlikely to generate B-waves, at least when ICP is <20 mmHg. A study of eight adult rhesus macaques showed that increasing CO_2 above the normal

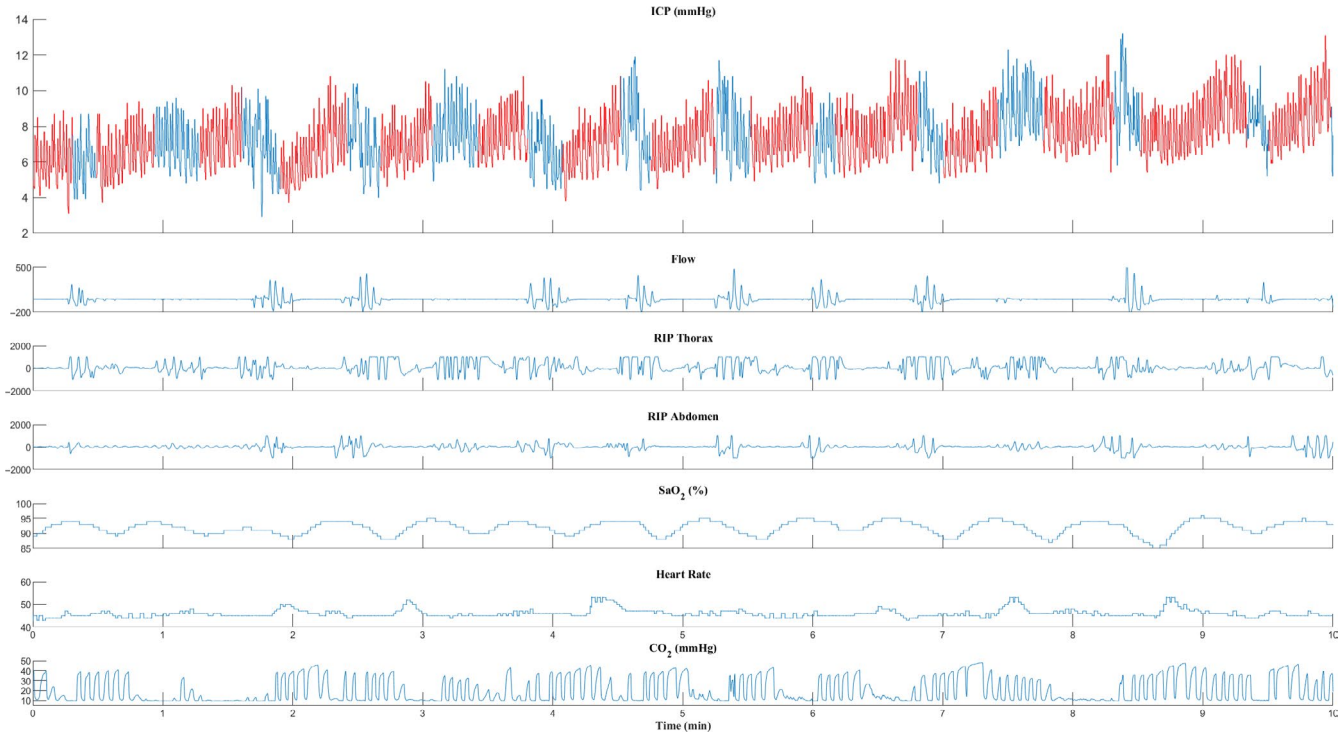

FIGURE 3 Example of intracranial pressure (ICP) B-waves during sleep-disordered breathing with CO_2 in patient 4. ICP is shown in blue, with red indicating apnea duration. Flow: nasal cannula registering flow changes (arbitrary units). RIP, respiratory inductance plethysmography; thorax and abdomen movements (arbitrary units). SaO_2 (%), oxyhaemoglobin saturation measured on the finger. Heart rate (beats/min) and end-tidal CO_2 (mmHg)

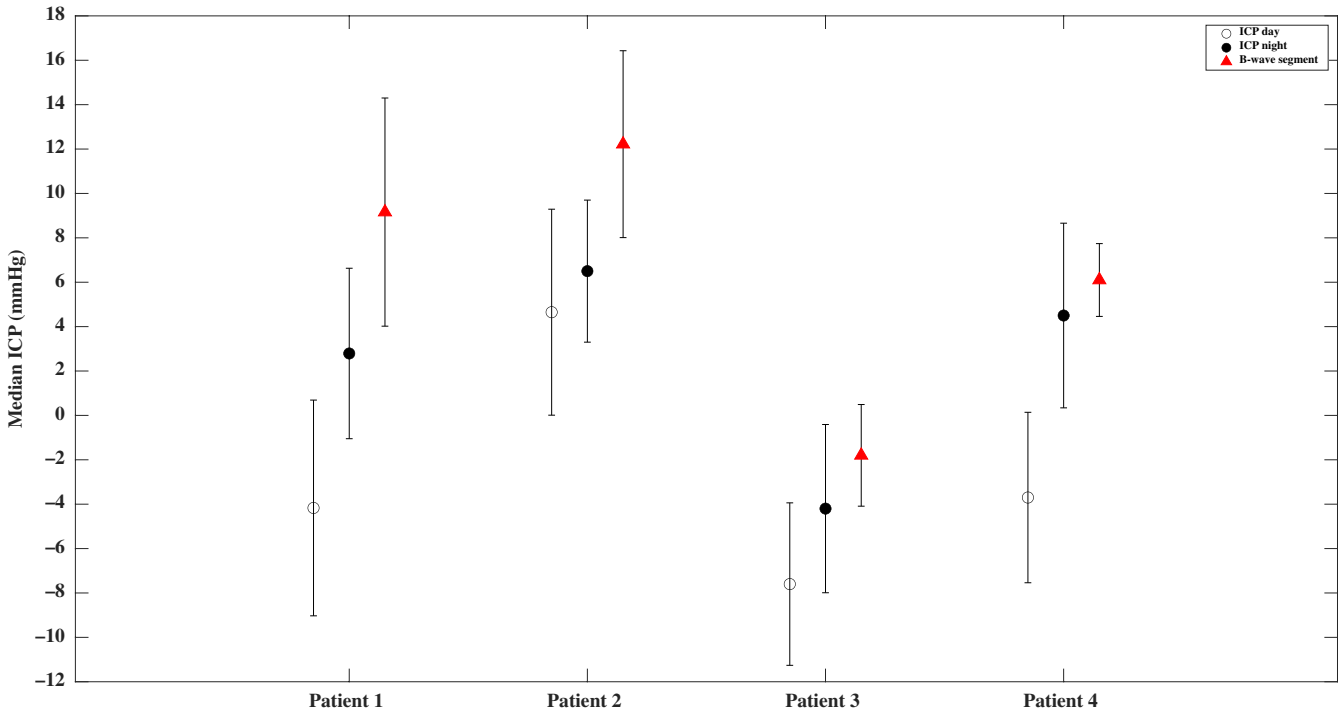

FIGURE 4 Median day and night intracranial pressure (ICP) values, and a representative 10-min B-wave segment for all four patients. The day and night segments were selected based on the hypnogram, and both contain different positions (upright, sitting, supine, lying on the left and right), which influences the median ICP values and standard deviation. All four patients have the same general pattern, with lowest ICP values during the day, followed by night ICP values, and B-wave segments (10-min B-wave segment measured with all patients in a supine position). Error bars indicate standard deviations

TABLE 4 Phenotype of B-waves and sleep stage

	Ramp-type B-waves high amplitude		Sinusoidal B-waves low amplitude		Sinusoidal B-waves high amplitude	
Patient	Non-REM	REM	Non-REM	REM	Non-REM	REM
1	÷	+++	+	÷	÷	÷
2	÷	++	+++	÷	+	÷
3	÷	+	+	÷	÷	÷
4	÷	÷	+++	÷	÷	+

TABLE 5 Intracranial pressure (ICP) during B-waves

Patient	Median	*SD*	Maximum	Minimum
1	4.98	5.97	35.60	−3.27
2	12.22	4.21	28.52	2.74
3	−1.80	2.29	8.82	−6.80
4	7.30	1.59	13.20	2.90

Median ICP of a 10-min representative B-waves segment, with standard deviation (*SD*) and maximum and minimum ICP values for each of the four patients.

range of 32–42 mmHg increased ICP by only a few mmHg, and increasing CO_2 up to 80 mmHg resulted in an increase in ICP of only ~5 mmHg. However, CO_2 had a more pronounced effect on ICP when the levels of the latter were clearly abnormal, at >20 mmHg. At severely elevated ICP levels of 50 mmHg, CO_2 at 30 mmHg already had a significant impact (Kindt & Gosch, 1972). Today, CO_2 fluctuations are not considered the main cause of B-waves, although CO_2 may be regarded as a potential modulator (Einhäupl et al., 1986; Russo et al., 2000). In contrast, according to our present findings, the mechanical changes during respiration could play an essential and hitherto unrecognised role in the generation of B-waves. This is supported by a highly significant phase correlation of B-waves with the peak of respiratory movements, central venous pressure, and arterial blood pressure, with or without changes in CO_2 (Einhäupl et al., 1986; Jennum & Børgesen, 1989). Breathing movements in the respiratory muscles during SDB, especially those of the diaphragm, could create B-waves by altering venous return and stroke volume. To test this hypothesis, future studies would need to measure diaphragm muscle movements and stroke volume in the heart during B-waves.

4.5 | Clinical implications

B-waves have attracted particular attention in patients with idiopathic normal pressure hydrocephalus (iNPH), including as a predictor of the effect of shunt surgery. However, those particular results were not conclusive (Halperin et al., 2015). Thus, B-waves are no longer accepted as a major predictor of the effect of shunt surgery (Marmarou et al., 2005). It is noteworthy that SDB is found in 65%–90% of patients with iNPH (Kristensen et al., 1998; Román et al., 2018), and combined with our present findings, could explain the high prevalence of B-waves in patients with iNPH, and why B-waves cannot predict the effect of shunt surgery. Furthermore, this also suggests that the assessment of iNPH should include a sleep evaluation with PSG. If ramp-type B-waves are found in clusters primarily during the latter half of the night, it is essential to rule out REM sleep-related SDB.

Our present results also suggest that continuous positive airway pressure (CPAP) could be a valuable component of the diagnostic assessment and possibly treatment, of patients who display B-waves during an overnight diagnostic invasive ICP study.

4.6 | Limitations

We cannot entirely discount the possibility that the aneurysm operation or the implementation of the telemetric ICP probe may have caused the abnormalities that gave rise to the observed B-waves. However, the very close relationship between B-waves and SDB and RDs makes this very unlikely. In addition, all surgical procedures were uncomplicated, and the applied technology made it possible for brain recovery to proceed for several weeks before the study.

The zero-offset drift of the telemetric probe is a potential source of error, but this becomes relevant only after very long-term implantation, well beyond the 3-month utility period set by the manufacturer (Norager et al., 2018). In any case, the zero-offset drift of the telemetric ICP probe does not impede the identification of waveforms (Lilja-Cyron et al., 2018; Norager et al., 2018), including B-waves.

The low sampling frequency (5 Hz) is another drawback of the telemetric probe, which gives a lower resolution and possible source of error. ICP pulse wave amplitude and morphology can be accessed, but are consistently underestimated as the low sampling frequency cuts off the peak of the signal (Norager et al., 2019). Long-term signal stability could also cause underestimation of B-waves if the ICP signal is lost due to displacement of the reader on the scalp caused by patient movements. The latter has unlikely influenced our present findings, as there were only short episodes of signal loss in two of the patients.

5 | CONCLUSION

We have found B-waves in patients without major structural brain lesions or disturbances of ICP. Their occurrence was associated with SDB. High-amplitude ramp-like B-waves waves were linked to REM

sleep, and smaller sinusoidal waves were associated with non-REM sleep stages. We conclude that B-waves are a normal physiological phenomenon associated with SDB and that the mechanical changes during respiration could have an essential and previously unrecognised role in the generation of B-waves.

ACKNOWLEDGMENTS

The authors gratefully acknowledge support in the form of research grants from the Lundbeck Foundation (R211-2015-2937), the Alzheimer's Research Fund, the IMK Almene Fund, and the Novo Nordisk Foundation (NNF17OC0024718). We also wish to thank Helle Leonthin and Christine Rehder Christensen for their skillful technical assistance in the evaluation of all the PSG data.

CONFLICTS OF INTEREST

All authors certify that they have no affiliations with, or involvement in, any organisation or entity with any financial or non-financial interest in the subject matter or materials discussed in this manuscript.

AUTHOR CONTRIBUTIONS

CSR, PJ, and MJ designed the study. CSR and NHN collected the data. CSR, IM-T, and LK wrote the Matlab code and analysed the data. CSR wrote the first version of the manuscript. All authors contributed to writing and editing the final version.

DATA AVAILABILITY STATEMENT

The data that support the findings of this study are available on request from the corresponding author. The data are not publicly available due to privacy or ethical restrictions.

ORCID

Casper Schwartz Riedel https://orcid.org/0000-0002-9393-0092
Isabel Martinez-Tejada https://orcid.org/0000-0003-4717-8597
Nicolas Hernandez Norager https://orcid.org/0000-0003-1896-7749
Poul Jennum https://orcid.org/0000-0001-6986-5254
Marianne Juhler https://orcid.org/0000-0003-2652-7495

REFERENCES

Andresen, M., & Juhler, M. (2014). Intracranial pressure following complete removal of a small demarcated brain tumor: A model for normal intracranial pressure in humans. *Journal of Neurosurgery*, *121*(4), 797–801. https://doi.org/10.3171/2014.2.JNS132209

Børgesen, S. E., & Espersen, J. (1986). The correlation between A- and B-waves and arterial CO_2 tension. In J. D. Miller, G. M. Teasdale, J. O. Rowan, S. L. Galbraith, & A. D. Mendelow (Eds.), *Intracranial pressure VI* (pp. 298–304). : Springer.

Brian, J. E. (1998). Carbon dioxide and the cerebral circulation. *Anesthesiology*, *88*(5), 1365–1386. https://doi.org/10.1097/00000542-199805000-00029

Cooper, R., & Hulme, A. (1966). Intracranial pressure and related phenomena during sleep. *Journal of Neurology, Neurosurgery & Psychiatry*, *29*(6), 564–570. https://doi.org/10.1136/jnnp.29.6.564

Droste, D. W., Berger, W., Schuler, E., & Krauss, J. K. (1993). Middle cerebral artery blood flow velocity in healthy persons during wakefulness and sleep: A transcranial Doppler study. *Sleep*, *16*(7), 603–609. https://doi.org/10.1093/sleep/16.7.603

Droste, D. W., & Krauss, J. K. (1997). Oscillations of cerebrospinal fluid pressure in nonhydrocephalic persons. *Neurological Research*, *19*(2), 135–138. https://doi.org/10.1080/01616412.1997.11740786

Einhäupl, K. M., Garner, C., Dirnagl, U., Schmieder, G., Schmiedek, P., Kufner, G., & Rieder, J. (1986). Oscillations of ICP related to cardiovascular parameters. . In J.D. Miller, G.M. Teasdale, J.O. Rowan, S.L.Galbraith, A.D. Mendelow (Eds.) *Intracranial pressure VI* (pp. 290–297). Berlin, Heidelberg: Springer. 10.1007/978-3-642-70971-5_55

Halperin, J. J., Kurlan, R., Schwalb, J. M., Cusimano, M. D., Gronseth, G., & Gloss, D. (2015). Practice guideline: Idiopathic normal pressure hydrocephalus: Response to shunting and predictors of response. *Neurology*, *85*(23), 2063–2071. https://doi.org/10.1212/WNL.0000000000002193

Hirsch, J. C., Pierre-Kahn, P., & Hirsch, J. F. (1978). Experimental study of intracranial pressure during rapid eye movement sleep in the chronic cat. *Neuroscience Letters*, *7*(2–3), 245–249.

Jennum, P., & Børgesen, S. E. (1989). Intracranial pressure and obstructive sleep apnea. *Chest*, *95*(2), 279–283. https://doi.org/10.1378/chest.95.2.279

Kindt, G. W., & Gosch, H. H. (1972). Arterial pCO_2 effect at various levels of intracranial pressure. In M. Brock, & H. Dietz (Eds.), *Intracranial pressure* (pp. 210–213). : Springer.

Krauss, J. K., Droste, D. W., Bohus, M., Regel, J. P., Scheremet, R., Riemann, D., & Seeger, W. (1995). The relation of intracranial pressure B-waves to different sleep stages in patients with suspected normal pressure hydrocephalus. *Acta Neurochirurgica*, *136*(3–4), 195–203. https://doi.org/10.1007/BF01410626

Kristensen, B., Malm, J., & Rabben, T. (1998). Effects of transient and persistent cerebrospinal fluid drainage on sleep disordered breathing in patients with idiopathic adult hydrocephalus syndrome. *Journal of Neurology Neurosurgery and Psychiatry*, *65*(4), 497–501. https://doi.org/10.1136/jnnp.65.4.497

Lilja-Cyron, A., Kelsen, J., Andresen, M., Fugleholm, K., & Juhler, M. (2018). Feasibility of telemetric intracranial pressure monitoring in the neuro intensive care unit. *Journal of Neurotrauma*, *35*(14), 1578–1586. https://doi.org/10.1089/neu.2017.5589

Lundberg, N. (1960). Continuous recording and control of ventricular fluid pressure in neurosurgical practice. *Acta Psychiatrica Scandinavica. Supplementum*, *36*(149), 1–193. https://doi.org/10.1097/00005072-196207000-00018

Madsen, P. L., Schmidt, J. F., Wildschiodtz, G., Friberg, L., Holm, S., Vorstrup, S., & Lassen, N. A. (1991). Cerebral O_2 metabolism and cerebral blood flow in humans during deep and rapid-eye-movement sleep. *Journal of Applied Physiology*, *70*(6), 2597–2601. https://doi.org/10.1152/jappl.1991.70.6.2597

Marmarou, A., Bergsneider, M., Klinge, P., Relkin, N., & Black, P. M. L. (2005). INPH guidelines, part III: The value of supplemental prognostic tests for the preoperative assessment of idiopathic normal-pressure hydrocephalus. *Neurosurgery*, *57*(3 Suppl.), , S2-17–S2-28. https://doi.org/10.1227/01.NEU.0000168184.01002.60

Martin, G. (1978). Lundberg's B waves as a feature of normal intracranial pressure. *Surgical Neurology*, *9*(6), 347–348.

Martinez-Tejada, I., Arum, A., Wilhjelm, J. E., Juhler, M., & Andresen, M. (2019). B waves: A systematic review of terminology, characteristics, and analysis methods. *Fluids and Barriers of the CNS*, *16*(33), 1–15. https://doi.org/10.1186/s12987-019-0153-6

Mautner-Huppert, D., Haberl, R. L., Dirnagl, U., Villringer, A., Schmiedek, P., & Einhaupl, K. (1989). B-waves in healthy persons. *Neurological Research*, *11*(4), 194–196. https://doi.org/10.1080/01616412.1989.11739891

Newell, D. W., Aaslid, R., Stooss, R., & Reulen, H. J. (1992). The relationship of blood flow velocity fluctuations to intracranial pressure B waves.

Journal of Neurosurgery, *76*(3), 415–421. https://doi.org/10.3171/jns.1992.76.3.0415

Norager, N. H., Lilja-Cyron, A., Bjarkam, C. R., Duus, S., & Juhler, M. (2018). Telemetry in intracranial pressure monitoring: Sensor survival and drift. *Acta Neurochirurgica*, *160*(11), 1–8. https://doi.org/10.1007/s00701-018-3691-9

Norager, N. H., Lilja-Cyron, A., Hansen, T. S., & Juhler, M. (2019). Deciding on appropriate telemetric intracranial pressure monitoring system. *World Neurosurgery*, *126*, 564–569. https://doi.org/10.1016/j.wneu.2019.03.077

Pierre Kahn, A., Gabersek, V., & Hirsch, J. F. (1976). Intracranial pressure and rapid eye movement sleep in hydrocephalus. *Child's Brain*, *2*(3), 156–166. https://doi.org/10.1159/000119611

Román, G. C., Verma, A. K., Zhang, Y. J., & Fung, S. H. (2018). Idiopathic normal-pressure hydrocephalus and obstructive sleep apnea are frequently associated: A prospective cohort study. *Journal of the Neurological Sciences*, *395*, 164–168. https://doi.org/10.1016/j.jns.2018.10.005

Russo, G., Lodi, C. A., & Ursino, M. (2000). Quantitative assessment of cerebral vascular reserve by means of transcranial Doppler ultrasound and rebreathing maneuver: Bedside test and mathematical modeling. *Neurological Sciences*, *21*(5), 292–302. https://doi.org/10.1007/s100720070066

Tindall, G. T., McGraw, C. P., Vanderveer, R. W., & Iwata, K. (1972). Cardiorespiratory changes associated with plateau waves in patients with head injury. In M. Brock, & H. Dietz (Eds.), *Intracranial pressure* (pp. 227–231). : Springer.

Venes, J. L. (1979). B waves. A reflection of cardiorespiratory or cerebral nervous systems rhythm? *Child's Brain*, *5*(3), 352–360. https://doi.org/10.1159/000119831

Yokota, A., Matsuoka, S., Ishikawa, T., Kohshi, K., & Kajiwara, H. (1989). Overnight recordings of intracranial pressure and electroencephalography in neurosurgical patients. Part II: Changes in intracranial pressure during sleep. *Journal of UOEH*, *11*(4), 383–391.

SUPPORTING INFORMATION

Additional supporting information may be found online in the Supporting Information section.

How to cite this article: Riedel CS, Martinez-Tejada I, Norager NH, Kempfner L, Jennum P, Juhler M. B-waves are present in patients without intracranial pressure disturbances. *J Sleep Res*. 2021;30:e13214. https://doi.org/10.1111/jsr.13214

A.3 Paper III

Title: Causal relationship between slow waves of arterial, intracranial pressures and blood velocity in brain

Authors: Isabel Martinez-Tejada, Marek Czosnyka, Zofia Czosnyka, Marianne Juhler, and Peter Smielewski

Journal: Computers in Biology and Medicine

Status: Submitted

Causal relationship between slow waves of arterial, intracranial pressures and blood velocity in brain

Isabel Martinez-Tejada · Marek Czosnyka · Zofia Czosnyka · Marianne Juhler · Peter Smielewski

Abstract *Purpose.* Slow vasogenic waves in arterial blood pressure (ABP), intracranial pressure (ICP) and cerebral blood flow velocity (FV) carry information on multiple brain homeostatic control mechanisms. This work presents an approach to evaluate causal relation between oscillatory modes of these signals as an alternative to time or frequency domain Granger analysis. *Methods.* Forty-five patients with simultaneous recordings of ICP, ABP and FV during CSF infusion studies were examined retrospectively. Each time series was decomposed into ten intrinsic mode functions (IMFs) via Ensemble Empirical Mode Decomposition (EEMD) and, afterwards, Granger causality (GC) was computed. *Results.* Slow waves of ICP, ABP and FV were reconstructed from mode functions $IMF_{6\text{-}9}$ of each time series, covering a frequency range between 0.013 and 0.155 Hz. Most significant connections were from FV to ICP, being stronger during elevation of mean ICP during infusion study. No G-causality was found between any of the IMFs during the baseline phase. *Conclusion.* Nonlinearity and nonstationarity of the cerebral and systemic signals can be addressed using EEMD decomposition There is a causal influence of slow waves of FV on slow waves on ICP during the plateau phase of the infusion study for a frequency band between 0.095 and 0.155 Hz. This relationship is magnified during mild intracranial hypertension.

Isabel Martinez-Tejada (Corresponding Author)
Clinic of Neurosurgery, Copenhagen University Hospital, Rigshospitalet, 2300 Copenhagen, Denmark
E-mail: isita.martinez93@gmail.com

Isabel Martinez-Tejada
Department of Health Technology, Technical University of Denmark, Kongens Lyngby, Denmark

Marek Czosnyka · Sofia Czosnyka · Peter Smielewski
Brain Physics Laboratory, Division of Neurosurgery, Department of Clinical Neurosciences, Cambridge University Hospitals, Cambridge CB2 0QQ, United Kingdom

Marianne Juhler
Clinic of Neurosurgery, Copenhagen University Hospital, Rigshospitalet, 2300 Copenhagen, Denmark

Keywords Granger Causality · Ensemble Empirical Mode Decomposition · Intracranial pressure · Slow waves

1 Introduction

Hydrocephalus is a well-recognized condition associated with the abnormal circulation of cerebrospinal fluid (CSF) within the brain. Although there is still a lack of agreement regarding its initiation, most neuroscientists agree that the cause is predominantly related to an imbalance between secretion, circulation and rate at which CSF is absorbed. Given the complexity of biological systems, the CSF compensatory reserve is likely to be governed by interactions between vascular, respiratory and CSF movement dynamics. Measurement and analysis of CSF pressure response to infusion of mock CSF/saline into CSF space [15], allow an objective analysis of the dynamic characteristics of the CSF system in patients where a hydrocephalus diagnosis is suspected. The procedure is called CSF infusion study.

Combining multiple physiological modalities during the infusion study (intracranial pressure [ICP], arterial blood pressure [ABP], and cerebral blood flow velocity [FV]) may provide new insights into the underlying mechanisms of cerebrovascular and CSF dynamics based on the analysis of connectivity and information flow between the systems represented by those measurements. Granger causality (GC) has emerged in recent years as a statistical technique for unraveling the directions of information flow in multivariate processes. A popular application in neuroscience for GC is functional neuroimaging, encompassing functional magnetic resonance (fMRI), electrocorticography (ECoG) and electroencephalogram/magnetoencephalogram (EEG/MEG). Moving beyond neuroimaging, GC has also been used to look at relations between time series [55]. For instance, causal inferences were studied between cardiovascular and respiratory parameters in TBI patients [12]. Also in TBI patients causal inference was identified within EEG and ICP signals [49]. A similar study evaluated the relationship between the spectral functions of these two signals [50], using the spectral metrics of GC. This is important because the causal connection may depend on oscillatory synchrony [10]. Yet, no previous studies have explored G-causality between ICP, ABP and FV time series in hydrocephalus patients. These patients very often exhibit pronounced slow waves in their intracranial pressure.

The frequency content of slow waves is limited to a fixed frequency range. However, there exists discrepancy on the limits spanning this range. Lundberg originally defined a frequency of 0.5-2 waves/min [38]. Czosnyka et al. defined a frequency window of 0.33 to 3 waves/min[13], while Lalou et al. and Hanlo et al. broadened the range to 4 waves/min [27,34]. Most methods for their detection utilize spectral analysis via Discrete Fourier Transform (DFT) combined with band-pass filtering [32]. The DFT is linear, that is, it presents with additivity and homogeneity properties. The aforementioned time series are all nonstationary, so utilizing a linear approach for their analysis may provide biased results. Instead of decomposing a signal into a finite number of pure sinusoids with fixed amplitude and frequency (as in DFT), any time series, also nonstationary, can be adaptively broken down into intrinsic mode components using the so-called Empirical Mode Decomposition (EMD) method [1]. An intrinsic mode represents an oscillatory mode with time-varying amplitude and frequency. EMD acts as a dyadic

filter bank that extracts these oscillatory modes, called Intrinsic Mode Functions (IMF), from the time series, each of them represented by a different frequency content. Oscillations that form the slow waves are contained in adjacent intrinsic modes. Decomposition into oscillatory modes could help in the identification of the frequency content of slow waves. Further, it may elucidate the source of slow waves, which remains unclear. Although they are commonly thought to be related to vasogenic activity, influences from respiration and baroreceptor activity have also been suggested. The contribution of these different systems in the generation of the slow waves analyzed in this work can vary in time. Thus, nonlinear methods like EMD perform better at capturing these variations than traditional stationary Fourier decomposition.

But EMD presents a significant mode mixing drawback as a result of intermittency and noise in the signal, causing signals of disparate time scales to appear in the same IMF, or signals of the same time scale to be present in different IMFs. This results in two successive IMFs waveform aliasing. A noise-assisted method known as Ensemble Empirical Mode Decomposition (EEMD) brilliantly solves this problem by first adding finite-amplitude white noise to the original signal and then breaking down the signal with added noise into IMFs via EMD [62].

In this study, we will investigate the possible link between ICP, ABP, and FV in patients diagnosed for hydrocephalus using time-domain conditional GC analysis between their intrinsic oscillatory modes obtained via Ensemble Empirical Model Decomposition (EEMD), a modified version of EMD.

2 Material and Methods

2.1 Patient selection

We retrospectively analyzed randomly selected data from 45 CSF infusion studies with simultaneous recordings of ICP, ABP, and TCD CBFV performed between 1994 and 2006 from a larger hydrocephalus group of patients. These studies were carried out in Addenbrookes Hospital (Cambridge, UK) in patients of all ages and etiologies. As a part of the clinical pathway, all patients required an infusion test as requested from a Neurosurgeon Consultant. These individuals presented a certain degree of ventricular enlargement on CT or MRI. Their clinical symptoms included cognitive decline, urinary incontinence, and unstable balance.

2.2 Data acquisition

The CSF infusion study aims at assessing the CSF absorptive capacity, since an abnormal rise in CSF pressure would indicate a lower absorptive capacity. The test involves infusion of fluid at a constant rate into the CSF space or subcutaneous reservoir connected to an intraventricular catheter. Two lines connected with two gage-25 needles were used. One line was connected to an infusion pump. The infusion pump was responsible for the infusion of Hartman's solution with a constant rate of 1 or 1.5 ml/minute (if the baseline pressure was below 18 mmHg). The second line was connected to a fluid-filled pressure transducer (Edwards Lifesciences™, Irvine, USA) and a pressure amplifier (Spiegelberg, Ham-

burg, Germany or Philips, Amsterdam, The Netherlands) for data collection and processing using ICM+ software (Cambridge Enterprise Ltd, University of Cambridge, https://icmplus.neurosurg.cam.ac.uk) [57]. A standard test starts with 10 minutes of baseline recording. Subsequently, the infusion is started and only terminated when a plateau in the ICP is reached or the pressure exceeds 40 mmHg. A detailed explanation of this methodology has been published previously [8,31, 59].

During the infusion study, simultaneous measurements of ABP using Finapres plethysmograph (Finapres Medical Systems B.V., Amsterdam, The Netherlands) and of cerebral FV in the middle cerebral artery using TCD (Neuroguard, Medasonics, Cremona, CA, USA) were recorded. Changes in FV represent changes in cerebral blood flow as long as the diameter of the insonated artery remains unchanged, since then there is a linear relationship between flow velocity and blood flow in the brain [47].

2.3 Data pre-processing

In the current work, the signals were first lowpass filtered using a finite impulse response (FIR) filter with a cut-off frequency of 0.12 Hz and then down-sampled to 1 Hz, as the frequencies of interest are below 0.1 Hz. Filtering is done before down-sampling to reduce the distortion caused by aliasing.

2.4 EEMD

The EEMD is an improved approach for decomposing the time series into intrinsic mode functions based on the original EMD method. IMFs are oscillatory modes with varying amplitude and frequency, which present the characteristics of having an equal number of extrema and zero-crossing and zero value for the average of its upper and lower envelopes. Based on the EMD method, EEMD defines true IMFs from the average of IMF trials generated by adding white noise of finite amplitude to the original time series. A more detailed mathematical explanation of this methodology can be found in Online Resource 1.

In our work, the total number of IMFs was fixed to 10, to ensure that components were not excessively extracted and only the last IMF generated contained the trend. IMFs were extracted in descending order of frequency content. In this work, the noise added had an amplitude of 0.1 of the standard deviation of the signal, and the ensemble number was set to 100.

The IMFs were tested for statistical significance to verify that noise was well separated from the data and we were therefore working with meaningful information [60]. Two statistical properties were calculated on both the extracted IMFs and the Gaussian noise added: the mean period and the RMS values [61]. The period was derived as the inverse of the instantaneous frequency. The confidence-limit level was set at 99% to determine the maximum and minimum values of each two of the statistical properties of noise. For a given significance level, the confidence limits encompassed the range of values for which we are confident that the extracted IMFs were noise. In other words, if the mean period and RMS values

of the extracted IMFs fell into the confidence limits, then the extracted IMF was noise.

EEMD for IMF generation was followed by a selection of relevant IMFs. In our work, IMF selection methodology selected those IMFs that best represented the signals in their time-frequency domain, while discarding redundant ones. From the set of extracted IMFs, we evaluated both the Jensen-Rényi divergence (JRD) [56] and the Minkowski distance (d_{mink}) [9]. If the original signal and the n-th IMF were somewhat identical, then d_{mink} and JRD would be very low and therefore selected as appropriate IMF.

2.5 Granger Causality

Given two physiological time series X_1 and X_2, bivariate GC determines whether one time series provides any statistically significant information useful in forecasting the other time series. If the inclusion of lagged values of X_1 contains information that helps predict X_2, then X_1 G-causes the time series X_2. To analyze the mutual influence among our three time series (ICP, ABP, and FV), a multivariate extension known as conditional Granger causality (cGC) was implemented. For example, we could say that FV Granger-causes ICP if ICP is better predicted by the inclusion of FV, while considering the influence of ABP. Detailed mathematical explanations are included in Online Resource 1. For cGC analysis we implemented the MATLAB code published by L.Barnett and A.K. Seth [4] (R2019a; MVGCA Matlab Toolbox, The MathWorks, Inc., Natick, MA.). The existence and strength of a connection must be ensured to construct a connectivity graph between the corresponding IMFs in ICP, ABP, and FV signals. No additional tests were performed to check the covariance stationarity because empirical mode components are stationary [5].

First, a MVAR model was fitted to the generated intrinsic mode functions using AIC criterion to determine the model order. The model was validated using a consistency test that calculated the percentage of the correlation structure of the IMFs that is explained by the MVAR model. An additional consistency test was carried out to validate the adjusted sum square error. A third validation test, the Durbin-Watson statistic [18], was performed to test for autocorrelation in the residuals to ensure that they were all white noise series.

For a single subject, the existence of a connection between two channels was determined by the conditional GC values under a Bonferroni-corrected significance threshold of $p = 0.01$. Bonferroni correction was implemented to counteract the problem of multiple comparisons, m, so that each individual null hypothesis was tested at a significance level: p/m. In this case $m = 6$ to account for the comparison between the three pairs of ICP, ABP, and FV signals, all tested for causality in both directions. At a group level, existence of connection between two signals was considered if the connection existed over 75% of subjects.

The strength of each connection was defined as the average GC values between two signals. The GC values of the subjects were averaged to establish one matrix whose elements denoted the average GC values from one signal to another, for those subjects for which the existence of a connection was significant.

2.6 Causal Flow

Knowledge of the presence and magnitude of the connection enables the construction of Event Calculus (EC) Graphs [48], from which several graph-theoretic measures can be calculated. GC interactions are graphically represented as edges and causality sources as nodes. In our work, we summarize causal connectivity using the causal flow (cf) index. The IMF_n of each of the three signals is considered as a node i in the graph ($i = 1, 2, 3$). The total number of edges outgoing and incoming from the node is called the out-degree and in-degree, respectively. Difference between out-degree and in-degree is denoted as causal flow [52]. The IMF of a signal with predominantly incoming edges (positive causal flow) can be seen as the causal sink of the network. Contrarily, if it mainly has outgoing connections (negative causal flow) it can be referred to as a causal source of the network. It is important to emphasize that ensuring mode mixing is removed ensures that causal oscillatory functions are not spread across the different IMFs [45].

3 Results

3.1 Patient Demographics

A total of 45 patients were enrolled in the study: 28 of them being male, and 17 female. The pooled mean age was 54 years; range: 25-78 years old. Ethnic data were not provided.

Clinical data were limited. The degree of ventriculomegaly in this group was calculated using the Bicaudate index (BCI). The mean BCI is 0.31 and ranged from 0.11 to 0.62; the mean width of the third ventricle is 13 mm and ranged from 7 to 27 m. They all presented with clinical symptoms, including gait difficulty, cognitive problems, memory loss, and urinary incontinence. Evidence of deep white matter ischemic lesions was found in seven patients using MRI (T_1 and T_2 weighted sequences) or computed tomography scans.

3.2 Data pre-processing

Fig. 1 shows an example of ICP, ABP, and FV signals of one subject after low-pass filtering and downsampling, with respiratory and pulse contributions to the signal removed. As shown in the figure, after approximately 10 minutes of baseline recording, a constant rate infusion was initiated and continued until a plateau was reached. The slow fluctuations of ICP were larger during infusion, as expected given that their presence has been associated to an increase in pressure. In general, four different epochs could be identified: baseline, infusion, plateau, and post-infusion (once infusion had stopped).

3.3 EEMD

We used the EEMD algorithm for IMF extraction after pre-processing.

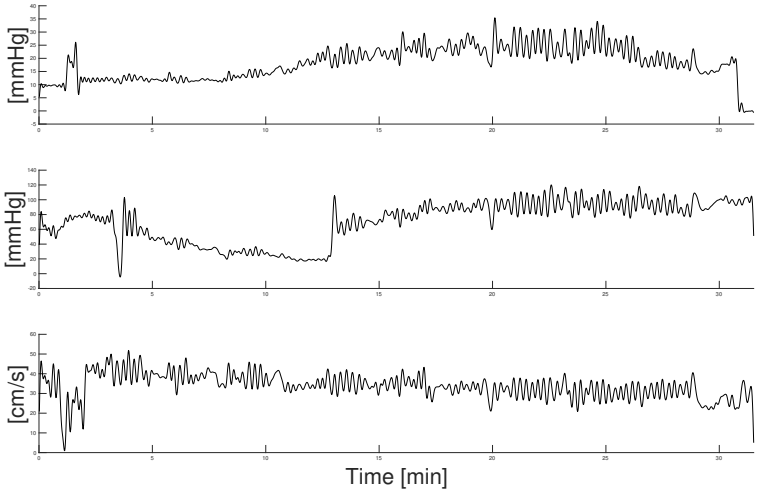

Fig. 1 ICP (top), ABP (middle) and FV (bottom) signals of one subject. The X-axis shows the time in minutes whereas the Y-axis represents the magnitude of the signals. Four epochs are identified in the ICP signal during the infusion test: (1) baseline – corresponding to the basal phase before infusion; (2) infusion – increasing slope as the infusion starts; (3) plateau – constant slope during infusion; and (4) post-infusion – recovery phase after infusion when ICP values return to the baseline state.

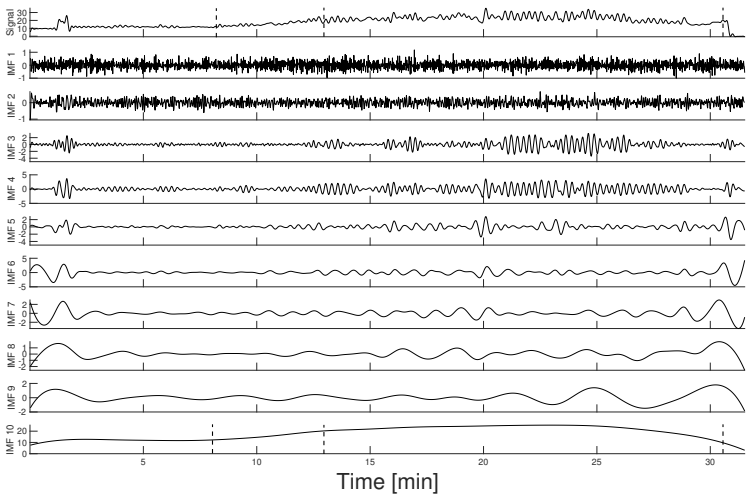

Fig. 2 An example of a filtered ICP waveform (first row) from one infusion test and its corresponding EEMD including the trend (last row), used for defining the four epochs/stages of the infusion test.

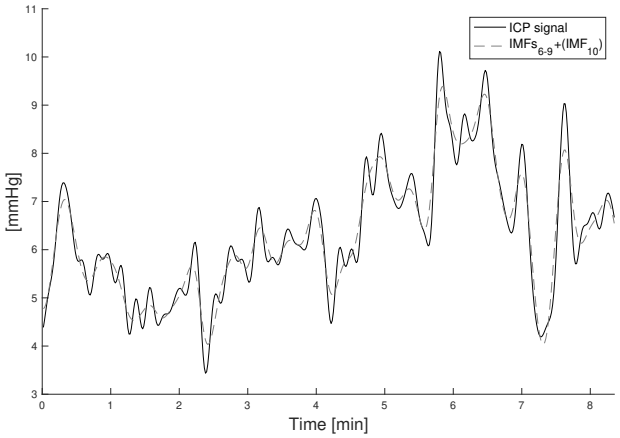

Fig. 3 ICP slow waves reconstructed using $IMF_{6\text{-}9}$, plus IMF_10 to better approach the magnitude of the oscillations (just for visualization purposes) during the plateau phase of infusion test. Selection of the appropriate IMFs is based on minimization of both Minkowski distance and Jensen Rényi divergence.

As illustrated in Fig. 2 after EEMD, the signals were decomposed into 10 IMFs. An initial visual inspection of these IMFs in the individual recordings suggested that the last IMF (IMF_{10}) contained the trend of the signal, in which the aforementioned epochs could be well identified. Fig. 3 visually depicted the reconstruction of slow waves from $IMF_{6\text{-}9}$. The trend could also play an important role in the reconstruction by helping to recover closer original values.

The results of the d_{mink} and JRD are shown in Fig. 4. As observed, both values decrease from the sixth IMF to the end. Following these criteria, we could select $IMF_{6\text{-}9}$ as the relevant IMFs of the ICP signal.

Average power spectral density (PSD) analysis [11] was performed to calculate the energy captured by the generated IMFs. The square of the root mean square level of each IMF was used to estimate the total power in baseline and infusion stages. Table 1 shows the average power of each IMF during the baseline and the infusion period, where the power increases with higher order IMFs. There is an increase in the power of slow waves from an average power of 0.330 (83.1 if the trend was included) in the baseline to 4.867 (378.310) in the infusion stage.

The frequency band contained in the selected IMFs is shown in Table 2. Thus, slow waves reconstructed with $IMF_{6\text{-}9}$ occupy a frequency range from 0.013 to 0.155Hz.

3.4 Directional Causality

Table 3 presents the percentage of subjects with existence of connection between signals. Table 4 shows the average GC values from one signal to another when existence of connection was present with significance of $p < 0.01$.

The significant connection was from FV to ICP. This connection was present during infusion in the reconstructed slow wave. The strength of this connection

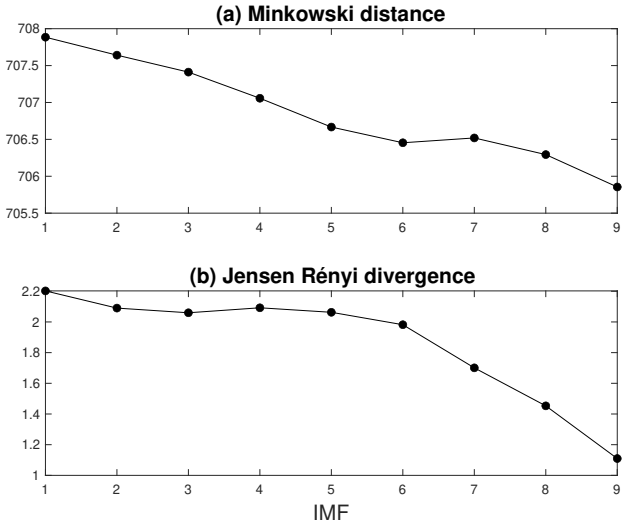

Fig. 4 The values of (a) the Minkowski distance and (b) Jensen Rényi divergence for $IMF_{1\text{-}9}$ averaged across all subjects. IMF_{10} showed very low values, so it was not included in the figure. The Minkowski distance decreases with increasing number of IMF. From the sixth IMF until the end, the divergence values start to rapidly decrease. This permits the selection of $IMF_{6\text{-}9}$ as the most representative IMFs of the ICP signal.

Table 1 Mean power of different IMFs during baseline (top row) and infusion (bottom row) stages.

Power / IMF	Baseline	Infusion
IMF_1	0.022	0.124
IMF_2	0.025	0.165
IMF_3	0.047	0.050
IMF_4	0.068	0.218
IMF_5	0.090	0.471
IMF_6	0.098	0.700
IMF_7	0.098	0.561
IMF_8	0.082	1.735
IMF_9	0.052	1.871
IMF_{10}	82.765	373.442

Table 2 Frequency band of IMFs used for slow waves reconstruction.

IMF	Frequency Band (Hz)
IMF_6	0.095 - 0.155
IMF_7	0.052 - 0.094
IMF_8	0.027 - 0.054
IMF_9	0.013- 0.030

Table 3 Percentage of patients with significant causal interaction.

	$IMF_{6\text{-}9}$ All Recording			$IMF_{6\text{-}9}$ Baseline			$IMF_{6\text{-}9}$ Infusion		
From/To	ICP	ABP	FV	ICP	ABP	FV	ICP	ABP	FV
ICP	-	24	66	-	20	42	-	13	68
ABP	24	-	33	26	-	48	28	-	44
FV	35	26	-	53	40	-	26	31	-
	IMF_6 All Recording			IMF_6 Baseline			IMF_6 Infusion		
ICP	-	31	60	-	22	48	-	17	75
ABP	37	-	48	31	-	66	35	-	51
FV	51	35	-	46	37	-	33	33	-
	IMF_7 All Recording			IMF_7 Baseline			IMF_7 Infusion		
ICP	-	17	66	-	22	42	-	15	46
ABP	31	-	42	44	-	55	22	-	42
FV	37	37	-	35	35	-	35	28	-
	IMF_8 All Recording			IMF_8 Baseline			IMF_8 Infusion		
ICP	-	28	42	-	24	53	-	20	37
ABP	33	-	35	55	-	62	20	-	28
FV	42	33	-	60	44	-	26	28	-
	IMF_9 All Recording			IMF_9 Baseline			IMF_9 Infusion		
ICP	-	22	33	-	33	48	-	28	35
ABP	35	-	26	44	-	46	33	-	28
FV	35	26	-	35	44	-	42	24	-

Percentage of patients with significant causal interaction. Connection significance was calculated using the conditional GC values under a Bonferroni-corrected significance threshold of $p = 0.01$. Marked in bold are those signals with existence of connection at group level (i.e., connection exists over 75% of subjects). In this case, only the connection from FV to ICP in IMF_6 is significant.

was 0.038 for IMF_6. No causalities in the baseline were reported since slow waves are of less power in this stage. In fact, Table 1 shows that the mean power of all IMFs is lower during baseline than during infusion.

3.5 Causal Flow

Causal connectivity graphs show the influence of interactions between the three studied signals during infusion, where the existence of connection was more significant. In only one out of the five cases of IMFs (IMF_6) analyzed, FV can be seen as a causal source, reflecting more outgoing causal influences. Thus, FV affects the remainder of the network. ICP remains as a causal sink in this case, hence affected by the FV signal. In the remaining IMFs there is no connection between nodes.

4 Discussion

Slow waves in ICP have been analyzed since Lundberg introduced them back in the 1960s [38]. Slow waves are described as short repeating oscillations with a frequency window of 0.33 to 3 waves/min [13]. However, there is still a lack of consensus on their physiological origin and morphological characteristics. Special

Table 4 Average GC value matrices across all subjects.

	Entire Recording	Baseline	Infusion
$IMF_{6\text{-}9}$	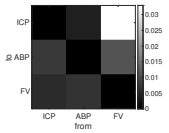	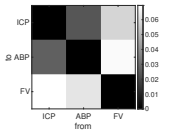	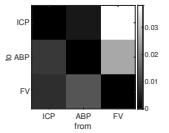
IMF_6	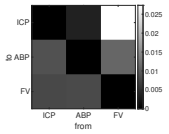	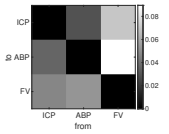	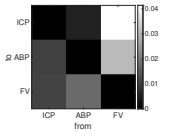
IMF_7	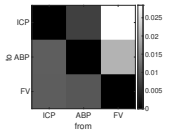	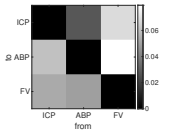	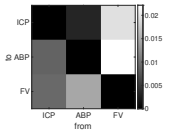
IMF_8	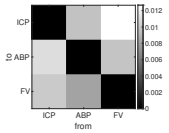	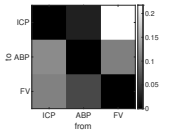	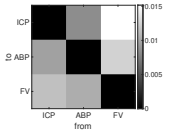
IMF_9	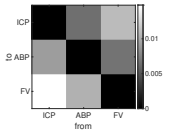	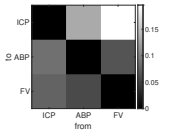	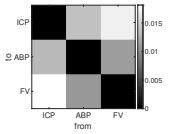

Darker colors represent a higher strength in the connection. All cases show highest strength in the connection from FV to ICP.

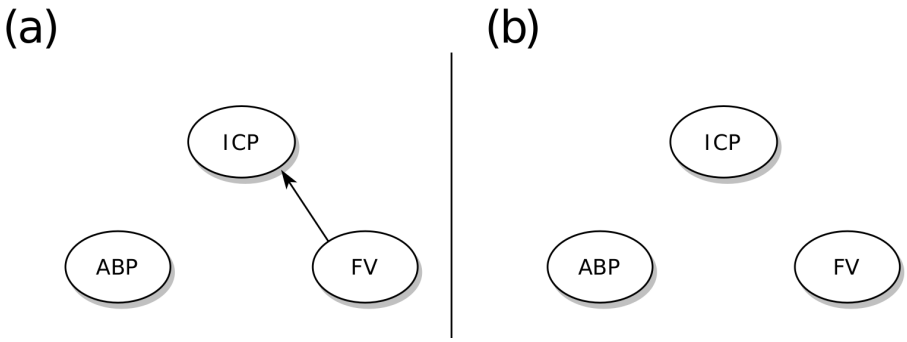

Fig. 5 Connectivity graphs of (a) IMF_6, (b) IMF_7, IMF_8, IMF_9 and $IMF_{6\text{-}9}$ during infusion. The connection is unidirectional, going from source to sink nodes. In our case, the connection goes from FV (source) to ICP (sink) for IMF_6. The remaining mode functions have no connection between nodes.

focus is placed on these waves since from the clinical point of view they are the most frequently encountered pattern. Although slow waves are originally defined in the ICP signal, slow oscillations can also be detected in other physiological signals, including those of extracranial origin (i.e., ABP).

The relationship between these oscillations remains unclear. Some studies reported that ICP lags behind ABP the time corresponding to the propagation of ABP waves into the cerebral microvasculature [39,58]. Others stipulated that ICP may lead ABP in these waves [17,35] suggesting that changes in ICP lead to vasomotor system instability that then causes arterial blood pressure to also change. The same controversy rises with the relationship between ICP and FV. While some findings state that FV leads ICP [41], others defined them as always being in phase (synchronous) [40].

The associations between ICP, ABP, and FV slow waves have been investigated through various techniques. Possibly the most commonly quoted metric, at least in the traumatic brain injury neuromonitoring scenario, is a running correlation coefficient between ABP and ICP slow waves [14], PRx, which is believed to reflect the state of cerebral vascular pressure reactivity. The correlation analysis approach has also been applied to slow waves in FV and ABP [25,37] as well as ICP and FV signals [36]. Transfer function analysis has also been applied to analyze the phase shift between pulse waveforms in ABP and ICP signals [42] and FV and ICP signals [33].

This work focused on an analysis of the relations between ICP, ABP, and FV in the low-frequency range encompassing slow waves. To achieve that, the signals were decomposed into oscillatory modes using an EMD extension, the so-called EEMD. EEMD addresses the mode mixing effect drawback present in EMD by averaging a certain number of repeated EMD decompositions of a white noise-added signal. This ensures that generated oscillatory modes with the same frequency are not spread across different IMFs. The true oscillatory modes for each trial are obtained by iteratively removing the highest frequency components from the data, generating progressively lower and lower frequency residual signals until only the data trend is left. Although EMD has previously been applied to ICP signals for the removal of artifacts [19,20], the use of EEMD in ICP signals has been limited to only one study by Zeiler et al. [63].

In this study, EEMD was chosen over traditional spectral decompositions because the latter ones incorporate a linear superposition of predefined fixed basis. If the signal is nonlinear and nonstationary, so that it contains more than just pure sine and cosine functions, then energy spreading will be present in the resulting Fourier spectrum. The nonlinearities will give rise to spurious high-order harmonics hindering the distinction between true and spurious energy in the spectrum. Instead, EEMD uses basis that are directly derived from the data [39]. Thus, each frequency band resulting from the EEMD may better describe the changes induced by a specific physiologic process.

We used EEMD results to identify patterns for each frequency range and used the information from only the ranges that allow the reconstruction of slow waves. We speculate that slow waves in all three signals are better described by $IMF_{6\text{-}9}$ obtained from the decomposition. Lundberg first defined a frequency of 0.0083-0.033 Hz for slow B waves [38], although an extended frequency window of 0.0055-0.05 Hz was later introduced to include an umbrella for all variations of slow B waves. Our data showed that the selected oscillatory modes cover a frequency range

between 0.013-0.155 Hz (76s to 6.5s) in all subjects analyzed. This frequency range includes the optimal index frequency range (55s to 15s) for causality analysis of slow waves suggested by Howells et al. [29].

Although higher than originally suggested for ICP signals, this frequency range supports the work from Raftopoulos et al. [44] where the frequency upper limit was 0.083 Hz, and that of Janny et al. [30], who described a frequency range for type 2 slow ICP waves from 0.008 to 0.05 Hz. Higher frequency waves with a central frequency approximating 0.1 Hz – the so-called Mayer waves – are also seen in ABP signals [24]. Mayer waves are thought to result from vascular changes, thus having a systemic vascular origin that could suggest the role of ABP as the source of ICP or FV.

Not only the characteristics of slow waves are not well defined, but the physiological origin underlying their existence also remains unclear. The use of causality analysis to find connections within complex networks should be encouraged for the better understanding of complex multisystem diseases like hydrocephalus or traumatic brain injury, where changes in autoregulation may disturb pure physiological mechanisms. For instance, ICP, ABP, and FV could be seen as nodes that reflect the behaviour of subsystems and changes in their information flow could be of clinical relevance for a certain disease. In addition, improved insight into these connections and their character could help in the development of a more robust mechanistic model to estimate ICP, whose measurement is very invasive, from the use of two noninvasively measured signals, which are ABP and FV, as well as shed light on the cause of variability in widely accepted slow-waves derived metrics like PRx.

GC is a well-established approach among connectivity methodologies to explore informational flow between signals. Increasingly, GC has been applied to study connectivity in brain dynamics [22, 43, 55]. Yet, our work is one of the first attempts on calculating conditional time-domain causality using both time and frequency information. By using conditional GC we were able to explore the information flow between IMFs of the aforementioned signals. The conditional GC of the data was established based on a MVAR model. Three validity tests confirmed the two requirements of the proposed MVAR model: (i) more than 90% of variance was accounted for by the model confirmed by both adjusted R-squared statistic and consistency tests, and (ii) all residuals were white noise series by Durbin-Watson test at significance 0.01.

In our work, conditional GC analysis focused on the sixth to ninth IMFs, provided their previously suggested key role in the composition of slow waves. Our observations show that FV dominates as the main source to ICP in the frequency band between 0.095 and 0.155 Hz during the infusion phase, i.e., when the slow waves are highly pronounced. The relative power change from baseline to infusion is 13.7. Steinmeier et al. also postulated that ICP follows FV with a mean time delay of 1.5s [58] in frequencies below 0.1 Hz. The nature of connectivity from FV to ICP can be perhaps best discussed using two prevailing theories. Some believe on the existence of intrinsic brain-stem sympathetic nerve discharges acting as a neural pacemaker that changes the cerebral blood volume [28]. A more popular opinion associates alterations in cerebral blood volume with regulatory mechanisms systemic to arterial smooth-muscle cells [3]. Changes in cerebral blood volume then result in alterations in ICP.

According to our results, FV also has some influence on ABP during elevation of ICP by infusion (51% of the subjects) in the aforementioned frequency band between 0.095 and 0.155 Hz. However, this result seems to oppose the theory of cerebral blood flow autoregulation, which describes changes in blood FV as a response to changes in ABP, thus with the causality implied as ABP leading FV. This apparent effect of FV leading ABP is related to the delay and nonlinear nature of the autoregulatory response, clearly seen with regular oscillations after the initial response of FV to the first ABP change. We must bear in mind that Granger causality does not necessarily imply true causality [54]. What we are actually testing is whether a particular variable comes before another in the signals. Hence, GC measure is heavily affected by the time lag between the signals. This time lag was previously described by Diehl et al. [16] and Blaber et al. [6], who reported slow waves of FV preceding those slow waves of ABP with working autoregulation, and no delay between FV and ABP in a situation where autoregulation is absent. This explains why we find Granger causality from FV to ABP in our data, although the true cause-and-effect link is from ABP to FV. Therefore, this effect is not in reality a contradiction to the autoregulatory principle.

Limitations

We acknowledge certain limitations in our work. As mentioned before, we need to be careful when interpreting GC analysis. GC only considers the three physiological signals introduced in the models, without giving any consideration to other variables (CO_2, heart rate...). Furthermore, the relations may not be constant throughout time. If ABP caused ICP during the first half of the infusion stage but this relation was reversed during the second half, no connectivity would have been identified. Finally, GC depends on the results obtained by the EEMD, which at the same time depend on the prescribed number of ensemble and noise amplitude.

The small group of subjects limited just to NPH clinical symptoms patients is an additional limitation to this work. For instance, results might have been different when looking at connectivity patterns in patients presenting with low and high baseline ICP, or in patients with increased or decreased resistance to CSF outflow. Further investigations are thus needed to clarify these potentially factors.

5 Conclusion

It is feasible to tackle the problem of nonlinearity and nonstationarity of the cerebral and systemic signals using EEMD decomposition. Therefore, slow waves in ICP, ABP, and FV can be described by oscillatory modes of frequencies between 0.013 and 0.155 Hz. Within the 0.095 and 0.155 Hz frequency band, there is an influence of slow waves of FV on slow waves of ICP.

Declarations

Funding. This project has received funding from the Novo Nordisk Tandem (NNF17OC0024718).

Conflicts of interest The authors have no conflicts of interest to report.
Availability of data and material Not applicable.
Code availability Not applicable.
Authors' contributions All authors contributed to the study conception and design. Data collection was performed by Zofia Czosnyka, Marek Czosnyka and Peter Smielewski, and data analysis was performed by Isabel Martinez-Tejada. The first draft of the manuscript was written by Isabel Martinez-Tejada and all authors commented on previous versions of the manuscript. All authors read and approved the final manuscript.
Ethics approval Data collection was done under approval of Ethical Committee (08/H0306/103).
Consent to participate Informed consent was obtained from all individual participants included in the study.
Consent for publication Patients signed informed consent regarding publishing their data.
Acknowledgements This project has received funding from the Novo Nordisk Tandem (NNF17OC0024718).

References

1. The empirical mode decomposition and the Hilbert spectrum for nonlinear and nonstationary time series analysis, vol. A454 (1998)
2. Akaike, H.: A new look at the statistical model identification. IEEE Trans. Autom. Control **AC-19**(6), 716–723 (1974)
3. Auer, L.M., Sayama, I.: Intracranial pressure oscillations (b-waves) caused by oscillations in cerebrovascular volume. Acta Neurochir (Wien) **68**(1-2), 93–100 (1983)
4. Barnett, L., Seth, A.K.: The mvgc multivariate granger causality toolbox: A new approach to granger-causal inference. Journal of Neuroscience Methods **223**, 50–68 (2014). DOI 10.1016/j.jneumeth.2013.10.018
5. Benali, J., Sayadi, M., Fnaiech, F., Morello, B., Zerhouni, N.: Importance of the fourth and fifth intrinsic mode functions for bearing fault diagnosis. 14th International Conference on Sciences and Techniques of Automatic Control and Computer Engineering, STA 2013 pp. 259–264 (2013). DOI 10.1109/STA.2013.6783140
6. Blaber, A.P., Bondar, R.L., Stein, F., Dunphy, P.T., Moradshahi, P., Kassam, M.S., Freeman, R.: Transfer Function Analysis of Cerebral Autoregulation Dynamics in Autonomic Failure Patients. Stroke **28**(9), 1686–1692 (1997). DOI 10.1161/01.STR.28.9.1686
7. Blinowska, K.J., Jaroslaw, Z.: Practical Biomedical Signal Analysis using MATLAB, Series in Medical Physics and Biomedical Engineering (2011)
8. Børgesen, S.E., Albeck, M.J., Gjerris, F., Czosnyka, M., Laniewski, P.: Computerized infusion test compared to steady pressure constant infusion test in measurement of resistance to CSF outflow. Acta Neurochirurgica **119**(1-4), 12–16 (1992). DOI 10.1007/BF01541775
9. Boutana, D., Benidir, M., Barkat, B.: On the selection of intrinsic mode function in emd method: Application on heart sound signal. 2010 3rd International Symposium on Applied Sciences in Biomedical and Communication Technologies, Isabel 2010 p. 5702895 (2010). DOI 10.1109/ISABEL.2010.5702895
10. Bressler, S.L., Seth, A.K.: Wiener-Granger Causality: A well established methodology. NeuroImage **58**(2), 323–329 (2011). DOI 10.1016/j.neuroimage.2010.02.059
11. Buttkus, B.: Spectral Analysis and Filter Theory in Applied Geophysics. Springer Berlin Heidelberg (2000)
12. Claassen, J., Rahman, S.A., Huang, Y., Frey, H.P., Schmidt, J.M., Albers, D., Falo, C.M., Park, S., Agarwal, S., Connolly, E.S., Kleinberg, S.: Causal structure of brain physiology after brain injury from subarachnoid hemorrhage. Plos One **11**(4), e0149878 (2016). DOI 10.1371/journal.pone.0149878
13. Czosnyka, M., Pickard, J.D.: Monitoring and interpretation of intracranial pressure. J. Neurol. Neurosurg. Psychiatry **75**(5), 813–821 (2004)

14. Czosnyka, M., Smielewski, P., Kirkpatrick, P., Piechnik, S., Laing, R., Pickard, J.D.: Continuous Monitoring of Cerebrovascular Pressure-Reactivity in Head Injury. In: Intracranial Pressure and Neuromonitoring in Brain Injury, pp. 74–77. Springer Vienna, Vienna (1998). DOI 10.1007/978-3-7091-6475-4_23
15. Di Rocco, C., Sutton, L.N., McComb, J.G., Rapoport, B.I., Park, E.H., Madsen, J.R.: Index of cerebrospinal compensatory reserve in hydrocephalus - comments. Neurosurgery **64**(3), 501–502 (2009)
16. Diehl, R.R., Linden, D., Lücke, D., Berlit, P.: Phase Relationship Between Cerebral Blood Flow Velocity and Blood Pressure. Stroke **26**(10), 1801–1804 (1995). DOI 10.1161/01.STR.26.10.1801
17. Droste, D.W., Krauss, J.K.: Intracranial pressure B-waves precede corresponding arterial blood pressure oscillations in patients with suspected normal pressure hydrocephalus. Neurological Research **21**(7), 627–630 (1999). DOI 10.1080/01616412.1999.11740987
18. Durbin, J., Watson, J.: Biometrika Trust Testing for Serial Correlation in Least Squares Regression . II. Biometrika **38**(1), 159–177 (1951)
19. Feng, M., Loy, L.Y., Sim, K., Phua, C., Zhang, F., Guan, C.: Artifact correction with robust statistics for non-stationary intracranial pressure signal monitoring. Proceedings - International Conference on Pattern Recognition (Icpr), 557–560 (2012)
20. Feng, M., Loy, L.Y., Zhang, F., Guan, C.: Artifact removal for intracranial pressure monitoring signals: A robust solution with signal decomposition. Proceedings of the Annual International Conference of the IEEE Engineering in Medicine and Biology Society, EMBS **1**, 797–801 (2011). DOI 10.1109/IEMBS.2011.6090182
21. Flandrin, P., Rilling, G., Gonçalvés, P.: Empirical mode decomposition as a filter bank. IEEE Signal Processing Letters **11**(2 PART I), 112–114 (2004). DOI 10.1109/LSP.2003.821662
22. Gao, L., Smielewski, P., Czosnyka, M., Ercole, A.: Early asymmetric cardio-cerebral causality and outcome after severe traumatic brain injury. Journal of Neurotrauma **34**(19), 2743–2752 (2017). DOI 10.1089/neu.2016.4787
23. Geweke, J.: Measurements of linear dependence and feedback between multiple time series. J. Amer. Statist. Assoc. **77**, 304–313 (1982)
24. Ghali, M.G., Ghali, G.Z.: Mechanisms contributing to the generation of mayer waves. Frontiers in Neuroscience **14**, 395 (2020). DOI 10.3389/fnins.2020.00395
25. Giller, C.: The frequency-dependent behavior of cerebral autoregulation. Neurosurgery **27**(3), 362–368 (1990). DOI 10.1097/00006123-199009000-00004
26. Granger, C.W.J.: Investigating causal relations by econometric models and cross-spectral methods. Econometrica **37**, 424–438 (1969)
27. Hanlo, P.W., Gooskens, R.H., Faber, J.A., Peters, R.J., Hermsen, A.A., Nijhuis, I.J., Vandertop, W.P., Tulleken, C.A., Willemse, J.: Relationship between anterior fontanelle pressure measurements and clinical signs in infantile hydrocephalus. Child's Nervous System: ChNS: Official Journal of the International Society for Pediatric Neurosurgery **12**(4), 200–209 (1996)
28. Higashi, S., Yamamoto, S., Hashimoto, M., Fujii, H., Ito, H., Kogure, Y., Tokuda, K.: The Role of Vasomotor Center and Adrenergic Pathway in B-Waves pp. 220–224 (1989). DOI 10.1007/978-3-642-73987-3_60
29. Howells, T., Johnson, U., McKelvey, T., Enblad, P.: An optimal frequency range for assessing the pressure reactivity index in patients with traumatic brain injury. Journal of Clinical Monitoring and Computing **29**(1), 97–105 (2015). DOI 10.1007/s10877-014-9573-7
30. Janny, P.: La pression intracrânienne chez l'homme. Ph.D. thesis (1950)
31. Juniewicz, H., Kasprowicz, M., Czosnyka, M., Czosnyka, Z., Gizewski, S., Dzik, M., Pickard, J.D.: Analysis of intracranial pressure during and after the infusion test in patients with communicating hydrocephalus. Physiological Measurement **26**(6), 1039–1048 (2005). DOI 10.1088/0967-3334/26/6/013
32. Kasprowicz, M., Asgari, S., Bergsneider, M., Czosnyka, M., Hamilton, R., Hu, X.: Pattern recognition of overnight intracranial pressure slow waves using morphological features of intracranial pressure pulse. Journal of Neuroscience Methods **190**(2), 310–318 (2010). DOI 10.1016/j.jneumeth.2010.05.015
33. Kim, D.J., Czosnyka, M., Kim, H., Balédent, O., Smielewski, P., Garnett, M.R., Czosnyka, Z.: Phase-shift between arterial flow and ICP pulse during infusion test. Acta Neurochirurgica **157**(4), 633–638 (2015). DOI 10.1007/s00701-015-2353-4
34. Lalou, D.A., Czosnyka, M., Donnelly, J., Lavinio, A., Pickard, J.D., Garnett, M., Czosnyka, Z.: Are slow waves of intracranial pressure suppressed by general anaesthesia? Acta Neurochirurgica, Supplementum **126**, 129–132 (2018). DOI 10.1007/978-3-319-65798-1_27

35. Lemaire, J.J., Burlat, J., Khalil, T., Chabane, A., Irthum, B., Chazal, J.: Computer software for frequential monitoring of slow intracranial pressure waves and related signals. In: Acta Neurochirurgica Supplementum, vol. 71, p. 388. Springer-Verlag (1998)
36. Lewis, P.M., Smielewski, P., Rosenfeld, J.V., Pickard, J.D., Czosnyka, M.: Monitoring of the Association Between Cerebral Blood Flow Velocity and Intracranial Pressure. pp. 147–151 (2012). DOI 10.1007/978-3-7091-0956-4_27
37. Liu, X., Czosnyka, M., Donnelly, J., Budohoski, K.P., Varsos, G.V., Nasr, N., Brady, K.M., Reinhard, M., Hutchinson, P.J., Smielewski, P.: Comparison of frequency and time domain methods of assessment of cerebral autoregulation in traumatic brain injury. Journal of Cerebral Blood Flow and Metabolism **35**(2), 248–256 (2015). DOI 10.1038/jcbfm.2014.192
38. Lundberg, N.: Continuous Recording and Control of Ventricular Fluid Pressure in Neurosurgical Practice. Journal of Neuropathology and Experimental Neurology **21**(3), 489 (1962). DOI 10.1097/00005072-196207000-00018
39. Magnæs, B.: Body position and cerebrospinal fluid pressure. part 1: Clinical studies on the effect of rapid postural changes. Journal of neurosurgery **44**(6), 687–697 (1976)
40. Newell, D.W., Aaslid, R., Stooss, R., Reulen, H.J.: The relationship of blood flow velocity fluctuations to intracranial pressure B waves. Journal of Neurosurgery **76**(3), 415–421 (1992). DOI 10.3171/jns.1992.76.3.0415
41. Panerai, R.B., Hudson, V., Fan, L., Mahony, P., Yeoman, P.M., Hope, T., Evans, D.H.: Assessment of dynamic cerebral autoregulation based on spontaneous fluctuations in arterial blood pressure and intracranial pressure. Physiological Measurement **23**(1), 59–72 (2002). DOI 10.1088/0967-3334/23/1/306
42. Piper, I.R., Miller, J.D.: An experimental study of cerebrovascular resistance, pressure transmission, and craniospinal compliance. Neurosurgery **34**(1), 199–201 (1994). DOI 10.1227/00006123-199401000-00042
43. Porta, A., Faes, L.: Assessing causality in brain dynamics and cardiovascular control. Philosophical Transactions of the Royal Society A: Mathematical, Physical and Engineering Sciences **371**(1997), 20120517 (2013). DOI 10.1098/rsta.2012.0517
44. Raftopoulos, C., Chaskis, C., Delecluse, F., Cantrainet, F., Bidauti, L., Brotchi, J.: Morphological quantitative analysis of intracranial pressure waves in normal pressure hydrocephalus. Neurological Research **14**(5), 389–396 (1992). DOI 10.1080/01616412.1992.11740091
45. Rodrigues, J., Andrade, A.: A New Approach for Granger Causality between Neuronal Signals using the Empirical Mode Decomposition Algorithm. In: Biomedical Engineering / 765: Telehealth / 766: Assistive Technologies. ACTAPRESS, Calgary,AB,Canada (2012). DOI 10.2316/P.2012.764-147
46. Rodrigues, J., Andrade, A.: Instantaneous Granger Causality with the Hilbert-Huang Transform. ISRN Signal Processing **2013**, 1–9 (2013). DOI 10.1155/2013/374064
47. Rosengarten, B., Rüskes, D., Mendes, I., Stolz, E.: A sudden arterial blood pressure decrease is compensated by an increase in intracranial blood volume. Journal of Neurology **249**(5), 538–541 (2002). DOI 10.1007/s004150200061
48. Sadri, F.: Intention recognition with event calculus graphs and weight of evidence. Icaart 2011 - Proceedings of the 3rd International Conference on Agents and Artificial Intelligence **1**, 470–475 (2011)
49. Sanz-García, A., Pérez-Romero, M., Pastor, J., Sola, R.G., Vega-Zelaya, L., Monasterio, F., Torrecilla, C., Vega, G., Pulido, P., Ortega, G.J.: Identifying causal relationships between EEG activity and intracranial pressure changes in neurocritical care patients. Journal of Neural Engineering **15**(6) (2018). DOI 10.1088/1741-2552/aadeea
50. Sanz García, A., Pérez Romero, M., Pastor Gómez, J., García de Sola, R., Vega Zelaya, L., Monasterio, F., Torrecilla López, C., Vega, G., Pulido Rivas, P., Ortega Rabbione, G.J.: ¿Es posible obtener información de la presión intracraneal a partir de la actividad electroencefalográfica? Revista de Neurología **68**(09), 375 (2019). DOI 10.33588/rn.6809.2018179
51. Schwarz, G.: Estimating the dimension of a model. Ann. Statist. **6**(2), 461–464 (1978)
52. Seth, A.: Causal connectivity of evolved neural networks during behavior. Network: Computation in Neural Systems **16**(1), 35–54 (2005). DOI 10.1080/09548980500238756
53. Seth, A.: Granger causality. Scholarpedia **2**(7), 1667 (2007). DOI 10.4249/scholarpedia.1667
54. Seth, A.K.: A MATLAB toolbox for Granger causal connectivity analysis. Journal of Neuroscience Methods **186**(2), 262–273 (2010). DOI 10.1016/j.jneumeth.2009.11.020

55. Seth, A.K., Barrett, A.B., Barnett, L.: Granger causality analysis in neuroscience and neuroimaging. Journal of Neuroscience **35**(8), 3293–3297 (2015). DOI 10.1523/JNEUROSCI.4399-14.2015
56. Singh, J., Darpe, A.K., Singh, S.P.: Bearing damage assessment using jensen-rényi divergence based on eemd. Mechanical Systems and Signal Processing **87**, 307–339 (2017). DOI 10.1016/j.ymssp.2016.10.028
57. Smielewski, P., Lavinio, A., Timofeev, I., Radolovich, D., Perkes, I., Pickard, J.D., Czosnyka, M.: ICM+, a flexible platform for investigations of cerebrospinal dynamics in clinical practice. pp. 145–151 (2008). DOI 10.1007/978-3-211-85578-2_30
58. Steinmeier, R., Bauhuf, C., Hübner, U., Bauer, R.D., Fahlbusch, R., Laumer, R., Bondar, I.: Slow Rhythmic Oscillations of Blood Pressure, Intracranial Pressure, Microcirculation, and Cerebral Oxygenation. Stroke **27**(12), 2236–2243 (1996). DOI 10.1161/01.STR.27.12.2236
59. Swallow, D.M., Fellner, N., Varsos, G.V., Czosnyka, M., Smielewski, P., Pickard, J.D., Czosnyka, Z.: Repeatability of cerebrospinal fluid constant rate infusion study. Acta Neurologica Scandinavica **130**(2), 131–138 (2014). DOI 10.1111/ane.12246
60. Veltcheva, A.D., Guedes Soares, C.: Analysis of abnormal wave records by the Hilbert-Huang transform method. Journal of Atmospheric and Oceanic Technology **24**(9), 1678–1689 (2007). DOI 10.1175/JTECH2067.1
61. Wu, Z., Huang, N.E.: A study of the characteristics of white noise using the empirical mode decomposition method. Proc. R. Soc. Lond. A, Math. Phys. Sci. **460**(2046), 1597–1611 (2004)
62. Wu, Z., Huang, N.E.: Ensemble empirical mode decomposition: A noise-assisted data analysis method. Advances in Adaptive Data Analysis **1**(1), 1–41 (2009). DOI 10.1142/S1793536909000047
63. Zeiler, A., Faltermeier, R., Tomé, A.M., Keck, I.R., Puntonet, C., Brawanski, A., Lang, E.W.: Sliding Empirical Mode Decomposition-Brain Status Data Analysis and Modeling. pp. 311–349 (2013). DOI 10.1007/978-3-642-28696-4_12

A Ensemble Empirical Mode Decomposition (EEMD)

EEMD was introduced by Huang et al. as an adaptive analysis method for time series generated by nonlinear and nonstationary systems [62]. EEMD is based on the original EMD approach [1], which is a sifting method for decomposing the signal, $X(t)$, into a finite number, n of intrinsic mode functions (IMFs), c_j and the residue, r_n: $X(t) = \sum_{j=1}^{n} c_j + r_n$. IMFs are oscillatory functions that fulfill two requirements: (1) the number of extrema and zero-crossing is either equal or differs by one over the entire length of the function, and (2) the mean value of the envelopes generated form the local maxima and minima is zero. But EMD suffers from the problem of mode mixing, causing either signals of the same time scale to appear in different IMFs or very different scales to be present in the same IMF.

To eliminate the shortcoming of mode mixing in EMD, EEMD is implemented instead. This noise-assisted signal analysis method generates the IMFs by adding white noise to the original signal. It turns out that EMD has a dyadic filter bank behaviour when decomposing white noise, preventing mode mixing from occurring [21]. The true IMFs are then computed as the mean of ensemble of the IMF decomposition.

B Granger Causality (GC)

Identifying the underlying relations of different temporal scales between signals gives rise to the concept of connectivity. However, this concept relates to the statistical relation between signal variables, without taking into account the influence of one variable to another. To study this cause-and-effect relation Granger formulated the measure of causality, often referred to as Granger Causality (GC) measure [26]. This measure is built on the idea that causes occur before their effects and help predict their effects.

Given two variables X_1 and X_2 in two physiological time series, bivariate GC analyzes whether the history of variable X_1 helps to improve the prediction of X_2, over the knowledge of just past information of X_2. Thus, we say that X_1 causes X_2, if X_2, can be at least partially

predicted from the past values of X_1, implying that past values of X_1 contribute to the current state of X_2. In our work, we want to understand the interaction between three signal variables, ICP, MAP, and FV, which requires a multivariate extension of the bivariate GC measure. This extension is known as conditional Granger causality analysis (GCCA), in which GC is investigated by fitting a multivariate autoregressive (MVAR) model to the time series. The third variable included is comprised of all the remaining signals that must be included in the model to analyze the flow between X and Y variables [46].

In our work, conditional GC using a MVAR model of order p. Suppose then that the dynamics of X_1 can be explained by the MVAR model as follows:

$$X_1(t) = \sum_{j=1}^{p} A_{1j} X_1(t-j) + \sum_{j=1}^{p} A_{2j} X_2(t-j) + \sum_{j=1}^{p} A_{3j} X_3(t-j) + E_1'(t) \tag{B.1}$$

where X_1, X_2 and X_3 are the three signal variables ICP, ABP and FV, E_1' is the error of the model, and A_k the regression coefficients. The model order p is determined using the lowest value of either Akaike Information Criterion (AIC) [2] or Bayesian Information Criterion (BIC) [51] so as to avoid overfitting. A more thorough mathematical description can be found elsewhere [7].

A causal flow from X_2 to X_1 exists when the inclusion of lagged observations of X_2 in the previous equation reduces the variance of E_1', after taking into account the influence of X_3. This implies that coefficients A12 reject the F-test null hypothesis that they are zero at a given significance level, i.e., they are different from zero [53]. The logarithm of the F-statistic measures the magnitude of the G-causality [23]:

$$cGCI_{2\to 1|3} = \ln \frac{var(E_1)}{var(E_{1'})} \tag{B.2}$$

where E_1 is the error of the model without lagged observations of X_2, and E_1' is the error of a similar MVAR model but including past observations of X_2.

A.4 Paper IV

Title: Empirical Mode Decomposition-Based Method for Artefact Removal in Raw Intracranial Pressure Signals

Authors: Isabel Martinez-Tejada, Jens E. Wilhjelm, Marianne Juhler, and Morten Andresen

Journal: Intracranial Pressure and Neuromonitoring XVII. Acta Neurochirurgica Supplement

Status: Published

DOI: 10.1007/978-3-030-59436-7_39

Empirical Mode Decomposition-Based Method for Artefact Removal in Raw Intracranial Pressure Signals

Isabel Martinez-Tejada, Jens E. Wilhjelm, Marianne Juhler, and Morten Andresen

Introduction

The most common way of analysing the intracranial pressure (ICP) signal in clinical practice is by visually inspecting the presence of macro patterns and waveform abnormalities. However, this approach relies on the experience of the observer, and hence the outcome might not be consistent. Automated and standardized methods of detecting wave patterns are thus desired to enable better detection of ICP deviations for diagnostic and therapeutic purposes. However, ICP signals are often contaminated by artefacts and the presence of segments of missing values. Some of these artefacts can be observed as very high and short spikes with a physiologically impossible high slope and value. These spikes can be generated by different sources, e.g. connection errors and movement of the monitoring system during data collection [1]. The presence of these spikes reduces the accuracy of pattern recognition techniques because they mask the characteristic appearance of ICP patterns.

Several methods have been used to identify the presence of spikes in ICP signals, from signal thresholding [2] to wavelet analysis. Signal thresholding fails to work if the signal-to-noise ratio (SNR) is low or if the ICP rises in an unphysiologically short time. Techniques using low-pass filtering are not appropriate in the case of the ICP signal since they are non-stationary (i.e. statistical properties change over time), as shown in the top graph of Fig. 1, where trends varying in time can be observed [3]. Alternative non-linear methods are based on wavelet transformation, whose output performance is highly influenced by the choice of a basis function [4]. These basis functions are fixed, hindering their match with the nature of the input signal at a given time. To overcome this drawback, more recent papers decompose the signal using the empirical mode decomposition (EMD) method, where the mother functions are derived from the signal, making the decomposition adaptive [4, 5].

Therefore, in this paper we propose a modified EMD method for automatic spike removal in raw ICP signals. The method is adaptive in non-linear and non-stationary signals because it involves breaking down signals into different frequency modes without leaving the time domain. It relies on the principle that some of these modes, also referred to as intrinsic mode functions (IMFs), capture the noise in signals so no a priori information on the data is required. This is important because there is no a priori knowledge of noise, so no procedures can be fixed beforehand to decrease the contribution of noise in signals.

Methods

EMD Algorithm

Huang et al. [6] presented EMD as a sifting method for adaptively decomposing non-stationary signals into a finite number of IMFs. An IMF is described as a function with two requirements: first, the number of extrema must be equal to zero-crossing or differ mostly by one and, second, the mean value of its lower and upper envelopes is zero. The EMD algorithm used for IMF extraction is briefly described for a given input ICP signal $s(t)$ as follows:

I. Martinez-Tejada (✉)
Clinic of Neurosurgery, Copenhagen University Hospital, Rigshospitalet, Denmark

Department of Health Technology, Technical University of Denmark, Lyngby, Denmark
e-mail: imate@dtu.dk

J. E. Wilhjelm
Department of Health Technology, Technical University of Denmark, Lyngby, Denmark
e-mail: jwil@dtu.dk

M. Juhler · M. Andresen
Clinic of Neurosurgery, Copenhagen University Hospital, Rigshospitalet, Denmark

B. Depreitere et al. (eds.), *Intracranial Pressure and Neuromonitoring XVII*, Acta Neurochirurgica Supplement 131, https://doi.org/10.1007/978-3-030-59436-7_39, © Springer Nature Switzerland AG 2021

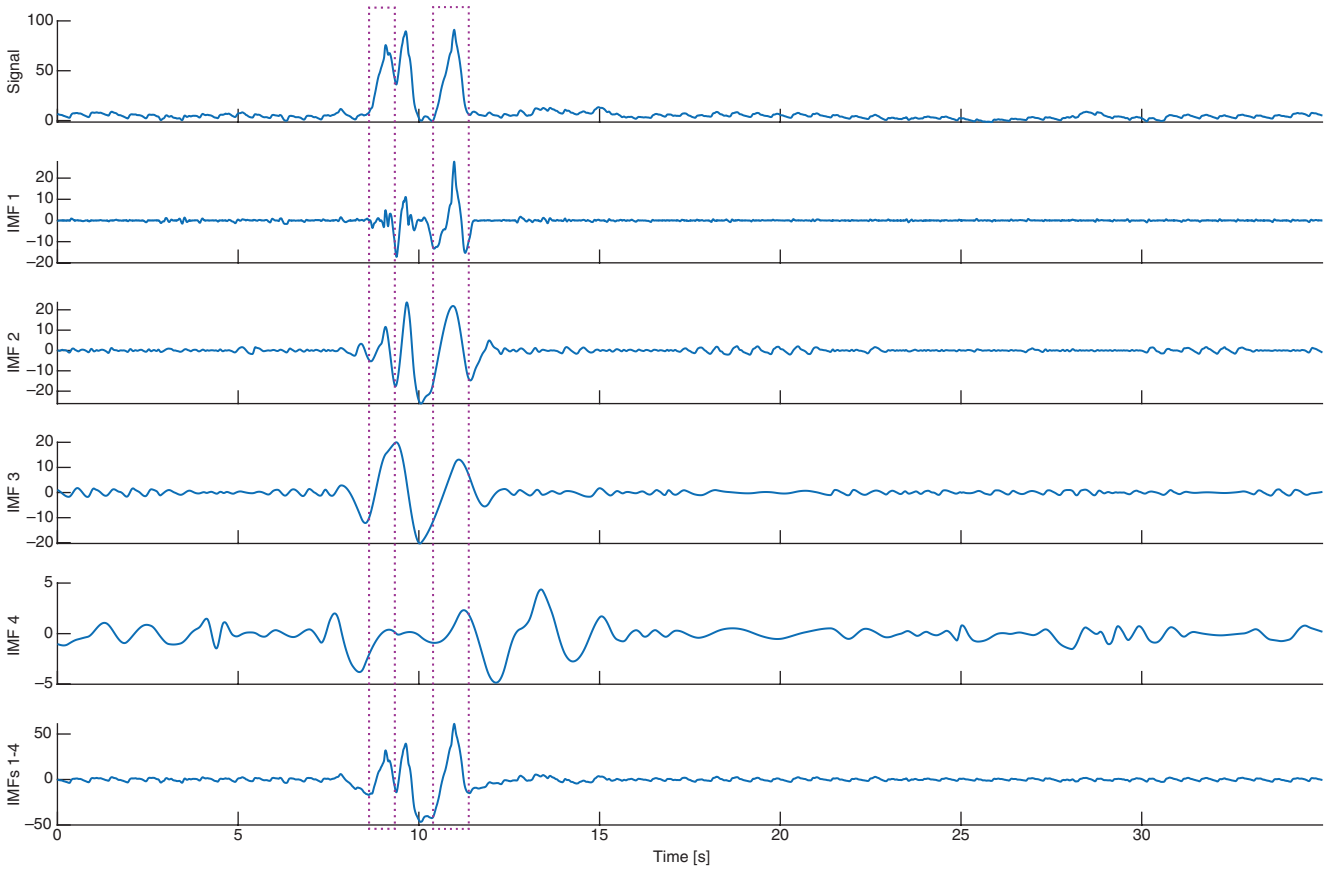

Fig. 1 Examples of peaks in ICP signals and IMF1–4

1. Find signal $x(t)$ extrema to which splines are fitted to generate both lower and upper envelopes. In the first iteration, $x(t) = s(t)$.
2. Calculate the arithmetic average of the two envelopes, $m(t)$.
3. Generate a candidate IMF $h(t)$ by subtracting the average envelope from the signal: $h(t) = x(t) - m(t)$.
4. If $h(t)$ is not an IMF according to the preceding requirements, then $x(t)$ must be replaced with $h(t)$ and steps 1–3 repeated. However, if $h(t)$ is treated as an IMF and the stopping criteria are not reached, the residue $r(t) = x(t) - h(t)$ is assigned to $x(t)$ and steps 1–3 are repeated. The stopping condition is usually a very small value to which the mean squared difference between the last two extracted successive IMFs is compared.

At the end of this iterative process, the original signal $s(t)$ can be expressed as the sum of all extracted IMFs plus the final residue. Note that the later an IMF is extracted, the lower will be its frequency content.

Proposed EMD-Based Algorithm

Spikes have a band-limited waveform, which implies that the frequency content is limited only to certain consecutive IMFs. *Band-limited* means that the frequency domain of the signal is zero beyond a certain finite frequency. The summation of the successive IMFs that contain part of a spike's dominant frequency would then help to temporally localize the spike event.

For localization and later removal of spikes from the ICP signal, we propose the following method:

1. Break down ICP signal into sixteen IMFs via EMD, as described above. Based on the physiological properties of the ICP signal as well as previous experiences by Feng et al. [7], breaking down the signal into 16 IMFs was considered the best trade-off between the signal length and computational time [8].
2. Spike detection from estimated IMFs.
3. Spike imputation in the original signal.

It must be noted that missing values are also randomly present in the ICP signal and they must be temporarily replaced with zeroes before EMD. In our monitored ICP signals, missing values are most likely due to sensor detachment during several minutes. Thus, temporal replacement by zeros during only the decomposition would not have any effect on higher frequency IMFs, which are the ones we are interested on for denoising. Instead, it will affect the low-frequency part, *i.e.* the local trend. Given the simplicity and lower computational time of this shortcoming and its ability to achieve

an effective technical solution, it is preferred over the interpolation of values.

After decomposition, as visually demonstrated in Fig. 1, high amplitude oscillations in the first IMF align with the location of spikes in the ICP signal. Because the spikes have band-limited waveforms, dominant oscillations are found in various consecutive IMFs. Thus, a more effective event duration estimation is obtained when various successive IMFs are taken into account. In our case, only the location of peaks in IMF_{1-4} aligns with the location of peaks in the ICP signal, so summing these four IMFs enhances spike episodes: $IMF_{1-4} = \sum_{k=1}^{4} IMF_k(t)$. It is assumed then that the oscillations that build a spike are present in these four successive IMFs at the same temporal location as the signal artefact.

To identify the peaks in the summed IMFs, an adaptive thresholding approach is proposed (Fig. 2). ICP samples outside the bounded region in $[-P_{th}, P_{th}]$ will be identified as spikes. The threshold is determined based on the noise level in the summed IMFs: $P_{th} = \widehat{\sigma}\sqrt{2 \times \log L}$, where σ is the standard deviation of the signal and L the number of samples in the summed IMF [1]. Because σ is always unknown given the presence of artefacts in the signal, it must be estimated using e.g. the median absolute deviation: $\hat{\sigma} = \frac{\text{MAD}}{0.6745}$, where $\text{MAD} = \text{Me} \mid IMF_{1-4} - \text{Me}(IMF_{1-4})\mid$ [9]. If two identified spikes lie within a window of 0.4 s, the ICP samples between them are also treated as spike events. ICP spikes identified can either be removed or imputed with a moving average calculated over a sliding window of 10 s. An example of the results can be seen in Fig. 3.

Results

To both prove the non-stationarity of the signals and test the ability of the proposed method to detect spikes, real ICP signals are used. A total of 26 h are investigated from five different monitoring sequences. The Kwiatkowski–Phillips–Schmidt–Shin (KPSS) test for stationarity is applied to selected artefact-free segments of increasing size [10]. With a 1-s window size, ICP signals are non-stationary with *p*-values around 0.03 for a significance level (critical alpha) equal to 0.05. Increasing window sizes reject the null hypothesis for the stationarity of the time series with even lower *p*-values (i.e. values close to 0.01).

To investigate the performance of the proposed algorithm, ICP segments containing unwanted dominant spikes are examined. Segments are visually inspected by an expert using a spike template. This template is established just for visual inspection purposes and is based on the determination of two spike characteristics: a duration shorter than 0.5 s and an abrupt ICP value increase. The artefact events visually

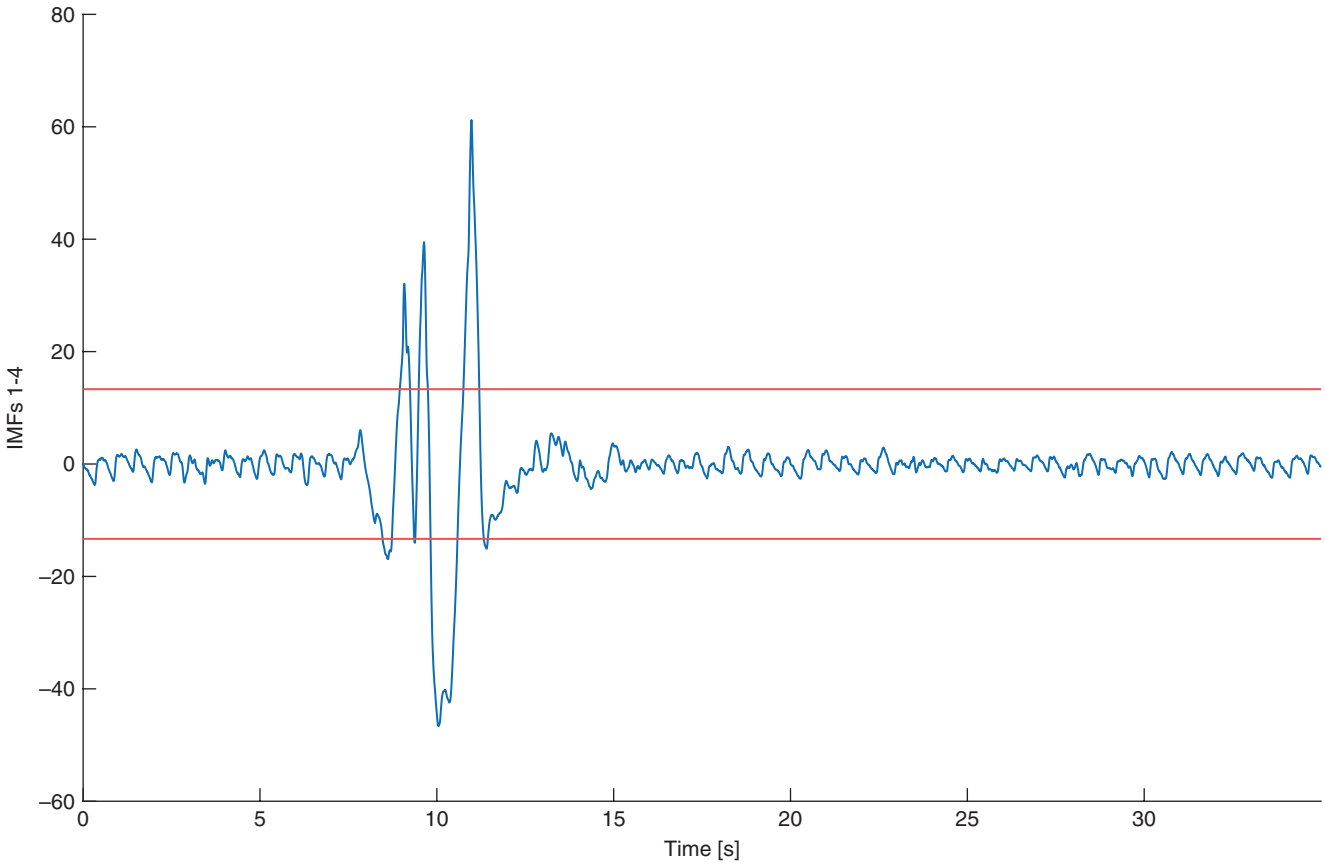

Fig. 2 ICP signals with lower and upper thresholds marked in red

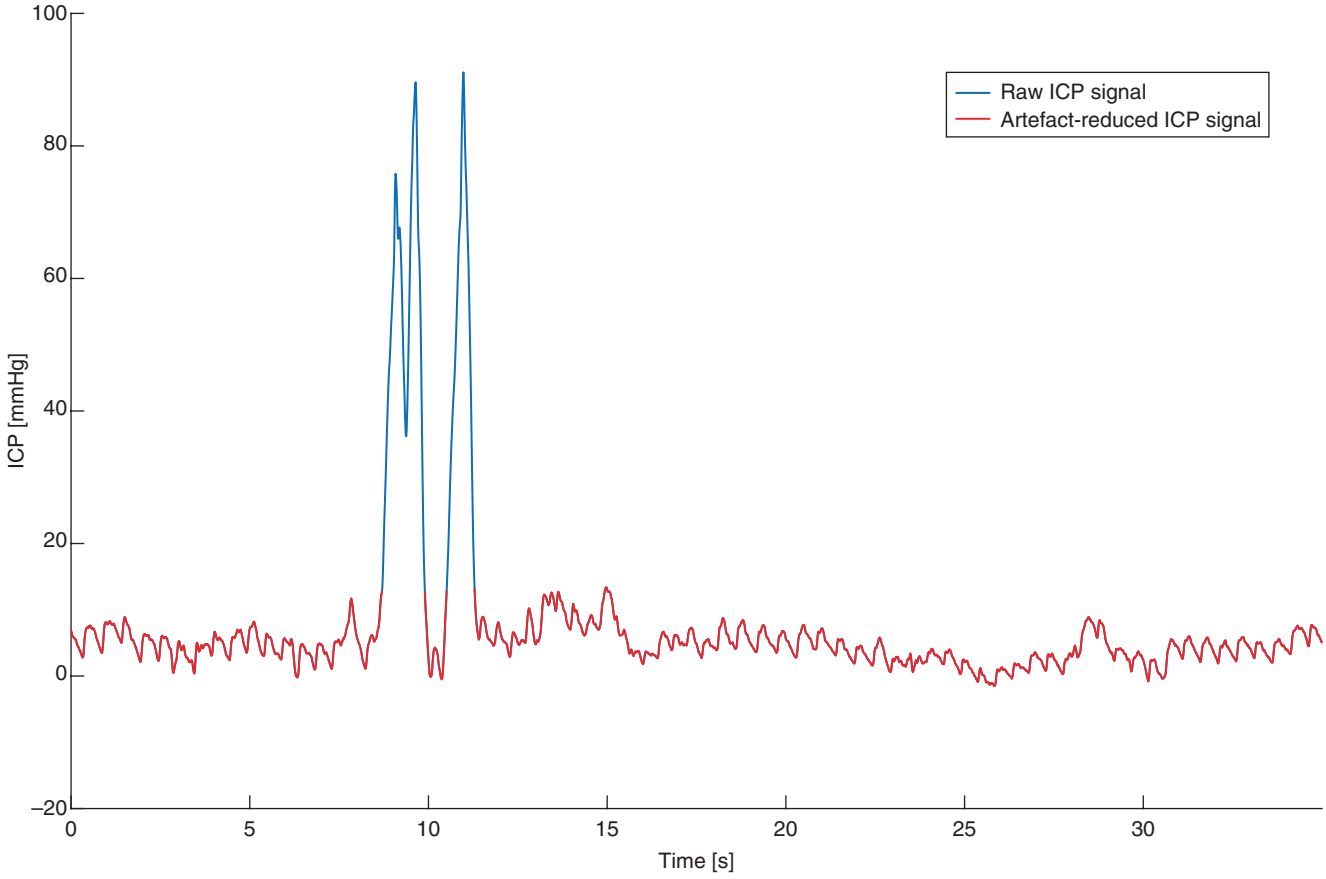

Fig. 3 Artefact-reduced ICP signal where detected spike has been removed

identified with the presence of the template are used as ground truth, and the ability of the method to identify them is then examined. The performance of the proposed method is quantified based on how well it estimates the location of the spikes using precision and recall metrics:

$$\text{precision} = \frac{\text{TP}}{\text{TP} + \text{FP}} \qquad \text{recall} = \frac{\text{TP}}{\text{TP} + \text{FN}}$$

where TP is the number of correctly identified spikes, FP is the number of spikes identified that were not spikes, and FN is the number of unidentified spikes. The goal is to get both values as close to 100% as possible. The proposed algorithm can detect spikes achieving an 84% precision and a 77% recall, given that TP = 114, FP = 21 and FN = 34.

Discussion

Results show that there are some artefact-free signal segments that are incorrectly classified as artefacts, given that the precision achieved is not 100%. The recall is lower, which shows that some artefact events are not identified. This is likely to be due to the magnitude of the episodes being smaller than the adaptive threshold P_{th} calculated. This limitation could be addressed by performing an additional spike identification iteration based on the slopes of the summed IMF peaks.

The algorithm also presents the drawback of not establishing a method to deal with the identified artefacts. We will further investigate this in our ongoing research, for which autoregressive moving average (ARMA) models [5] will be considered.

Conclusion

In this paper, a new methodology based on EMD is proposed for the removal of unphysiological spikes in clinical ICP signals, which is essential for correct patient evaluation and diagnosis in clinical practice.

Acknowledgement The authors are thankful for contributions from the Novo Nordisk Fonden Tandem Programme and Otto Mønsteds Fond.

Conflict of Interest **The authors declare that they have no conflict of interest.**

References

1. Andresen M, Juhler M, Thomsen OC (2013) Electrostatic discharges and their effect on the validity of registered values in intracranial pressure monitors. J Neurosurg 119:1119–1124
2. Obeid I, Wolf PD (2004) Evaluation of spike-detection algorithms for a brain-machine interface application. IEEE Trans Biomed Eng 51(6):905–911. https://doi.org/10.1109/TBME.2004.826683
3. Han B, Muma M, Feng M, Zoubir AM (2013) An online approach for intracranial pressure forecasting based on signal decomposition and robust statistics. In: 2013 IEEE International Conference on Acoustics, Speech and Signal Processing (ICASSP), pp. 6239–6243
4. Andrade AO, Nasuto S, Kyberd P, Sweeney-Reed CM, Van Kanijn FR (2006) EMG signal filtering based on empirical mode decomposition. Biomed Signal Process Control 1(1):44–55
5. Farashi S, Abolhassani M, Kani M (2014) An empirical mode decomposition based method for action potential detection in neural raw data. World Academy of Science, Engineering and Technology, Open Science Index 85. Int J Med Health Sci 8(1):45–49
6. Huang NE, Shen Z, Long SR, Wu MC, Shih HH, Zheng Q, Yen N, Tung C, Liu HH (1998) The empirical mode decomposition and the Hilbert spectrum for nonlinear and non-stationary time series analysis. Proc Math Phys Eng Sci 454(1971):903–995
7. Feng M, Loy LY, Zhang F, Guan C (2011) Artifact removal for intracranial pressure monitoring signals: a robust solution with signal decomposition. In: Proceedings of the annual international conference of the IEEE Engineering in Medicine and Biology Society, EMBS, vol 6090182. IEEE, pp 797–801
8. Sanchez JL, Ortigueira M, Rato R, Trujillo J (2016) An improved empirical mode decomposition for long signals. In: SIGNAL 2016: The First International Conference on advances in signal, image and video processing
9. Signal noise reduction. Proceedings of World Academy of Science, Engineering and Technology, 2, 93–96
10. Kwiatkowski D, Phillips PCB, Schmidt P, Shin Y (1992) Testing the null hypothesis of stationarity against the alternative of a unit root. J Econ 54(54):159–178. https://doi.org/10.1016/0304-4076(92)90104-Y

A.5 Paper V

Title: k-Shape clustering for extracting macro-patterns in intracranial pressure signals

Authors: Isabel Martinez-Tejada, Casper Schwartz Riedel, Marianne Juhler, Morten Andresen, and Jens E. Wilhjelm

Journal: Neurocomputing

Status: Submitted

k-Shape clustering for extracting macro-patterns in intracranial pressure signals

Isabel Martinez-Tejada[a,b,*], Casper Schwartz Riedel[a], Marianne Juhler[a], Morten Andresen[a], Jens E. Wilhjelm[b]

[a] *Clinic of Neurosurgery, Copenhagen University Hospital, Rigshospitalet, Copenhagen, Denmark*
[b] *Department of Health Technology, Technical University of Denmark, Kongens Lyngby, Denmark*

Abstract

Intracranial pressure (ICP) monitoring is a core component of neurosurgical diagnostics. With the introduction of telemetric monitoring devices in the last years, ICP monitoring has become feasible in a broader clinical setting including monitoring during full mobilization and at home, where a greater diversity of ICP waveforms are present. The need for identification of these variations, the so-called macro-patterns lasting seconds to minutes - emerges as a potential tool for better understanding the physiological underpinnings of patient symptoms. We introduce a new methodology that serves as a foundation for future automatic macro-pattern identification in the ICP signal to comprehensively understand the appearance and distribution of these macro-patterns in the ICP signal and their clinical significance. Specifically, we describe an algorithm based on k-Shape clustering to build a standard library of such macro-patterns. This library may be used as a basis for the classification of new ICP variation distributions based on clinical disease entities. We provide the starting point for future researchers to use a computational approach to characterize ICP recordings from a wide cohort of disorders.

*Corresponding author
Email addresses: isita.martinez93@gmail.com (Isabel Martinez-Tejada), casper.schwartz.riedel@regionh.dk (Casper Schwartz Riedel), marianne.juhler@regionh.dk (Marianne Juhler), andresen@gmail.com (Morten Andresen), jwil@dtu.dk (Jens E. Wilhjelm)

Keywords: intracranial pressure, macro-pattern, k-Shape clustering

1. Introduction

Intracranial pressure (ICP) monitoring is a mainstay of neurosurgical diagnostics both for intensive care management in acute neurosurgical conditions [1] and for aiding diagnosis in conditions outside the ICU for milder degrees of disease such as hydrocephalus, normal pressure hydrocephalus (NPH), or idiopathic intracranial hypertension (IIH).

In the clinical setting, ICP is often interpreted purely as a number within a certain range. Yet, ICP signals are complex time series with wave patterns that go beyond just a simple number. Analysis of ICP waveforms on either a subsecond beat-to-beat basis or in patterns over longer durations, the so-called macro-patterns, gives further insight into brain function [2]. Machine learning tools have the potential to identify these patterns faster and –more importantly– objectively, helping to characterize their appearance and distribution in a standardized fashion compared to the current primary visual inspection by clinicians. Until now, most studies have employed these techniques to analyze the ICP in acute conditions. Mariak et al. used artificial neural networks (ANN) to extract global properties of the entire ICP time series to assess the severity of the clinical state in intensive care patients [3]. Hornero et al. analyzed the complexity of the ICP signal estimated by approximate entropy (ApEn) to determine the presence of patterns in periods of acute elevations in ICP of pediatric patients in intensive care [4].

In the last decade, new telemetric ICP monitoring devices have become available, allowing easier access to perform ICP recordings that are representative of daily life conditions, compared to previous cable-based solutions [5, 1]. Thus, ICP can now be monitored in patients with milder degrees of disease in disease categories such as hydrocephalus, normal pressure hydrocephalus, or idiopathic intracranial hypertension. The ICP signals recorded with these systems ensure sufficient clinical and technical quality to be analyzed as part of the ICP inter-

pretation procedure carried out by neurosurgeons and other clinicians [6, 7, 8], but the increased monitoring period and signal diversity also means that the analysis of ICP data becomes more demanding.

In this study, we explore the use of machine learning tools to extract macro-patterns from the ICP signal in a diverse cohort of patients with different disease entities. We introduce a new methodology based on k-Shape clustering as a basic building block for future day-to-day ICP evaluation and update of models on stored patient data. Given that ICP monitoring can now safely take place out of hospital borders, our main context for considering this new approach moves away from ICP monitoring exclusively in the neurointensive care setting as the cornerstone of Traumatic Brain Injury (TBI) care. Specifically, it aims to permit a more adequate description of the longer timescale ICP variations seen in the broader clinical setting nowadays including disease types like NPH or IIH. Our approach created a universal library of representative macro-patterns that can later be used to automatically segment each individual ICP signal into shorter sequences based on clinical input. Also, we developed a template matching framework to classify these shorter sequences -which we will refer to as ICP subsequences- into what we estimate to be clinically significant macro-patterns. Finally, we propose a possible visualization strategy to display the pattern-annotated ICP signal in a fashion that is clinically useful.

2. Methods

Our goal was to create a scalable library of a few macro-pattern templates to use for ICP subsequence classification. We used k-Shape clustering as a method to efficiently group together subsequences characterized by their shape similarity despite differences in amplitude, duration and alignment. We first describe our data selection and processing approach for artifact removal (Sections 2.1 and 2.2). Next, we discuss our k-Shape based clustering approach to construct the templates (Section 2.3). Finally, we show how the stored library can be used to characterize new incoming ICP signals by reproducible macro-patterns. The

components of the entire approach are illustrated in Figure 1.

2.1. Data selection

We used a collection of eight randomly selected anonymized overnight monitoring sessions that belong to different subjects from our database in the Department of Neurosurgery, Rigshospitalet, Denmark. A commercially available cable ICP probe (Neurovent-P; Raumedic AG, Germany) was used for these measurements. The length of the sessions spanned from nine to 22 hours, summing up to a total of 88 hours. The sampling frequency of the recordings was 100 Hz. The dataset was made up of five monitoring sessions (five patients) for a total of 88 hours, and an additional set of three monitoring sessions (three patients) for a total of 55 hours. By adding the latter dataset, template matching results can provide an indication of whether the algorithm is general enough to cover subjects with different disease entities.

2.2. Data preprocessing

The ICP signal recorded is often contaminated by very high and sharp spikes, with unphysiologically high values. These artifacts mask the characteristic appearance of the signal, rendering accurate pattern recognition impossible. We used an Empirical Mode Decomposition (EMD) based method for spike removal [9].

EMD decomposes the signal into a set of intrinsic mode functions (IMFs, i.e., IMF_1, IMF_n, ..., IMF_N). The first function of this set corresponds to fast oscillations, while the last one corresponds to the slowest ones. The first IMFs, containing high-frequency oscillations, indicate the presence of artifacts. Because the spikes have band-limited waveforms, their dominant oscillations are found in a subset of consecutive IMFs. In our case, the location of unphysiologically high and rapid spikes aligned with the location of spike events in IMF_1 to IMF_4, so summing these four IMFs enhances spike episodes. The summation result reveals the peaks with dominant amplitude at the temporal location of the spike, and attenuates the effect of non-spike events. The term g_r will be

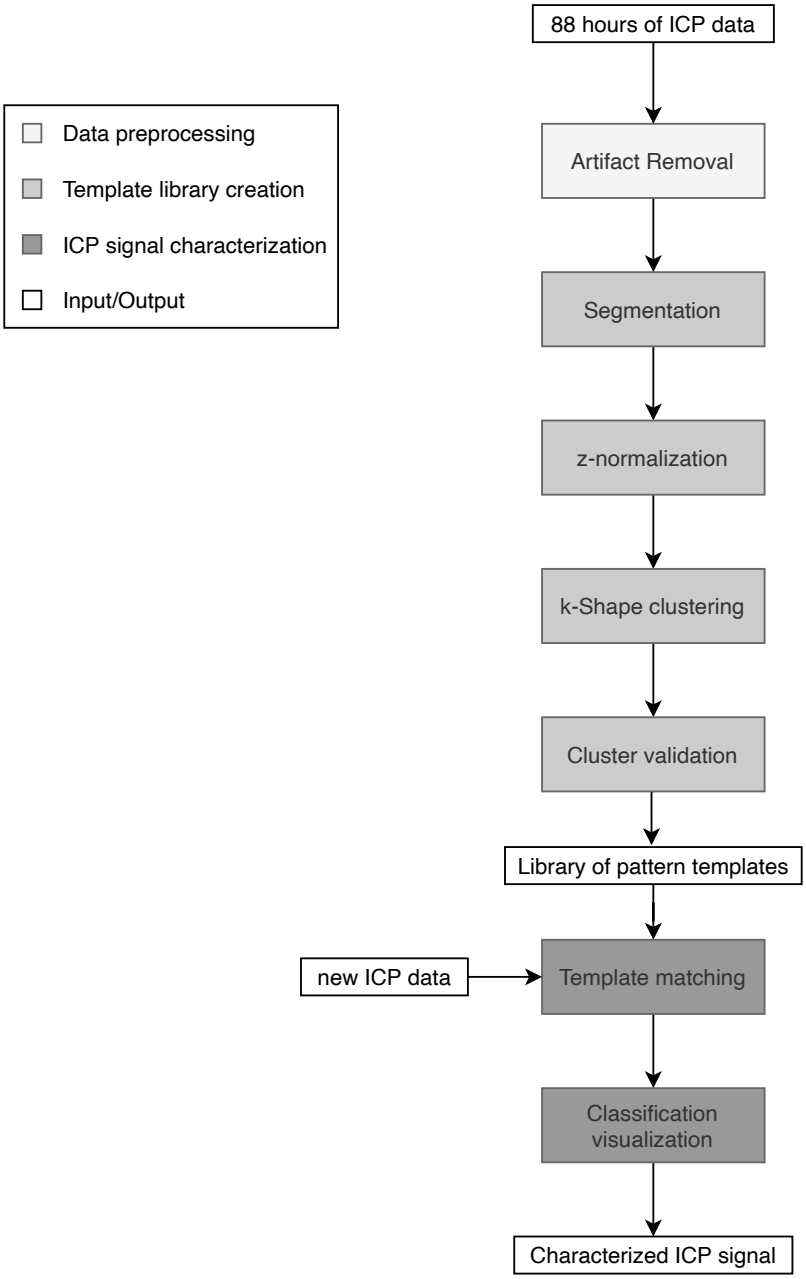

Figure 1: Workflow of methodology developed in this paper for 88 hours of ICP data, and an additional data set of 55 hours purely for investigating how new incoming ICP data in the future can be labelled.

used to refer to the partially reconstructed signal calculated as the sum of the first to fourth IMFs.

To identify the peak events in g_r, an adaptive thresholding approach was implemented. ICP values outside the bounded region between $[-\eta_s,\ \eta_s]$ were identified as spikes. The threshold was calculated as $\eta = \sigma\sqrt{2 \cdot \log(L)}$, where σ and L are the standard deviation (noise level) and number of samples of g_r, respectively. It is a universal threshold first proposed by Donoho and Johnstone [10] for determining a value above background noise. Identified spikes were then imputed with a moving average calculated over a sliding window of 10s.

2.3. Template library creation

We implemented the algorithm in MATLAB (R2020b; The MathWorks, Inc., Natick, MA.) using the platform: Intel® with core i7 processor and clock speed 2.6 GHz and 16 GB RAM.

2.3.1. Segmentation

Time series segmentation plays an important role in data mining and refers to the tool for decomposing the signal into a discrete number of contiguous subsequences. The proposed algorithm for segmentation of the ICP signal can be broken down into four sequential steps, as seen in Figure 2. The following section will cover the details regarding each of the steps.

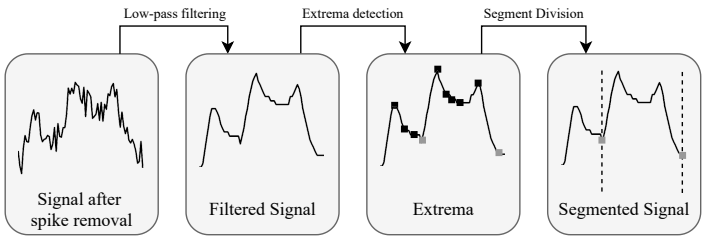

Figure 2: Workflow of the steps involved in the generation of the ICP subsequences, describing the segmentation step in Figure 1

ICP segmentation was applied to divide the signal into subsequences of duration varying from seconds to minutes. This poses the challenge of deciding

the time location at which to anchor both the start and end points of each subsequence. To address this problem, we first smoothed the signal via a linear phase FIR lowpass filter. The filtered signal will only be used in the segmentation step. The cut-off frequency (F_{pass}) was set to 0.05-0.1 Hz, depending on the degree of smoothing desired for the removal of cardiac and respiratory contributions in each subject. Other filter parameters were F_{stop} = 0.02-0.05 Hz, A_{pass} = 0.001 dB, A_{stop} = 60 dB, and minimum order.

From the smoothed ICP signal, the major extrema were extracted (maxima and minima). However, we only used the minima to define the start and endpoints for each of the ICP subsequences. Because some minima are located very close - both time and amplitude wise - to a neighboring maxima, we implemented the following rule to identify suitable minima for the segmentation. If we suppose that the discrete ICP signal at this stage can be written as g_n, $n = 1, 2, ..., N$, we removed a minima g_i from being a candidate as a boundary point if:

1. the time difference between the minima g_i and its neighboring maxima g_j was smaller than a predefined value η_{dur}, between 0.5 and 2 minutes, i.e. $|t_j - t_i| < \eta_{dur}$, or
2. the magnitude difference between a minima g_i and its neighboring maxima g_j was smaller than a predefined value η_{mag}, between 0.5 and 1.5, i.e. $|g_j - g_i| < \eta_{mag}$.

We can then define the segmented window (i.e., ICP subsequence) as $g[i, j]$ with i and j corresponding to the discrete indices of the selected boundary points. An example of these steps is shown in Figure 5A-C.

2.3.2. Z-normalization

Z-normalization of the derived subsequences was required before clustering. As many recent studies [11, 12] suggest, this procedure is necessary for data mining algorithms to deal with scale and translation invariance to prioritize shape features over amplitude ones. By z-normalizing each subsequence we

ensured that they were linearly transformed to have zero mean and standard deviation close to one:

$$z(g[i,j]) = \frac{g[i,j] - \mu_{g[i,j]}}{\sigma_{g[i,j]}} \tag{1}$$

where $\mu_{g[i,j]}$ and $\sigma_{g[i,j]}$ refer to the mean and standard deviation of the ICP subsequence $g[i,j]$, respectively. For the sake of simplicity, we will refer to each z-normalized ICP subsequence $z(g[i,j])$ as z_{icp} in the rest of the paper.

2.3.3. k-Shape clustering

k-Shape was used to divide our extracted ICP subsequences into a number of characteristic-preserving groups, the so-called clusters, such that sequences in the same group were similar in shape. Each cluster is represented by a central vector, the centroid, which is not necessarily part of the original dataset [13]. Each centroid in k-Shape is determined as a sequence that minimizes the sum of squared distances to the rest of the z-normalized ICP subsequences. This novel centroid-based clustering algorithm is fundamentally a variant of k-means with a distance measure derived from the cross-correlation coefficient [14]. As a result, one template is built for each centroid and subsequently stored together with a class label.

Through an iterative procedure, k-Shape:

(i) assigned each z-normalized ICP subsequence to the centroid with the maximum shape similarity in the assignment step, and

(ii) updated the centroids based on the new members of each cluster, in the refinement step.

Shape similarity was defined by the so-called Shape-Based Distance (SBD):

$$SBD(\overrightarrow{x}, \overrightarrow{c_k}) = 1 - max_w \left(\frac{CC_w(\overrightarrow{x}, \overrightarrow{c_k})}{\sqrt{R_0(\overrightarrow{x}, \overrightarrow{x}) \cdot R_0(\overrightarrow{c_k}, \overrightarrow{c_k})}} \right) \tag{2}$$

where w is the position at which the cross-correlation $CC_w(\overrightarrow{x}, \overrightarrow{c_k})$ between the z-normalized ICP subsequence ($\overrightarrow{x} = z_{icp}$) and the centroid vector of each cluster ($\overrightarrow{c_k}$) was maximized; and R_0 the autocorrelation of each sequence $\overrightarrow{x}$

or $\overrightarrow{c_k}$. Cross-correlation adds shift-invariance to the SBD measure and can be computed on sequences of different lengths. The previous two steps of the algorithm were repeated either until there was no change in cluster configuration or until the maximum number of 100 iterations was reached [14].

Determining the optimal number of clusters, K, is a fundamental challenge within partitional clustering and unfortunately, there is not an ideal approach to identify K. Given that we had a large amount of data to be clustered into a number of clusters, and this number was dependent on medical practical experience, the need for an initial estimate of clusters is clear. We relied on a direct method, the so-called silhouette index, as the metric to evaluate the quality of the clustering structure. This metric evaluates the clustering quality based on the similarity between subsequences within the same cluster and across different clusters [15]:

$$S(i) = \frac{b(l) - a(i)}{max\{b(l), a(l)\}} \tag{3}$$

In Equation 3, $a(l)$ is the average distance between subsequence l and every subsequence within the same cluster and $b(l)$ is the minimum average distance between subsequence l and every subsequence in different clusters [16]. The optimal estimate of K was the value that maximized the silhouette metric over a range of possible values for K. The window of solutions for which the silhouette index was calculated ranged from five to 20.

2.3.4. Cluster validation

Visual inspection of the clustering results is crucial for verifying the accuracy of the partitioning. However, a visual approach is subject to the level of expertise and subjectivity of the investigator. Thus, visualization needs to be combined with standardized cluster validation indices (CVI) tailored to quantitatively evaluate clustering results. Quantitative evaluation of extracted clusters is not straightforward if there is a lack of annotated data. Thus, we need to rely on internal indices. Conclusions from previous studies have shown that there is no best single CVI in each context [17, 18]. Therefore, multiple validation indices

will be used in the validation process: Silhouette Index, Davies-Bouldin index (DBI), and Calinski-Harabasz index (CHI).

Silhouette index, introduced in the previous section, is a common metric to measure how well an object lies within a cluster and our selected internal clustering validation index. DBI is the ratio between the average distance of all subsequences of each cluster to their respective centroids and the distance of the centroids of the two clusters, i.e., the ratio between within-cluster compactness and between-cluster separation [19, 20]:

$$DBI = \frac{1}{K}\sum_{a=1}^{K} max\Big\{\frac{d_a + d_b}{d(c_a, c_b)}\Big\}\, a \neq K \tag{4}$$

where K is the number of clusters, a, b are cluster labels, d_a, d_b the average distance of all subsequences in clusters a and b to their respective centroids, and $d(c_a, c_b)$ the distance between centroids. Smaller values indicate better clustering results, as clusters are more separated from each other and less disperse within each cluster. To be in line with the rest of CVIs, we use $1 - DBI$ for comparison of clustering results and thus higher values indicate better clustering solutions.

CHI relates the sum between the cluster dispersion calculated as the distance, S_B, between each within-cluster subsequence and its centroid, to the inter-cluster dispersion calculated as the distance (S_W) between each centroid to the global centroid ($\overline{c}$) [21]:

$$CHI = \frac{tr(S_B)}{tr(S_W)} \cdot \frac{n_p - 1}{n_p - K} \tag{5}$$

where S_B and S_W are the between and within cluster scatter matrices, respectively, tr the trace defined by the sum of the elements of the main diagonal of the scatter matrices, K the number of clusters and n_p the number of clustered subsequences. The higher the index value, the better the performance of the clustering.

2.4. Characterization of ICP signals

2.4.1. Shape-based template matching

The primary goal was to learn what the distinctive shapes for differentiating pattern clusters from each other were. Therefore, when an uncharacterized ICP subsequence entered into our system, we were able to automatically determine if it belonged to a template from the library of patterns or not. For labeling ICP subsequences based on the generated templates, new ICP subsequences from the additional dataset were retrieved and z-normalized to address scaling invariance, as explained in Section 2.3.2. To deal with the horizontal shifts and stretching of the subsequence on the templates, we rescaled the time dimension. Query subsequences were then compared to each template for the closest match. For this comparison, we computed the SBD so that the shape similarity could be measured.

This template matching approach is done under the assumption that all queries must be classified to a template, even if the closest match shows a high SBD. This is why apart from defining our template library, we also defined a rule to ensure that the correlation to the closest match is meaningful. Although this parameter can be specified by the user, a reasonable rule is: $CC(z_{icp}, \overrightarrow{c_k}) > 0.50$.

2.4.2. Classification visualization

The amount of data in each ICP recording is very large. With our current template library, we are able to classify a subset of the ICP signal. Visualizing this information must be presented to a clinical end-user in a fashion that is operationally useful. For this purpose, we represented each ICP subsequence as colored boxes with varying dimensions according to their characteristics (Figure 3). The height of the box was defined by the difference between the absolute maximum and minimum values of the non-normalized sequence (of the raw unfiltered ICP signal), and the width by the duration of the sequence. The vertical center of the box corresponded to the median ICP value of the non-z-normalized subsequence. Each box was colored after the label their corresponding subsequence had been matched to, being black if the matching correlation coefficient

was below 0.50.

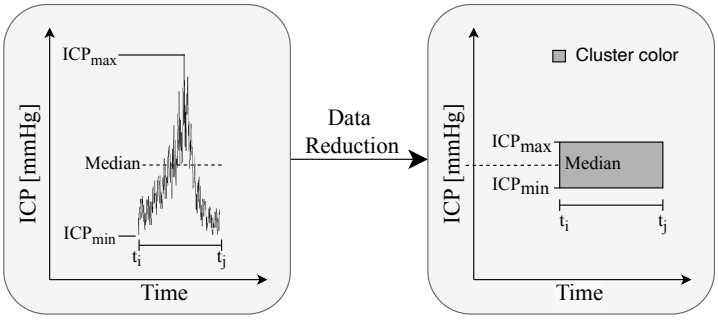

Figure 3: Detailed description of data reduction for each labeled ICP subsequence.

3. Results

3.1. Data Demographics

Eight patients were selected for the study: two male and six female. The pooled median age was 55 years; range: 20-74 years old. Subjects were fetched randomly from a continuously updated clinical ICP database. The clinical conditions were hydrocephalus, aneurysm and craniotomy, but signal analysis was performed on the anonymized recordings without reference to clinical information.

3.2. Data pre-processing

We decomposed the ICP signal via EMD into sixteen IMFs and a residual. Figure 4 shows an example of an ICP signal of one subject after EMD-based filtering, with unphysiologically high and rapid spikes removed.

On average, 18 spikes of less than one second duration are identified in each ICP monitoring. These spikes are found within a range that spans from two to 43 spikes per recording, that account on average for less that 0.000087% of the total monitoring time. Thus, removing the few samples corresponding to

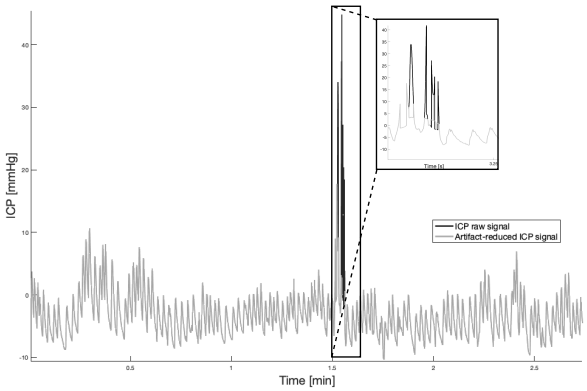

Figure 4: Example of EMD-based filtering of an ICP signal for removal of high spikes.

these spikes should not have any major consequences on later processing steps, especially since we will be looking at longer variations of the ICP signal.

3.3. Template library creation

3.3.1. Segmentation and normalization

We now show how the ICP signal is segmented and illustrate the segmentation results for the five patients whose recordings made up the main dataset. Figure 5 displays the segmentation process described in Figure 2. From the figure, we can see that some of the minima extracted, marked as black squares, are not minima that could potentially be considered boundary points. To keep only the minima of our interest, marked as squares, we specified η_{dur} and η_{mag} for each ICP signal. From the main dataset of 88 hours, we were able to generate 5579 ICP subsequences. The last Figure 5(d) presents how the segmentation results are z-normalized. Z-normalization of a subsequence was done with the mean and standard deviation of that subsequence.

3.3.2. k-Shape clustering

5579 ICP subsequences of varying length generated from the 88 hours of the ICP main dataset were clustered with the k-Shape algorithm into seven

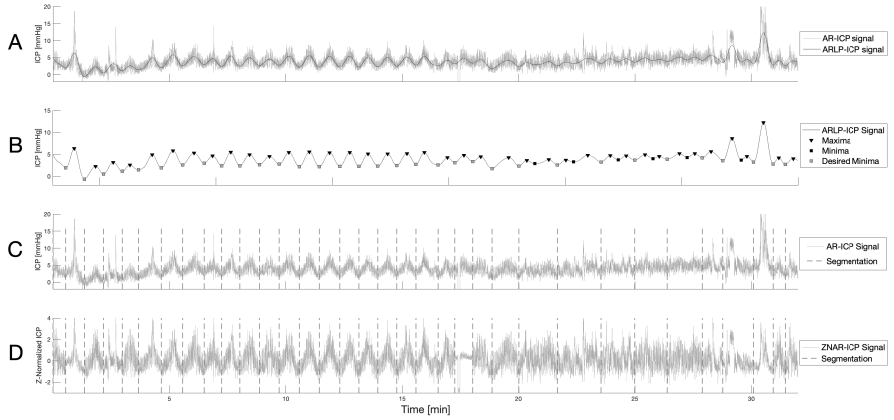

Figure 5: Example of the Artifact removed (AR)-ICP signal segmentation of one subject. (A) After low-pass filtering the AR-ICP signal, with respiratory and pulse contributions to the signal removed to generate the AR-low-pass (ARLP)-ICP signal; (B) After extracted extrema from ARLP-ICP signal; (C) After segmentation using desired minima; and (D) After z-normalization of the segmented AR (ZNAR)-ICP signal.

clusters. The number of optimal clusters to generate the most distinct patterns was calculated using the Silhouette index. We set $K = 7$ because it gave us the maximum silhouette value after performing k-Shape clustering for $k = 5 - 20$, as seen in Figure 6. Going beyond twenty will not contribute to generating distinctive clusters with sufficient information about the ICP data and it will only make our clusters more complicated.

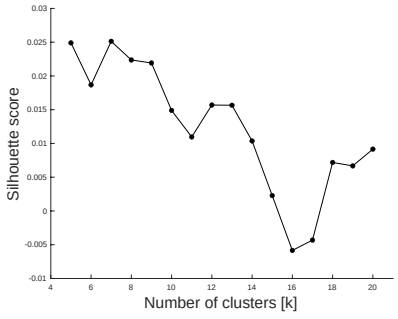

Figure 6: Number of optimal K using Silhouette score on the main ICP subsequences.

To better understand what shapes of centroids were generated, Figure 7 visualizes the cluster centroids with their corresponding ICP subsequences. This means that the five ICP recordings can be represented by a combination of these seven patterns which can vary in duration and amplitude.

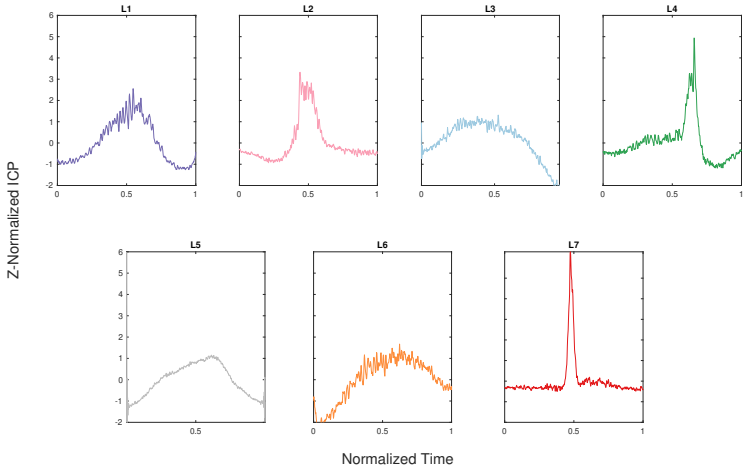

Figure 7: Main extracted reproducible subsequences from the 88 hours of ICP recordings (main dataset). These patterns are the foundation for identifying clinically relevant macro-patterns across a wide cohort of patients, moving away from Lundberg's A and B waves. In contrast to the classical approach, our subsequences could be combined to generate a new macro-pattern. For instance, the ascending *L6* subsequence could be followed by the descending *L3* subsequence, generating a new macro-pattern.

3.4. Cluster validation

Silhouette index was used to compare the clustering results of k-Shape applied to the main data with and without the addition of the correlation rule. Figure 8 shows that for Silhouette index, k-Shape together with the correlation rule shows better results over just k-Shape.

The value of the Silhouette index lies within the range -1 to 1. The closer the index is to 1, the more dense and well-separated from other clusters it is. The addition of the correlation rule increases the silhouette average from 0.024 to 0.056. Another aspect to look for is the thickness (in the vertical axis) of the

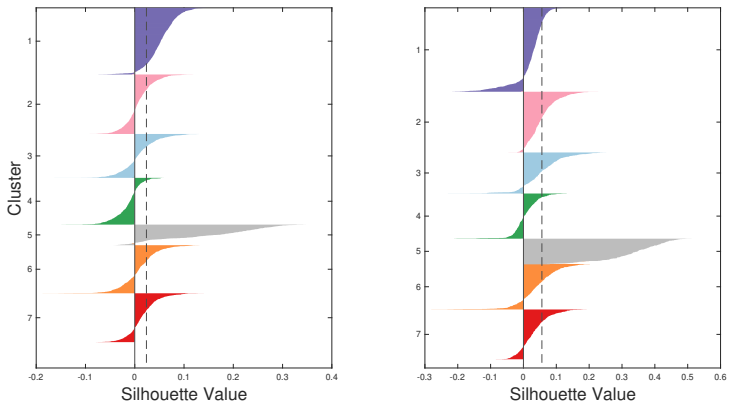

Figure 8: Graphical silhouette values for each clusters when $K = 7$ of the main dataset (left), main dataset and correlation rule (right). The dashed vertical line indicates the average silhouette score across all clusters.

CVI	k-Shape	k-Shape with correlation rule
Sil	0.02	0.06
1-DBI	-9.96	-8.19
CHI	115.91	123.15

Table 1: Three CVIs for k-Shape clustering without and with correlation rule for the main dataset.

silhouette plot representing each cluster, being more uniform between clusters when the correlation rule is considered. This idea is reinforced by the results seen in Table 1, with all CVIs increasing when the correlation rule is added.

Cluster validation indices highly depend on the complexity of the cluster analysis and on the vague definition of what the nature of the cluster is. Such validation requires a visual approach [22]. We used the additional set to visually confirm that the patterns found in the main set can also be observed in this new data.

3.5. ICP signal characterization

To allow searching for the minimum distance between each new z-normalized ICP subsequence and each pattern template, we used SBD. Results from the previous section (Section 3.4) showed the importance of the introduction of a correlation-based rule to ensure that the closest match was significant. We need to bear in mind that if clinicians are our end-users, the ICP template matching output should be clinically intelligible. Figure 9 shows an example of our ICP signal characterization output described in Section 2.4.

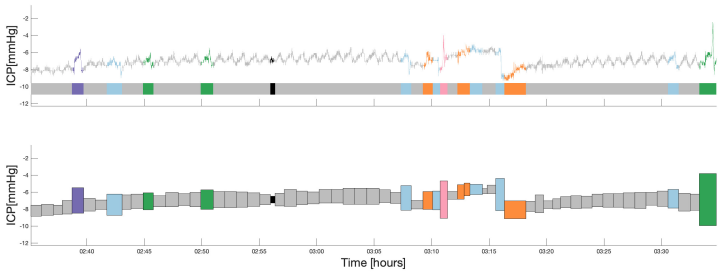

Figure 9: Example of the ICP signal segmentation and classification into labels for one subject visualized in the raw signal (top) and in the data reduced signal representation (bottom).

Using the pipeline solution we propose in this paper, we are able to characterize an average of 54% of the ICP signal. Further classification details are presented in Table 2

Figure 10 provides further visualization of the macro-pattern amplitude and duration in each subject. The presence of specific patterns in unique subjects, in this case $L5$ in Subject 1, could suggest that the occurrence frequency of specific macro-patterns could potentially be used to describe the pathological state of each subject.

4. Discussion

Typical A and B waves are described and classified differently by various authors [23] and do no longer adequately address the waveforms encountered in

Patient	Monitoring Duration [hours]	Duration of classified subsequences [%]
1	8.8	90.4
2	20.1	54.4
3	22.1	52.8
4	17.9	48.6
5	19.3	47.4
6	18.6	50.1
7	18.4	33.0
8	17.7	56.3

Table 2: Percentage duration of the classified subsequences in the ICP monitoring of each patient. The first five patients correspond to the main set, while the remaining three are part of the additional set.

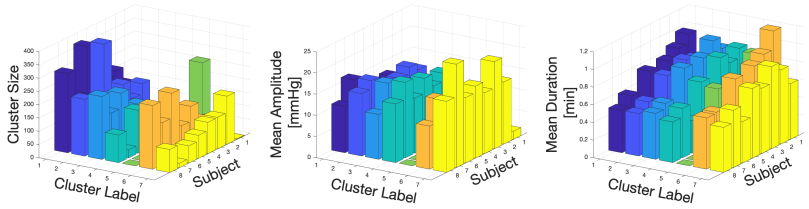

Figure 10: Variation between patients and labels for how often the seven types of patterns occur (left), pattern mean amplitude (middle) and pattern mean duration (right).

clinical practice today, where patients are investigated also in non-acute scenarios. Therefore, building on top of these classical macro-patterns, a new workflow was developed for the characterization and visualization of long-term ICP variations. Our adaptable pipeline steps includes Empirical Mode Decomposition (EMD) for artifact removal, segmentation into variable-duration subsequences, z-normalization, k-Shape clustering to divide the extracted ICP subsequences into a number of characteristic preserving labels, template-matching to locate the labels in the segmented ICP signal, and finally produces a box-based subsequence labeling display.

k-Shape outperforms traditional scalable and non-scalable clustering, such as k-means with Dynamic Time Warping (DTW) as distance metrics or k-medoids, in terms of both accuracy and/or efficiency [14, 24, 25]. Unfortunately, k-Shape

also presents a limitation: the number of clusters needs to be pre-specified by the user. If the assumed K value is above the optimal, the algorithm will generate unnecessary additional groups; if below, we will be under-representing associations between subsequences. There is no perfect method to determine the optimal number, as there is no clear definition of a cluster. We tackled this issue by combining visual inspection with the Silhouette index. Initial visual exploration by clinicians suggested that the search for the optimal K should not go beyond $k = 20$, as they do not believe in the existence of a number of clinically relevant macro-patterns beyond that value. Thus, the choice of search range was $k = 5 - 20$, with $K = 7$ as the optimal value for our data. We are aware that our methods for selecting K are heuristics, and subject to interpretation. A different choice of K could yield different results if our study is to be replicated with the same methodology by different research groups.

Besides using CVIs for estimating the quality of the clustering, it is important to visually inspect the results. Clusters *L1*, *L2*, and *L5* could fall into the same category of clinically well-known waveforms since they highly relate to A and B waves. Previous studies classify B waves according to their shape into symmetrical (sinousoidal) and asymmetrical (ramp-like) waveforms [26, 27, 28, 29]. Cluster *L1* in our template library resembles the so-called asymmetrical waves, since the duration of the ascending phase is longer than that of the descending. Clusters *L2* and *L5* present more symmetry, with ascending and descending phases of closer duration. They differ in the presence (*L2*) or not (*L5*) of a plateau. For *L2* waveforms, the pressure magnitude will determine its degree of similarity to either A or B waves. Remaining extracted clusters have not been described as such in the literature. Clusters *L6* and *L3* represent ascending and descending segments leading or ending a plateau segment, respectively. This plateau can vary in duration and in some cases contain other clinically relevant macro-patterns. Cluster *L7* is likely to represent subsequences containing artifacts, given the shape of the peak. Finally, cluster *L4* appears as a new non-classified macro-pattern, whose clinical relevance needs to be further analyzed. It must be noted that the templates in our library are

normalized in time, meaning that they can be stretched and compressed when matched to incoming ICP subsequences, but constrained by the correlation rule.

With these templates, approximately half of the ICP recording ends up being labeled. This means that for the data considered in this paper, half of it can be represented by just seven shapes (properly scaled horizontally and vertically). This suggests that many ICP signals are often made up of the same patterns repeated again and again. As we have selected to look for one particular macro-pattern type (B wave) to investigate the feasibility of our approach, and the occurrence of macro-pattern types is related to the clinical diagnosis, it is to be expected that the current macro-pattern library does not cover the entire curve length and that the percentage covered can vary between datasets, as we have included these randomly. With this in mind, we have developed the building blocks of a methodology that - with additional retrospective data - could allow identification of previously unencountered macro-patterns in addition to the immediately useful potential of systematic quantitative multidimensional analysis of ICP data. It would be interesting to investigate whether an increased number of templates, K, would increase the fraction of ICP recording being labeled, and especially whether such an increase in the fraction comes at the price of an exponential increase in K. Finally, in this context, one should bear in mind that if K increases to e.g., 100, then the clinical clarity with respect to visual classification might suffer seriously.

The universal scalable library produced so far is the result of combining clinical knowledge of how ICP changes in different clinical conditions, with an engineering approach that moves ICP signal analysis in a more robust quantitative direction with fewer subjective judgments. The results of the present work may be considered benchmarks for the shape clustering method that will be used in our ongoing research. The evident next step is to relate the generated macro-pattern templates with clinical data to ensure that macro-patterns are reproducible and identifiable across a wide cohort of patients with different disease entities. Subsequently, we aim to investigate if it is possible to match disease categories with the occurrence frequency and distribution of the spe-

cific macro-patterns. Knowledge of some macro-patterns possibly being more indicative of particular pathological conditions opens opportunities to individualize management and treatment of each patient and obtain a better prediction and understanding of the possible outcome. Furthermore, looking at each label together with additional monitoring of other physiological signals could help to elucidate the origin of each waveform.

The output of our labeling method must be displayed in a way that ensures readability and clarity for clinicians to easily interpret and to integrate it as a new tool in their daily clinical practice. Our visualization strategy is one of the many alternative ways of looking at the raw ICP signal that could be used to accentuate specific features that might not be easily spotted during the visual interpretation of the ICP monitoring. It can be seen as a prototype, among all possibilities of graphical representations, for how the ICP data analysis workflow can be structured. The box approach highlights the presence of the seven identified labels, with many other visualization alternatives yet to be considered, some of them maybe aiming for a report of a certain clinical state. Internal distribution and clinical weighting of the boxes could reflect the pathological state of the patient.

Limitations

The selection of subjects for the creation of the template library is likely to affect the result, since some patients appear to have more distinguishable macro-patterns than others. Applying this approach to a larger group of subjects is one of the future objectives.

5. Conclusion

In this paper, a flexible time series pattern recognition scheme customized to handle ICP time series patterns was introduced. In particular, a clustering algorithm k-Shape clustering was first applied to cluster ICP subsequences to generate a standard scalable library of macro-patterns that can further be used

for classification of new incoming ICP signals. We worked with 88 hours of ICP recordings and showed the resulting seven clusters that best describe them. Our further research will investigate the clinical use of this technique and look at the practicality of its automatic use to quantitatively interpret ICP data, hoping to reveal a better understanding of the patients underlying physiological status.

Declarations

Funding. This project has received funding from the Novo Nordisk Tandem (NNF17OC0024718).

Conflicts of interest The authors have no conflicts of interest to report.

Availability of data and material Not applicable.

Code availability Not applicable.

Authors' contributions All authors contributed to the study conception and design. Data analysis was performed by Isabel Martinez-Tejada. The first draft of the manuscript was written by Isabel Martinez-Tejada and all authors commented on previous versions of the manuscript. All authors read and approved the final manuscript.

Ethics approval Not applicable.

References

[1] A. Lilja-Cyron, J. Kelsen, M. Andresen, K. Fugleholm, M. Juhler, Feasibility of Telemetric Intracranial Pressure Monitoring in the Neuro Intensive Care Unit, Journal of Neurotrauma 35 (14) (2018) 1578–1586. doi:10.1089/neu.2017.5589.

[2] M. Czosnyka, J. D. Pickard, Monitoring and interpretation of intracranial pressure, Journal of Neurology, Neurosurgery and Psychiatry 75 (6) (2004) 813–821. doi:10.1136/jnnp.2003.033126.

[3] Z. Mariak, M. Swiercz, J. Krejza, J. Lewko, T. Lyson, Intracranial pressure processing with artificial neural networks: Classification of signal

properties, Acta Neurochirurgica 142 (4) (2000) 407–412. doi:10.1007/s007010050450.

[4] R. Hornero, M. Aboy, D. Abasolo, J. McNames, W. Wakeland, B. Goldstein, Complex analysis of intracranial hypertension using approximate entropy*, Critical Care Medicine 34 (1) (2006) 87–95. doi:10.1097/01.CCM.0000190426.44782.F0.

[5] M. Andresen, M. Juhler, T. N. Munch, Quality and Safety of Home ICP Monitoring Compared with In-Hospital Monitoring, 2012, pp. 187–191. doi:10.1007/978-3-7091-0923-6{_}37.
URL http://link.springer.com/10.1007/978-3-7091-0923-6_37

[6] M. Andresen, M. Juhler, Intracranial pressure following complete removal of a small demarcated brain tumor: a model for normal intracranial pressure in humans, Journal of Neurosurgery 121 (4) (2014) 797–801. doi:10.3171/2014.2.JNS132209.

[7] M. Andresen, A. Hadi, L. G. Petersen, M. Juhler, Effect of postural changes on ICP in healthy and ill subjects, Acta Neurochirurgica 157 (1) (2015) 109–113. doi:10.1007/s00701-014-2250-2.

[8] M. Andresen, M. Juhler, O. C. Thomsen, Electrostatic discharges and their effect on the validity of registered values in intracranial pressure monitors, Journal of Neurosurgery 119 (5) (2013) 1119–1124. doi:10.3171/2013.7.JNS13506.

[9] I. Martinez-Tejada, J. E. Wilhjelm, M. Juhler, M. Andresen, Empirical Mode Decomposition-Based Method for Artefact Removal in Raw Intracranial Pressure Signals, 2021, pp. 201–205. doi:10.1007/978-3-030-59436-7{_}39.

[10] D. L. Donoho, I. M. Johnstone, Ideal spatial adaptation by wavelet shrinkage, Biometrika 81 (3) (1994) 425–455. doi:10.1093/biomet/81.3.425.

[11] S. Aghabozorgi, T. Ying Wah, T. Herawan, H. A. Jalab, M. A. Shaygan, A. Jalali, A hybrid algorithm for clustering of time series data based on affinity search technique, The Scientific World Journal 2014. doi:10.1155/2014/562194.

[12] A. Javed, B. S. Lee, D. M. Rizzo, A benchmark study on time series clustering, arXiv 1 (July) (2020) 100001. doi:10.1016/j.mlwa.2020.100001.

[13] M. R. Karim, O. Beyan, A. Zappa, I. G. Costa, D. Rebholz-Schuhmann, M. Cochez, S. Decker, Deep learning-based clustering approaches for bioinformatics, Briefings in Bioinformatics 22 (1) (2021) 393–415. doi:10.1093/bib/bbz170.

[14] J. Paparrizos, L. Gravano, K-shape: Efficient and accurate clustering of time series, Proceedings of the ACM SIGMOD International Conference on Management of Data 2015-May (2015) 1855–1870. doi:10.1145/2723372.2737793.

[15] A. Sardá-Espinosa, Comparing time-series clustering algorithms in R using the dtwclust package, R Journal 11 (1) (2019) 1–45.

[16] A. Starczewski, A. Krzyżak, Performance Evaluation of the Silhouette Index, 2015, pp. 49–58. doi:10.1007/978-3-319-19369-4{_}5.

[17] J. Hämäläinen, S. Jauhiainen, T. Kärkkäinen, Comparison of Internal Clustering Validation Indices for Prototype-Based Clustering, Algorithms 10 (3) (2017) 105. doi:10.3390/a10030105.

[18] U. Maulik, S. Bandyopadhyay, Performance evaluation of some clustering algorithms and validity indices, IEEE Transactions on Pattern Analysis and Machine Intelligence 24 (12) (2002) 1650–1654. doi:10.1109/TPAMI.2002.1114856.

[19] H. Li, S. Zhang, X. Ding, C. Zhang, P. Dale, Performance Evaluation of Cluster Validity Indices (CVIs) on Multi/Hyperspectral Remote Sensing Datasets, Remote Sensing 8 (4) (2016) 295. doi:10.3390/rs8040295.

[20] K. Kryszczuk, P. Hurley, Estimation of the Number of Clusters Using Multiple Clustering Validity Indices, 2010, pp. 114–123. doi:10.1007/978-3-642-12127-2{_}12.

[21] T. Calinski, J. Harabasz, A dendrite method for cluster analysis, Communications in Statistics - Theory and Methods 3 (1) (1974) 1–27. doi:10.1080/03610927408827101.

[22] M. Ng, J. Huang, M-FastMap: A Modified FastMap Algorithm for Visual Cluster Validation in Data Mining, 2002, pp. 224–236. doi:10.1007/3-540-47887-6{_}22.

[23] P. K. Eide, A. D. Fremming, A new Method and Software for Quantitative Analysis of Continuous Intracranial Pressure Recordings, Acta Neurochirurgica 143 (12) (2001) 1237–1247. doi:10.1007/s007010100020.

[24] J. Paparrizos, L. Gravano, Fast and Accurate Time-Series Clustering, ACM Transactions on Database Systems 42 (2) (2017) 1–49. doi:10.1145/3044711.

[25] J. Yang, C. Ning, C. Deb, F. Zhang, D. Cheong, S. E. Lee, C. Sekhar, K. W. Tham, k-Shape clustering algorithm for building energy usage patterns analysis and forecasting model accuracy improvement, Energy and Buildings 146 (2017) 27–37. doi:10.1016/j.enbuild.2017.03.071.

[26] I. Martinez-Tejada, A. Arum, J. E. Wilhjelm, M. Juhler, M. Andresen, B waves: a systematic review of terminology, characteristics, and analysis methods, Fluids and Barriers of the CNS 16 (1) (2019) 33. doi:10.1186/s12987-019-0153-6.

[27] A. Spiegelberg, M. Preuß, V. Kurtcuoglu, B-waves revisited, Interdisciplinary Neurosurgery 6 (2016) 13–17. doi:10.1016/j.inat.2016.03.004.

[28] C. Raftopoulos, C. Chaskis, F. Delecluse, F. Cantrainet, L. Bidauti, J. Brotchi, Morphological quantitative analysis of intracranial pressure

waves in normal pressure hydrocephalus, Neurological Research 14 (5) (1992) 389–396. doi:10.1080/01616412.1992.11740091.

[29] D. Santamarta, E. González-Martínez, J. Fernández, A. Mostaza, The Prediction of Shunt Response in Idiopathic Normal-Pressure Hydrocephalus Based on Intracranial Pressure Monitoring and Lumbar Infusion, 2016, pp. 267–274. doi:10.1007/978-3-319-22533-3{_}53.

CHAPTER B Mathematical Remarks

B.1 Empirical Mode Decomposition

Empirical Mode Decomposition (EMD), is a local and adaptive data-driven technique used for the decomposition of nonstationary and nonlinear signals [115]. EMD breaks down each signal $X(t)$ into intrinsic mode functions (IMFs), c_i, and a residue, r_n, that provide instantaneous frequency data to elucidate hidden features [120]:

$$X(t) = \sum_{i=1}^{n} c_i + r_n \tag{B.1}$$

IMFs are oscillatory functions of varying amplitude and frequency that fulfill two conditions: (1) the number of extrema is equal to the number of zero-crossings or differ at most by one; and (2) the mean of the upper and lower envelopes calculated from the local maxima and minima extracted, respectively, must always equal to zero [121]. IMFs are sequentially calculated from high to low frequency as follows [122]:

1. Envelope extraction: first, all the local extrema in the signal are identified. Then, the local maxima are connected by a cubic spline to produce the upper envelope, and the same is done with the local minima to generate the lower envelope. The mean between the two envelopes is $m_1(t)$.
2. The envelope mean is then subtracted from the original signal to generate the first IMF candidate, $h_1(t)$: $h_1 = X(t) - m_1(t)$. If h_1 satisfies the IMF conditions, it is denoted as $c_1(t)$, otherwise steps 1 and 2 are repeated until $h_{1k}(t)$ is a IMF.
3. The first IMF is then subtracted from the original signal to generate the first residual, $r_1(t)$: $r_1(t) = X(t) - c_1(t)$. This residual component is then treated as a new original signal, and subjected to steps 1 and 2 to calculate the second IMF.
4. The previous steps are repeated until the final residual becomes a monotonic or constant function.

Although EMD is an effective technique to tackle the non-stationarity and non-linearity of signals, it still faces some drawbacks, especially the mode mixing one. This means that one IMF might contain components from different time scales, or one time scale might appear in different IMFs. Intermittency of the signal due to discontinuous frequency components is responsible for the presence of multifrequency components in one IMF. High frequency pulses with frequency components closely spaced cause the decomposition of one frequency component into different IMFs [123].

B.2 Ensemble Empirical Mode Decomposition

EEMD has been recently proposed to alleviate the mode mixing problem of the EMD [99]. Basically, EEMD decomposes the original signal with different white noise series added each time into IMFs using the original EMD technique. A more detailed process explanation, summed up in Figure B.1, is as follows [99]:

1. Addition of white noise to the original signal. White noise series should have finite amplitude and equal mean and variance as the original signal:

$$X_j(t) = X(t) + A \cdot w_j(t)\ j = 1...M \tag{B.2}$$

where A is the amplitude of the added white noise w and M the total number of trials.

2. Decomposition of the signal with added noise into IMFs using EMD:

$$X_j(t) = \sum_{i=1}^{N_j} c_{ij} + r_{n_j} \tag{B.3}$$

where c_{ij} and r_{n_j} are the ith IMF or residual of the jth trial, respectively, and N_j the number of IMF in the jth trial.

3. Repetition of steps 1 and 2 with different white noise added in step 1 a total of M times.

4. Calculation of the average (ensemble) of all the corresponding IMFs of the EMD to eliminate the influence of white noise:

$$c_i(t) = \frac{\sum_{j=1}^{M} c_{ij}}{M}\ i = 1, 2, ..., K \tag{B.4}$$

where K is the number of IMFs in the trials.

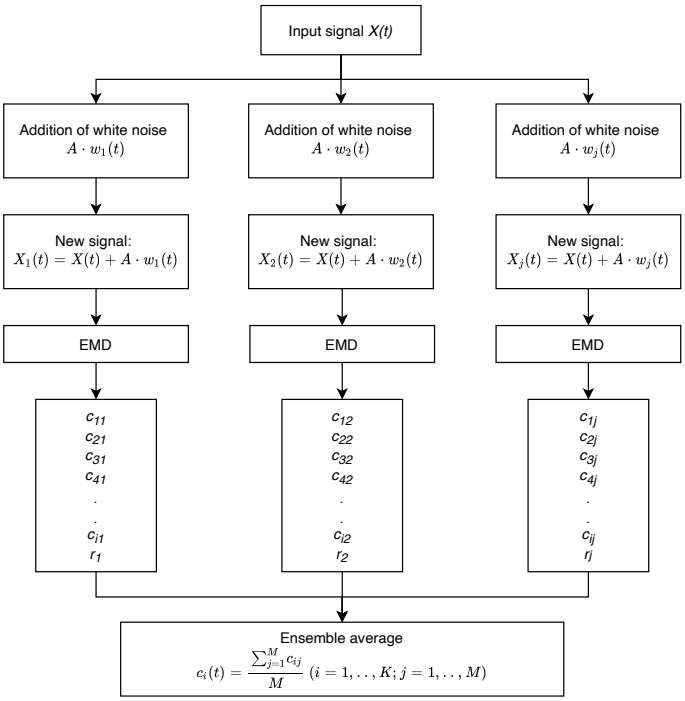

Figure B.1: The flowchart of the EEMD algorithm.

EEMD effectively mitigates the problem of mode mixing, but presents the challenge of defining the noise amplitude and the number of ensembles, which are both key parameters in the performance of the technique [124]. If the amplitude of the added noise is too low, mode mixing will still be present. On the contrary, if too high, redundant IMFs will be created. The number of ensemble trials is a trade-off between completely canceling out the influence of the added white noise and the computational cost.

B.3 Granger Causality

Bivariate Granger Causality (GC) is a statistical test that determines whether one time series X_1 is statistically useful in forecasting another time series X_2. A time series X_1 is said to Granger-cause X_2 if lagged values of X_1 provide information that helps to better predict X_2 [125]. This measure is built on the foundation that effects come after the cause, and these causes help to better predict their effects. To analyze the mutual influence between more than two time series, an extension of the bivariate modality is considered: conditional Granger causality analysis (cGC). For instance, X_1 is said to G-causes X_2 if X_2 conditional on X_3 can be better predicted using the past values of both X_1 and X_2, influenced by X_3 (full model) compared with the prediction of using only the past values of X_1 (restricted model). Conditional GC analysis was implemented using the MATLAB code published by L.Barnett and A.K. Seth [126] (R2019a; MVGCA Matlab Toolbox, The MathWorks, Inc., Natick, MA.).

GC was investigated by fitting a multivariate autoregressive (MVAR) model of order p to the three time series of interest. Next, an MVAR model between all three random processes $X_1(t)$, $X_2(t)$, and $X_3(t)$ is assumed:

$$\begin{aligned} X_1(t) &= \sum_{j=1}^{p} A_{11,j} X_1(t-j) + \sum_{j=1}^{p} A_{12,j} X_2(t-j) + \sum_{j=1}^{p} A_{13,j} X_3(t-j) + E_1'(t) \\ X_2(t) &= \sum_{j=1}^{p} A_{22,j} X_2(t-j) + \sum_{j=1}^{p} A_{21,j} X_1(t-j) + \sum_{j=1}^{p} A_{23,j} X_3(t-j) + E_2'(t) \\ X_3(t) &= \sum_{j=1}^{p} A_{33,j} X_3(t-j) + \sum_{j=1}^{p} A_{32,j} X_2(t-j) + \sum_{j=1}^{p} A_{31,j} X_1(t-j) + E_3'(t) \end{aligned} \tag{B.5}$$

where E_1', E_2', and E_3' are the error of each model, and A_{kj} the regression coefficients. The model order p was determined using the lowest value of either Akaike Information Criterion (AIC) [127] so as to avoid overfitting. The model was validated using three tests: (1) a consistency test that calculated the percentage of the correlation structure of the IMFs that is explained by the MVAR model, (2) an additional consistency test to validate the adjusted sum square error, and (3) the Durbin-Watson statistic [128] to test for autocorrelation in the residuals to ensure that they were all white noise series.

Based on the models above, a causal flow from one signal (source) to another (target) exists if the inclusion of past observations of the target reduces the variance of the model error of the source, while taking into account the influence of the third variable. For instance, a causal flow from X_2 to X_1 exists if the addition of past observations of X_2 in the model reduces the variance of E_1', after taking into account the influence of X_3. This implies that the coefficients A_{12} reject the F-test null hypothesis that they are zero at a given significance level, i.e., they are different from zero [129]. The logarithm of the F-statistic measures the magnitude of the G-causality [130]:

$$cGCI_{2\to 1|3} = \ln \frac{var(E_1)}{var(E_{1'})} \tag{B.6}$$

where E_1 is the error of the model without lagged observations of X_2 (reduced model), and E_1' is the error of a similar MVAR model but including past observations of X_2 (full model).